A SOLUTION METHODOLOGY FOR THE UNIT COMMITMENT PROBLEM IN TRADITIONAL-AND-WIND INTEGRATED HYBRID POWER SYSTEMS UNDER SUPPLY/DEMAND UNCERTAINTY AND EMISSION LIMITATIONS

A THESIS SUBMITTED TO
THE GRADUATE SCHOOL OF NATURAL AND APPLIED SCIENCES
OF
MIDDLE EAST TECHNICAL UNIVERSITY

BY

TOLGA KARABAŞ

IN PARTIAL FULFILLMENT OF THE REQUIREMENTS
FOR
THE DEGREE OF MASTER OF SCIENCE
IN
INDUSTRIAL ENGINEERING

SEPTEMBER 2020

Approval of the thesis:

A SOLUTION METHODOLOGY FOR THE UNIT COMMITMENT PROBLEM IN TRADITIONAL-AND-WIND INTEGRATED HYBRID POWER SYSTEMS UNDER SUPPLY/DEMAND UNCERTAINTY AND EMISSION LIMITATIONS

submitted by **TOLGA KARABAŞ** in partial fulfillment of the requirements for the degree of **Master of Science in Industrial Engineering, Middle East Technical University** by,

Prof. Dr. Halil Kalıpçılar
Dean, Graduate School of **Natural and Applied Sciences** _____

Prof. Dr. Esra Karasakal
Head of the Department, **Industrial Engineering** _____

Assoc. Prof. Dr. Sedef Meral
Supervisor, **Industrial Engineering, METU** _____

Examining Committee Members:

Assoc. Prof. Dr. Seçil Savaşaneril Tüfekci
Industrial Engineering, METU _____

Assoc. Prof. Dr. Sedef Meral
Industrial Engineering, METU _____

Assist. Prof. Dr. Ayşe Selin Kocaman
Industrial Engineering, Bilkent University _____

Assist. Prof. Dr. Sakine Batun
Industrial Engineering, METU _____

Assist. Prof. Dr. Mustafa Kemal Tural
Industrial Engineering, METU _____

Date: 11.09.2020

I hereby declare that all information in this document has been obtained and presented in accordance with academic rules and ethical conduct. I also declare that, as required by these rules and conduct, I have fully cited and referenced all material and results that are not original to this work.

Name, Last name : Tolga Karabaş

Signature :

ABSTRACT

A SOLUTION METHODOLOGY FOR THE UNIT COMMITMENT PROBLEM IN TRADITIONAL-AND-WIND INTEGRATED HYBRID POWER SYSTEMS UNDER SUPPLY/DEMAND UNCERTAINTY AND EMISSION LIMITATIONS

Karabaş, Tolga
Master of Science, Industrial Engineering
Supervisor: Assoc. Prof. Dr. Sedef Meral

September 2020, 248 pages

Unit commitment problem (UCP) is one of the essential problems in operations planning of power generation systems. The objective is to minimize total operating cost while meeting the forecasted load requirements and satisfying several operational and technical constraints. Nevertheless, the UCP is a mixed integer, non-linear, combinatorial and NP-hard problem, making it difficult to develop any rigorous optimization method for a real-size system. In this thesis, we address two variants of the UCP: (1) the deterministic UCP in conventional power systems, (2) the stochastic UCP in wind integrated hybrid power systems. For the first one, an effective and efficient Genetic Algorithm-based approach is developed. For the second one, Mixed-Integer Quadratic Programming-based approaches are developed. In these approaches for the stochastic UCP, novel expected energy not served (EENS) approximation methods are proposed to model both load demand uncertainties and supply uncertainties due to intermittent nature of wind power generation and outages in conventional generation. Furthermore, the proposed approaches are extended to consider: (i) the Valve Point Loading Effect in efficiencies of conventional generating units by proposing efficient multi-area

piecewise linear approximation, (ii) the impacts of Emission Control Technologies and Emission Trading and Taxing Mechanisms in mitigating greenhouse gas and air pollutant emissions caused by conventional generating units. According to numerical experiments and sensitivity analysis results, both Genetic Algorithm-based and Quadratic Programming-based approaches are proven to be valid and effective, and they can provide satisfactorily good power generation schedules for large scale power systems in a reasonable computational time.

Keywords: Unit Commitment Problem, Genetic Algorithm, Supply/Demand Uncertainty, Quadratic Programming, Emissions Control

ÖZ

ARZ/TALEP BELİRSİZLİĞİ VE EMİSYON SINIRLAMALARI ALTINDA GELENEKSEL-VE-RÜZGAR ENTEGRE HİBRİT ENERJİ SİSTEMLERİNDE BİRİM YÜKLENME PROBLEMİ İÇİN ÇÖZÜM YÖNTEMLERİ

Karabaş, Tolga
Yüksek Lisans, Endüstri Mühendisliği
Tez Yöneticisi: Doç. Dr. Sedef Meral

Eylül 2020, 248 sayfa

Enerji üretim sistemlerinin operasyon planlamasındaki en temel problemlerden biri Birim Yüklenme Problemidir (UCP). Problemin amacı; tahmini enerji gereksinimlerini ve çeşitli operasyonel ve teknik kısıtları sağlarken, toplam işletme maliyetlerini en aza indirmektir. Ancak, UCP karışık tamsayılı, doğrusal olmayan, kombinatoryal ve NP-zor bir problemdir. Bu durum gerçek boyutlu bir enerji sistemi için bütünleşik bir optimizasyon yöntemi geliştirmeyi zorlaştırmaktadır. Bu tezde UCP'nin iki versiyonu ele alınmıştır: (1) konvansiyonel enerji sistemlerindeki deterministik UCP, (2) rüzgar entegre hibrit enerji sistemlerindeki rassal UCP. İlki için etkili ve verimli bir Genetik Algoritma tabanlı yaklaşım geliştirilmiştir. İkincisi için, Karışık Tamsayılı Karesel Programlama tabanlı yaklaşımlar geliştirilmiştir. Rassal UCP için bu yaklaşımlarda hem enerji talebindeki belirsizliklerden hem de rüzgar enerjisi üretiminin kesintili doğasından ve konvansiyonel üretimdeki olası kesintilerden kaynaklanan arz belirsizliklerinden dolayı karşılanamayacak enerji miktarını (EENS) hesaplama yöntemleri önerilmiştir. Ayrıca, önerilen yaklaşımlar şunları da dikkate alarak genişletilmiştir: (i) verimli bir çok-alanlı parçalı doğrusal yakınlaştırma yöntemi ile Vana Noktası Yükleme Etkisinin konvansiyonel üretim tesislerinin verimliliklerinde yarattığı dalgalanmalar, (ii) konvansiyonel üretim

tesislerinin neden olduğu sera gazı ve hava kirliliğine sebep olan gazların emisyonlarının azaltılmasında Emisyon Kontrol Teknolojilerinin ve Emisyon Ticareti ve Vergi Mekanizmalarının etkileri. Yapmış olduğumuz sayısal deneylerin ve duyarlılık analizlerinin sonuçlarına göre hem Genetik Algoritma tabanlı hem de Karesel Programlama tabanlı yaklaşımların, geçerli ve etkili olduğu kanıtlanmış, ve büyük ölçekli enerji sistemleri için makul bir hesaplama süresinde tatmin edici derecede iyi enerji üretim çizelgeleri sağlayabildikleri saptanmıştır.

Anahtar Kelimeler: Birim Yüklenme Problemi, Genetik Algoritma, Arz/Talep Belirsizliği, Karesel Programlama, Emisyon Kontrolü

To my family…

ACKNOWLEDGMENTS

First, I would like to thank my thesis supervisor, Dr. Sedef Meral, for her guidance, advice, criticism, encouragements and insight throughout the research. I would like to acknowledge the examining committee members, Dr. Seçil Savaşaneril Tüfekci, Dr. Ayşe Selin Kocaman, Dr. Sakine Batun and Dr. Mustafa Kemal Tural for their valuable reviews and comments.

I would like to thank The Scientific and Technological Research Council of Turkey (TÜBİTAK), for their financial support during this thesis work.

I would like to thank my managers in EnerjiSA; Nuri Osman Çalışkan, Arif Coşkun and Sezgin Şen, for their support during my graduate education.

Finally, I would like to express my deepest gratitude to my dearest mother, father, brother, aunt and grandmothers; Feray Karabaş, Kemal Karabaş, Toygun Karabaş, Funda Köksal, Necla Köksal and Naciye Karabaş, for their endless supports and encouragements.

TABLE OF CONTENTS

LIST OF TABLES

TABLES

LIST OF FIGURES

FIGURES

CHAPTER 1

INTRODUCTION

Power systems are one of the crucial and fundamental infrastructures in a modern society. Therefore, it is necessary to maintain a secure, reliable and continuous power supply (Roque, 2014). For this purpose, one of the most critical problems in modern power systems is the Unit Commitment Problem (UCP) in which the main objective is to optimize commitment statuses and productions of generating units in a power system on an hourly basis to meet forecasted load demand requirements, while satisfying various operational and technical constraints. However, the problem environment of the UCP contains several complexities.

First of all, in power systems, hourly load demands have a variable nature during the day. To illustrate, the load demands during the daytime tend to be extremely higher than the ones during nights and early mornings (Mallipeddi and Suganthan, 2014). In traditional power generation, this cyclic nature may cause some of the conventional generating units working at their minimum power output level during nights and early mornings. Hence, it is indispensable to efficiently make commitment decisions of conventional units in a day-ahead power generation planning.

Secondly, supply and demand uncertainties are inevitable in power generation systems. Hourly load demands cannot be exactly determined since they are dependent on the human activities during the day. Thus, they can only be forecasted, which causes load demand uncertainty. Furthermore, conventional generating units may cause supply uncertainty as a result of the unexpected unit outages. In addition, renewable energy sources such as water, wind and sunlight have gained a significant attention in modern power systems thanks to their zero marginal production costs

and lower maintenance costs when compared to the ones in conventional power plants due to potential fossil fuel scarcity (Kåberger, 2018). Hence, renewable energy sources have started to be used synchronously with conventional generating units for the last two decades. Those systems are known as hybrid power systems. Nonetheless, in hybrid power systems, the intermittent nature of renewable energy sources also causes uncertainty in power supply. To deal with those uncertainties, an easy and straightforward method is to commit more reserve from conventional generating units to guarantee more reliable power generation. For this purpose, deterministic reserve policies have been used when renewable energy sources are not integrated into modern power systems. Nevertheless, those policies are not sufficient in the evaluation of the system risk levels in wind and solar integrated hybrid power systems, so stochastic solution approaches are required to overcome this problem (Lin et al., 2014).

Thirdly, in recent years, environmental considerations have become another important factor when operating modern power generation systems due to increasing concerns on adverse effects of global warming and air pollution on the environment and human health. To increase the public awareness and mitigate those emissions, several environmental agreements such as Kyoto Protocol (1997) and Paris Agreement (2016) have been introduced and signed by most of the industrial countries over the world under the leadership of the United Nations Framework Convention on Climate Change (UNFCCC). Those agreements dictate signing countries to gradually reduce their Greenhouse Gas (GHG) and air pollutant emissions by setting horizon-based targets (see Chapter 5). For this purpose, emission trading mechanisms and emission taxing schemes have been introduced by those countries to abate and control their emissions. Conventional power plants are one of the major emission producers. One of the solutions is to modernize fuel-based conventional power plants by installing emission reduction technologies while considering possible efficiency reductions (see Chapter 5). Another solution is to increase the share of renewable energy sources in the overall power generation mix as much as possible. For this purpose, since 2010, several feasibility studies have

been published to achieve 100% renewable share in world's power generation mix. Jacobson and Delucchi (2011) propose that 30% of world's total energy need can be met from hydro, wind and solar energy by 2030, and it is also possible that they can meet the whole energy demand by 2050. According to simulation results of Jacobson et al. (2018) and Jacobson et al. (2019), they suggest a new roadmap to achieve 100% transition to hydro, wind and solar energy combined with storage systems by 2050 for 20 regions containing 139 countries. That means effective production and operations planning in hybrid power systems will remain the main topic in the modern power industry for at least 30 more years to come. Hence, in order to achieve ambitious targets for emission abatement, conventional generating units should be modernized with emission reduction techniques, and their effects on overall production should be evaluated cautiously under the supervision of strict emission trading and taxing mechanisms.

Lastly, solving the UCP is computationally intensive because of its nonconvex, nonlinear, high dimensional and combinatorial nature especially when power systems consist of too many conventional generating units. The nonconvexity of the UCP is due to the binary nature of the commitment decisions of generating units, which is also the reason of its combinatorial nature, whereas the nonlinearities are caused by nonlinear generation cost curves, and nonlinear GHG and air pollutant emission curves. In addition, the UCP has various time-dependent constraints such as minimum uptime/downtime and ramp-up/down constraints. That is, those constraints affect decisions in a period by linking them to decisions in the previous period, which complicates the solution even more.

Under that background, the aim of the thesis is to develop efficient and optimal/near-optimal solution methods that can be implemented to the UCP in large-scale traditional and wind integrated hybrid power systems. For this reason, we propose a Genetic Algorithm based approach for the UCP in traditional power systems ignoring the inherent uncertainties. For the UCP in wind integrated hybrid power systems, we propose time-decoupled, stochastic and environmental mathematical models. It is important to note that hydro and solar generating units are excluded

from our scope, so the hybrid power systems examined throughout the study consist of numerous wind turbines and conventional power plants burning fossil fuels such as coal, gas and oil.

The rest of the thesis is organized as follows: In Chapter 2, Genetic Algorithm based approaches for the conventional UCP are reviewed first. Then, current studies on the UCP under supply and demand uncertainty for wind integrated hybrid power systems are briefly explained. Lastly, solution approaches for the UCP under emission considerations in traditional and wind integrated hybrid power systems are summarized. In Chapter 3, a mathematical formulation for the deterministic UCP in conventional power systems is presented first. Then, the proposed Mixed Integer Coded Genetic Algorithm (MICGA) combined with Improved Lambda Iteration Method (I-LIM) is provided to solve the deterministic UCP with/without ramp-rate limits in conventional generation. The MICGA is implemented to 10-unit, 20-unit and 40-unit standard problem instances in the literature after one-factor-at-a-time (OFAT) experiments are conducted to fine tune the proposed algorithm. Then, statistical analyses are carried out to test the robustness and precision of the algorithm. Lastly, the performance of the MICGA is compared with other GA techniques developed in the last two decades. In Chapter 4, uncertainty models of load demand, wind power and conventional power generation are presented for wind integrated hybrid power systems. Then, commonly used reliability indices in the literature are reviewed in detail. In the second part of the chapter, under supply/demand uncertainty, time-decoupled and stochastic Mixed Integer Quadratic Programming (MIQP) models consisting of two different expected energy not served (EENS) approximations are presented. By using those EENS approximation methods, other MIQP models that also piecewise linearly approximate the rippling efficiencies, also known as valve point loading effect (VPLE), of conventional generating units are proposed in this part. In the last part of the chapter, two EENS approximation methods are compared by applying the associated MIQP models to 6-unit and 26-unit problem instances while ignoring the VPLE. Then, the proposed MIQP models with/without the VPLE are applied to 6-unit, 12-unit and 26-unit

standard problem instances. To examine the sensitivity of the MIQP models to problem parameters, sensitivity analyses are conducted for each model. Then, the most widely used deterministic policies to cope with uncertainties related to conventional generation and forecasts of load demand and wind power are briefly reviewed. Accordingly, the time-decoupled and stochastic MIQP models are compared with mathematical models involving those deterministic reserve policies. In Chapter 5, emission considerations are studied and integrated for wind integrated hybrid power systems. First, current emission reduction agreements and regulations such as emission trading and taxing mechanisms in European Union, United States, China and Turkey are reviewed in detail. Then, emission reduction technologies against GHG and air pollutants, and their impacts on the conventional power plants are explained in detail. In the third part of the chapter, under supply/demand uncertainty and emission considerations, a time-decoupled, stochastic and environmental Mixed Integer Quadratically Constrained Programming (MIQCP) model, to which clean energy technologies, emission trading and taxing schemes, and the VPLE are integrated, is presented. Lastly, the proposed MIQCP model is applied to 6-unit and 12-unit standard problem instances. To examine the sensitivity of the model to problem parameters, sensitivity analyses are carried out for each problem instance. Then, the time-decoupled, stochastic and environmental MIQCP model is compared with the final stochastic model without emission considerations introduced in Chapter 4, and mathematical models involving deterministic reserve policies. In Chapter 6, the main achievements of the study and future research directions are discussed.

CHAPTER 2

LITERATURE REVIEW

The literature on the UCP for traditional and hybrid power systems has been proliferating especially in the last two decades. Hence, we firstly review Genetic Algorithm based approaches for the conventional UCP. Then, we briefly explain studies on the UCP under supply and demand uncertainty for wind integrated hybrid power systems. Lastly, we summarize solution approaches for the UCP under emission considerations in traditional and wind integrated hybrid power systems.

2.1 Genetic Algorithm Based Approaches for the Unit Commitment Problem in Traditional Power Systems

Literature on the UCP for traditional power systems includes several metaheuristic implementations such as Genetic Algorithm (GA), Ant Colony Optimization (ACO), Simulated Annealing (SA), Particle Swarm Optimization (PSO), Dynamic Programming (DP). However, we limit our review to the GA applications only. Several GAs have been proposed for the UCP thanks to its feature being a powerful stochastic global search technique, since the search is carried out by randomly exploiting information from different regions of the solution space. For the chromosome representation, in most of the GA implementations so far, binary coding has been used. One of them is proposed by Kazarlis et al. (1996). In their GA, they use conventional genetic operators and problem specific operators for the scheduling part of the problem which is assisted by an economic load dispatch technique for solving the optimal power output of the committed units. For constraint handling, they use penalty function for the violated constraints. Similar to Kazarlis

et al. (1996), Xing and Wu (2002) and Senjyu et al. (2002) also propose a similar approach to solve the UCP. They calculate the fitness of each chromosome as the reciprocal of the sum of both total generation cost and penalty costs. Swarup and Yamashiro (2003) also use binary representation for the chromosome structure. Different from Kazarlis et al. (1996), Xing and Wu (2002) and Senjyu et al. (2002); they do not use a penalty mechanism for constraint violation rather they apply some problem specific operators to repair and correct the violated schedules. Likewise, Madraswala and Deshpande (2016) propose a GA application similar to Swarup and Yamashiro (2003). For the Economic Load Dispatch (ELD) part of the problem, they use the Lambda Iteration Method (LIM). Mantawy et al. (1997) propose a different approach for the chromosome representation which is a combination of binary and decimal numbers to save both memory space and computation time. They convert the binary chromosomes (NxT matrix) into decimal ones (Nx1 array) before performing the genetic operations. After genetic operations are applied, they convert it to its binary equivalent. They also use repair mechanisms with problem specific operators to handle the constraint violations. Rudolf and Bayrleithner (1999) propose a special Binary Coded GA (BCGA) where the generating units are scheduled by automatically satisfying the uptime/downtime constraints. For the ELD part, they implement a Lagrangian Relaxation approach. Singhal et al. (2014) develop an enhanced BCGA in which commitment decisions are made by genetic operations and dispatching decisions by LIM. They also introduce some problem specific operators to speed up calculations and use repairing mechanisms to avoid infeasible solutions. Dudek (2013) proposes another BCGA variant in which chromosomes are designed in a more intelligent way to save memory space. When making ELD decisions, they also use LIM. For infeasible solutions, they apply penalty measures in fitness calculations. Sundararajan et al. (2013) use a similar coding scheme to Dudek (2013). For the constraint violations, they introduce some repairing procedures. They solve the ELD subproblem via Quadratic Programming.

Different from the studies above, Damousis et al. (2004) propose a completely new chromosome structure which is integer coded. They divide schedules to the "On/Off"

cycles and represent their chromosomes with the cycle lengths using positive and negative numbers (+: "On" cycles, -: "Off" cycles). They use different crossover and mutation techniques such as swapping crossover and Michalewicz's mutation for evolution from one generation to the next. They also use some problem specific operators like unit swapping operator and chromosome length augmentation. For constraint handling, they apply penalty mechanisms. Similarly, Amjady and Shirzadi (2008) modify the Integer Coded GA (ICGA) proposed by Damousis et al. (2004) by using hybrid operators such as swapping and bound operators for the crossover. They claim that ICGA can perform a more complete search of the solution space; thus, increasing the possibility of finding the global optimal solution. They use a combination of uniform and non-uniform mutations so as to improve diversity of the search in ICGA. To the best of our knowledge, Datta (2013) addresses both scheduling and load dispatching parts of the UCP by using GA approach for the first time and proposes a Binary-Real Coded GA (BRCGA) to handle both parts of the UCP with only genetic operators. The binary part tackles the unit scheduling part whereas the real part tackles the load dispatch part of the problem. They introduce new crossover and mutation operators for the real part of the GA and make use of repairing mechanisms and elite preservation strategies. Farag et al. (2015) propose a similar BRCGA, but they also integrate *k*-means clustering before applying genetic operations. They divide the population into *k* subpopulations and then apply different genetic operations to members of each subpopulation to introduce extended diversity; thus, avoiding BRCGA from being stuck in local optima.

Apart from these pure GA implementations, hybridized versions of GA with other metaheuristics are also common in literature. Yazdandoost et al. (2018) propose a modified GA approach based on Multicellular Organisms Mechanisms. Their GA has two phases as normal and modified; the normal one replicates the meiosis process on sexual chromosomes while the modified one uses mitosis for asexual chromosomes. By doing so, the convergence speed of the algorithm is increased. Salimian and Ameli (2015) hybridize GA and PSO (HGAPSO) to benefit from their good features such as GA's rapid convergence rate and PSO's high solution quality.

All constraints are satisfied while calculating the fitness function without introducing any penalty mechanism. Similarly, Marrouchi et al. (2018) suggest a hybrid metaheuristic algorithm combining GA and PSO. In their fitness function, total cost consists of total energy production cost and a Lagrangian function defined by the set of equality and inequality constraints. Effatnejad and Rouhi (2015) add Dynamic Programming (DP) to their HGAPSO so that they can avoid any repetition in calculations to save computing time. Reddy et al. (2019) propose a novel hybrid approach consisting of GA and SA. They use GA-SA to cluster the units as Base load (BL), intermittent load (IL), semi-peak load (SPL) and peak load (PL) categories according to their fitness values. After clusters are obtained, they also construct priority lists for the units in each cluster before applying LIM to make ELD decisions. Tsalavoutis et al. (2019) develop a GA to solve Multi-objective UCP (MO-UCP) with the objective function consisting of total operating cost and total emission of air pollutants. They utilize real coding for the chromosome representation and repairing mechanisms for constraint violations. The commitment and dispatching decisions are made simultaneously by hybridizing two-step local search procedures such as Pareto dominance and scalar fitness function. Similarly, Li et al. (2013) design a memetic evolutionary algorithm combining Non-dominated Sorting Genetic Algorithm-II for global exploration and local search procedure for local exploitation to solve MO-UCP whose ELD subproblem is solved by LIM. Kyu-Hyung and Mun-Kyeom (2018) propose an Improved GA (IGA) to solve stochastic UCP. The main difference of IGA from other GAs is that it only searches the feasible regions owing to its special repairing operators. Saber et al. (2016) develop a hybrid procedure where the commitment decisions are made by Priority Lists (PL) whereas ELD decisions are made by Hybrid Modified Genetic-Imperialist Competitive Algorithm (HGICA). In their approach, they use binary coding in the chromosomes and a new crossover technique called as “mime crossover” making the offspring resemble its parents and generation elite with specific ratios. Different from the conventional GAs, elite preservation is also applied after each genetic operation in order not to lose any elite solution after crossover and mutation operations. Bukhari

et al. (2016) also propose a binary coded GA in which they use a special type crossover called as “ring crossover” and repairing mechanisms for violated constraints. In their approach, “On/Off” decisions are made by GA and ELD decisions are made by LIM. Trivedi et. al (2016) suggest using BCGA with Differential Evolution (DE) since these two can efficiently handle binary variables (commitment) and continuous variables (dispatching), respectively. In their procedure, infeasible solutions are not repaired rather they are preserved. Besides, they also propose a special priority list-based initial population generation method to enhance performance of the algorithm by integrating domain-specific knowledge. Roque et al. (2014) introduce a Hybrid Biased Random Key GA (HBRKGA) in which several local search techniques are also incorporated to concentrate the search close to good solutions and random keys are used to create bias during both parent selection and crossover operations, since HBRKGA does not allow searching on infeasible solutions.

Different from the pure and hybridized versions of the GA approaches so far, we propose a novel approach based on GA combined with an improved LIM (I-LIM) to solve the UCP in traditional power systems. Our GA-based approach adopts a mixed integer coding scheme, uses an intelligent algorithm for the initial population generation, and contains various problem specific genetic operators to lessen the computing time. With these features, our approach can be considered one of the most efficient and effective GAs. The detailed explanation of the proposed GA approach and its implementation are provided in Chapter 3.

2.2 Solution Approaches for the Unit Commitment Problem in Wind Integrated Hybrid Power Systems

Literature on the UCP and its subproblem ELD for wind-integrated power systems involves different solution approaches such as mathematical programming formulations including stochastic programming, robust optimization and chance constrained modelling and several metaheuristic implementations as well. The

reason why we also include solution methods for ELD is that this subproblem can be considered as the single period UCP. Therefore, we limit our review to the most recent methods proposed for the UCP and ELD problem in the last decade particularly.

Hetzer et al. (2008) use a mathematical modelling approach for ELD with wind farms. Their objective is to minimize expected operating cost comprising of fuel costs and wind-based costs. Wind-based costs consist of operating cost of wind farms, the cost of wasted wind power due to underestimation in wind power generation and the cost of load not served due to overestimation cost in wind power generation. Wind speeds are assumed to follow Weibull distribution. Wind power is represented by using a simplified version of Wind Energy Conversion System (WECS) from wind speeds. Liu (2012) develops a nonlinear mathematical model for ELD problem in a combined heat and power (CHP) system integrated with wind power generation. The objective is to minimize heat and power production costs. The generation level of wind turbines is taken as a random variable. Similar to Hetzer et al. (2008), they also characterize the wind power by using the simplified version of WECS. Zhou et al. (2010) develop a stochastic model for Dynamic Economic Dispatch (DED) problem with large scale wind power penetration. In their model, generation forced outages, variabilities in load demand forecasts and wind speed forecasts are taken into account. They use a special type of WECS when converting wind speed forecasts into wind power forecasts. Since there are numerous causes of uncertainty, a sufficient reserve should be allocated in order to prevent generation shortages. For this purpose, they take reserves as decision variables which are used in chance constraints for satisfying risk thresholds. They solve their DED model by using Nonlinear Primal-Dual Interior-Point Method. Xia et al. (2012) propose a stochastic programming model for conventional ELD problem in which the objective is to minimize total fuel costs with valve point loading effect (VPLE). In this formulation, they use a joint probability density function for the uncertainty of load demand and wind power approximated by a simplified WECS. To deal with those uncertainties, they use chance constraints for two risk levels such as up spinning

reserve and down spinning reserve, respectively. Reddy et al. (2013) study the effect of wind integration to thermal power system. The only source of uncertainty is wind power forecasts following Weibull distribution. They take VPLE in fuel costs and transmission losses into account in their formulation where the objective is to minimize total operating cost, reserve allocation costs and underestimation and overestimation costs of wind power generation. They propose a new algorithm called as Covariant Matrix Adaptation with Evolution Strategy (CMA-ES) with mean learning technique (MLT) to solve their ELD formulation. Wang et al. (2017) propose a chance constrained ELD formulation under wind power uncertainty which does not necessarily follow Normal distribution. They use Gaussian Mixture Model (GMM) to represent joint probability distribution of wind power generation in different wind farms. They consider wind-based costs that consist of operating cost of wind farms, the cost of wasted wind power due to underestimation of wind power generation and the cost of load not served due to overestimation of wind power generation. They formulate power flow limits on a transmission line as chance constraints converted into deterministic linear constraints.

Ortega-Vazquez and Kirschen (2007) develop a bilevel optimization approach for the UCP under uncertainty due to the outages in conventional generation. First, they solve time-decoupled subproblems to determine the optimal spinning reserves for each period by taking generating unit outages into account. To illustrate, hourly reserve decisions are made according to the cost/benefit analysis between total operating costs and socioeconomic cost of expected energy not served (EENS) subject to some of the UCP constraints. They use three-point grid search technique to solve these subproblems prior to the exact UCP solution. Then, they solve traditional UCP with optimal spinning reserves. Later, Ortega-Vazquez and Kirschen (2009) improve the first level of this bilevel optimization by also incorporating the uncertainty due to load demand forecasts and wind power forecasts as the net load demand. For this purpose, they discretize the net load demand and apply their previous spinning reserve optimization method for each interval to find reserves corresponding to each interval. By taking the expectation of these reserves over

possible net load demand intervals, they find optimal spinning reserves. Then, they solve traditional UCP with optimal spinning reserves. Similar to Ortega-Vazquez and Kirschen (2009), Wu et al. (2015) develop a spinning reserve optimization method called as Cost-conditional value at risk (CVaR) model to assess the risk due to the uncertainties of load and wind power forecasts. In their method, they consider the loss of load when wind power is overestimated, and the wasted wind power when it is underestimated. They determine reserves by using CVaR and those reserve requirements are calculated prior to main UCP formulation. In their formulation, they also take transmission losses and transmission security verifications into consideration. Wang et al. (2015) propose a UCP formulation with risk reserve constraints. They use two types of reserves as correction reserve and emergency reserve. The former deals with the uncertainty in load demand and wind power generation while the latter is used for random breakdowns of conventional generating units. The emergency reserves are determined as the maximum of 10 percent of total generation and the largest capacity of conventional units. After determining the optimal reserves, they solve traditional UCP. Different from Wang et al. (2015) and Wu et al. (2015), Chen et al. (2016) incorporate CVaR method into mixed integer linear programming (MILP) type UCP formulation to minimize total generation cost that gives generation and spinning reserve schedules simultaneously.

Ortega-Vazquez et al. (2006) propose a stochastic programming model to schedule power generation and reserves for a power system under reliability issues in conventional generation. Instead of using deterministic spinning reserves or risk thresholds, they account for loss of load due to generation outages and the cost of providing extra reserve to prevent such losses. They show the nonlinear relationship between the available installed capacity of conventional generating units and EENS, which is then linearized in their model. The objective in their UCP formulation is to minimize the total operating costs, reserve allocation costs and expected cost of lost energy subject to several operational and technical constraints. Bouffard and Galiana (2008) develop a two-stage stochastic programming approach for a power system consisting of hydrothermal units and wind turbines. By ignoring hydrothermal

generator contingencies in their model, load demand and wind power forecasts are considered as the only sources of uncertainty which are integrated as the net load demand forecasts by considering the wind generation as a negative load demand. They construct the scenarios by discretizing the net load demand. The objective is to minimize the expected social cost where the first stage components are reserve costs, fixed operating costs and start-up costs, and the second stage components are demand benefits, variable operating costs and the expected cost of load not served. Pappala et al. (2008) develop a nonlinear mixed integer multistage stochastic model for the UCP in which the power system has wind farms, pumped storage and thermal power plants. The objective is to minimize total operating costs of thermal power plants. Wind forecasts and load demand forecasts are considered as two separate causes of uncertainty that are integrated to the model as scenario trees. They also propose a PSO based scenario reduction technique for a huge set of associated scenarios. Alabedin et al. (2012) propose two special types of stochastic UCP formulation for microgrids having two operational modes such as grid connected mode and isolated mode. In the grid connected mode, upstream grid behaves like a virtual generating unit when there are power generation shortages by conventional and wind power generation while it behaves like a virtual load demand point when more power is generated than the actual load demand realization. In this mode, the total cost consists of operating costs of conventional generating units, costs of reserve and power imported from the upstream grid. In the isolated mode, there are only conventional generating units and wind turbines so excess power generation is lost. In this case, total cost consists of operating and expected cost of load not served. The uncertainties related to load demand and wind power are handled using both additional reserves and scenarios. Liu and Tomsovic (2012) develop a security constrained UCP MILP formulation to deal with uncertainties related to conventional generator outages, wind power generation and load demand. The last two sources of uncertainty are continuous random variables combined as the net load whereas conventional generator outages are discrete random variables. When constructing their scenarios, they use only single order contingency events of

generator outages to save computation time. To integrate net load demand into EENS, they discretize the net load demand by using seven-interval approximation. Then they take the expectation over possible load intervals. The objective is to minimize total operating costs, reserve allocation costs and the expected cost of lost load. Moreover, they consider the effect of transmission line capacities as well. Chen et al. (2013) propose a stochastic multi-objective programming model to investigate how uncertainties due to conventional generation reliability, load demand and wind power generation affect the UCP. The objectives are penalty cost of wind curtailment (overestimation), fuel costs of conventional thermal units and operating risk index of the system. By using fuzzy optimization method, the multi-objective formulation is transformed to a single objective model. As a risk index, they use loss of load expectation (LOLE) which is known as the percentage of time the available capacity will be lower than the load demand. The constraint set includes LOLE threshold constraint and transmission capacities. When calculating LOLE, they use three scenarios which are no generator outage but load demand and wind power variabilities, single generator outage with load demand and wind power variabilities, and two generators outage with load demand and wind power variability. They use PSO to solve this non-linear and non-convex optimization model. Chaiyabut and Damrongkulkumjorn (2014) develop a nonlinear stochastic UCP formulation with EENS constraint under load demand and wind power variabilities. The objective is to minimize total operating costs and the expected cost of lost energy. The load demand uncertainty is handled by a deterministic spinning reserve whereas wind power uncertainty is imposed by enforcing a reliability index EENS. This index is used in both the objective function as the expected cost of lost energy due to wind power variability, and in the constraint set by defining a maximum threshold for EENS. Seven-interval approximation method is used for wind power forecasts which is assumed to follow Normal distribution to calculate the EENS. To reflect the stochastic nature of load forecasts, wind power forecasts and fault outages in conventional generation, Cui et al. (2015) devise a stochastic UCP model, in which the objective is to minimize total operating cost and reserves are the decision

variables. Since fault outages are discrete random variables, they are approximated to follow exponential distribution so that they can be combined with load demand and wind power forecasts following Normal distribution. Khazali and Kalantar (2015) formulate a two-stage stochastic programming model for the UCP under variabilities in load demand, wind power generation and unit outage in conventional generation. They use two kinds of variables for reserves. One of the variables is used to overcome imbalances between load demand following Normal distribution and wind power generation following Rayleigh distribution. These reserves are determined as expected values by using scenarios. The other variable is used to overcome unit outages and determined by using linearized formulations of reliability constraints for the EENS for each scenario and total EENS after removing the load-generation imbalances. Govardhan (2016) formulates the UCP under the variability in wind power generation as a stochastic nonlinear programming model with the objective of minimizing total operating costs, reserve allocation costs and wind-based costs. Wind-based costs consist of operating cost of wind farms, the cost of wasted wind power due to underestimation in wind generation and the overestimation cost of wind generation assumed to follow Weibull distribution. She solves this nonlinear model by using Modified Teaching-Learning Based Optimization (M-TLBO). Shao et al. (2018) develop a stochastic risk decision-making model for scheduling a wind integrated power system. The multi-probability wind scenarios are constructed based on Discrete Time Markov Chains, and they use a scenario reduction technology to extract representative scenarios. The aim is to minimize total fuel costs and risk related costs such as expected cost of loss of load and wind spillage while obtaining optimal generation and reserve schedules. Hedayati-Mehdiabadi et al. (2018) describe a scenario-based two-stage stochastic energy and reserve scheduling formulation by considering the uncertainty in the short-term wind farm generation forecasts. The objective is to minimize the total cost consisting of the operating costs, reserve allocation costs and the expected risk costs associated with insufficient reserve allocation. First, they solve this stochastic model and then they test the robustness of the solution by running a risk analysis model.

Apart from the aforementioned studies for the UCP under wind power uncertainty, there are also robust optimization, chance constrained optimization and simulation-based optimization methods in the literature. Alvarez-Miranda et al. (2015) propose a two-stage robust UCP formulation to model the uncertainties related to wind forecasts. They use bootstrap predictive inference approach to make interval-based wind power scenarios instead of distribution-based scenarios. Commitment decisions are considered as the first stage variables and dispatching decisions are taken as the second stage variables. Cobos et al. (2018) also propose two-stage robust energy and reserve scheduling formulation for the UCP under wind uncertainty. They also study the effects of slow and fast acting generating units in a power system. By using chance constraints associated with system security risk levels for EENS and expected wind spillage (EWS), Qian et al. (2016) integrate the uncertainty in wind power generation having β distribution into the UCP formulation for thermal-gas-wind power system. Penalty costs of EENS and EWS are added to the objective function by linearizing them to speed up the computation. Ummels et al. (2007) develop a simulation-based unit commitment and load dispatch optimization method, also known as the so-called equal marginal cost method, for thermal power system that mainly consists of CHP under wind power uncertainty. Atmospheric high-resolution limited area model (HIRLAM) is used to approximate atmosphere state for 6-hour intervals; accordingly, average wind speeds are forecasted. Then, wind speed forecasts are postprocessed and wind power forecasts are made by using the wind power forecasting method Aanbod Voorspeller Duurzame Energie (AVDE) developed by Energy Research Centre of the Netherlands. The optimization tool uses three different time buckets such as annual, weekly and hourly. Annual time buckets are used for maintenance scheduling, weekly time buckets are used for production cost optimization, and hourly time buckets are used for load dispatching. Lee (2007) designs an evolutionary iteration particle swarm optimization (EIPSO) algorithm to solve the nonlinear UCP problem for a wind-thermal power system. The objective of his formulation is to minimize the total operating costs and the outage costs subject to the standard operational and technical constraints. Besides, reserves from thermal

units and wind turbines are considered as decision variables. Wind speed forecasts and their probabilities (according to Weibull distribution) are generated by using Hybrid Optimization of Multiple Electric Renewables (HOMER). Accordingly, the wind power generation is approximated by third order polynomial WECS.

Different from the solution methods summarized above, we propose stochastic time-decoupled quadratic programming-based approaches to solve the UCP under supply/demand uncertainty for the hybrid power systems with significant wind power penetration. In our approach, we consider several causes of uncertainty such as load and wind power forecast errors and random outages in conventional generation. We also propose a novel approach to integrate the VPLE causing rippling effect in the efficiencies of conventional generating units as well. The detailed explanation of the proposed approach and its implementation is provided in Chapter 4.

2.3 Solution Approaches for the Unit Commitment Problem with Emission Considerations in Traditional-and-Wind Integrated Hybrid Power Systems

Since the integration of renewable energy generation and emission models into the UCP brings additional difficulties and complexities to the problem scope, efficient mathematical models and solution methods such as Lagrangian relaxations or metaheuristics are required to solve complex versions of this problem. For the last two decades, the UCP with emission considerations has been extensively studied for both traditional and hybrid power systems. To make our literature review more comprehensible and easier to follow in this section, we classify it into two categories. In subsection 2.3.1, mathematical models and solution methods for the UCP and its subproblem ELD in traditional power systems are briefly summarized. In subsection 2.3.2, mathematical formulations and algorithms to solve the UCP and ELD in the wind integrated hybrid power systems are concisely explained.

2.3.1 Emission Considerations in Traditional Power Systems

Nanda et al. (1994) utilize a weighted sum approach in their Economic Emission Dispatch (EED) formulation in which two conflicting objectives such as total operating costs and total emissions of SO_2 and NO_x are minimized by using a compromise factor subject to transmission line flow constraints. Emissions are represented by quadratic functions. They develop a new algorithm that use coordination equations to handle line flow constraints. Similarly, Ramanathan (1994) propose a weighted sum formulation for EED problem where unit-based and area-based NO_x and SO_2 emission limitations are also taken into account. Therefore, the problem can be called as Emission Constrained Economic Dispatch (ECED) problem. To represent emissions, second order polynomial functions are used. He also devises an efficient technique to determine binding constraints in the problem by linearizing the emission constraints. The proposed technique rapidly converges to the Kuhn-Tucker optimality conditions. Wang et al. (1995) propose a new approach based on the augmented Lagrangian relaxation method and the decomposition and coordination technique to solve environmentally constrained UCP (EC-UCP). The objective is to minimize total fuel costs while satisfying system, transmission and emission constraints. Similar to Wang et al. (1995), Gjengedal (1995) devise a Lagrangian relaxation-based algorithm to solve EC-UCP. CO_2 and SO_2 emissions are modelled via quadratic functions whereas NO_x emissions are represented via cubic functions. He also considers start-up and shutdown emissions. Start-up emissions are characterized as an exponential function of unit's downtime while shut-down emissions are assumed to be constant. For emission constraints, he uses an overall limit on total emissions in the planning horizon. Marwali and Shahidehpour (1999) propose an algorithm based on Double Benders Decomposition for long-term transmission and generation maintenance scheduling problem in which linearly defined NO_x and SO_2 emissions are not taken as objectives to be minimized, rather they are considered as area-based and overall emission limits in the problem. Raglend and Padhy (2006) formulate the EC-UCP by using price

penalty factor for emissions, which enables them to convert the bi-objective problem into single-objective optimization problem with total cost minimization. Emissions and fuel costs are characterized as quadratic functions. They also take unit and transmission constraints into account. Yamashita et al. (2010) come up with a weighted sum formulation for the UCP with CO_2 emissions by normalizing total operating cost and total CO_2 emissions and assigning weight factors for both objectives. Emissions are modelled by quadratic functions. They implement decommitment procedure to attain Pareto optimal curves for the analysis of trade-offs between CO_2 emissions and total cost. Nazari et al. (2010) propose an EC-UCP solution method in which Cap & Trade mechanism is applied for total emissions. That is, emission costs are added to total operating cost whenever quadratically defined emissions exceed the total cap value. They also study impacts of pumped storage units integrated into thermal power systems. Catalão et al. (2010) develops a multi-objective optimization method for the Profit-Based UCP (PBCUP) by using ε-constraint method for one of the objectives such as maximizing total revenue and minimizing total emissions. Accordingly, depending on electricity price profiles, Pareto optimal trade-off curves are obtained for the compromise between the revenue and emissions. For emission modelling, quadratic and exponential functions are combined. Anita and Raglend (2013) develop a Shuffled Frog Leaping Algorithm to solve EC-UCP in which the objective is to minimize total operating costs and total emission costs. NO_x and SO_2 emissions are modelled via second order polynomial functions, and no constraints are imposed on them. Xia et al. (2013) differently formulate ECED problem taking intertemporal constraints and transmission losses into consideration. The objective is to minimize total operating cost of thermal units and pumped-hydro storage units. Emissions are represented by quadratic functions and a total emission limit is defined for the entire system. They devise a Simultaneous Perturbation Method for Lagrangian relaxation for both standard ED constraints and intertemporal constraints to solve this problem. Tang and Che (2013) propose a variable splitting-based Lagrangian relaxation algorithm to solve EC-PBUCP in the deregulated electricity market. The objective is to maximize total

profit calculated as the difference between the revenue obtained from electricity sold and total cost of operations and CO_2 emissions calculated by piecewise linear emission penalty factors. Saravanan and Vasudevan (2014) develop an invasive weed optimization algorithm to solve EC-UCP with the objective of minimizing the weighted sum of total operating cost and total emission levels. Emissions are characterized as second order polynomial functions. Ahmadian et al. (2014) suggest a multi-objective optimization formulation for the EC-UCP by minimizing the weighted sum of total pollutant emission and total operating costs. They devise a new Honey Bee Mating Optimization Algorithm to solve this problem in which emissions are modelled by quadratic functions. Laia et al. (2014) propose a stochastic mixed-integer linear programming formulation to cope with the UCP under emission limitations and uncertainty in a deregulated electricity market involving day-ahead bidding and bilateral contracts. The uncertainty is caused by variable electricity prices and modelled by scenarios. In the PBUCP formulation, the objective is to maximize expected profit obtained from sales of electricity subject to the system-wide emission limitation and standard UCP constraints. Che and Shi (2014) present a mixed-integer linear programming (MILP) formulation for the PBUCP with nonlinear emissions penalty. To apply MILP, quadratic fuel cost and emission functions are piecewise linearly approximated. Haddadian et al. (2015) propose MILP formulation for the EC-UCP with the integration of distributed energy storage devices. Quadratic CO_2 emissions are handled by introducing system-wide emission limit instead of incurring emission costs. Similar to Che and Shi (2014), they also apply piecewise linear approximation for quadratic functions. To speed-up the processing required for large power systems, they use Benders Decompositions and Cuts. Geng et al. (2015) suggest a novel mixed-integer nonlinear programming (MINLP) type ECED formulation in which clean energy technologies are employed for the reduction of NO_x, SO_2 and PM_x emissions. Emissions are modelled with quadratic functions in operational mode and with linear functions in start-up mode by considering effects of emission reduction devices. The aim is to minimize total operating cost and total emission taxes levied. They employ area-based emission

limits as constraints and tiered emission taxes. Moreover, Geng et.al. (2017) extend their ECED formulation for the EC-UCP and apply it for the Chinese power system. Navin and Sharma (2016) develop a Modified Differential Evolution (MODE) optimization technique to solve EC-UCP in which emission costs and unit-based emission limits are used to cope with emissions characterized by quadratic functions. They also incorporate priority lists and a random search algorithm to tackle with classical spinning reserve requirements and minimum uptime/downtime constraints, respectively. Zhang et al. (2016) formulate EC-UCP for smart grids by applying the unit-based carbon emission trading (CET) mechanism for emissions. In their formulation, emissions are quadratically characterized and emission costs are incurred whenever allowable emission limits of thermal units are exceeded. They devise an Improved PSO Algorithm to solve the problem. Liu et al. (2014) present both mixed-integer quadratic programming (MIQP) and mixed-integer linear programming (MILP) formulation for the PBUCP that aims to maximize profit under carbon taxing in a deregulated electricity market. To convert MIQP into MILP, quadratic fuel cost and emission functions are piecewise linearly approximated. Ghadi et al. (2016) propose a bi-objective nonlinear PBUCP under a deregulated environment. The aim is to maximize the profit while minimizing CO_2 emission levels subject to emission limits defined for each period. Emissions are represented by second order polynomial functions They devise an Imperialist Competitive algorithm combined with a metaheuristic constraint handling technique to solve their bi-objective formulation. Sen and Mathur (2016) propose a metaheuristic algorithm using the framework of Ant Colony Optimization-Artificial Bee Colony-Harmonic Search (ACO-ABC-HS) algorithm to solve ECED problem. The aim is to minimize total fuel cost with valve point loading effect while satisfying emission limits, transmission losses and other standard ELD constraints. Quadratic emission models are used in their formulation. Sundaram et al. (2017) develop Tabu Search-Enhanced ABC algorithm to solve the PBUC in a deregulated electricity market by taking emission limitations into consideration. Both fuel costs and emissions are represented by quadratic functions. In the proposed algorithm, unit commitment part

of the problem is solved by an ABC algorithm and dispatch part of the problem is solved by the Lambda Iteration Method (LIM) whereas TS is used to explore and exploit the solution space. Geng et al. (2018) propose a two-stage stochastic programming formulation for the EC-UCP under variable emission limits depending on variable Air Quality Index (AQI). The first stage represents day-ahead UCP and the second stage is used to simulate power system operation under scenario-dependent emission limits for NO_x and SO_2. Quadratic costs and emissions are piecewise linearly approximated, so their formulation is based on MILP in which the objective is to minimize total operating cost. Olamaei et al. (2018) develop a nonlinear EC-UCP formulation for power systems consisting of CCHP, thermal and heat units. The objective is to minimize total cost comprising of fuel costs with valve point loading effect and the penalty cost of CO_2 emissions defined by second order polynomial functions.

2.3.2 Emission Considerations in Hybrid Power Systems

Kuo (2009) develops an efficient metaheuristic that combines SA and PSO for the bi-objective economic emission dispatch (EED) problem in which wind turbines are taken as more flexible units having zero emissions. Objectives are to minimize total fuel costs and total emissions. Both terms are represented by quadratic functions; in addition, emissions are superimposed by exponential functions. Complex operational constraints like prohibited operation zones, ramp-up/ramp-down limits and transmission losses are also added in the formulation. Liu and Xu (2010) propose a MINLP formulation for EED problem under wind power uncertainty. Different from other formulations, the main objective is to minimize environmental impact index that is total NO_x emissions, so the total cost consisting of fuel costs of thermal units and penalty costs for wind curtailment (overestimation) and wind spillage (underestimation) is taken as a constraint specifying an upper bound for total cost. They also set a limit for wind power generation. Emissions are modelled via the combination of quadratic functions and exponential function. Wind power is

assumed to follow Gamma distribution; accordingly, they derive expressions for expectations of overestimation and underestimation of wind generation. Piperagkas et al. (2010) formulate ECED problem for both heat and power generation system under variabilities in the wind power and emission limitations for NO_x, SO_2 and CO_2. Those emissions are characterized by linear functions for CHP units. For thermal units, NO_x and SO_2 emissions are represented by quadratic functions with an exponential factor whereas CO_2 emissions are modelled for CHP units. Instead of taking emissions into account in the objective, they define maximum emission limits for each gas. Thence, fuel costs and the expected cost of wind curtailment forms the objective to be minimized. Furthermore, transmission losses are also formulated according to Kron's B-loss function. To solve the ECED problem, they use a PSO-based optimization technique. Verma and Kumar (2011) formulate the bi-objective EC-UCP under wind power uncertainty and pumped storage integration. The variabilities in wind power are described by wind speed scenarios which are transformed into wind power scenarios by using simplified WECS. They convert bi-objective formulation into a single objective by defining emission penalty. Hence, the single objective comprises of total operational costs of thermal and pumped storage units and emission penalties. They do not use underestimation and overestimation costs for wind power generation since these situations are compensated by pumped storage units. Besides, quadratic expressions are used to model emissions. Liao (2011) devises a Chaotic Quantum GA to solve EED problem in which both total operating costs, overestimation cost of wind farms, and emission costs of NO_x are minimized. Several technical aspects such as transmission losses, prohibited operation zones and valve point loading effect are also considered in the formulation. Wind power generation is calculated from wind speed forecasts by using simplified WECS. Fuel costs with valve point loading effect are represented by quadratic functions having absolute sinusoidal rippling whereas quadratic functions superimposed by exponential functions are used to represent NO_x emissions. Azizipanah-Abarghooee et al. (2011) develop a Modified Teaching-Learning Algorithm to solve a stochastic multi-objective wind-thermal EED

problem. The conflicting objectives are to minimize total fuel costs with valve point loading effect and expected overestimation and underestimation cost of wind power, and to minimize NO_x emissions. Emissions are modelled as the sum of quadratic and exponential functions. For wind power forecasts of each wind farm, WECS is used. Van Dinter et al. (2012) propose a MINLP model for the environmental UCP in which the objective is to minimize the sum of piecewise linearly approximated fuel costs, shortage costs, and concave NO_x emission costs in wind-thermal-storage power system. They also introduce several cuts to reinforce their formulation and to increase the tractability of the problem. Then, they apply Bender's Decomposition to solve their MINLP model. Jadhav and Roy (2013) formulate the probabilistic bi-objective wind-thermal EED problem with the objective of minimizing the sum of fuel costs with valve point loading effect, expected costs of wind spillage and wind curtailment. The exact WECS is used to represent wind power from wind speed following Weibull distribution. Emissions are represented with quadratic functions. They also consider transmission losses and prohibited operation zones. Gbest Guided ABC is utilized to optimize the EED problem. Wu et al. (2013) devise a method based on the framework of multi-objective PSO and Primal-Dual Interior Point Method to solve EC-UCP. In the problem formulation, the objective is to minimize total operating costs and total air pollutant emissions. Wind power uncertainty is characterized by using interval forecasting techniques and assigning an occurrence probability for each interval. Both emissions and fuel costs are expressed with quadratic functions. Roy and Hazra (2014) present a Chemical Reaction Optimization Algorithm (CROA) to solve nonlinear EED problem in wind-fossil fuel-based power systems. This algorithm is extended by Hazra and Roy (2019) who also use quasi-opposition based learning with CROA. The aim of the problem is to minimize fuel costs with valve point loading effect, emission costs and wind related expected costs as overestimation and underestimation costs. Wind power is characterized by using Weibull distribution and exact WECS. Emissions are modelled via combined second order polynomial and exponential functions. They also take power transmission losses into consideration. Zhang et al. (2014) model the

EC-UCP for wind-thermal power systems with the objective that minimizes total operating costs of thermal units, expected underage and overage cost of wind power and costs of quadratic CO_2 and NO_x emissions. Wind speeds are expressed via Weibull distribution and WECS is used to convert wind speed into wind power. They design a hybrid algorithm based on Sequential Quadratic Programming (SQP) and PSO. Haddi and Bouktir (2015) develop an ABC algorithm to solve EED under wind power uncertainty. Wind speeds are assumed to follow Gamma distribution, so are wind powers. The problem is formulated as the weighted sum of total system cost consisting of fuel costs, wind related expected costs, and total emissions which are modelled via quadratic functions combined with exponential functions. Trivedi et al. (2016) propose a multi-objective environmental UCP under significant wind penetration with objectives that are total operating costs, total emissions and EENS cost due to load demand and wind power forecasts, and uncertainty based on thermal unit outages. Apart from considering these costs in the objective, maximum limits are also defined for each cost, which makes the problem optimized in the constrained objective space. Emissions are characterized as quadratic functions. Wind power is represented by using simplified WECS. To solve the problem, they devise a Multi-Objective Evolutionary Algorithm Based on Decomposition and Differential Evolution. Alham et al. (2016) formulate EED as a weighted sum of total fuel cost and total emissions to be minimized. They also integrate time-dependent ramp-rate limits and transmission losses into their formulation. Both fuel costs and emissions are taken as second order polynomial functions. Stochastic nature of wind power is modelled via Weibull distribution and it is represented by taking power balance constraint as a chance constraint in the formulation. Wang et al. (2016) establish a VaR-based multi-objective formulation for EC-UCP with wind penetration. Objectives are to minimize the sum of total operating costs and emission taxes, and to minimize generalized fuzzy VaR-based reliability index. For NO_x and SO_2, single level tax is levied on emission levels whereas carbon emission trading scheme is applied for CO_2 emissions. Uncertainty of wind power is characterized as Weibull distribution. They use a Fuzzy Simulation-Based Multi-Objective PSO Algorithm to

solve EC-UCP problem. Qu et.al. (2016) develop a Summation Based Differential Evolution Algorithm for the solution of bi-objective EED problem in wind-thermal systems. Total operating cost and total emission levels are tried to be minimized. Emissions are modelled via quadratic functions combined with exponential functions. Besides, the stochastic nature of wind power is represented from wind speed following Weibull distribution by using simplified WECS. Wind power uncertainties are handled by introducing chance constraints instead of power balance and spinning reserve constraints. Negi et al. (2016) formulate the environmental UCP by minimizing total operating costs of thermal units, expected costs of overestimation and underestimation of wind power and emission taxes for NO_x and CO_2 emissions. Wind power is assumed to follow Weibull distribution as a result of WECS conversion of wind speeds following Weibull distribution. They take standard emission constraints and valve point loading effect into account. To solve the problem, they develop Improved Binary PSO. Qu et al. (2017) propose a different EED formulation under load and wind power uncertainty, which are incorporated as spinning reserve constraints modified to integrate variabilities in forecasts of load demand and wind power. They define two objectives, namely the minimization of total fuel cost and the minimization of total emission levels. The valve point loading effect is considered in fuel cost representation as a sinusoidal term. Emissions are modelled as the sum of quadratic and exponential functions. They solve this formulation by using Selection Method Based Multi-Objective Differential Evolution Algorithm. Hu et al. (2017) propose a novel EED model taking economic and environmental aspects of a wind integrated power system into account. Both fuel costs and NO_x, SO_2 and CO_2 emissions are characterized as cubic functions. When incurring emission costs, NO_x and SO_2 emissions are converted into associated CO_2-equivalents by using conversion factors. Wind speeds are represented with Weibull distribution and they are transformed into wind power by using simplified WECS. In their model, both emission costs and fuel costs are minimized by satisfying several system constraints and allowable emission limits. Hybrid GA-SQP algorithm is employed to solve the EED problem. Zhang et al. (2017) build a stochastic EC-UCP

model that simultaneously analyses operational economy, emission, and reliability of the whole system. Wind power uncertainty is characterized as interval-based scenarios. Therefore, unit commitment decisions are made in the first stage, whereas load dispatch decisions, accordingly emission levels are set at the second stage depending on scenarios. The overall objective is to minimize total operating cost consisting of quadratic fuel costs and two-step start-up costs and emissions levels which are expressed with combined usage of quadratic and exponential functions. Zhang et al. (2017) propose a cost-benefit analysis method to solve environmental UCP with load and wind power forecast variabilities along with forced outages of generators. The objective is the joint minimization of carbon trading costs, operating costs, the expected cost of load shedding, the penalty cost of wind power curtailments. In order to combine uncertainties of load demand and wind power forecasts with forced outages, they discretize them. Emissions and costs involve linear representations. Franz et al. (2018) propose a MILP type formulation for environmental UCP with pumped storages and renewable energy sources such as wind and solar. Renewables are integrated to the problem by considering them in residual demands. Emission costs are added to variable cost of thermal power units, which have a linear relationship with the cost of production. The aim is to minimize total generation cost, emission cost and the expected cost of load shedding. They use time-oriented, unit-oriented, and generic fix-and-optimize procedures as a decomposition method. Guo et al. (2018) formulate an AQI-driven SCUC incorporating wind power uncertainties. Different from other formulations, impacts of thermal units on regional air quality is modelled by using Gaussian puff dispersion model and pollutant equivalent method. Wind power uncertainty is modelled via scenarios generated from uncertain wind speed following Weibull distribution. NO_x, SO_2 and PM_x emissions are modelled via quadratic expressions. Chinnadurrai and Victoire (2019) suggest a multi-objective EED formulation that consists of two levels. In the first level, the bi-objective to be minimized includes total fuel costs with valve point loading effect and total emissions represented with quadratic functions superimposed by exponential functions. In the second level, wind

curtailment as a result of the overestimation of expected wind power is minimized. To solve the problem, the combined framework of Enhanced Multi-Objective Crisscross Optimization and Linear Programming is employed. Franz et al. (2020) build a MILP model for EC-UCP with hydrothermal coordination to minimize total production and emission costs. They employ Cap & Trade mechanism when incurring emission costs and using residual demands for renewable generation. Also, they develop a two-stage heuristic to analyze the trade-off between power generation and emission costs.

Different from the aforementioned solution methods, we propose a stochastic time-decoupled quadratic programming-based approach to solve the UCP under both supply/demand uncertainty due to unexpected outages in conventional generation and forecast errors of wind power and load demands, and emission limitations for the wind integrated hybrid power systems. In our approach, we model emissions of CO_2, one of the most important Greenhouse Gases (GHGs), and NO_x, SO_2 and PM_x, the most dangerous air pollutants by taking the potential implementation of emission control technologies and strict regulations into account. We extend our approaches explained in Chapter 4 by integrating emission considerations as well. The detailed explanation of the proposed approach and its implementation is provided in Chapter 5.

CHAPTER 3

UNIT COMMITMENT PROBLEM FOR TRADITIONAL POWER SYSTEMS

The unit commitment problem (UCP) in traditional power systems is a mixed integer, nonlinear, and combinatorial optimization problem. The main objective is to effectively schedule operations of conventional generating units in a power system on an hourly basis to meet forecasted load demand requirements, while satisfying various operational and technical constraints. Moreover, the UCP has a challenging issue of non-convexity, high dimensionality and combinatorial nature especially when a power network contains too many conventional generating units, which makes it difficult to use any rigorous optimization approach to solve the problem for a real-size power system. In this chapter, we first develop a mathematical model for the traditional UCP, and then a novel Mixed Integer Coded Genetic Algorithm (MICGA) is proposed and applied to standard problem instances in the literature to test the efficiency and effectiveness of the MICGA. Our main motivation for developing a GA for the UCP is that it employs fundamentals of natural genetics that are proven very efficient in the search of global optimal solution for complex and nonlinear problems in a relatively short computing time.

3.1 Problem Formulation

The UCP is a well-known generator scheduling problem basically comprising of two decisions. The first one is to specify commitment statuses of conventional generating units for each time period in the planning horizon. After determining the commitment statuses, the second decision is to determine how much energy should be produced by each committed unit in each time period. In order to perform these decisions, the main objective of the problem is to minimize the total operating cost

consisting of fuel costs and start-up costs over the planning horizon. Besides, it includes several constraints that can be classified in two main categories such as load-driven constraints and technological constraints. These constraints are status restrictions of individual generating units, minimum uptime and minimum downtime constraints, generation capacity limits, limited ramp rates, and power balance constraint. There are also several operational uncertainties such as random outages of conventional generating units that should also be considered when formulating and solving the UCP. This stochastic nature of traditional power systems is generally alleviated by pursuing several deterministic reserve policies requiring a spare capacity generally defined as a certain proportion of the peak load or the largest capacity of committed units. In this section, we develop a Mixed Integer Nonlinear Programming (MINLP) model which can even be made simpler and more compact. In the formulation, ramp-up and ramp-down constraints, which aggravate the problem's tractability, are also taken into consideration.

Assumptions

- The electricity market is vertically integrated. Hence, a power generation company is obliged to meet the load demand of its customers exactly.
- The load demands during the planning horizon are accurately forecasted. No deviation beyond 10% of the forecasted load is expected.
- The conventional power generation system is reliable enough, so the failure events (unexpected outages) of conventional units can be neglected.
- The efficiency of a conventional generating unit shows a monotonic increase as it is more heavily loaded.
- A conventional generating unit can produce power within its available power generation limits.
- The power produced can be transmitted to the demand points without any transmission limits.
- Power losses during power transmission are negligible.

Sets and Indices

N: Set of conventional generating units

$i \in N$: Conventional generating units

T: Set of time periods (hours)

$t \in T$: Time period

Parameters

a_i, b_i, c_i: Fuel cost coefficients of unit *i* (\$, \$/MW, \$/MW^2, respectively)

S_i^H: Hot startup cost of unit *i* (\$)

S_i^C: Cold startup cost of unit *i* (\$)

$T_{c,i}$: Startup time threshold of unit *i* (hours)

$T_{Min,\,i}^{off}$: Minimum downtime of unit *i* once it is shutdown (hours)

$T_{Min,\,i}^{on}$: Minimum uptime of unit *i* once it is started up (hours)

P_i^{Min}: Minimum power output level of unit *i* (MW)

P_i^{Max}: Maximum power output level of unit *i* (MW)

R_i^{up}: Ramp-up limit of unit *i* (MW)

R_i^{down}: Ramp-down limit of unit *i* (MW)

D_t: Load demand in period *t* (MW)

SR_t^{Min}: Minimum spinning reserve requirement in period *t* (MW)

Decision Variables

u_{it}: Commitment status of unit *i* in period *t*:

$$u_{it} = \begin{cases} 1 \text{ if unit } i \text{ is "On" in period } t \\ 0 \text{ otherwise} \end{cases} \quad (3.1)$$

P_{it}: Amount of electricity produced by unit *i* in period *t*

$FC(P_{it}, u_{it})$: Fuel Cost of unit *i* in period *t* generally given by a quadratic cost function as follows:

$$FC(P_{it}, u_{it}) = a_i u_{it} + b_i P_{it} + c_i {P_{it}}^2 \quad (3.2)$$

T_{it}^{off}: Number of consecutive time periods that unit *i* remained decommitted up to period *t*

T_{it}^{on}: Number of consecutive time periods that unit *i* remained committed up to period *t*

S_{it}: Start-up cost of unit *i* in period *t* generally depends on the number of consecutive time periods in which the unit is in "Off" status. According to the length of the "Off" periods, start-up costs are classified as hot start-up or cold start-up costs:

$$S_{it} = \begin{cases} S_i^H & \text{if} \quad T_{Min,\,i}^{off} \le T_{it}^{off} \le T_{Min,\,i}^{off} + T_{c,i} \\ S_i^C & \text{if} \quad T_{it}^{off} > T_{Min,\,i}^{off} + T_{c,i} \end{cases} \quad (3.3)$$

P_{it}^{Min}: Minimum power output level of unit *i* in period *t*:

$$P_{it}^{Min} = \begin{cases} \text{Max}\{P_i^{Min}, P_{it-1} - R_i^{down}\} & \text{if} \quad u_{it-1} = u_{it} = 1 \\ P_i^{Min} & \text{otherwise} \end{cases} \quad (3.4)$$

P_{it}^{Max}: Maximum power output level of unit *i* in period *t*:

$$P_{it}^{Max} = \begin{cases} \text{Min}\{P_i^{Max}, P_{it-1} + R_i^{up}\} & \text{if} \quad u_{it-1} = u_{it} = 1 \\ P_i^{Max} & \text{otherwise} \end{cases} \quad (3.5)$$

Auxiliary Binary Variables for Logical Constraints:

- δ_{it}: Start-up type indicator of unit *i* in period *t*:

$$\delta_{it} = \begin{cases} 1 & \text{if} \quad T_{Min,\,i}^{off} \le T_{it}^{off} \le T_{Min,\,i}^{off} + T_{c,i} \\ 0 & \text{if} \quad T_{it}^{off} > T_{Min,\,i}^{off} + T_{c,i} \end{cases} \quad (3.6)$$

- α_{it}^{1}: Auxiliary variable indicating unit *i* has been working beyond its minimum uptime requirement in period *t*:

$$\alpha_{it}^{1} = \begin{cases} 1 & \text{if} \quad T_{it}^{on} \geq T_{Min,i}^{on} \\ 0 & \text{otherwise} \end{cases} \tag{3.7}$$

- α_{it}^{2}: Auxiliary variable indicating unit *i* has not been working till period *t*:

$$\alpha_{it}^{2} = \begin{cases} 1 & \text{if} \quad T_{it}^{on} = T_{Min,i}^{on} \\ 0 & \text{otherwise} \end{cases} \tag{3.8}$$

- β_{it}^{1}: Auxiliary variable indicating unit *i* has not been working beyond its minimum downtime requirement in period *t*:

$$\beta_{it}^{1} = \begin{cases} 1 & \text{if} \quad T_{it}^{off} \geq T_{Min,i}^{off} \\ 0 & \text{otherwise} \end{cases} \tag{3.9}$$

- β_{it}^{2}: Auxiliary variable indicating unit *i* has been working till period *t*:

$$\beta_{it}^{2} = \begin{cases} 1 & \text{if} \quad T_{it}^{off} = T_{Min,i}^{off} \\ 0 & \text{otherwise} \end{cases} \tag{3.10}$$

Mathematical Model

$$Min \quad \sum_{t=1}^{|T|} \sum_{i=1}^{|N|} \left(FC(P_{it}, u_{it}) + S_{it} \left(1 - u_{i,t-1}\right) u_{it} \right) \tag{3.11}$$

subject to

$$\sum_{i=1}^{|N|} P_{it} \geq D_t \qquad \forall t \tag{3.12}$$

$$\sum_{i=1}^{|N|} P_{it}^{Max} \geq D_t + SR_t^{Min} \qquad \forall t \tag{3.13}$$

$$P_{it}^{Min} \leq P_{it} \leq P_{it}^{Max} \qquad \forall i, \forall t \tag{3.14}$$

$$T_{it+1}^{on} \leq M_1 u_{it} \qquad \forall i, \forall t - \{T\} \tag{3.15}$$

$$T_{it+1}^{on} \geq T_{it}^{on} + 1 + m_1(1 - u_{it}) \qquad \forall i, \forall t - \{T\} \tag{3.16}$$

$$T_{it+1}^{off} \leq M_2(1 - u_{it}) \qquad \forall i, \forall t - \{T\} \tag{3.17}$$

$$T_{it+1}^{off} \geq T_{it}^{off} + 1 + m_2 u_{it} \qquad \forall i, \forall t - \{T\} \tag{3.18}$$

$$T_{it}^{off} \geq T_{Min,i}^{off} + T_{c,i} + \varepsilon + (m_3 - \varepsilon)\delta_{it} \qquad \forall i, \forall t \tag{3.19}$$

$$S_{it} = S_i^H \delta_{it} + S_i^C (1 - \delta_{it}) \qquad \forall i, \forall t \tag{3.20}$$

$$T_{it}^{off} \leq T_{Min,i}^{off} + T_{c,i} + M_3(1 - \delta_{it}) \qquad \forall i, \forall t \tag{3.21}$$

$$T_{it}^{on} \geq T_{Min,i}^{on} + m_4(1 - \alpha_{it}^1) \qquad \forall\, i, \forall t \tag{3.22}$$

$$T_{it}^{on} \leq M_4(1 - \alpha_{it}^2) \qquad \forall i, \forall t \tag{3.23}$$

$$\alpha_{it}^1 + \alpha_{it}^2 \leq 1 + u_{it} \qquad \forall i, \forall t \tag{3.24}$$

$$T_{it}^{off} \geq T_{Min,i}^{off} + m_5(1 - \beta_{it}^1) \qquad \forall i, \forall t \tag{3.25}$$

$$T_{it}^{off} \leq M_5(1 - \beta_{it}^2) \qquad \forall i, \forall t \tag{3.26}$$

$$\beta_{it}^1 + \beta_{it}^2 \leq 1 + (1 - u_{it}) \qquad \forall i, \forall t \tag{3.27}$$

$$P_{it}^{Max} \leq P_i^{Max} u_{it} \qquad \forall i, \forall t \tag{3.28}$$

$$P_{it}^{Max} \leq P_{it-1} + R_i^{up} + M_6(2 - u_{it-1} - u_{it}) \qquad \forall i, \forall t \tag{3.29}$$

$$P_{it}^{Min} \geq P_i^{Min} u_{it} \qquad \forall i, \forall t \tag{3.30}$$

$$P_{it}^{Min} \geq P_{it-1} - R_i^{down} + m_6(2 - u_{it-1} - u_{it}) \qquad \forall i, \forall t \tag{3.31}$$

$$P_{it}, S_{it}, T_{it}^{on}, T_{it}^{off}, P_{it}^{Max}, P_{it}^{Min} \geq 0 \qquad \forall i, \forall t \tag{3.32}$$

$$u_{it}, \delta_{it}, \alpha_{it}^1, \alpha_{it}^2, \beta_{it}^1, \beta_{it}^2 \in \{0,1\} \qquad \forall i, \forall t \tag{3.33}$$

Objective Function

The objective is to minimize the sum of fuel costs and start-up costs associated with uncommitted units. In the mathematical model, the objective function is given by its closed form representation as in (3.11). Its open form representation is provided below.

$$Min \quad \sum_{i=1}^{|N|} (a_i u_{it} + b_i P_{it} + c_i {P_{it}}^2 + S_{it} \left(1 - u_{i,t-1}\right) u_{it}) \qquad (3.34)$$

Constraints

The constraints can be categorized in two main classes such as load demand constraints (3.12, 3.13) and technological constraints (3.14,…, 3.31). The first set consists of load requirements and spinning reserve requirements. The second set of constraints consists of limits on the unit output range, and on the minimum number of time periods that the unit must be continuously in "On" or "Off" status.

Load Requirement Constraint (3.12): Also known as the power balance constraint guaranteeing that total power generated by the committed units in period *t* should be greater than or equal to the load demand in period *t*.

Spinning Reserve Constraint (3.13): Total available capacity of the committed units in period *t* should be greater than or equal to the sum of the power demand and minimum spinning reserve requirement in period *t*. Minimum spinning reserve requirement is conventionally taken as 10 percent of the load demand in period *t*.

Unit Output Range Constraints (3.14): Unit *i* can generate power within its minimum and maximum generation limits in period *t*.

Consecutive Number of Committed Periods (3.15, 3.16): Constraints to calculate the number of consecutive periods that unit *i* stayed in "On" status up to time period *t*+1. If the unit is in "Off" status in period *t* then, T_{it+1}^{on} should be equal to 0. Otherwise, calculate T_{it+1}^{on} by adding one more period to T_{it}^{on}.

In (3.15), M_1 is a very big number denoting upper bounds for the Consecutive Number of Committed Periods. In (3.16), m_1 is a very small number denoting upper bounds for the Consecutive Number of Committed Periods.

Consecutive Number of Uncommitted Periods (3.17, 3.18): Constraints to calculate the number of consecutive periods that unit *i* stayed in "Off" status up to time period t+1. If the unit is in "On" status in period *t*, then T_{it+1}^{off} should be equal to 0. Otherwise, calculate T_{it+1}^{off} by adding one more period to T_{it}^{off}.

In (3.17), M_2 is a very big number denoting upper bounds for the Consecutive Number of Uncommitted Periods. In (3.18), m_2 is a very small number denoting upper bounds for the Consecutive Number of Uncommitted Periods.

Start-up Cost Constraints (3.19, 3.20, 3.21): If the number of time periods in which unit *i* stayed in "Off" status is less than the sum of minimum downtime requirement and threshold level of unit *i*, then the start-up cost is equal to hot start-up value. Otherwise, the start-up cost is equal to cold start-up value.

In (3.19), m_3 is a very small number denoting upper bounds for Start-up Cost Constraints. In (3.21), M_3 is a very big number denoting upper bounds for Start-up Cost Constraints.

Minimum Uptime Constraints (3.22, 3.23, 3.24): A unit cannot be turned off instantaneously once it is committed. The minimum uptime constraint imposes a minimum number of working time periods that must elapse before the unit *i* can be turned off.

In (3.22), m_4 is a very small number denoting upper bounds for Minimum Uptime Constraints. In (3.23), M_4 is a very big number denoting upper bounds for Minimum Uptime Constraints.

Minimum Downtime Constraints (3.25, 3.26, 3.27): A unit cannot be turned on instantaneously once it is decommitted. The minimum downtime constraint imposes

a minimum number of idle time periods that must elapse before the unit *i* can be turned on.

In (3.25), m_5 is a very small number denoting upper bounds for Minimum Downtime Constraints. In (3.26), M_5 is a very big number denoting upper bounds for Minimum Downtime Constraints.

Ramp-up Constraints (3.28, 3.29): Due to the thermal stress limitations and mechanical characteristics of the generating units, the increase in the power output level of committed unit *i* is restricted by its ramp-up rate over consecutive time periods during which it remains committed.

In (3.29), M_6 is a very big number denoting upper bounds for Ramp-up Constraints.

Ramp-down Constraints (3.30, 3.31): Due to the thermal stress limitations and mechanical characteristics of the generating units, the decrease in the power output level of committed unit *i* is restricted by its ramp-down rate over consecutive time periods during which it remains decommitted.

In (3.31), m_6 is a very small number denoting upper bounds for Ramp-down Constraints.

(3.32, 3.33): Sign restrictions of decision variables.

3.2 Proposed Genetic Algorithm Based Approach

Since the UCP is shown to be one of the NP-hard problems in the OR literature by Bendotti et al. (2017), efficient algorithms for the solution of the UCP are required by system operators in traditional power systems. For this reason, we develop an effective and efficient evolutionary metaheuristic algorithm, also called as Mixed Integer Coded Genetic Algorithm, to solve the UCP in negligible computation time and to obtain high solution quality, since GA-based approaches are proven to be very efficient in the search of global optimum in large and complex problems like the UCP in a relatively short computational time. The commitment scheduling part of

the UCP in which commitment statuses ("On/Off") of units are determined for each period is dealt with genetic operators. On the other hand, the load dispatching part in which how much power should be produced by each committed unit is determined for each period is coped with a modified version of Lambda Iteration Method (I-LIM).

The main difficulty in developing a GA for the UCP is that it has several constraints involving both continuous and binary variables. Therefore, a somehow more-involved algorithm is required in order to tackle with those constraints. For this purpose, minimum uptime/downtime constraints are handled in the chromosome representation. In other words, chromosomes attained in the initial population and during genetic operators always satisfy the minimum uptime/downtime constraints. Similarly, unit output range constraints and ramp-rate limits are always satisfied as a result of the rules enforced by the I-LIM. Different from the minimum uptime/downtime constraints, unit output range and ramp-rate limits; load requirement constraints and spinning reserve constraints are not guaranteed to be satisfied during genetic operations. To cope with violations of these two constraints, penalty mechanisms are adopted.

3.2.1 Improved Lambda Iteration Method to Solve Economic Load Dispatch Subproblem

In power electronics, the LIM is one of the most practical and useful heuristics to obtain an optimal or near-optimal solution for the Economic Load Dispatch (ELD) subproblem of the UCP (Wood, 1996). It is an iterative algorithm which stops computations when either one of the stopping conditions as the specified tolerance level for the difference between total load demand and total power generated by the committed units, and the maximum limit for the number of iterations are satisfied. The LIM is implemented instead of a commercial optimization solver like CPLEX for the ELD subproblem because of two reasons. One is its fast convergence to near-optimal solution for this problem, while the other reason is that the LIM can easily

be coded in any programming environment. The main logic behind the LIM is that it defines an initial incremental cost rate λ first. Then, it calculates the amount of power generated by each committed unit by taking the derivative of the convex fuel cost, and equating it to this incremental cost rate λ as it is depicted in (3.35).

$$FC(P_i) = a_i + b_i P_i + c_i {P_i}^2 \rightarrow \quad \frac{dFC(P_i)}{dP_i} = b_i + 2c_i P_i = \lambda \qquad (3.35)$$

where a_i, b_i and c_i are positive fuel cost coefficients of generating unit *i*, P_i and $FC(P_i)$ is the power generation level and the fuel cost of generating unit *i*, respectively.

According to the difference between total power generated by the committed units and total load demand, the algorithm incrementally increases or decreases λ. By iteratively repeating this calculation, the LIM finds the load dispatch decisions of conventional generating units. Nevertheless, the most efficient dispatching decisions cannot be obtained by applying original LIM iterations. For some instances, it is observed that a unit, which is more cost-effective in terms of average fuel cost, is scheduled to produce less power than those with higher average fuel costs. As a result, dispatching schedules obtained by the original LIM are more expensive in terms of fuel costs which is the primary contributor to the total operating cost. As it can be inferred from the second order derivative of the average fuel cost of unit *i*, it is a convex function, so it has its minimum value when its first order derivative takes the value of zero, which is illustrated in (3.36).

$$\overline{FC(P_i)} = \frac{a_i}{P_i} + b_i + c_i P_i \rightarrow \quad \frac{d^2\overline{FC(P_i)}}{d{P_i}^2} = 2\frac{a_i}{{P_i}^3} > 0 \quad \ni P_i > 0 \qquad (3.36)$$

Therefore, we improve the LIM by incorporating Average Fuel Cost Optimization as well. With this modification the amount of power to be produced by committed units according to the LIM is adjusted as shown in (3.37, 3.38).

$$\overline{FC(P_i)} = \frac{a_i}{P_i} + b_i + c_i P_i \rightarrow \quad \frac{d\overline{FC(P_i)}}{dP_i} = -\frac{a_i}{{P_i}^2} + c_i = 0 \rightarrow {P_i}^* \qquad (3.37)$$

$${P_i}^{**} = \min(P_i^{Max}, {P_i}^*) \qquad (3.38)$$

In this improved LIM (I-LIM), we perform original LIM iterations to obtain schedules that are cost-effective by means of Total Fuel Cost Optimization first. Then, we perform improvement iterations for the committed units to adjust their power output level in order to minimize Average Fuel Cost. In Figure 3.1, dispatching decisions of the LIM and I-LIM are illustrated for a 10-Unit system being subject to different load demands. Total fuel costs of meeting 1500 MW of load demand for the LIM and I-LIM are calculated as $33,945 and $33,890, respectively. By applying Average Fuel Cost Optimization iterations, the total fuel cost is reduced by $55. Similarly, for 1000 MW of load demand, associated fuel costs are found as $20,758 for the LIM and $20,642 for the I-LIM, which corresponds to $116 of reduction in total fuel costs.

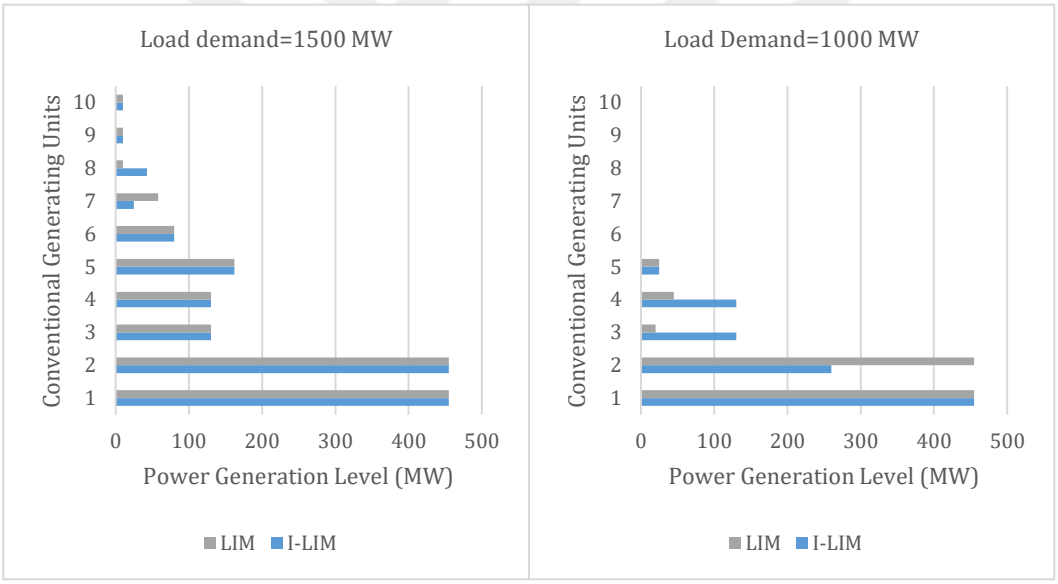

Figure 3.1. Dispatching Decisions of the LIM and I-LIM for a Power System with 10 Conventional Generating Units for Different Load Demands

It is also important to note that we improve the original LIM even more by adding Step 3.1.2 into the algorithm in order to handle ramp up and ramp down constraints. For the UCP without ramp rate limits, the I-LIM can be applied by removing Step 3.1.2 from the algorithm. The pseudocode of I-LIM is provided below.

The pseudocode of the I-LIM:

1. Set iteration limit (*MaxIter*), tolerance (ε) and initial incremental cost rate (λ).
2. Set the counter *k=0*;
3. While (*k<MaxIter*)

k=k+1

3.1. For each unit *i*

3.1.1. Calculate power value to be dispatched:

$$P_{it} = \frac{\lambda - b_i}{c_i}$$

3.1.2. Adjust power output limits by considering ramp-rate limits:

If $u_{it-1} = u_{it} = 1$

$$P_{it}^{Min} = \text{Max}\{P_i^{Min}, P_{it-1} - R_i^{down}\}$$
$$P_{it}^{Max} = \text{Min}\{P_i^{Max}, P_{it-1} + R_i^{up}\}$$

Else

$$P_{it}^{Min} = P_i^{Min}$$
$$P_{it}^{Max} = P_i^{Max}$$

End if

3.1.3. If $P_{it} < P_{it}^{Min}$

$$P_{it} = P_{it}^{Min}$$

Else if $P_{it} > P_{it}^{Max}$

$$P_{it} = P_{it}^{Max}$$

End if

End for

3.2. Sum all P_{it}'s up as total load supply.

3.3. Calculate the difference between the demand and load supply as P_{net}.

3.3.1. If $P_{net} > \varepsilon$; $\lambda = \lambda - \frac{\lambda}{4}$;

Else if $P_{net} < \varepsilon$; $\lambda = \lambda + \frac{\lambda}{4}$;

Else; Break

End if

End while

4. Find $\overline{FC(P_i)}$ of each unit *i* by using P_i^{**}.
5. Sort units in ascending order according to $\overline{FC(P_i)}$.
6. For each unit *i* [starting from the beginning of the sorted list].

6.1. If $0 < P_{it} < P_{it}^{Max}$

6.1.1. For each unit *j* [starting from the last of the list && *ind(j)>ind(i)*]

6.1.1.1. If $P_{jt} - P_{jt}^{Min} + P_{it} \leq P_{it}^{Max}$

$$P_{it} = P_{jt} - P_{jt}^{Min} + P_{it}$$
$$P_{jt} = P_{jt}^{Min}$$

Else

$$P_{jt} = P_{jt} - (P_{it}^{Max} - P_{it})$$

$P_{it} = P_{it}^{Max}$
End if
6.1.1.2. If $P_{it} = P_{it}^{Max}$
Break
End if
End for
End if
End for

3.2.2 Mixed Integer Coded Genetic Algorithm to Solve the Unit Commitment Problem

3.2.2.1 Chromosome Representation

The standard GA approaches for the UCP generally adopt the binary chromosome representation strategy in which chromosomes are represented by using |*N*|x|*T*| matrix having binary elements of 0 and 1. Different from those GA approaches, we propose a GA in which a mixed integer chromosome representation strategy is adopted in order to reduce the excessive memory usage of the pure binary coded ones, which slows down the computation in return. For this purpose, we aggregate consecutive time periods in which a unit has the same commitment status by forming "On/Off" cycles for each unit. As a result of this aggregation, a chromosome is represented by two subsets:

- **InitialStat:** It is the red |*N*|x1 array storing the initial commitment status of each unit as shown in Figure 3.2. If a unit is committed during the first period; that is, its commitment status is "On", then the element in the InitialStat array takes the value of 1. On the contrary, it takes the value of 0 if its commitment status is "Off" during the first period.
- **Schedule:** It is the concatenated matrix whose elements in each row are associated with the "On/Off" cycles of a unit. Each element in a row takes a positive integer value representing the ending hour of an "On/Off" cycle for a unit during the planning horizon as shown in Figure 3.2.

According to the value in InitialStat subset, the "On" and "Off" cycles are determined for each unit as shown in Figure 3.2 for a system such that $|N|$=7 units and $|T|$=24 hours.

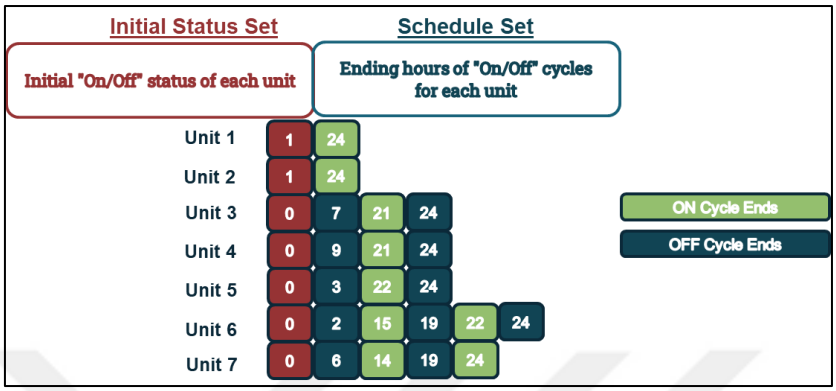

Figure 3.2. Chromosome Representation for a Power System with 7 Conventional Generating Units over a 24-h Planning Horizon

3.2.2.2 Initial Population Generation

The minimum uptime/downtime requirements must be met when generating the initial population, which cannot be satisfied by pure random generation. Thus, we define an additional set of rules to generate the initial population. The first subset (InitialStat) of a chromosome is generated by randomly selecting 0 or 1. However, the generation of the second subset is not as straightforward as the first subset, so the following algorithm is applied to each unit in a chromosome. The pseudocode of the initial population generation algorithm is provided below**:**

1. Determine the number of cycles (c) that the unit will have by randomly selecting an integer from the set Q.

$$Q = \left[1, \left\lfloor \frac{T}{max\left(T_{Min,\,i}^{on}, T_{Min,\,i}^{off}\right)} \right\rfloor\right] \tag{3.39}$$

2. If c is even, define remaining number of "On" & "Off" cycles as $c_{ON} = c_{OFF} = \frac{c}{2}$ Otherwise, look at its status in the InitialStat array. If it is "On" ("Off") during the first period, then $c_{ON\,(OFF)} = \left\lceil \frac{c}{2} \right\rceil$, $c_{OFF\,(ON)} = \left\lfloor \frac{c}{2} \right\rfloor$

3. Set ending hour of the previous cycle (*B*) as 1.
4. Set the last cycle's ending hour *T* for each unit.
5. For each cycle except the last one,
   5.1. According to its cycle status ("On" or "Off") (the determination of these statuses are explained at the end of the previous section), randomly generate an integer (*EndCycle*) between $[B + T_{Min,\,i}^{on},\ T - c_{OFF} * T_{Min,\,i}^{off} - c_{ON} * T_{Min,\,i}^{on}]$ and $c_{ON} = c_{ON} - 1$ if it is an ON cycle; otherwise between $[B + T_{Min,\,i}^{off},\ T - c_{OFF} * T_{Min,\,i}^{off} - c_{ON} * T_{Min,\,i}^{on}]$ and $c_{OFF} = c_{OFF} - 1$.
   5.2. *B=B+ EndCycle*

3.2.2.3 Penalty Mechanisms

Load requirement constraints and spinning reserve constraints are not guaranteed to be satisfied during genetic operations. To cope with violations of these two constraints, penalty mechanisms are adopted in a way that penalties are incurred for the amount of violations, not for the number of violations. The reason for adopting such a heavy penalty mechanism is to prevent chromosomes violating all or one of these two constraints from passing to the next generation and being selected for the mating pool. The penalty of not meeting load requirements is denoted as *PwrP* ($/MW). Similarly, the penalty for the violation of spinning reserve constraints is denoted as *SRP* ($/MW).

3.2.2.4 Fitness Function

The fitness function in the MICGA is calculated by taking the reciprocal of the sum of the total operating cost and total penalty costs for violations of spinning reserve and load requirement constraints. To preclude premature convergence, the fitness function is linearly scaled according to the method proposed by Mantawy et al. (1997) as expressed in (3.40).

$$f_s = a\,f + b \tag{3.40}$$

where f and f_s denote the original fitness value and the scaled fitness value; c, a and b is defined as in (3.41, 3.42, 3.43), respectively.

$$c \in [1.2, 2] \tag{3.41}$$

$$a = (c-1)\frac{f_{avg}}{f_{max} - f_{min}} \tag{3.42}$$

$$b = (1-a) * f_{avg} \tag{3.43}$$

where f_{avg}, f_{max} and f_{min} are the population average, maximum and minimum of the original fitness functions.

3.2.2.5 Selection Operation

In the MICGA, roulette wheel selection method is employed to choose chromosomes from the mating pool. In this selection method, each slot on the wheel represents a chromosome from the parent generation; the width of each slot represents the relative scaled fitness of a given chromosome. Chromosomes having larger scaled fitness values tend to be selected most likely since they are represented with larger slots on the roulette wheel.

3.2.2.6 Crossover Operation

The MICGA utilizes a horizontal two-point crossover technique. In other words, generating unit schedules are not taken apart and exchanged, which is the case in the horizontal crossover, rather whole schedules of the units between two points determined randomly are exchanged with the corresponding schedules of the other parent as illustrated in Figure 3.3.

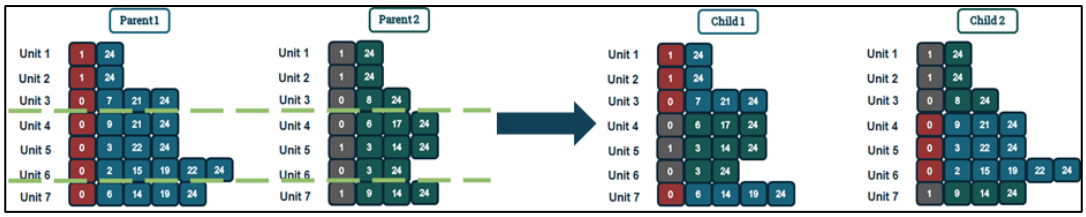

Figure 3.3. The Two-Point Horizontal Crossover Operation for a Power System with 7 Conventional Generating Units over a 24-h Planning Horizon

The pseudocode of the two-point horizontal crossover operation is provided below:

Crossover (Par_I; Par_{II}; C_I; C_{II}): where *Par* defines parent chromosomes and *C* denotes child chromosomes

If rand (0,1) ≤ P_c;

1. Randomly select two crossover points horizontally, that is, select the two points between which whole schedules of the units will be exchanged by the crossover.
2. Apply two-point crossover to both sets (InitialStat and Schedule sets)

Else; set $C_I = Par_I$ *and* $C_{II} = Par_{II}$

End if

3.2.2.7 Mutation Operations

In the MICGA, several mutation operators are used to obtain a diversity of chromosomes and to explore the neighborhood of a child chromosome for a better solution quality. For this purpose, five mutation operators are used to change schedules in child chromosomes. Moreover, an additional mutation operator is introduced to eliminate excessive reserves of power generation schedules since the ELD subproblem of the UCP is not solved by using genetic operations, rather it is externally solved by applying the I-LIM.

Mutation 1

In this mutation, two units in a chromosome are randomly selected. For each unit, one of its cycle lengths is reduced. Similarly, cycles to be curtailed are also randomly selected. It is important to note that minimum uptime and downtime constraints are

also taken into consideration while reducing cycle lengths. Operations of Mutation 1 is illustrated in Figure 3.4.

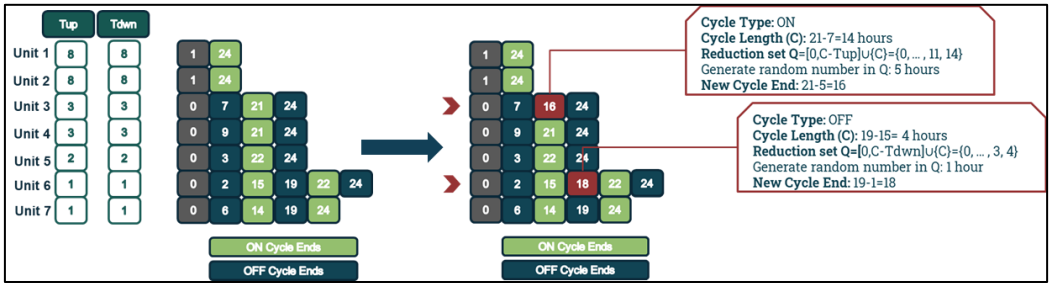

Figure 3.4. Mutation 1 for a Power System with 7 Conventional Generating Units over a 24-h Planning Horizon

The pseudocode of Mutation 1 is provided below.

Mutation1 (C): P_m1 is the occurrence probability of Mutation 1 and C denotes the child chromosome.

If rand (0,1) ≤ P_m1;

1. Select two units randomly.

For each unit;

If the schedule length>1

1.1. Randomly select a mutation point (one of the cycle ends).

If (the status of unit i during 1st period is "On" && cycle number is EVEN) || (the status of unit i during 1st period is "Off" && cycle number is ODD)

1.2. Calculate the cycle length as Δ.

If $\Delta \geq T^{off}_{Min,i}$

1.2.1. Construct the following reduction set $Q = [0, \Delta - T^{off}_{Min,i}] \cup \{\Delta\}$

1.2.2. Select a random integer k among Q.

If $k \neq \Delta$

1.2.2.1. Reduce the cycle end by k.

Else

1.2.2.2. Remove the selected cycle end and the previous cycle end.

End if

End if

Else if (the status of unit i during 1st period is "On" && cycle number is ODD) || (the status of unit i during 1st period is "Off" && cycle number is EVEN)

1.3. Calculate the cycle length as Δ.
If $\Delta \geq T_{Min,i}^{on}$
1.3.1. Construct the following reduction set $Q = [0, \Delta - T_{Min,i}^{on}] \cup \{\Delta\}$
1.3.2. Select a random integer k among Q.
If $k \neq \Delta$
1.3.2.1. Reduce the cycle end by k.
Else
1.3.2.2. Remove the selected cycle end and the previous cycle end.
End if
End if
End if
End if
End for
Else; Return C
End if

Mutation 2

In this mutation, units are clustered according to their minimum uptime and downtime requirements so that units will have the same minimum uptime and downtime requirements. Then, one cluster having at least 2 units is randomly chosen. Accordingly, two units in that cluster are randomly selected. Mutation 2 is used to exchange a part of their schedules as illustrated in Figure 3.5. This mutation can be considered as one-point crossover within a chromosome.

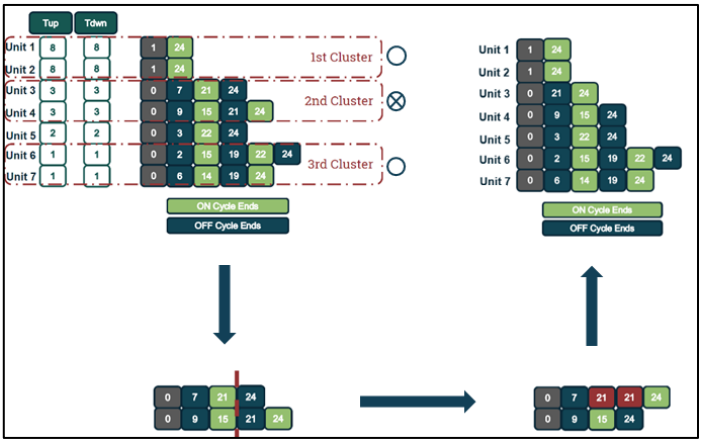

Figure 3.5. Mutation 2 for a Power System with 7 Conventional Generating Units over a 24-h Planning Horizon

The pseudo code of Mutation 2 is provided below:

Mutation2 (*C*): P_m2 is the occurrence probability of Mutation 2 and *C* denotes the child chromosome

If rand (0,1) ≤ P_m2;

1. Cluster the units having same minimum uptime (T_{Min}^{on}) and downtime (T_{Min}^{off}) limits.
2. Select a cluster consisting of more than 1 unit.
3. Select two units randomly which have the schedule length being at least 2, from that cluster.
4. Select a crossover point from the set of [2, Min(schedule length of 1st and 2nd units)-1]
5. Apply one-point crossover to the schedules of these units.

For each unit;

5.1. Calculate cycle length of unit *i* at the crossover point as Δ_i.

If (the status of unit *i* during 1st period is "On" && crossover point is EVEN) || (the status of unit during *i* 1st period is "Off" && cycle number is ODD)

If $\Delta_i = 0$

5.2. Remove each cycle end just before and just after the crossover point.

Else if $\Delta_i < T_{Min,i}^{off}$

5.3. Calculate the lengths of the cycles just before and just after the crossover point as Δ_1^* *and* Δ_2^*

If $\Delta_1^* + \Delta_i < T_{Min,i}^{on} + T_{Min,i}^{off}$

5.3.1. Reduce the cycle end just before the crossover point by $T_{Min,i}^{off} - \Delta_i$

5.3.2. Break

Else if $\Delta_2^* + \Delta_i < T_{Min,i}^{on} + T_{Min,i}^{off}$

5.3.3. Increase the cycle end at the crossover point by $T_{Min,i}^{off} - \Delta_i$

5.3.4. Break

Else if (the status of the unit i during 1st period is "On" && crossover point is ODD) || (the status of the unit during i 1st period is "Off" && cycle number is EVEN)

If $\Delta_i = 0$

5.4. Remove both cycle ends just before and just after the crossover point.

Else if $\Delta_i < T_{Min,i}^{on}$

5.5. Calculate the lengths of the cycles just before and just after the crossover point as Δ_1^* *and* Δ_2^*

If $\Delta_1^* + \Delta_i < T_{Min,i}^{on} + T_{Min,i}^{off}$

5.5.1. Reduce the cycle end just before the crossover point by $T^{on}_{Min,i} - \Delta_i$

5.5.2. Break

Else if $\Delta^*_2 + \Delta_i < T^{on}_{Min,i} + T^{off}_{Min,i}$

5.5.3. Increase the cycle end at the crossover point by $T^{on}_{Min,i} - \Delta_i$

5.5.4. Break

End if

End if

End for

Else; Return *C*

End if

Mutation 3

In this mutation, two units in a chromosome are randomly selected. For each unit, one of its cycle lengths is increased. Similarly, cycles are also randomly selected. It is important to note that minimum uptime and downtime constraints are also taken into consideration while increasing cycle lengths. Operations of Mutation 1 is illustrated in Figure 3.6.

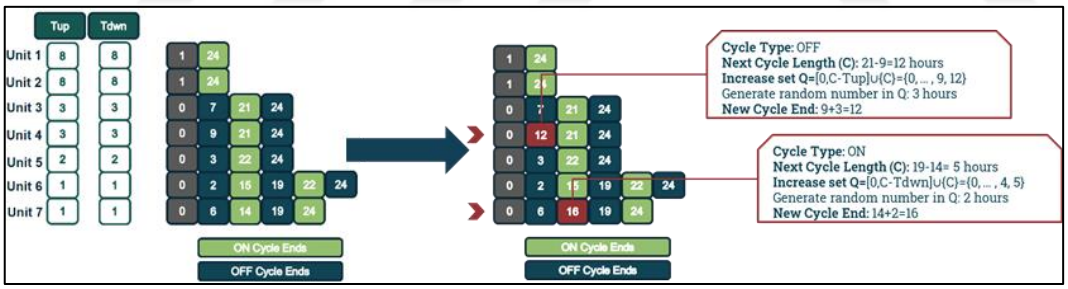

Figure 3.6. Mutation 3 for a Power System with 7 Conventional Generating Units over a 24-h Planning Horizon

The pseudocode of Mutation 3 is provided below:

Mutation3 (*C*): P_m3 is the occurrence probability of Mutation 3 and *C* denotes the child chromosome

If rand (0,1) ≤ P_m3;

1. Select two units randomly.

For each unit;

If the schedule length > 1

1.1. Randomly select a mutation point (one of the cycle ends).
If (the status of unit *i* during 1st period is "On" && cycle number is EVEN) || (the status of unit *i* during 1st period is "Off" && cycle number is ODD)
1.2. Calculate the next cycle's length as Δ.
If $\Delta \geq T_{Min,i}^{on}$
1.2.1. Construct the following reduction set $Q = [0, \Delta - T_{Min,i}^{on}] \cup \{\Delta\}$
1.2.2. Select a random integer *k* among *Q*.
If $k \neq \Delta$
1.2.3. Increase the cycle end by *k*.
Else
1.2.4. Remove the selected cycle end and the next cycle end.
End if
End if
Else if (the status of unit *i* during 1st period is "On" && cycle number is ODD) || (the status of unit *i* during 1st period is "Off" && cycle number is EVEN)
1.3. Calculate the next cycle's length as Δ.
If $\Delta \geq T_{Min,i}^{off}$
1.3.1. Construct the following reduction set $Q = [0, \Delta - T_{Min,i}^{off}] \cup \{\Delta\}$
1.3.2. Select a random integer *k* among *Q*.
If $k \neq \Delta$
1.3.3. Increase the cycle end by *k*.
Else
1.3.4. Remove the selected cycle end and the next cycle end.
End if
End if
End if
End if
End for
Else; Return *C*
End if

Mutation 4

In this mutation, two units in a chromosome are randomly selected. For each unit, its first cycle is removed and "On/Off" statuses of the remaining cycles are adjusted as depicted in Figure 3.7.

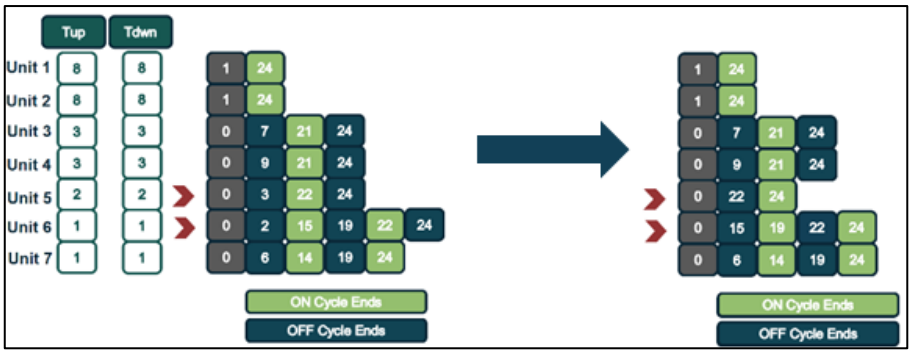

Figure 3.7. Mutation 4 for a Power System with 7 Conventional Generating Units over a 24-h Planning Horizon

The pseudocode of Mutation 4 is provided below:

Mutation4 (C): P_m4 is the occurrence probability of Mutation 4 and C denotes the child chromosome
If rand (0,1) ≤ P_m4;
1. Select two units randomly.
For each unit;
If the schedule length > 1
1.1. Remove the first cycle end.
End if
End for
Else; Return C
End if

Excessive Reserve Elimination Operator

After implementing standard genetic operations such as crossover and mutations, there might be many units operating at their minimum power output limit in several time periods. It is an indicator that an excessive number of units is committed in periods involving excessive reserves. The commitment and dispatching decisions could be improved by considering the option of turning off several units operating at their minimum output levels. For this purpose, this operator evaluates whether the new commitment cycles attained by turning off some of those units could satisfy both time dependent constraints and meet load demand and spinning reserve requirements in those time periods as well. If one of these constraints is not satisfied,

then the original chromosome is retained. Otherwise, the new chromosome is encoded back as a new child solution.

3.2.2.8 Elite Preservation Mechanism

In order not to lose any fittest solution during the genetic operations, parents and children in the population are sorted according to their fitness values in descending order. The first *PS* (initial population size) of chromosomes is preserved for the reproduction of the further genetic process in the next generations.

3.3 Implementation of the Genetic Algorithm Based Approach

The MICGA combined with the I-LIM is applied to problem instances in the order specified in the flowchart demonstrated in Figure 3.8.

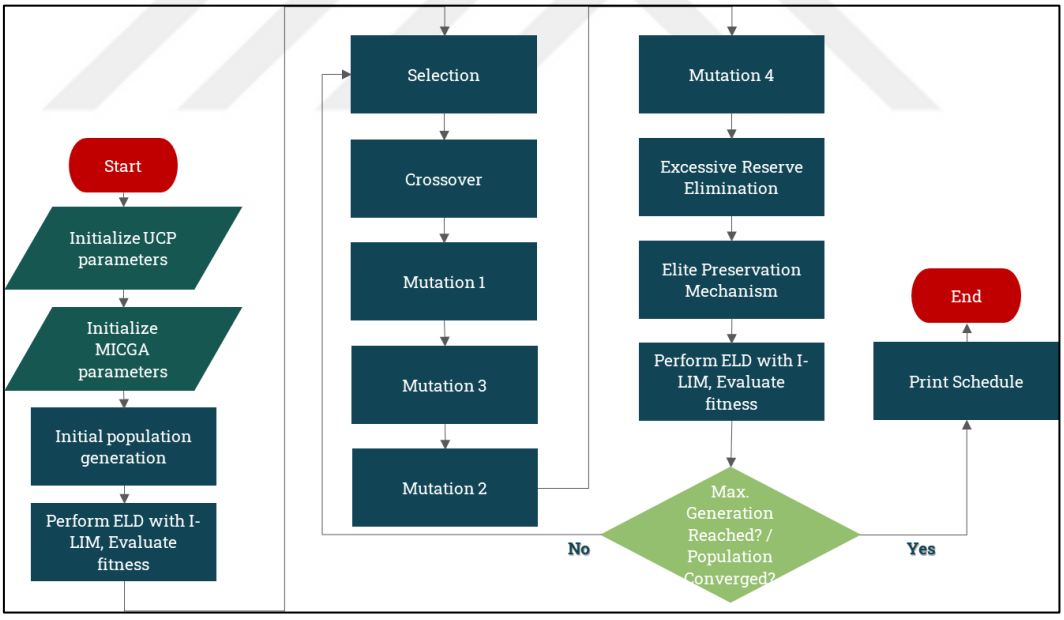

Figure 3.8. Flowchart of the MICGA

The pseudocode of the MICGA is provided below:

1. Initialization of the parameters such as *PS*, P_c, P_m1, P_m2, P_m3, P_m4, P_m5, and maximum number of generations (*G*) as the termination criterion.
2. Generate *PS* many chromosomes in accordance with the rules in Section 3.2.2.2.
3. Determine the generation mix of the committed units by performing I-LIM on the generated solutions.
4. Calculate production cost of each unit for every hour by using the cost function defined in Section 3.1. Then, sum them up to calculate total operation cost.
5. Determine the periods with load requirement and spinning reserve violation. If there is any, then calculate the amount of violation of each constraint and multiply them with the corresponding penalty term. Then, sum them up to find total penalty cost.
6. Evaluate fitness using equation defined in Section 3.2.2.3.
7. Use Roulette Wheel Selection technique to select parent chromosomes for formation of mating pool.
8. Randomly perform two-point crossover on parents selected to produce new off-springs.
9. Perform mutation operations except Excessive Reserve Elimination operator to diversify the solution space and modify off-springs. If the generation number is greater than 6, also apply Excessive Reserve Elimination operator.
10. Perform I-LIM for calculating production cost and penalty cost for the infeasible solutions. Evaluate the fitness of offspring.
11. Apply elite preservation mechanism for preserving the best solutions.
12. If the maximum number of generations (*G*) is not reached or the population does not converge, go to 7,

    Otherwise, stop and print UC schedule (both schedule and load dispatch mix) and plot graphs.

3.4 Computational Study

The MICGA is coded in MATLAB programming language and it is executed in Windows 10 environment in a Lenovo ultrabook with Intel(R) Core (TM) i7-6500U 2.6 GHz CPU and 8 GB RAM. Numerical experiments on the performance of the MICGA are conducted by using a set of three problem instances of the Institute of Electrical and Electronics Engineers (IEEE) (Datta, 2013). Moreover, the robustness of the proposed approach is validated by applying statistical analysis to solutions obtained by the proposed approach. Then, we compare the results of the MICGA with other GA approaches for each problem instance.

3.4.1 Problem Instances

To conduct numerical experiments, the MICGA is applied to the original and modified versions of IEEE 39-bus problem instances. The reason of choosing these problem instances is that they are the most widely studied benchmark instances to compare the performances of different solution techniques for the UCP in traditional power systems with/without ramp rate limits. For each problem instance, the minimum spinning reserve requirement in any time period and the ramp-rate limits are taken as 10% of the forecasted load demand at that period and 20% of the unit's maximum power output limit, respectively.

Problem Instance 1

This problem instance consists of 39-bus with 10 units. The length of the scheduling horizon is 24 hours. The conventional unit related data for the 10-Unit power system are provided in Table 3.1. Hourly forecasted load demands of the system over 24 hours are provided in Table 3.2.

Table 3.1. Conventional Unit Related Data for IEEE 39-bus Problem Instance

	Unit 1	Unit 2	Unit 3	Unit 4	Unit 5	Unit 6	Unit 7	Unit 8	Unit 9	Unit10
P_i^{Max} (MW)	455	455	130	130	162	80	85	55	55	55
P_i^{Min} (MW)	150	150	20	20	25	20	25	10	10	10
a_i ($)	1000	970	700	680	450	370	480	660	665	670
b_i($/MW)	16.19	17.26	16.60	16.50	19.70	22.26	27.74	25.92	27.27	27.79
c_i ($/$MW^2$)	0.00048	0.00031	0.00200	0.00211	0.00398	0.00712	0.00079	0.00413	0.00222	0.00173
$T_{Min,i}^{on}$ (h)	8	8	5	5	6	3	3	1	1	1
$T_{Min,i}^{off}$ (h)	8	8	5	5	6	3	3	1	1	1
S_i^H($)	4500	5000	550	560	900	170	260	30	30	30
S_i^C ($)	9000	10000	1100	1120	1800	340	520	60	60	60
$T_{c,i}$ (h)	5	5	4	4	4	2	2	0	0	0
Initial Status (h)	8	8	-5	-5	-6	-3	-3	-1	-1	-1

NOTE: 1. In Initial Status parameters, (+) sign means a unit has been "On" while (-) sign means a unit has been "Off" for the specified hours

Table 3.2. Hourly Load Demand Forecasts for IEEE 39-bus Problem Instance

Hour	**1**	**2**	**3**	**4**	**5**	**6**	**7**	**8**	**9**	**10**	**11**	**12**
Demand (MW)	700	750	850	950	1000	1100	1150	1200	1300	1400	1450	1500
Hour	**13**	**14**	**15**	**16**	**17**	**18**	**19**	**20**	**21**	**22**	**23**	**24**
Demand (MW)	1400	1300	1200	1050	1000	1100	1200	1400	1300	1100	900	800

Problem Instance 2

This problem instance is obtained by appropriately scaling Problem Instance 1. For this purpose, generating units in Table 3.1 are replicated two times to form 20-Unit problem instance. Also, forecasted load demand requirements in Table 3.2 are doubled.

Problem Instance 3

Similarly, this problem instance is obtained by also appropriately scaling Problem Instance 1. For this purpose, generating units in Table 3.1 are replicated four times

to form 40-Unit problem instance. Also, forecasted load demand requirements in Table 3.2 are quadruplicated.

3.4.2 Fine Tuning and Test Results

Before solving the UCP with/without ramp rate limits by the MICGA, we apply one-factor-at-a-time (OFAT) experiments, in which only one variable is changed at a time, for all algorithm parameters such as population size, crossover and mutation probabilities instead of a factorial design. The main reason of preferring OFAT experiments is that all parameters are continuous type whose values can be discretized by at least nine potential levels, which makes at least 531,441 parameter combinations. Also, we have three problem instances, each consisting of two cases, namely with/without ramp-rate limits, which makes 6 problem categories. Hence, it is not plausible to design full factorial experiments with the required combinations. One way of dealing with such a heavy requirement is to design reduced factorial experiments such as fractional factorial experiments in which each factor consists of two levels, or experiments with the representative runs. However, all parameters are very effective for exploration and exploitation abilities of the MICGA, so reducing factor levels of some parameters may cause misleading judgements. Thus, we conduct OFAT experiments in order to test more levels of each parameter.

Since Problem Instances 2 and 3 are obtained by appropriately scaling the original IEEE-39 bus problem instance, OFAT experiments are made for only the first instance. For this purpose, the algorithm parameters for Problem Instance 1 are arbitrarily set as shown in Table 3.3. MICGA is replicated for 10 times with these settings for the UCP with/without ramp rate constraints. The average operation costs of schedules obtained by the MICGA are found as $580,878.63 and $568,794.8, respectively; for cases with and without ramp rate constraints.

Table 3.3. Parameter Settings before Fine Tuning for IEEE 39-bus Problem Instance

MICGA without Ramp Rate Limits				**MICGA with Ramp Rate Limits**			
PS	50	P_m4	0.4	***PS***	50	P_m4	0.4
G	250	P_m5	0.7	***G***	250	P_m5	0.7
P_c	0.6	***SRP* ($)**	2490	P_c	0.6	***SRP* ($)**	2490
P_m1	0.4	***PwrP* ($)**	1736	P_m1	0.3	***PwrP* ($)**	1736
P_m2	0.1	***p***	0.5	P_m2	0.2	***p***	0.5
P_m3	0.4	***c***	1.2	P_m3	0.3	***c***	1.2

During the fine-tuning process, same random number generators are used for each 10 replications so that effects of different parameter values on the solution quality can be fairly compared.

Having fixed other parameter values, the crossover rate (P_c) is changed in each run starting from 0.9. As shown in Table 3.4., the best level of P_c is found as 0.6 with average operation cost of $ 580,878.6 for the case without ramp rate limits whereas the rate of 0.5 is chosen for the case with ramp rate limits.

Table 3.4. OFAT Results for Crossover Rates for IEEE 39-bus Problem Instance

	MICGA without Ramp Rate Constraints		**MICGA with Ramp Rate Constraints**	
Crossover Rate (P_c)	**Average Operation Costs ($)**	**Average Computing Times (sec)**	**Average Operation Costs ($)**	**Average Computing Times (sec)**
0.9	587,067.1	28.8	568,034.0	36,2
0.8	588,996.7	19.2	568,827.8	37,2
0.7	588,155.5	12.9	568,794.8	36,4
0.6	**580,878.6**	**9.8**	568,794.8	76,7
0.5	585,071.8	7.8	**568,794.8**	**28,8**
0.4	603,587.4	6.2	568,827.8	28,0
0.3	588,864.1	4.9	568,794.8	22,3
0.2	620,222.6	6.6	569,077.8	26,0
0.1	637,405.0	2.5	568,692.3	13,4

After setting the best value of P_c, the rate of Mutation 1 (P_m1) is changed in a similar manner for every 10 replications. The best level of P_m1 is found as 0.3 and 0.1 for each case respectively. The associated additional reductions in average operation costs are \$2,303.8 and \$830.2 as illustrated in Table 3.5.

Table 3.5. OFAT Results for Mutation 1 Rates for IEEE 39-bus Problem Instance

	MICGA without Ramp Rate Constraints		**MICGA with Ramp Rate Constraints**	
Mutation 1 Rate (P_m1)	**Average Operation Costs (\$)**	**Average Computing Times (sec)**	**Average Operation Costs (\$)**	**Average Computing Times (sec)**
0.9	611,966.7	9.6	568,794.8	64.1
0.8	615,248.5	9.2	569,378.3	65.1
0.7	584,981.3	9.5	569,755.6	64.7
0.6	607,723.1	9.6	569,077.8	68.4
0.5	612,006.7	9.6	568,794.8	55.4
0.4	580,878.6	9.5	569,077.8	35.9
0.3	**580,453.9**	**9.7**	568,794.8	29.5
0.2	594,345.4	10.3	569,882.2	22.8
0.1	579,978.9	9.1	**567,964.6**	**14.8**

Table 3.6. OFAT Results for Mutation 3 Rates for IEEE 39-bus Problem Instance

	MICGA without Ramp Rate Constraints		**MICGA with Ramp Rate Constraints**	
Mutation 3 Rate (P_m3)	**Average Operation Costs (\$)**	**Average Computing Times (sec)**	**Average Operation Costs (\$)**	**Average Computing Times (sec)**
0.9	620,443.2	9.8	568,794.8	64.1
0.8	599,398.4	9.2	569,378.3	65.1
0.7	594,844.6	15.7	569,755.6	64.7
0.6	582,666.4	9.2	569,077.8	68.4
0.5	581,126.9	9.4	568,794.8	55.4
0.4	580,453.9	9.4	569,077.8	35.9
0.3	**578,150.1**	**9.2**	568,794.8	29.5
0.2	581,317.8	9.4	569,882.2	22.8
0.1	580,077.3	10.4	**567,964.6**	**14.8**

After setting the best values of P_c and P_m1, the rate of Mutation 3 (P_m3) is changed in a similar manner for every 10 replications. For cases without and with ramp rate limits, the best level of P_m3 is found as 0.3 with an additional decrease of $1,579.9 in the average operation cost, and 0.1 with no further change, respectively. The results of the experiments are summarized in Table 3.6.

After setting the best values of P_c, P_m1 and P_m3, the rate of Mutation 2 (P_m2) is changed in a similar manner for every 10 runs. For cases without and with ramp rate limits, the best level of P_m2 is found as 0.2 with an additional decrease of $1,579.9 in the average operation cost, and 0.5 with no further change in the average cost, respectively. The results of the experiments are reported in Table 3.7.

Table 3.7. OFAT Results for Mutation 2 Rates for IEEE 39-bus Problem Instance

	MICGA without Ramp Rate Constraints		**MICGA with Ramp Rate Constraints**	
Mutation 2 Rate (P_m2)	**Average Operation Costs ($)**	**Average Computing Times (sec)**	**Average Operation Costs ($)**	**Average Computing Times (sec)**
0.9	659,302.5	11.9	568,794.8	21.3
0.8	589,988.9	28.7	569,699.7	36.1
0.7	632,412.4	12.2	568,827.8	30.9
0.6	579,248.1	11.4	571,913.8	35.0
0.5	619,967.3	14.0	**567,964.6**	**10.5**
0.4	584,235.5	13.0	569,882.3	16.0
0.3	577,825.2	14.3	568,794.8	36.2
0.2	**576,570.2**	**10.7**	567,964.6	14.8
0.1	578,150.1	11.5	572,003.3	34.1

After setting the best values of P_c, P_m1 P_m3 and P_m2, the rate of Mutation 4 (P_m4) is changed in a similar manner for every 10 runs. For cases without and with ramp rate limits, the best level of P_m4 is found as 0.4 with an extra reduction of $351.5, and with no reduction in the average operation cost, respectively. The results of the experiments are illustrated in Table 3.8.

Table 3.8. OFAT Results for Mutation 4 Rates for IEEE 39-bus Problem Instance

	MICGA without Ramp Rate Constraints		MICGA with Ramp Rate Constraints	
Mutation 4 Rate (P_m4)	**Average Operation Costs ($)**	**Average Computing Times (sec)**	**Average Operation Costs ($)**	**Average Computing Times (sec)**
0.9	605,461.7	12.2	571,796.3	60.8
0.8	620,505.7	9.4	569,882.3	52.2
0.7	581,179.7	9,0	569,963.1	64.7
0.6	616,425.0	11.1	567,964.6	11.4
0.5	581,987.4	11.3	569,077.8	19.9
0.4	**576,218.7**	**9.2**	**567,964.6**	**10.6**
0.3	578,962.3	9.4	567,964.6	7.7
0.2	576,570.2	9.1	572,533.7	26.1
0.1	581,275.9	9.7	568,827.8	16.6

Table 3.9. OFAT Results for Mutation 5 Rates for IEEE 39-bus Problem Instance

	MICGA without Ramp Rate Constraints		MICGA with Ramp Rate Constraints	
Mutation 5 Rate (P_m5)	**Average Operation Costs ($)**	**Average Computing Times (sec)**	**Average Operation Costs ($)**	**Average Computing Times (sec)**
0.9	576,382.4	11.7	**567,964.6**	**30.2**
0.8	580,067.9	12.1	572,485.3	14.3
0.7	**576,218.7**	**16.0**	567,964.6	10.5
0.6	580,998.3	17.3	569,077.8	25.8
0.5	576,560.0	10.1	568,794.8	23.3
0.4	578,804.3	9.1	568,794.8	15.4
0.3	589,182.7	9.0	571,721.0	31.4
0.2	616,216.0	9.0	569,077.8	14.2
0.1	581,474.7	9.1	568,794.8	21.8

After setting the best values of P_c, P_m1, P_m3, P_m2 and P_m4, the rate of Mutation 5, also called as Excessive Reserve Elimination Operator (P_m5) is changed in a similar manner for every 10 replications. As illustrated in Table 3.9, the best level of P_m5 is

found as 0.7 with no further reduction in the average operation cost for the case without ramp rate limits whereas 0.9 is chosen for the case with ramp rate limits although the average operation cost does not change and the average computing time increases. This operator is used to exploit solutions nearby by trying to eliminate excessive reserves, so we prefer higher rates for this operation.

Lastly, according to the best values of rates of genetic operators, the population size (PS) is increased by 10 individuals starting from a population size of 10 for every 10 replications. For the case without ramp-rate limits, the best level of PS is found as 50 with no further decrease in the average operation cost. Moreover, we investigate the marginal effect of removing and adding an individual for the population sizes between 40 and 60. At this point, the maximum number of generation (G) is changed as a function of the population size to see the interaction between PS and G. Similar adjustments are also made for the case with ramp-rate limits. Accordingly, the best pairs of *PS* and *G* for each case are found as (45, 250) and (40, 200), respectively.

As a result of fine tuning the algorithm parameters, the best parameter settings of the MICGA for the cases with/without ramp rate limits are listed in Table 3.10.

Table 3.10. The Best Parameter Settings for MICGA after Fine Tuning for IEEE 39-bus Problem Instance

MICGA without Ramp Rate Limits				**MICGA with Ramp Rate Limits**			
$\boldsymbol{PS}$	45	$\boldsymbol{P_m4}$	0.4	$\boldsymbol{PS}$	40	$\boldsymbol{P_m4}$	0.4
$\boldsymbol{G}$	250	$\boldsymbol{P_m5}$	0.7	$\boldsymbol{G}$	200	$\boldsymbol{P_m5}$	0.9
$\boldsymbol{P_c}$	0.6	***SRP* ($)**	2490	$\boldsymbol{P_c}$	0.5	***SRP* ($)**	2490
$\boldsymbol{P_m1}$	0.3	***PwrP* ($)**	1736	$\boldsymbol{P_m1}$	0.1	***PwrP* ($)**	1736
$\boldsymbol{P_m2}$	0.2	$\boldsymbol{p}$	0.5	$\boldsymbol{P_m2}$	0.5	$\boldsymbol{p}$	0.5
$\boldsymbol{P_m3}$	0.3	$\boldsymbol{c}$	1.2	$\boldsymbol{P_m3}$	0.1	$\boldsymbol{c}$	1.2

Without considering the ramp rate constraints, MICGA is implemented to 10-Unit, 20-Unit and 40-Unit problem instances for 30 times with different initial solutions and predetermined parameter settings. For each instance, the best, average and the worst solutions in terms of total operating costs are summarized in Table 3.11.

Likewise, the minimum, average and maximum computing times are provided in Table 3.12.

Table 3.11. Best, Average and Worst Results of Total Operating Costs for All Problem Instances without Ramp Rate Constraints

	Total Operating Cost ($)		
Problem Instance	**Best**	**Average**	**Worst**
1 (10-Unit)	563,937.7	566,918.1	569,913.2
2 (20-Unit)	1,124,432.0	1,124,738.5	1,125,285.7
3 (40-Unit)	2,246,312.5	2,247,320.4	2,248,714.5

Table 3.12. Computing Times for All Problem Instances without Ramp Rate Constraints

	Computing Time (Min)			
Problem Instance	**Minimum**	**Average**	**Maximum**	**Standard Deviation**
1 (10-Unit)	0.17	0.45	0.71	0.18
2 (20-Unit)	0.17	0.65	1.09	0.30
3 (40-Unit)	0.17	1.11	1.66	0.47

MICGA is implemented to 10-Unit, 20-Unit and 40-Unit problem instances for 30 times with different initial solutions and predetermined parameter settings by also considering the ramp rate constraints. For each instance, the best, average and the worst solutions in terms of total operating costs are summarized in Table 3.13. Likewise, the minimum, average and maximum computing times are provided in Table 3.14.

Table 3.13. Best, Average and Worst Results of Total Operating Costs for All Problem Instances with Ramp Rate Constraints

	Total Operating Cost ($)		
Problem Instance	**Best**	**Average**	**Worst**
1 (10-Unit)	565,964.6	568,252.3	571,752.3
2 (20-Unit)	1,130,388.7	1,134,692.1	1,142,828.1
3 (40-Unit)	2,259,981.2	2,262,163.2	2,264,752.5

Table 3.14. Computing Times for All Problem Instances with Ramp Rate Constraints

	Computing Time (Min)			
Problem Instance	**Minimum**	**Average**	**Maximum**	**Standard Deviation**
1 (10-Unit)	0.11	0.45	0.84	0.22
2 (20-Unit)	0.17	0.49	1.09	0.30
3 (40-Unit)	0.96	1.60	1.70	0.15

3.4.3 Statistical Analysis on Robustness

Since the GA based approaches have a stochastic nature, it is very important to validate their robustness in the solution quality. For this purpose, we first conduct variability analysis for the best solutions with/without ramp rate limits. Secondly, we make an interval estimation for the average solutions by constructing two-sided confidence intervals to test the precision of the MICGA.

To analyze the robustness of MICGA, three performance measures are calculated by using best, average and worst operating costs as listed in Table 3.15. The first one compares the best and the average solutions for each problem instance and it is always below 0.55% for all instances. The second one indicates the difference between the best and worst solutions, which is never larger than 1.1%. Similarly, the last one is the ratio between the standard deviation of the total operating costs over 30 replications and the best solution which is always smaller than 0.35% for any problem instance. Those values are even smaller in 20-Unit and 40-Unit problem instances. That is because the best solution obtained in the 10-Unit problem instance is appropriately scaled and put as a seed solution in initial populations to reduce the computing time required for Problem Instances 2 and 3, also to increase solution quality.

Table 3.15. Variability Analysis on Total Operating Costs for All Problem Instances without the Ramp Rate Constraints

Problem Instance	(Average-Best)/Best	(Worst-Best)/Best	Standard Deviation/Best
1 (10-Unit)	0.53%	1.06%	0.32%
2 (20-Unit)	0.03%	0.08%	0.02%
3 (40-Unit)	0.04%	0.11%	0.03%

Thanks to 30 independent replications, we apply Central Limit Theorem to construct two-sided confidence intervals for the average total costs of each problem instance with 5% and 2% significance levels. As it can be inferred from the results reported in Table 3.16, the confidence intervals are narrow and indicate high precision for the cases without ramp rate constraints.

Table 3.16. Two-Sided Confidence Intervals on Average Total Costs for All Problem Instances without Ramp Rate Constraints

	95 % Confidence Interval		98 % Confidence Interval	
Problem Instance	**Lower Bound**	**Upper Bound**	**Lower Bound**	**Upper Bound**
1 (10-Unit)	566,250.8	567,585.2	566,114.8	567,721.2
2 (20-Unit)	1,124,669.3	1,124,806.7	1,124,655.3	1,124,820.7
3 (40-Unit)	2,247,071.3	2,247,568.7	2,247,020.6	2,247,619.4

Similar analyses are also performed for each problem instance considering the ramp-rate constraints and the results are listed in Table 3.17. For all instances, the variability between the best and the average solutions is always below 0.4%. Secondly, the difference between the best and worst solutions is never larger than 1.1%. Lastly, the ratio between the standard deviation of the total operating costs over 30 replications and the best solution is always smaller than 0.35% for any problem instance.

Table 3.17. Variability Analysis on Total Operating Costs for All Problem Instances with Ramp Rate Constraints

Problem Instance	(Average-Best)/Best	(Worst-Best)/Best	Standard Deviation/Best
1 (10-Unit)	0.40%	1.02%	0.29%
2 (20-Unit)	0.38%	1.10%	0.32%
3 (40-Unit)	0.10%	0.21%	0.08%

In a similar manner, we construct two-sided confidence intervals for the average total costs of each problem instance with 5 percent and 2 percent significance level. As it can be inferred from the results reported in Table 3.18, the confidence intervals are narrow and indicate high precision for the cases with ramp rate constraints as well.

Table 3.18. Two-Sided Confidence Intervals on Average Total Costs for All Problem Instances with Ramp Rate Constraints

	95 % Confidence Interval		98 % Confidence Interval	
Problem Instance	**Lower Bound**	**Upper Bound**	**Lower Bound**	**Upper Bound**
1 (10-Unit)	567,634.5	568,870.2	567,508.5	568,996.1
2 (20-Unit)	1,133,352.8	1,136,031.4	1,133,079.7	1,136,304.5
3 (40-Unit)	2,261,510.9	2,262,815.6	2,261,377.9	2,262,948.6

As a result of the variability analyses and precision tests, the MICGA is robust in terms of solution quality for both cases, ie., with and without ramp rate constraints, which is very important for a conventional power generation system since the generation companies are reluctant and hesitant to implement solution techniques with high variability and less precision to avoid schedules with poor solution quality.

3.4.4 Comparison with other Genetic Algorithm Based Approaches

The MICGA is comparable with other techniques in terms of several performance measures such as the best solution quality and the required computing time. By using these measures, MICGA is compared with some other GA techniques developed in the last two decades as reported in Table 3.19. These algorithms are implemented for

the same problem instances subject to the same set of constraints (but without the ramp-rate constraints) explained in Section 3.1. The results of these algorithms are directly taken from the original publications. Hence, comparing the algorithms in terms of their computation times will not be fair and informative enough since those algorithms are executed in different programming languages in different computational environments. For the UCP variant with the ramp-rate constraints, MICGA could not be compared with those GA techniques since the results of this variant were not reported in any publication.

Table 3.19. Comparison of the Best Solution Qualities and Average Computing Times for All Problem Instances without Ramp Rate Constraints

		Total Operating Cost ($)			**Average Computing Time (Min)**		
GA Approach	**Test Runs**	**Problem Instance 1 (10-Unit)**	**Problem Instance 2 (20-Unit)**	**Problem Instance 3 (40-Unit)**	**Problem Instance 1 (10-Unit)**	**Problem Instance 2 (20-Unit)**	**Problem Instance 3 (40-Unit)**
Senjyu (2002)	20	563,977.0	1,125,516.0	2,249,715.0	<1.5	<4	<11
Valenzuela (2002)	N/A	578,566.0	1,272,845.2	2,545,690.4	<5	<9	<18
Swarup (2003)	N/A	603,423.6	1,327,532.1	2,655,064.2	<1.5	<4	<8
Damousis (2004)	10	566,404.0	1,127,244.0	2,254,123.0	<0.5	<0.5	<1
Lazo (2011)	20	563,938.0	-	-	-	-	-
Datta (2013)	30	563,938.0	1,124,290.0	2,246,165.0	<0.5	<0.5	<0.5
Li (2013)	20	563,938.0	-	-	-	-	-
Roque (2014)	20	563,938.0	1,123,955.0	2,244,345.0	<0.5	<0.5	<1.5
Singhal (2014)	10	563,938.0	-	-	<0.5	-	-
Farag (2015)	10	564,230.0	-	-	-	-	-
Salimian (2015)	N/A	563,939.5	-	-	-	-	-
Bukhari (2016)	25	563,938.0	1,123,297.0	2,242,887.0	-	-	-
Saber (2016)	32	563,938.0	1,124,565.0	-	<0.5	<0.5	-
Trivedi (2016)	20	563,959.0	1,123,410.0	2,243,971.0	<0.6	<1.5	<3.5
Proposed MICGA	30	563,937.7	1,124,432.0	2,246,312.5	<0.55	<0.65	<1.1

For Problem Instance 1, in terms of the solution quality, the proposed MICGA is able to obtain the best known solution with the parameter setting found in Section 3.4.2 like Lazo (2011), Datta (2013), Li (2013), Roque (2014), Singhal (2014),

Bukhari (2016) and Saber (2016), as shown in Table 3.19 where the number of test runs when obtaining the corresponding results are also reported for each approach. Besides, it is observed that the average computing time of the MICGA is much smaller than some of the previous approaches whereas it is closer to ones obtaining the best solution quality. Similarly, for Problem Instance 2 and 3, it is observed that the computational time of MICGA is much smaller than those of most of the previous approaches and comparable with those of Damousis (2002), Datta (2013) and Singhal (2016). Apart from the average computing times, the proposed MICGA has also good performance in terms of the solution quality since the total operating cost of the best schedule attained by the MICGA is at most 0.1% and 0.15% greater than the best solutions obtained by Roque (2014), Bukhari (2016), Trivedi (2016) and Datta (2013) for Problem Instances 2 and 3. Furthermore, the MICGA can handle the ramp rate constraints, which are important for operations planning of conventional generating units, while others cannot.

CHAPTER 4

UNIT COMMITMENT PROBLEM FOR WIND INTEGRATED HYBRID POWER SYSTEMS UNDER SUPPLY/DEMAND UNCERTAINTY

Since there is a global tendency to integrate renewable energy sources in a power network to mitigate greenhouse gas emissions and to replace traditional generation, wind power generation has gained significant attention around the world, especially in European countries, for the last decade. Due to intermittent nature of wind, one of the most challenging issues that most of the power system operators are facing is how to manage uncertainty in a power system with significant penetration of wind power generation. In such an environment, there are three major sources of uncertainty. The first one arises from the errors in load demand forecasts for a specific time period. The second one stems from unexpected deviations by wind based generating units from their forecasted production schedules. The third one is caused by sudden outages of traditional generating units. Especially, the last two sources of uncertainty have to be handled very carefully when making unit commitment and load dispatch decisions for conventional generating units. An easy and straightforward method to deal with those uncertainties is to commit more spinning reserve (SR) from the conventional generating units so that they can guarantee more reliable power generation.

4.1 Uncertainty Modelling of Supply and Demand

In general, uncertainty due to load demand and wind power generation is modelled via continuous random variables since they cannot be accurately forecasted, and the errors have a continuous nature. However, outages in conventional generation are modelled via discrete random variables because of their discrete nature.

4.1.1 Forecasts for Load Demand

According to Gross et al. (1987) and Kirschen et al. (2009), load demand forecasts are modelled as the real load plus a random error term following symmetrical probability distribution such as Normal distribution having zero mean and positive variance with the following expression:

$$L_t^f = E(L_t^a) = L_t^a + \varepsilon_t^L \tag{4.1}$$

where $L_t^f, L_t^a, \varepsilon_t^L$ represent forecasted load, actual load and an error related to load forecast in period *t*, respectively. The mean and variance of the error term of the load forecast in period *t* are calculated as follows:

$$E(\varepsilon_t^L) = E(L_t^a) - E(L_t^a) = 0 \tag{4.2}$$

$$(\sigma_t^L)^2 = E((\varepsilon_t^L)^2) - \left(E(\varepsilon_t^L)\right)^2 = E((\varepsilon_t^L)^2) = E((E(L_t^a) - L_t^a)^2) \tag{4.3}$$

$$(\sigma_t^L)^2 \approx \frac{k^L}{10000}(L_t^a)^2 \tag{4.4}$$

where σ_t^L and k^L represent the standard deviation of ε_t^L and the accuracy of the forecasting method, respectively.

4.1.2 Forecasts for Wind Power Generation

In power systems, the wind power forecasts are generated from wind speed forecasts. According to Liu et al. (2012), wind speed forecast can also be modelled as the sum of expected wind speed and an error term following Normal distribution with mean zero. Since a wind turbine has a nonlinear relationship while converting wind speed into wind power, wind power forecast error does not follow a Normal distribution. Instead, it is observed to follow a β distribution in different studies carried out by Bofinger et al. (2002) and Fabbri et al. (2005). Although wind power forecast error follows a β distribution, since we are considering the integration of a large number of wind farms located in different regions or areas in a power system, it could be

approximated as Normal distribution thanks to the central limit theorem. Besides, such an approximation can be applied to any form of a smooth probability distribution (Ross, 2007), which is one of the commonly used methods in the literature. With the assumption that a hybrid power system contains many wind turbines dispersed in a wide geographical area, the wind power forecasts are also modelled by the same relation as in load demand forecasts:

$$W_t^f = E(W_t^a) = W_t^a + \varepsilon_t^W \tag{4.5}$$

where W_t^f, W_t^a and ε_t^W represent forecasted wind power, actual wind power and an error related to wind power forecast in period *t*, respectively. The mean of the error term in period *t* is calculated as follows:

$$E(\varepsilon_t^W) = E(W_t^a) - E(W_t^a) = \sum_{f=1}^{|NF|} \sum_{i=1}^{n_f} \left(E\left(W_{ift}\right) - E\left(W_{ift}\right) \right) = 0 \tag{4.6}$$

where NF, n_f and W_{ift} denote the set of wind farms in a power system and number of wind turbines in wind farm *f*, the random wind power generated by wind turbine *i* in wind farm *f* in period *t*, respectively.

The calculation of the variance of wind power forecast errors are not as straightforward as in the case of load demand forecast errors since the wind power generation is dependent on weather conditions of wind farms located in different regions. Hence, correlations of the wind power generation within a wind farm and between wind farms must also be taken into account when calculating the overall variance. The relationship of wind power forecast errors in the same wind farm f can be approximated by a correlation coefficient ρ_{ff} depending on the dispersion of wind turbines within the wind farm and wind speeds in the region. Similarly, the relationship of wind power forecast errors between wind farms f and g can be approximated by a correlation coefficient ρ_{fg}. When those wind farms are located in regions that are far away from each other, the dependence between wind farms significantly decrease, so ρ_{fg} takes very small values, even a value of zero.

$$(\sigma_t^W)^2 = E((\varepsilon_t^W)^2) - E(\varepsilon_t^W)^2 = E((\varepsilon_t^W)^2) \tag{4.7}$$

$$\begin{aligned} E((\varepsilon_t^W)^2) &= E\left[\left(\sum_{f=1}^{|NF|}\sum_{i=1}^{n_f} W_{ift} - \sum_{f=1}^{|NF|}\sum_{i=1}^{n_f} E(W_{ift})\right)^2\right] \\ &= \sum_{f=1}^{|NF|}\sum_{i=1}^{n_f} E(W_{ift}^2) \\ &+ 2\sum_{f=1}^{|NF|}\sum_{i=1}^{n_f-1}\sum_{j=i+1}^{n_f}\left(\rho_{ff}\sigma_{ift}\sigma_{jft} + E(W_{ift})E(W_{jft})\right) \\ &+ 2\sum_{f=1}^{|NF|-1}\sum_{g=f+1}^{|NF|}\sum_{i=1}^{n_f}\sum_{j=1}^{n_g}\left(\rho_{fg}\sigma_{ift}\sigma_{jgt} + E(W_{ift})E(W_{jgt})\right) \\ &- \left(\sum_{f=1}^{|NF|}\sum_{i=1}^{n_f} E(W_{ift})\right)^2 \end{aligned} \tag{4.8}$$

When identical wind turbines are used in all wind farms, then the variance of wind power forecast errors is simplified down to the following expression (Söder, 1993):

$$\begin{aligned} (\sigma_t^W)^2 &= \sum_{f=1}^{|NF|} n_f E(W_{ift}^2) + \sum_{f=1}^{|NF|} n_f(n_f-1)E(W_{ift}W_{jft}) \\ &+ \sum_{f=1}^{|NF|-1}\sum_{g=f+1}^{|NF|} n_f n_g E(W_{ift}W_{jgt}) - \left(\sum_{f=1}^{|NF|} n_f E(W_{ift})\right)^2 \\ &= \sum_{f=1}^{|NF|}\left[n_f\left(1+(n_f-1)\rho_{ff}\right)\sigma_{ift}^2 + \left(n_f E(W_{ift})\right)^2\right. \\ &\left. + 2\sum_{g=f+1}^{|NF|} n_f n_g\left(\rho_{fg}\sigma_{ift}\sigma_{jgt} + E(W_{ift})E(W_{jgt})\right)\right] \\ &- \left(\sum_{f=1}^{|NF|} n_f E(W_{ift})\right)^2 \end{aligned} \tag{4.9}$$

where σ_{ift} denotes the standard deviation of wind power generated by wind turbine i in wind farm f in period t and σ_t^W represents the standard deviation of ε_t^W.

4.1.3 Forecasts for Net Load Demand

Load demand forecasts and wind power generation forecasts are linked with each other by considering generation of the renewable energy sources as a negative load under certain assumptions, which are listed below:

- No interdependency between load demand forecasts and wind power forecasts
- Identically distributed forecast errors (Normal distribution)

By doing so, the net load demand in each period can be represented as the subtraction of total power generated by the renewable energy resources from system's total load demand in each period:

$$D_t^f = L_t^f - W_t^f = D_t^a + \varepsilon_t^D \quad (4.10)$$

where $D_t^a = L_t^a - W_t^a$ representing the net load demand in period *t* and $\varepsilon_t^D = \varepsilon_t^L + \varepsilon_t^W$ representing forecast error of the net load demand in period *t*.

Accordingly, the forecast error of the net load demand in period *t* follows Normal distribution with expectation zero and the variance as:

$$(\sigma_t^D)^2 = (\sigma_t^L)^2 + (\sigma_t^W)^2 \quad (4.11)$$

4.1.4 Reliability Model for Conventional Generation

A conventional generating unit's availability in each period can be modeled as a two-state Discrete Time Markov Process in which states represent whether a generating unit is available (fully functional) or it is not available (broken down) (Billinton and Allan, 1996). That is, there are two types of events that can occur at the beginning of each period, which are failure and repair. The repair and failure durations are exponentially distributed with rates λ_i and μ_i, respectively. A rate diagram for two-state Discrete Time Markov Process is depicted in Figure 4.1.

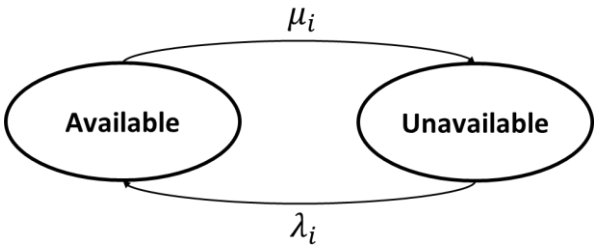

Figure 4.1. Two-State Discrete Time Markov Process Rate Diagram for the Reliability Model of a Conventional Generating Unit

For a conventional generating unit *i*, its availability and unavailability status should be defined as time-dependent. The expressions for unavailability and availability probabilities are summarized below:

$$U_i(t) = \frac{\mu_i}{\mu_i + \lambda_i} * \left(1 - e^{-(\mu_i+\lambda_i)t}\right); \qquad A_i(t) = 1 - U_i(t) \qquad (4.12)$$

The first term in $U_i(t)$ is the probability of "Failure" type of event that occurs first for unit *i*, and the second one is the proability of an event occurrence in a time interval with length of *t* for unit *i*. In power systems, $U_i(t)$ can also be referred to as Failure Probability or Outage Replacement Rate of unit *i* (ORR_i).

Since we are solving a day ahead UCP with hourly time periods, we can assume that a unit cannot be repaired or renewed in such a short time, so the repair rates λ_i can be ignored in the reliability model shown in Figure 4.1. With this simplifying assumption, unavailability and availability probabilities of unit *i* can be expressed as:

$$U_i(t) = 1 - e^{-\mu_i t}; \qquad A_i(t) = 1 - U_i(t) \qquad (4.13)$$

4.1.4.1 Capacity Outage Probability Table

To calculate the expected energy not served (EENS) for a given load level, it is essential to know the probability of the specific capacity outage or the loss of generation level. For this purpose, Capacity Outage Probability Table (COPT) is

constructed for a specific set of conventional generating units. As the name implies, it is a table that consists of capacity outage levels and the corresponding probabilities. Those probabilities can easily be calculated by using Binomial distribution if all generating units were identical; that is, each had the same capacity level and failure probability. However, in general, it is not the case for a real power generation system. Hence, it is needed to develop an efficient algorithm to evaluate each combination having same the capacity outage level in order to find the corresponding outage probability. The steps of our algorithm is provided below.

1. Evaluate every possible failure combination for a given set of generating units.
2. For each combination, calculate the capacity outage and the probability of the associated combination.
3. For each capacity outage, sum the failure probabilities and let it be the probability of the associated capacity outage.

Consider a system with three generating units, two of which have a 12 MW capacity while one of which has a 20 MW capacity with a failure probability of 0.02. By using the abovementioned algorithm, COPT can be easily constructed for this 3-Unit system and it is shown in Table 4.1.

Table 4.1. Capacity Outage Probability Table for a 3-Unit System

Unit(s) Out of Service	**Capacity Outage (MW)**	**Probability**
None	0	0.941192 = (0.98) (0.98) (0.98)
Unit 1 or Unit 2	12	0.038416 = (0.02) (0.98) (0.98) + (0.98) (0.02) (0.98)
Unit 3	20	0.019208 = (0.98) (0.98) (0.02)
Units 1 and 2	24	0.000392 = (0.02) (0.02) (0.98)
Units 1 and 3 or Units 2 and 3	32	0.000784 = (0.02) (0.98) (0.02) + (0.98) (0.02) (0.02)
Units 1, 2 and 3	44	0.000008 = (0.02) (0.02) (0.02)

There are also other algorithms to build a capacity outage probability table by constructing it in a recursive manner, by taking the continuous approximation of outages or by applying Fourier transform method based on the Gram-Charlier expansion to the continuous approximation. These are explained in detail by Billinton and Allan (1996).

4.1.4.2 Reliability Indices for Power Generation

In general, there are deterministic and probabilistic power system reliability assessment methods to evaluate the adequacy of generation capacity. Deterministic indices have an important drawback, since they do not take the stochastic nature of the load demand and conventional generation system into account when assessing the reliability of the whole system, whereas the probabilistic indices can indicate more significant insights on the reliability performance of the whole system. The probabilistic methods can be further divided into two classes, namely, Monte Carlo simulation and analytical techniques. In Monte Carlo simulation, the reliability indices are calculated as mean statistics found by actual system simulation. In analytical techniques, these indices are directly expressed by mathematical and probabilistic expressions. The most commonly used reliability indices are Loss of Load Probability (LOLP), Loss of Load Expectation (LOLE), Expected Load Not Served (ELNS) and Expected Energy Not Served (EENS) which are summarized below (Billinton and Allan, 1996; Prada, 1999).

Loss of Load Probability

$LOLP_t$ is used to evaluate the generation adequacy to meet the load demand in a conventional generation system in period *t*. It can also be considered how many times the available generation capacity is expected to be insufficient to satisfy the load demand in the long run. Its value is evaluated by the probability of the available capacity being less than the load demand. It is given by the expression below, where L_t is a continuous random variable corresponding to the load demand in period t, C_t

is a discrete random variable corresponding to the available capacity in period *t*. It is not possible to explicitly know the distribution of $L_t - C_t$ since they are different types of random variables. Thus, by using Bayesian Theorem, this probability expression can be evaluated by conditioning L_t on the possible discrete values of C_t as follows:

$$LOLP_t = P(L_t > C_t) = \sum_k \left(P(L_t > C_t | C_t = C_k)\, P(C_t = C_k)\right) \qquad (4.14)$$

The probability $P(C_t = C_k)$ can be found from the COPT tables easily. For a capacity outage amount of O_k, C_k is the capacity in use when k^{th} outage occurs and it is found by the difference $C_t^I - O_k$ where C_t^I is the installed capacity level in period t. When the load is assumed to be known and constant, L_t will be equal to its expected value $\bar{L_t}$ for period *t*. In this case, the conditional probability $P(L_t > C_t | C_t = C_k)$ can take two distinct values. It will be 0 if $\bar{L_t} \leq C_t$ and 1 if $\bar{L_t} > C_t$. For this constant load assumption, $LOLP_t$ can be found directly from the COPT tables. When the load demand is expressed in terms of forecasts with an error having a known distribution, this conditional probability $P(L_t > C_t | C_t = C_k)$ can be calculated for a given capacity in use C_k with the help of its probability density function of $f_l(L_t)$ as follows:

$$P(L_t > C_t | C_t = C_k) = \int_{C_k}^{\infty} f_l(L)\, dl \qquad (4.15)$$

Loss of Load Expectation

When the load is expressed in terms of load duration curves, the conditional probability for $LOLP_t$ has a different meaning which is the percentage of time that the load demand cannot be met by the capacity in use in period *t* and denoted by T_k. As a result, the following expression defines the expected loss of load duration or the expected percentage of time the load demand will be less than or equal to the capacity in use during period *t*.

$$LOLE_t = \sum_k \left(T_k \, P(C_t = C_k)\right) \tag{4.16}$$

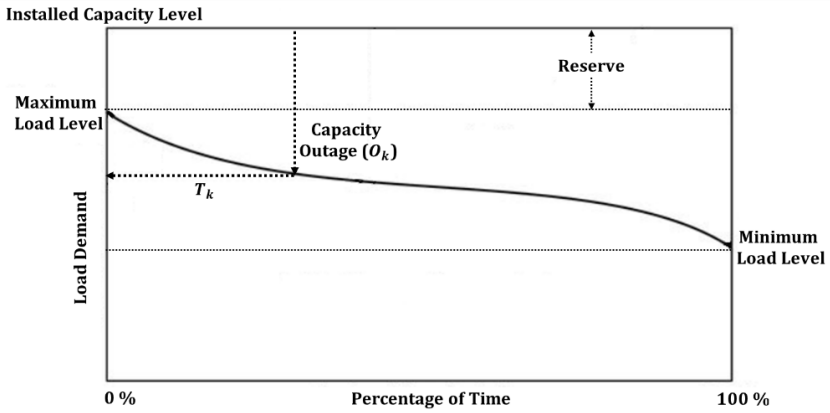

Figure 4.2. Representation of a Load Duration Curve

To find T_k, load duration curves are used. In these curves, the load level in a time period (hour) is estimated by a nonlinear curve between maximum and minimum expected load levels. In Figure 4.2, the horizontal axis represents the percentage of time the load demand will exceed the capacity in use, and the vertical axis represents the system load level and the installed capacity level. T_k is found by locating O_k on this curve as shown in Figure 4.2. The value projected on horizontal axis gives T_k as the percentage of time in which the load demand will be greater than the available generation capacity when there is a capacity outage level of O_k.

Expected Load Not Served

Since $LOLE_t$ just gives an information on the expected duration of the loss of load during period *t*, another reliability index is used to estimate the expected amount of load demand that cannot be served during period *t* which is denoted by $ELNS_t$ as follows:

$$ELNS_t = \sum_k \left(E[L_t > C_t | C_t = C_k] \, P(C_t = C_k)\right) \tag{4.17}$$

where $E[L_t > C_t | C_t = C_k]$ is the expected load demand that cannot be served during period *t*, given that the capacity in use in period *t* is equal to C_k. This conditional expectation is calculated by a probability density function of $f_l(L)$ with the following integral:

$$ELNS_t^k = E[L_t > C_t | C_t = C_k] = \int_{C_k}^{\infty} (L - C_k)\, f_l(L) dl \qquad (4.18)$$

When the load duration curves are used to evaluate this conditional expectation, it is simply the difference between the maximum load level of period *t* and the capacity in use during this period as shown in Figure 4.3. By multiplying this conditional expectation with the corresponding probability of the capacity outage, and summing them up for all possible outages, $ELNS_t$ for period *t* is estimated.

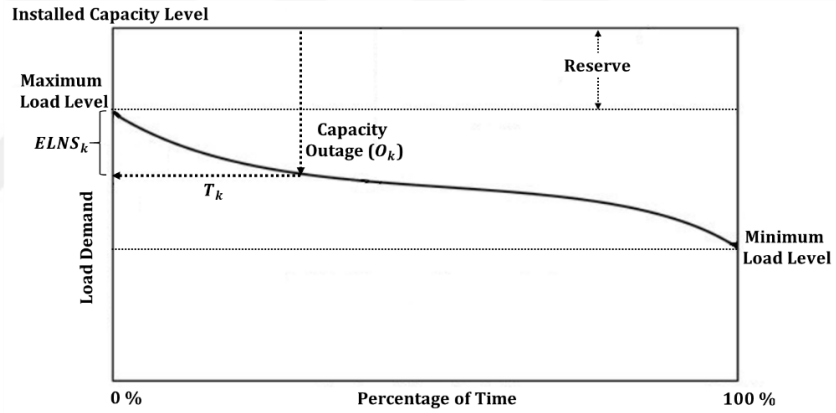

Figure 4.3. Expected Load Not Served for the k^{th} Outage by Using the Load Duration Curve

Expected Energy Not Served

Another reliability index is defined for estimating the expected amount of energy that cannot be served during a period. $EENS_t$ is one of the most commonly used indices in power generation scheduling since it represents the expected lost amount of energy (MWh) in terms of the consumer's point of view. It is calculated by the following expression where h denotes the length of time period *t*:

$$EENS_t = \sum_k \left(h\, E[L_t > C_t | C_t = C_k]\, P(C_t = C_k) \right) \qquad (4.19)$$

The conditional expectation in this expression is calculated by using the probability density function of the load demand as explained in $ELNS_t$. It should be noted that when the length of the time period is 1 hour, then $EENS_t$ and $ELNS_t$ are equal.

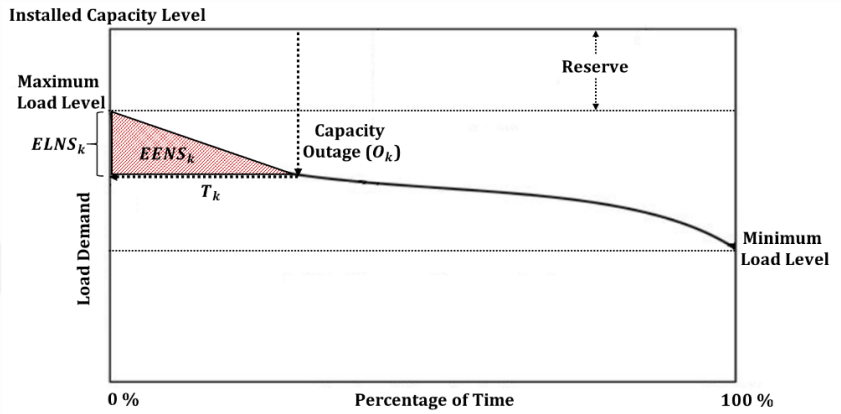

Figure 4.4. Expected Energy Not Served for the k^{th} Outage by Using the Load Duration Curve

When the load duration curves are used to evaluate $EENS_t$ of an outage *k*, it is the area between the load duration curve and the capacity in use when k^{th} outage occurs in this period. It is shown by the shaded area in Figure 4.4 and calculated by the following integral where $g_l(L)$ denotes the load duration function in terms of load and $h_x(X)$ denotes the same function in terms of percentage of time that the load exceeds the capacity in use, and L_t^{Max} is the maximum load level in period *t*:

$$EENS_t^k = \int_{C_k}^{L_t^{Max}} (L - C_k)\, g_l(L) dl = \int_0^{T_k} x\, h_x(X) dx \qquad (4.20)$$

By multiplying the $EENS_t^k$ with the corresponding probability of the capacity outage, and summing them up for all possible outages, $EENS_t$ for period *t* is estimated as follows:

$$EENS_t = \sum_k \left(EENS_t^k \; P(C_t = C_k) \right) \qquad (4.21)$$

4.2 Proposed Time-decoupled Quadratic Programming Based Approach

In the proposed approach, the unit commitment problem with supply/demand uncertainty is time-decoupled by decomposing the original UCP into *T* many subproblems each of which is a single-period UCP defined for each period in the planning horizon. Accordingly, each subproblem is optimally solved by balancing the potential benefits to be obtained by reducing $EENS_t$, and potential losses caused by not committing enough reserve in period *t*. In time-decoupled subproblems, time dependent UCP constraints, namely minimum uptime, minimum downtime, ramp-up and ramp-down constraints, are also taken into account. Although our time-decoupled method may yield near optimal solutions, it is very difficult to optimize the UCP under supply/demand uncertainties for the whole planning horizon without using some kind of risk levels like maximum allowable $EENS_t$, $LOLP_t$ or $LOLE_t$ for the periods. However, defining such risk levels results in overlooking the costs due to variabilities in load demand forecasts, wind power forecasts, and potential outages. For this reason, unit commitment (UC), economic load dispatch (ELD) and spinning reserve decisions are individually determined for each period through time-decoupled cost-benefit optimization rather than multi-period optimization.

4.2.1 Uncertainty Caused by Net Load Demand Forecast Errors

As it is pointed out in Section 4.1 it is not possible to know exact load and power generation by the renewable energy sources before solving UC and ELD problem. That is, their values should be estimated by using forecasting tools prior to their actual realizations so that the day-ahead UC, ELD and SR decisions can be made.

To cope with the forecasting errors of load and wind power generation, the term net load demand (D_t^f) has been defined in Section 4.1.3. According to this new

definition, it is shown that the standard deviation of aggregate forecast error (ε_t^D) can be calculated as the square root of the sum of the variances of corresponding Normally distributed forecast errors. However, D_t^f is a continuous random variable as a result of ε_t^D whereas the uncertainties related to the reliability of conventional generating units are discrete random variables; in addition, the Normal distribution has a complex and nonlinear nature. To tackle with this situation, the probability distribution of D_t^f is discretized by using a multi-interval approximation. For this purpose, the cumulative density function of D_t^f is divided into K_L odd number of intervals whose probability values (p_l) are represented by the following expression:

$$p_l = \phi_{\left(D_t^f - \left(\frac{K_L}{2} - l\right)\sigma_t^D\right)} - \phi_{\left(D_t^f - \left(\frac{K_L}{2} - l + 1\right)\sigma_t^D\right)} \quad (4.22)$$

The mid-value of each interval (a_l) is considered as the value of the whole interval. They are represented by the following expression:

$$a_l = D_t^f - \left(\frac{K_L}{2} - l + 0.5\right)\sigma_t^D \quad (4.23)$$

In our approach, the seven-interval approximation is used for the discretization of the Normally Distributed D_t^f in each period *t* as shown in Figure 4.5.

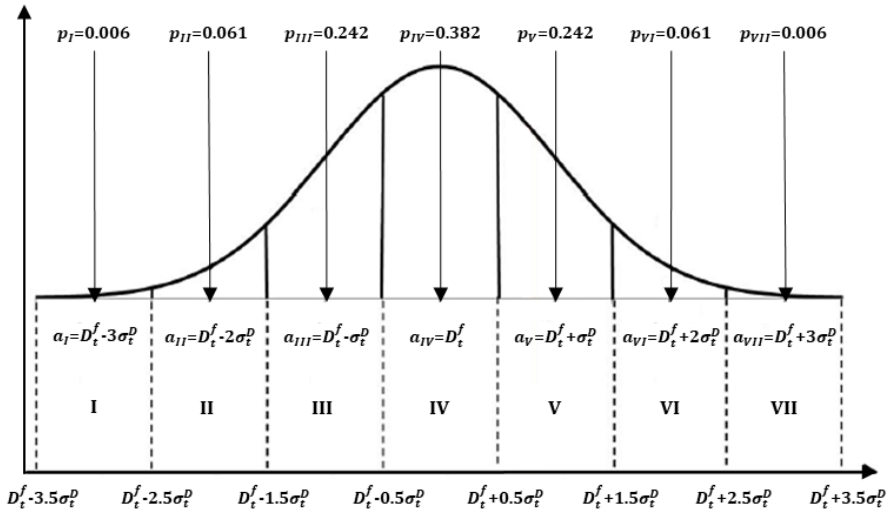

Figure 4.5. Seven-Interval Approximation for the Normally Distributed Net Load Demand for Period *t*

4.2.2 Reliability Based Uncertainty in Conventional Generation

To compute $EENS_t$ in a conventional generation system, there are several factors such as conventional units operating, their forced outage probabilities, amount of SR to be committed by "On" units and the load demand. For a given set of units in "On" status, the COPT could be constructed by using our algorithm explained in Section 4.1.4. Hence, it is essential to make commitment decisions before making COPT calculations. By using the COPT and the conditional expectation method explained in Section 4.1.4, $EENS_t$ can be computed for a given combination of "On" units, but EENS calculations for all possible committed capacity levels require a significant computational burden in a complex power system. The reason is that the number of outage combinations to be evaluated increases exponentially as the number of "On" units in the system increases.

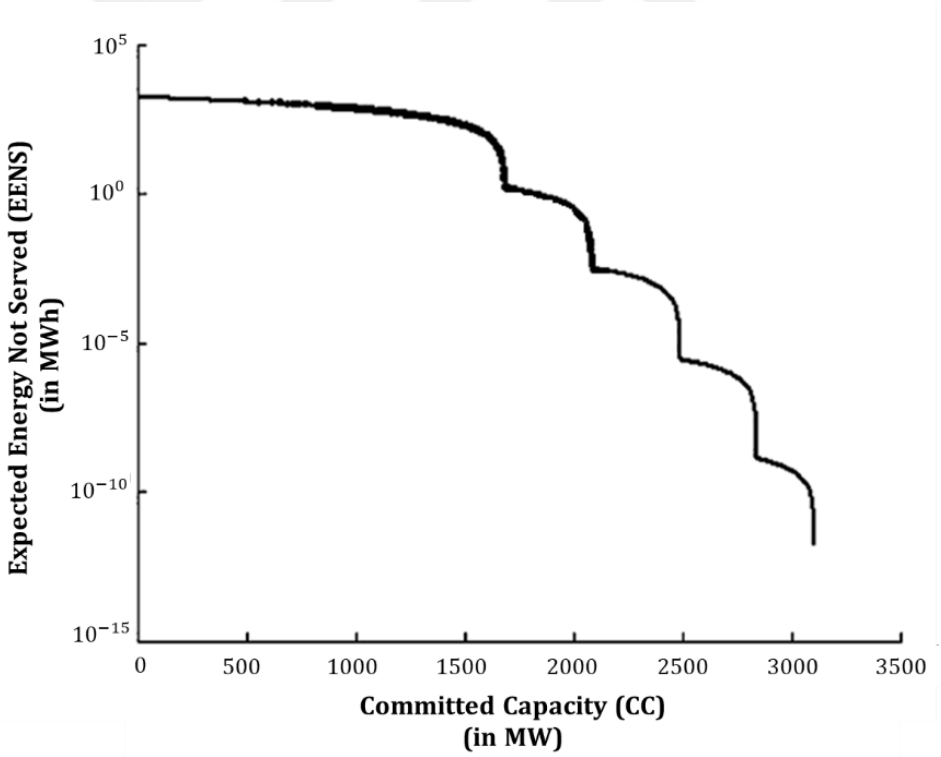

Figure 4.6. Relationship between Expected Energy Not Served and Committed Capacity, Adapted from Ortega-Vazquez et al. (2006)

Ortega-Vazquez et al. (2006) shows the nonlinear relationship between $EENS_t$ and Committed Capacity (CC) for IEEE Reliability Test System having 26 units with a generation capacity of 3105 MW for a constant load demand level of 1690 MW as demonstrated in Figure 4.6. There is an inverse relationship between $EENS_t$ and CC. Thus, smaller CC indicates that most of the generating units are loaded heavily whereas higher CC indicates that generation units are loaded partially.

The concept that such a nonlinear relationship can be approximated by its piecewise linear equivalent is first proposed by Ortega-Vazquez et al. (2006). Starting from upper left to lower right in Figure 4.6, they show that the first breakpoint represents *CC=Load Level*, the second one corresponds to *CC=Load Level + Capacity of the Largest "On" unit*, the third one denotes *CC=Load Level + Capacities of the Largest and the Second Largest "On" units*, and so on. The reason of a sudden drop between adjacent break points is that one more unit should fail simultaneously with the other ones at that break point. To determine $EENS_t$ of any breakpoint, they propose an auxiliary optimization method instead of full search for the unit combination having maximum $EENS_t$ with CC of a breakpoint since such a search would be very time-consuming. Thus, they suggest using a weighted sum approach with three main objectives:

- The committed capacity should be very small
- The number of committed units should be very small
- The unit combination with the most unreliable units should be in operation

However, the combination obtained by the weighted sum approach depends heavily on the weights given to those objectives. Hence, finding the right set of weights requires extensive experimentation for each load level in each period, which is a computationally prohibitive operation for a day ahead UCP.

To overcome this problem, we propose the use of preemptive (lexicographic) optimization instead of a weighted sum approach to find the right combination owing to its parameter-free structure. To apply this method, the objectives are sorted from the most important one to the least important one as follows:

1. The most important objective: Having the smallest committed capacity is the top priority objective since CC being closer to the value on the break point results in a more accurate approximation:

$$z_1 = \sum_i C_i \gamma_i \tag{4.24}$$

where z_1 is the objective function representing the total committed capacity, γ_i and C_i are binary variable representing "On (1) / Off (0)" status of unit i and maximum generation capacity of unit i, respectively.

2. The second important one: Having the smallest number of committed units for a given CC is the second priority objective since $EENS_t$ is maximized when there is a smaller number of units that yields the same CC value:

$$z_2 = \sum_i \gamma_i \tag{4.25}$$

where z_2 is the objective function representing the total number of committed units.

3. The least important one: Having the most unreliable units for a given CC is the third priority objective since $EENS_t$ is maximized with the most unreliable set of units that yields the same CC value:

$$z_3 = \prod_i \left((1 - ORR_i)\gamma_i\right) \tag{4.26}$$

where z_3 is the objective function representing the reliability of the units committed, ORR_i is the outage replacement rate of unit i. To handle the nonlinearity in z_3, it can be represented as follows:

$$z_3 = \sum_i \left(\ln(1 - ORR_i)\, \gamma_i\right) \tag{4.27}$$

Then, the following lexicographic optimization method is applied to each breakpoint in Figure 4.6. Its pseudocode is provided below where *N* is the set of units and *M* is the CC value on a breakpoint.

Step 1: Let k=1 and solve the following linear mathematical model.

$$Min\{ z_1\}$$

$$s.to. \quad \sum_i C_i\gamma_i \geq M$$

$$\gamma_i \in \{0,1\} \quad \forall\, i \in N$$

Let the optimal solution for the 1st objective, $z_1^* = d_1$

Step 2: k=k+1

If k >3; Stop, the resulting γ_i (s) are the unit combination that will maximize $EENS_t$ on the breakpoint.

Otherwise, solve the following linear mathematical model.

$$Min\{ z_k\}$$

$$s.to. \quad \sum_i C_i\gamma_i \geq M$$

$$z_j = d_j \quad \forall\, j = 1, \dots, k-1$$

$$z_j \geq 0 \quad \forall\, j = 1, \dots, k-1$$

$$\gamma_i \in \{0,1\} \quad \forall\, i \in N$$

Let the optimal objective value for the k^{th} objective, $z_k^* = d_k$ and repeat Step 2.

4.2.3 Expected Energy Not Served (EENS) under Supply/Demand Uncertainty: Piecewise Linear Approximation

When approximating $EENS_t$, we are inspired from the work of Ortega-Vazquez et al. (2006) in which they model $EENS_t$ by assuming that the load demand is

deterministic and the reliability of conventional generating units is the only source of uncertainty. Different from their work, we consider uncertainties in the load demand, wind power generation and the reliability of conventional generating units. In our approach, we propose two methods for integrating the net load uncertainty with the reliability model of conventional generation. In Method I, $EENS_t$ is approximated with one piecewise linear model whereas, in Method II, $EENS_t$ is approximated with seven piecewise linear models corresponding to the intervals in the seven-interval approximation of D_t^f explained in Section 4.2.1.

4.2.3.1 Approximation Method I

In Figure 4.7, the black lines indicate the nonlinear relationship between $EENS_t$ and CC, and the red lines show its piecewise linear approximation.

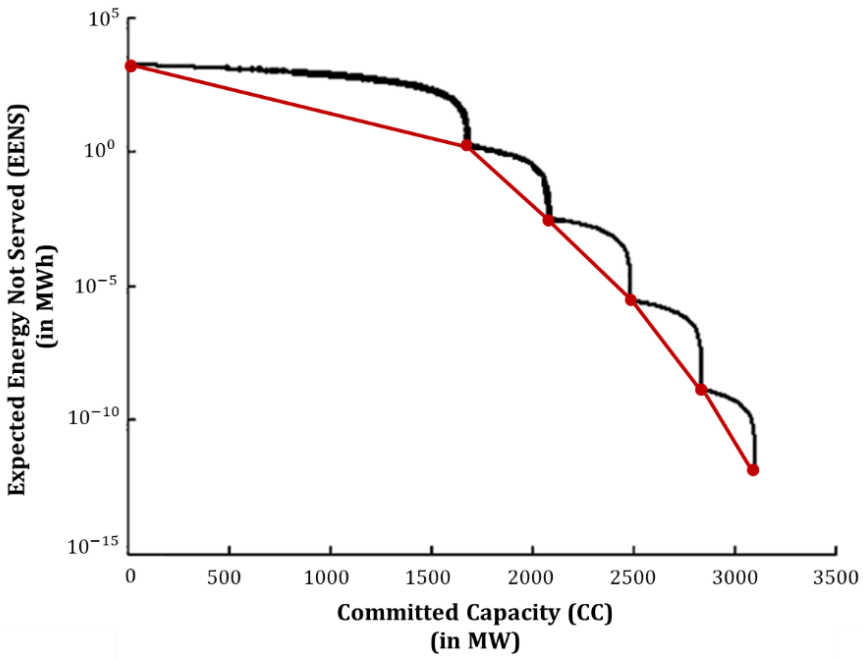

Figure 4.7. Piecewise Linear Approximation of Expected Energy Not Served and Committed Capacity

With this method, the *CC* values at each breakpoint can be modeled as:

- At the first breakpoint: *CC=Expected Net Load Level in period t*,
- At the second breakpoint: *CC=Expected Net Load Level in period t + Capacity of the Largest conventional generating unit available in period t*,
- At the third breakpoint: *CC=Expected Net Load Level in period t + Capacities of the Largest and the Second Largest conventional generating units available in period t*,

  ⋮
- At the last breakpoint: *CC=Total installed capacity available in period t*

After determining the committed capacities at each breakpoint, the right combination of units that will maximize the expected energy not served at each breakpoint is found by using the lexicographic optimization method explained in Section 4.2.2. According to the combinations of units for each breakpoint *b*, the corresponding $EENS_{bt}^{l}$ values are calculated by using the seven-interval approximation of D_t^f and the COPT tables. For each mid-value (a_l) of the net load demand in the seven-interval approximation, $EENS_{bt}^{l}$ at breakpoint *b* corresponding to interval *l* is calculated by summing the load shedding level with the probabilities of outage *k* causing a load shedding over all possible outages. Since the planning horizon (24 h) in our UCP formulation consists of 1-hour time periods, the $EENS_{bt}^{l}$ and $ELNS_{bt}^{l}$ will be equal as shown below:

$$EENS_{bt}^{l} = ELNS_{bt}^{l} = \sum_{k} \left(\text{Max}(a_l - C_t, 0)\, P(C_t = C_k) \right) \qquad (4.28)$$

By taking the expected value of $EENS_{bt}^{l}$ over all possible intervals in the seven-interval approximation, the $EENS_{bt}$ value of the breakpoint *b* is calculated:

$$EENS_{bt} = E\left[EENS_{bt}^{l}\right] = \sum_{l} \left(p_l\, EENS_{bt}^{l} \right) \qquad (4.29)$$

It is important to note that this procedure to find $EENS_{bt}$ estimation must be repeated for each breakpoint and for each period in the planning horizon prior to

implementing our approach so that the nonlinear concave relationship between *CC* and $EENS_t$ can be modelled for each period.

4.2.3.2 Approximation Method II

In this method, the uncertainty in the net load demand is separately integrated into the $EENS_t$ approximation. Since the uncertainty is discretized by the seven-interval approximation as discussed in Section 4.1, $EENS_t$ can be approximated by separate piecewise linear models associated with the mid-values of each load demand interval as shown in Figure 4.8.

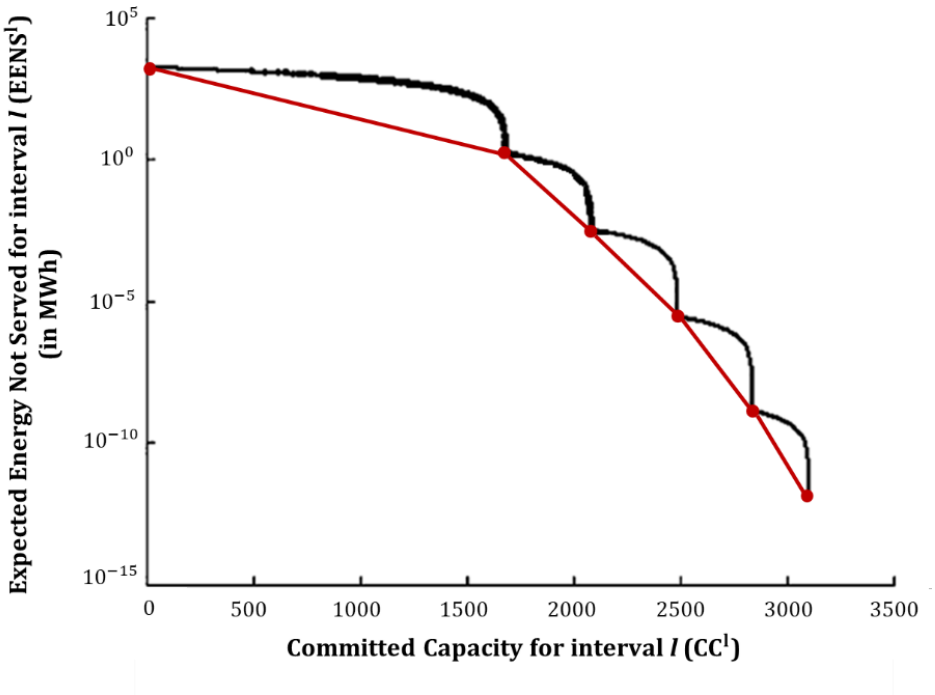

Figure 4.8. Piecewise Linear Approximation of Expected Energy Not Served and Committed Capacity for Interval *l* in Seven Interval Approximation

With this method, the mid-value a_l is considered as the load demand in each piecewise linear model of interval *l* so the CC^l values at each breakpoint can be modeled as:

- At the first breakpoint: *CC^l=The mid-value of interval l in period t,*
- At the second breakpoint: *CC^l=The mid-value of interval l in period t + Capacity of the Largest conventional generating unit available in period t,*
- At the third breakpoint: *CC^l=The mid-value of interval l in period t + Capacities of the Largest and the Second Largest conventional generating units available in period t,*

  ⋮
- At the last breakpoint: *CC^l=Total installed capacity available in period t*

After determining the committed capacities at each breakpoint, the right combination of units that will maximize the expected energy not served at each breakpoint is found by using the lexicographic optimization method explained in Section 4.2.2. According to the combinations of units for each breakpoint *b*, the corresponding $EENS_{bt}^{l}$ values are calculated by using the seven-interval approximation and the COPT tables. $EENS_{bt}^{l}$ at breakpoint *b* for interval *l* is calculated by summing the load shedding level with the probabilities of outage *k* causing a load shedding over all possible outages:

$$EENS_{bt}^{l} = ELNS_{bt}^{l} = \sum_{k} \left(\text{Max}(a_l - C_t, 0)\, P(C_t = C_k)\right) \qquad (4.30)$$

Similar to Method I, this procedure must also be repeated for each breakpoint, for each interval of load demand, and for each period in the planning horizon prior to implementing our approach so that the nonlinear concave relationship between CC^l and $EENS_t^l$ can be modelled for each load demand interval in each period.

4.2.4 Mixed Integer Quadratic Programming (MIQP) Formulations

The proposed method consists of two MIQP formulations distinguished by the type of expected energy not served approximation used in each formulation. Those formulations have been implemented in MATLAB by using CPLEX Optimizer. In these formulations, standard UCP constraints such as power balance constraints and

minimum/maximum generation limits are taken into account. Furthermore, the time-dependent constraints like the minimum uptime/downtime constraints and the ramp-up/ramp-down limits are separately included in the mathematical models of each period since the UCP is solved in a time-decoupled manner. Different from the standard formulations of the UCP, for each period, the reserves are taken as decision variables whose values are determined by the trade-off between total operational costs and the expected cost of load shedding (energy not served) instead of using standard spinning reserve requirements. For this purpose, $EENS_t$ is piecewise linearly approximated as described in Section 4.2.3, and the value of lost load ($VOLL$) is used to calculate the expected cost of lost shedding. $VOLL$ is defined as the dollar value that users place on the loss for outage of 1 MWh of electricity; that is, it is the opportunity cost for households and businesses that are deprived of 1 MWh electricity. According to Kariuki et al. (1996), in general, it is estimated by consumer surveys.

4.2.4.1 Time-decoupled MIQP Formulation I

In this formulation, the objective function consists of fuel costs, start-up costs, reserve allocation costs and expected cost of load shedding. The last two of these costs have a linear relationship with the corresponding decision variables as reserves and $EENS_t$ modelled by Approximation Method I explained in Section 4.2.3. $EENS_t$ is piecewise linearly approximated with additional auxiliary variables, and constraints by using λ-*method* (Bradley et al., 1977).

The start-up costs depend on the commitment status in consecutive two time periods and the number of time periods in which a unit is in "Off" status. According to the length of the "Off" periods, the start-up costs are modelled by a two-step function comprising of hot start-up and cold start-up costs. This nonlinear relationship could be linearized by defining additional auxiliary binary variables and additional logical constraints. This conversion is not needed in our time-decoupled formulation, so the

start-up costs are calculated as parameters prior to implementing our formulation for each time period.

For conventional generating units, by assuming that their efficiencies increase monotonically with their power generation levels, the fuel costs are represented by a convex quadratic function which can also be approximated piecewise linearly by using *λ-method*. However, this approximation is not necessary in our formulation, because it is a MIQP type model in which the objective function contains both separable, strictly convex quadratic terms and linear terms; the decision variables include both binary and continuous ones, and the constraint set is linear. Furthermore, Quadratic Programming (QP) models have similar optimality conditions with Linear Programming (LP) models; owing to this property, there are specialized algorithms like Phase I Simplex to solve QP. The detailed explanation of the optimality conditions and some algorithms for QP can be found in Bradley et al. (1977). The mathematical model for Formulation I (MIQP I), is provided in this section. For each period in the planning horizon, this model is sequentially solved to obtain near-optimal schedules for the commitment, generation and reserve.

Assumptions

- The electricity market is vertically integrated, and customers place a high value on the energy not served. Hence, a power generation company is obliged to meet the load demand of its customers exactly.
- The load demands during the planning horizon are forecasted, so their actual realizations might be different.
- Similarly, the wind power generation during the planning horizon is also forecasted. Thus, the overproduction or underproduction by the wind turbines are possible.
- The errors in wind power and load demand forecasts are Normally distributed.
- During the planning horizon, conventional generating units are subject to unexpected outages which are exponentially distributed.

- The efficiency of a conventional generating unit shows a monotonic increase as it is more heavily loaded.
- A conventional generating unit can produce power within its available power generation limits.
- The power produced can be transmitted to the demand points without any transmission limits.
- Power losses during power transmission are negligible.

Sets and Indices

$N:$ Set of conventional generating units

$i \in N:$ Conventional generating unit *i*

T: Set of time periods (hours)

$t \in T$: Time period *t*

$N_t^{on} \subset N$: Set of conventional generating units that should remain committed in period *t* to satisfy minimum uptime requirement:

$$N_t^{on} = \{i \in N: 0 < T_{it}^{on} < T_{Min,\,i}^{on}\} \tag{4.31}$$

$N_t^{off} \subset N$: Set of conventional generating units that should remain uncommitted in period *t* to satisfy minimum downtime requirement:

$$N_t^{off} = \{i \in N: 0 < T_{it}^{off} < T_{Min,\,i}^{off}\} \tag{4.32}$$

Additional Sets and Indices for $EENS_t$ Approximation:

$B_t:$ Set of breakpoints in the piecewise linear $EENS_t$ approximation in period *t*

$b \in B_t:$ Breakpoint *b* for the piecewise linear $EENS_t$ approximation in period *t*

$E_t:$ Set of segments in the piecewise linear $EENS_t$ approximation in period $t \ni |E_t| = |B_t| - 1$

$e \in E_t:$ Segment *e* for the piecewise linear $EENS_t$ approximation in period *t*

Parameters

a_i, b_i, c_i: Fuel cost coefficients of unit *i* (\$, \$/MW, \$/MW^2, respectively)

q_i: Reserve allocation costs of unit *i* (\$/MW)

$VOLL$: Value of lost load (\$/MWh)

S_i^H: Hot startup cost of unit *i* (\$)

S_i^C: Cold startup cost of unit *i* (\$)

$T_{c,i}$: Startup time threshold of unit *i* (hour)

$T_{Min,\,i}^{off}$: Minimum downtime of unit *i* once it is shutdown (hour)

$T_{Min,\,i}^{on}$: Minimum uptime of unit *i* once it is started up (hour)

P_i^{Min}: Minimum power output level of unit *i* (MW)

P_i^{Max}: Maximum power output level of unit *i* (MW)

R_i^{up}: Ramp-up limit of unit *i* (MW)

R_i^{down}: Ramp-down limit of unit *i* (MW)

D_t^f: Net load demand in period *t* (MW)3

T_{it}^{off}: Number of periods that unit *i* remained decommitted up to period *t* (hour)

T_{it}^{on}: Number of periods that unit *i* remained committed up to period *t* (hour)

S_{it}: Start-up cost of unit *i* in period *t* generally depends on the number of time periods in which the unit is in "Off" status. According to the length of the "Off" periods, start-up costs are classified as hot start-up or cold start-up costs (\$):

$$S_{it} = \begin{cases} S_i^H & \text{if} \quad u_{it-1} = 0 \quad \& \quad T_{Min,\,i}^{off} \le T_{it}^{off} \le T_{Min,\,i}^{off} + T_{c,i} \\ S_i^C & \text{if} \quad u_{it-1} = 0 \quad \& \quad T_{it}^{off} > T_{Min,\,i}^{off} + T_{c,i} \\ 0 & \text{if} \quad u_{it-1} = 1 \end{cases} \qquad (4.33)$$

Additional Parameters for $EENS_t$ Approximation:

x_{bt}: *CC* value on breakpoint *b* in the piecewise linear $EENS_t$ approximation for period *t* (MW)

y_{bt}: $EENS_t$ value on breakpoint *b* in the piecewise linear $EENS_t$ approximation for period *t* (MWh)

CV_{be}^{t}: $|B_t|\ x\ |E_t|$ coverage matrix for adjacent breakpoints on each segment in the piecewise linear $EENS_t$ approximation for period *t*:

$$CV_{be}^{t} = \begin{cases} 1 \quad \text{if} \quad b = e \ and \ b = e + 1 \text{ in period } t \\ 0 \quad \text{otherwise} \end{cases} \tag{4.34}$$

Decision Variables

u_{it}: Commitment status of unit *i* in period *t*:

$$u_{it} = \begin{cases} 1 \text{ if unit } i \text{ is committed in period } t \\ 0 \text{ otherwise} \end{cases} \tag{4.35}$$

P_{it}: Amount of electricity generated by unit *i* in period *t*

R_{it}: Reserve allocated by unit *i* in period *t*

CC_t: Committed capacity in period *t*

$EENS_t$: Expected energy not served in period *t*

P_{it}^{Min}: Minimum power output level of unit *i* in period *t*:

$$P_{it}^{Min} = \begin{cases} \text{Max}\{P_i^{Min}, P_{it-1} - R_i^{down}\} & \text{if} \quad u_{it-1} = u_{it} = 1 \\ P_i^{Min} & \text{otherwise} \end{cases} \tag{4.36}$$

P_{it}^{Max}: Maximum power output level of unit *i* in period *t*:

$$P_{it}^{Max} = \begin{cases} \text{Min}\{P_i^{Max}, P_{it-1} + R_i^{up}\} & \text{if} \quad u_{it-1} = u_{it} = 1 \\ P_i^{Max} & \text{otherwise} \end{cases} \tag{4.37}$$

Additional Variables for $EENS_t$ Approximation:

λ_{bt}: Weight of breakpoint *b* on the piecewise linear $EENS_t$ approximation for period *t*

v_{et}: Segment *e* that CC_t lies on the piecewise linear $EENS_t$ approximation for period *t*:

$$v_{et} = \begin{cases} 1 \text{ if } CC_t \text{ lies on segment } e \text{ in period } t \\ 0 \text{ otherwise} \end{cases} \quad (4.38)$$

Mathematical Model: MIQP I

$$Min \sum_{i=1}^{|N|} (a_i u_{it} + b_i P_{it} + c_i {P_{it}}^2 + q_i R_{it} + S_{it} u_{it}) + (VOLL)(EENS_t) \quad (4.39)$$

$subject\ to$

$$\sum_{i=1}^{|N|} P_{it} \geq D_t^f \quad (4.40)$$

$$P_{it}^{Min} \leq P_{it} \leq P_{it}^{Max} \quad \forall i \quad (4.41)$$

$$P_{it}^{Max} \leq P_i^{Max} u_{it} \quad \forall i \quad (4.42)$$

$$P_{it}^{Max} \leq P_{it-1} + R_i^{up} + M_1(2 - u_{it-1} - u_{it}) \quad \forall i \quad (4.43)$$

$$P_{it}^{Min} \geq P_i^{Min} u_{it} \quad \forall i \quad (4.44)$$

$$P_{it}^{Min} \geq P_{it-1} - R_i^{down} + m_1(2 - u_{it-1} - u_{it}) \quad \forall i \quad (4.45)$$

$$R_{it} = \text{Min}\{R_i^{up} + P_{it-1} + M_2(1 - u_{it-1}), P_i^{Max}\} u_{it} - P_{it} \quad \forall i \quad (4.46)$$

$$CC_t = \sum_{i=1}^{|N|} (P_{it} + R_{it}) \quad (4.47)$$

$$u_{it} = 1 \quad \forall i \in N_t^{on} \quad (4.48)$$

$$u_{it} = 0 \quad \forall i \in N_t^{off} \quad (4.49)$$

$$CC_t = \sum_{b=1}^{|B_t|} x_{bt}\, \lambda_{bt} \tag{4.50}$$

$$EENS_t = \sum_{b=1}^{|B_t|} y_{bt}\, \lambda_{bt} \tag{4.51}$$

$$\sum_{b=1}^{|B_t|} \lambda_{bt} = 1 \tag{4.52}$$

$$\sum_{e=1}^{|E_t|} v_{et} = 1 \tag{4.53}$$

$$\begin{bmatrix} \lambda_{1t} \\ \vdots \\ \lambda_{|B_t|t} \end{bmatrix} \leq CV^{t}_{|B_t|\ x\ |E_t|} \begin{bmatrix} v_{1t} \\ \vdots \\ v_{|E_t|t} \end{bmatrix} \tag{4.54}$$

$$P_{it}, P_{it}^{Max}, P_{it}^{Min}, R_{it} \geq 0 \quad \forall i \tag{4.55}$$

$$\lambda_{bt} \geq 0 \quad \forall b \tag{4.56}$$

$$CC_t, EENS_t \geq 0 \tag{4.57}$$

$$u_{it} \in \{0,1\} \quad \forall i \tag{4.58}$$

$$v_{et} \in \{0,1\} \quad \forall e \tag{4.59}$$

Objective Function (4.39)

The objective is to minimize the sum of the fuel costs and the reserve allocation costs of committed units, the start-up costs of uncommitted units, and the expected cost of load shedding due to supply/demand uncertainty.

Constraints

Net Load Requirement Constraint (4.40): Also known as the power balance constraint which guarantees that total power generated by the committed units in period *t* should be greater than or equal to the net load demand in that period.

Unit Output Range Constraints (4.41): Unit *i* can generate power within its minimum and maximum generation limits available for period *t*.

Maximum Generation Limit Constraints (4.42): The maximum generation limit of unit *i* can be at most equal to its maximum generation capacity if it is committed in period *t.*

Ramp-up Constraints (4.43): Due to the thermal stress limitations and mechanical characteristics of the conventional generating units, the increase in the power output level of a committed unit is restricted by its ramp-up rate over consecutive time periods during which it remains committed.

In (4.43) M_1 is a very large number denoting upper bounds for Ramp-up Constraints.

Minimum Generation Limit Constraints (4.44): The minimum generation limit of unit *i* should be at least equal to its maximum generation capacity if it is committed in period *t.*

Ramp-down Constraints (4.45): Due to the thermal stress limitations and mechanical characteristics of the conventional generating units, the decrease in the power output level of a committed unit is restricted by its ramp-down rate over consecutive time periods during which it remains committed.

In (4.45), m_1 is a very small number denoting lower bounds for Ramp-down Constraints

Reserve Constraints (4.46): Reserve allocated by unit *i* in period *t* should be equal to the difference between its maximum generation capacity and generation level in that period if unit *i* is not committed in the previous period *t-1*. Otherwise, it can take the difference between the minimum of the sum of its ramp-up rate and generation level in the previous period *t-1* and maximum capacity for period *t*, and its generation level in that period.

In (4.46), M_2 is a very large number for Reserve Constraints.

Committed Capacity Constraint (4.47): Committed capacity in period *t* is the sum of power generations and reserves in that period.

Minimum Uptime Constraints (4.48): A unit cannot be turned off instantaneously once it is committed. The minimum uptime constraint imposes a minimum number of working time periods that must elapse before unit *i* can be turned off.

Minimum Downtime Constraints (4.49): A unit cannot be turned on instantaneously once it is decommitted. The minimum downtime constraint imposes a minimum number of idle time periods that must elapse before unit *i* can be turned on.

Piecewise Linear Approximation Constraints for $EENS_t$ (4.50,…,4.54): The values of CC_t and $EENS_t$ at each breakpoint for period *t* are determined according to the rules defined for Approximation Method I in Section 4.2.3. Accordingly, the concave nonlinear relationship between CC_t and $EENS_t$ is converted into its piecewise linear approximation with the following constraints:

- *(4.50)*: The approximation of Committed Capacity in period *t*.
- *(4.51)*: The approximation of Expected Energy Not Served in period *t*.
- *(4.52)*: The weights in the approximation for period *t* should add up to 1.
- *(4.53)*: Committed capacity can lie on one of the segments in the approximation for period *t*.
- *(4.54)*: There is a concave relationship between CC_t and $EENS_t$. Since we are trying to minimize the cost of $EENS_t$, we need to define the following set of constraints to satisfy the adjacency criterion (*at most two adjacent weights can be non-zero*) in the piecewise linear approximation for period *t*.

(4.55,…,4.59): Sign restrictions of decision variables.

4.2.4.2 Time-decoupled MIQP Formulation II

The only difference of this formulation from the MIQP I is that the approximation of $EENS_t$ which is modelled by using Approximation Method II explained in Section

4.2.3. $EENS_t$ of each interval in the seven-interval approximation of the net load demand is piecewise linearly approximated with additional auxiliary variables, and constraints by using *λ-method* (Bradley et al., 1977). The associated modifications for Formulation II (MIQP II) are provided below.

Sets and Indices

For each interval *l* in the seven-interval approximation of D_t^f, the following sets are defined instead of additional sets defined in the MIQP I.

Additional Sets and Indices for $EENS_t$ Approximation:

L: Set of net load demand intervals in the seven-interval approximation of D_t^f

$l \in L$: Net load demand interval *l*

B_t^l: Set of breakpoints in the piecewise linear $EENS_t$ approximation of interval *l* in period *t*

$b_l \in B_t^l$: Breakpoint b^l for the piecewise linear $EENS_t$ approximation of interval *l* in period *t*

E_t^l: Set of segments in the piecewise linear $EENS_t$ approximation of interval *l* in period *t* $\ni \left|E_t^l\right| = |B_t^l| - 1$

$e_l \in E_t^l$: Segment e_l for the piecewise linear $EENS_t$ approximation of interval *l* in period *t*

Parameters

For each interval *l* in the seven-interval approximation of D_t^f, the following parameters are defined instead of the additional parameters defined in the MIQP I.

Additional Parameters for $EENS_t$ Approximation:

A_t^l: Net load demand value (mid-value) of interval *l* in period *t* (MW)

p_l: Probability that load demand takes a value of A_t^l

$x_{b_l t}^l$: *CC* value at breakpoint b_l in the piecewise linear $EENS_t$ approximation for interval *l* in period *t* (MW)

$y_{b_l t}^{l}$: $EENS_t$ value on breakpoint b_l in the piecewise linear $EENS_t$ approximation for interval *l* in period *t* (MWh)

$CV_{b_l e_l}^{t}$: $\left|B_t^l\right| x \left|E_t^l\right|$ coverage matrix for adjacent breakpoints on each segment in the piecewise linear $EENS_t$ approximation for interval *l* and period *t*:

$$CV_{b_l e_l}^{lt} = \begin{cases} 1 \text{ if } b_l = e_l \text{ and } b_l = e_l + 1 \text{ in period } t \\ 0 \text{ otherwise} \end{cases} \quad (4.60)$$

Decision Variables

For each interval *l* in the seven-interval approximation of D_t^f, the following decision variables are defined instead of the additional variables defined in the MIQP I.

Additional Variables for $EENS_t$ Approximation:

$EENS_t^l$: Expected energy not served for interval *l* in period *t*

$\lambda_{b_l t}^{l}$: Weight of breakpoint b_l on the piecewise linear $EENS_t$ approximation for interval *l* in period *t*

$v_{e_l t}^{l}$: Segment e_l that CC_t lies on the piecewise linear $EENS_t$ approximation for interval *l* in period *t*:

$$v_{e_l t}^{l} = \begin{cases} 1 \text{ if } CC_t \text{ lies on segment } e_l \text{ in period } t \\ 0 \text{ otherwise} \end{cases} \quad (4.61)$$

Constraints

The constraints other than the piecewise linear approximation constraints for $EENS_t$ remain the same. λ_{bt} and v_{et} are removed from the sign restriction constraints in MIQP I.

Piecewise Linear Approximation Constraints for $EENS_t$: The values of CC_t and $EENS_t^l$ at each breakpoint for interval *l* in period *t* are determined according to the rules defined for Approximation Method II in Section 4.2.3. Accordingly, the

concave nonlinear relationship between CC_t and $EENS_t^l$ is converted into its piecewise linear approximation for each interval *l* with the following constraints:

- The approximation of Committed Capacity in period *t*:

$$CC_t = \sum_{b_l=1}^{|B_t^l|} x_{b_l t}^l \, \lambda_{b_l t}^l \quad \forall l \tag{4.62}$$

- The approximation of Expected Energy Not Served for interval *l* in period *t*:

$$EENS_t^l = \sum_{b_l=1}^{|B_t^l|} y_{b_l t}^l \, \lambda_{b_l t}^l \quad \forall l \tag{4.63}$$

- The weights in the approximation for interval *l* in period *t* should add up to 1:

$$\sum_{b_l=1}^{|B_t^l|} \lambda_{b_l t}^l = 1 \quad \forall l \tag{4.64}$$

- Committed capacity can lie on one of the segments in the approximation for interval *l* in period *t*:

$$\sum_{e_l=1}^{|E_t^l|} v_{e_l t}^l = 1 \quad \forall l \tag{4.65}$$

- As shown in Section 4.2.3, there is a concave relationship between CC_t and $EENS_t^l$. Since we are implicitly trying to minimize the cost of $EENS_t^l$, we need to define the following set of constraints to satisfy the adjacency criterion (*at most two adjacent weights can be non-zero*) in the piecewise linear approximation for interval *l* in period *t*:

$$\begin{bmatrix} \lambda_{1t}^l \\ \vdots \\ \lambda_{|B_t^l|t}^l \end{bmatrix} \leq CV_{|B_t^l| \, x \, |E_t^l|}^{lt} \begin{bmatrix} v_{1t}^l \\ \vdots \\ v_{|E_t^l|t}^l \end{bmatrix} \quad \forall l \tag{4.66}$$

- $EENS_t$ in period *t* is found by taking the expected value of $EENS_t^l$ over all possible net load demand intervals:

$$EENS_t = \sum_{l=1}^{|L|} p_l \, EENS_t^l \tag{4.67}$$

Sign Restrictions of Decision Variables for $EENS_t$:

$$EENS_t^l \geq 0 \quad \forall l \tag{4.68}$$

$$\lambda_{b_l t}^l \geq 0 \quad \forall b_l, \forall l \tag{4.69}$$

$$v_{e_l t}^l \in \{0,1\} \quad \forall e_l, \forall l \tag{4.70}$$

Mathematical Model: MIQP II

$$Min \quad \sum_{i=1}^{|N|} (a_i u_{it} + b_i P_{it} + c_i {P_{it}}^2 + q_i R_{it} + S_{it} u_{it}) + (VOLL)(EENS_t)$$

$$subject\ to$$

$$(4.40), \ldots, (4.49), (4.55), (4.57), (4.58), (4.62), \ldots, (4.70)$$

4.2.5 Valve Point Loading Effect (VPLE)

Due to the VPLE, a conventional generating unit has a rippling efficiency curve as its power generation level increases; that is, the efficiency of a conventional generating unit does not increase monotonically as it is more heavily loaded in practice. There are valves that control its fuel consumption rate by using separate nozzle groups. Each nozzle group achieves its best efficiency when generating at its maximum power output level which is also known as the valve point. As a result, when the power generation level is tried to be increased, valves are sequentially opened to achieve the highest possible efficiency for a given power generation level. This situation causes a rippling effect on the efficiency of a conventional generating unit as its fuel consumption rate increases. This rippling effect is demonstrated in Figure 4.9 for a steam turbine. Decker et al. (1958) show that a turbine loaded at a

valve point is operating with its maximum efficiency at that loading level before the next valve opens whereas its efficiency reduces as it is working off a valve point until its loading level reaches the next valve point. This is a result of a sudden increase in the incremental heat rate because of a rapid increase in the throttling losses when an extra valve first opens (Zobaa et al., 2018). Hence, in a complex power system, most of the conventional generating units should generate power output at one of their valve points to maximize the power generation efficiency of the whole system.

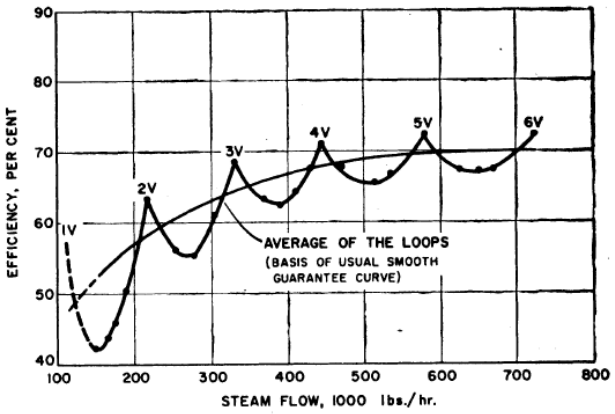

Figure 4.9. Valve Point Loading Effect on Efficiency of a Steam Turbine, Adapted from Decker et al. (1958)

Mathematical models in Section 4.2.4 somehow ignore this important fact by assuming that the efficiency of a conventional generating unit increases monotonically with its power generation level. The UCP with valve point loading effects brings a change in the fuel cost representation. For this purpose, the convex quadratic fuel cost function is superimposed with an absolute sine function; that is, the valve point loading part of the fuel cost, with the following modification where d_i and e_i are valve point loading coefficients of unit *i*:

$$FC(P_i) = a_i + b_i P_i + c_i\, P_i^2 + |d_i \sin(e_i\, (P_i - P_i^{Min}))| \qquad (4.71)$$

The absolute sine function models the efficiency reduction beyond the valve points by increasing the fuel consumption rate, which causes an absolute sinusoidal fluctuation in the convex quadratic fuel cost as shown in Figure 4.10.

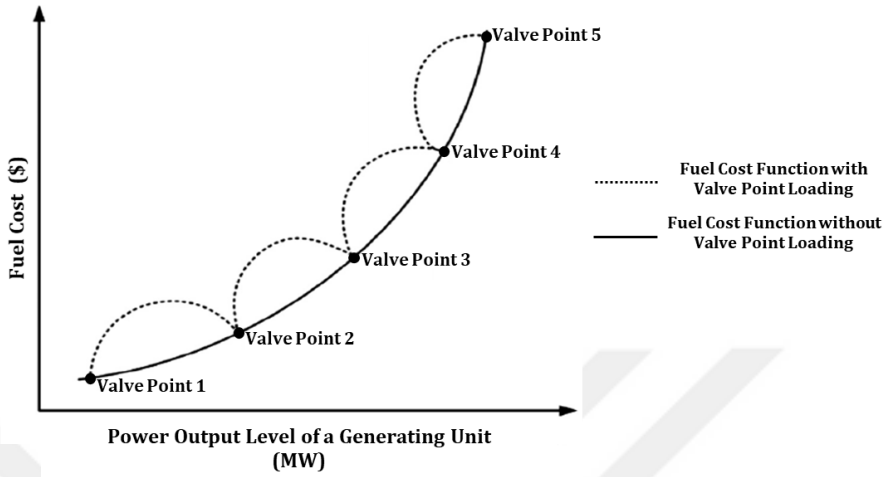

Figure 4.10. Fuel Cost Curve with/without Valve Point Loading Effect

Because of the valve point loading cost, the objective function becomes non-convex, non-smooth and hence hard to solve. To overcome this situation, the absolute sine function in the modified fuel cost representation is converted into its multi-area piecewise linear equivalent that consists of absolute sine areas K_i^{VP} as shown in Figure 4.11. The number of areas in the sine approximation for unit *i* is calculated with the following expression:

$$\left|K_i^{VP}\right| = \left\lceil e_i \frac{P_i^{Max} - P_i^{Min}}{\pi} \right\rceil \qquad (4.72)$$

It is to be noted that the quality of the multi-area piecewise linear approximation can be improved by increasing the number of breakpoints in a sine area. In Figure 4.11, the five-point piecewise linear approximation of the valve point loading cost is demonstrated with red lines.

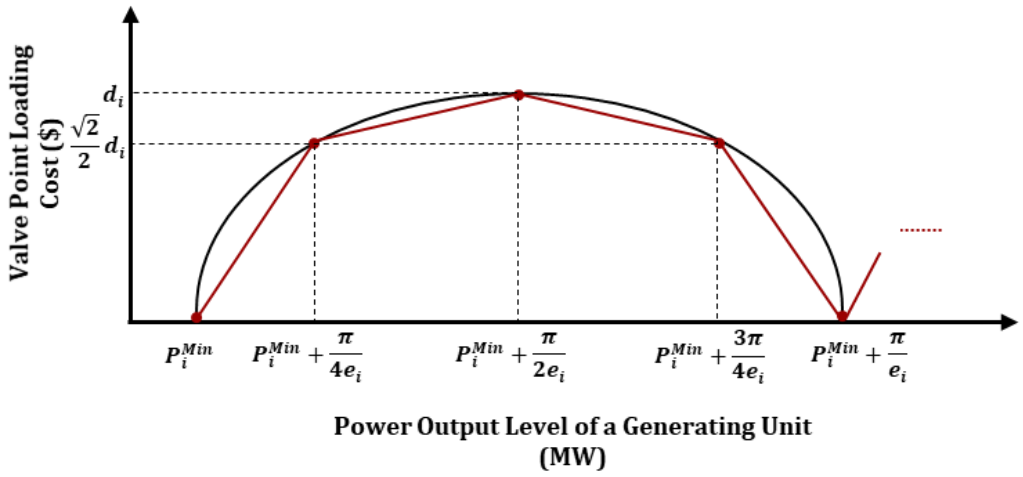

Figure 4.11. Five Point Piecewise Linear Approximation of the 1st Sine Area of the Valve Point Loading Cost

4.2.5.1 Time-decoupled MIQP Formulations with the VPLE

In our multi-area piecewise linear approximation of the VPLE, we reduce the total number of decision variables necessary for the approximation. For this purpose, for each conventional generating unit, we define the weight variables of breakpoints and binary variables indicating the segments for only the first sine area since there is a similar relationship between power generation level and valve point loading cost in each area. In other words, for each generating unit, the same sine area of the VPLE repeats in every $\frac{\pi}{e_i}$ power generation level starting from P_i^{Min}, so the approximation of the first sine area is shifted by $\frac{\pi}{e_i}$ for the successive sine areas. By reducing the total number of decision variables, the total number of constraints required for the approximation is also reduced accordingly. As a result, the model size with the VPLE becomes more manageable for real power systems with many conventional generating units.

By relaxing the monotonic efficiency increase assumption; accordingly, modifying the objective function and the constraint set, the multi-area piecewise linear

approximation of the VPLE can be integrated into each mathematical model explained in Section 4.2.4. These modifications do not change the model type since we are adding valve point loading costs as linear terms into the objective function; similarly, additional constraints defined for the piecewise linear approximation of the VPLE are also linear. Thus, modified formulations are still MIQP. Different from MIQP I and MIQP II, for each conventional generating unit, valve point loading costs are now added to the objective function. The power balance constraints, minimum/maximum generation limits, the minimum uptime/downtime constraints, the ramp-up/ramp-down limits, the reserve allocation and committed capacity constraints are modelled in the same way as in MIQP I and MIQP II. Besides, $EENS_t$ can be modelled by using both approximation methods described in Sections 4.2.3. Therefore, only modifications for the VPLE are provided in this section, and the associated modified models are called as MIQP I-VPLE and MIQP II-VPLE. For each period in the planning horizon, the modified formulations are sequentially solved to obtain near-optimal schedules for the commitment, generation and reserve similarly.

Sets and Indices

For the multi-area piecewise linear approximation of VPLE, the following sets are defined.

Additional Sets and Indices for VPLE Approximation:

K_i^{VP}*:* Set of sine areas in the multi-area VPLE approximation for unit *i*

$k_i \in K_i^{VP}$: Sine area k_i in the multi-area VPLE approximation for unit *i*

G_i: Set of breakpoints in a sine area of the multi-area VPLE approximation for unit *i*

$g_i \in G_i$: Breakpoint g_i in a sine area of the multi-area VPLE approximation for unit *i*

H_i: Set of segments in a sine area of the multi-area VPLE approximation for unit *i*

$\ni |H_i| = |G_i| - 1$

$h_i \in H_i$: Segment h_i in a sine area of the multi-area VPLE approximation for unit *i*

Parameters

For the multi-area piecewise linear approximation of VPLE, the following parameters are defined.

Additional Parameters for VPLE Approximation:

d_i, e_i: Valve point loading cost coefficients of unit *i* ($ and MW, respectively)

$x_{g_i i}^{VP}$: Power generation level of unit *i* at breakpoint g_i in the VPLE approximation (MW):

$$x_{g_i i}^{VP} = P_i^{Min} + (g_i - 1)\frac{\pi}{|G_i|e_i} \tag{4.73}$$

$y_{g_i i}^{VP}$: Valve point loading cost of unit *i* at breakpoint g_i in the VPLE approximation ($):

$$y_{g_i i}^{VP} = \left| d_i \sin\left(e_i\left(x_{g_i i}^{VP} - P_i^{Min}\right)\right)\right| \tag{4.74}$$

$CM_{g_i h_i}^{i}$: $|G_i|\ x\ |H_i|$ coverage matrix for adjacent breakpoints on each segment in the VPLE approximation for unit *i*:

$$CM_{g_i h_i}^{i} = \begin{cases} 1 & \text{if } g_i = h_i \text{ and } g_i = h_i + 1 \text{ in period } t \\ 0 & \text{otherwise} \end{cases} \tag{4.75}$$

Decision Variables

For the multi-area piecewise linear approximation of VPLE, the following variables are defined.

Additional Variables for VPLE Approximation:

VP_{it}: Valve point loading cost of unit *i* in period *t*

$\delta_{k_i it}^{VP}$: Sine area k_i that P_{it} lies on the VPLE approximation for unit *i* in period *t*:

$$\delta_{k_i it}^{VP} = \begin{cases} 1 & \text{if } P_{it} \text{ lies on sine area } k_i \text{ for unit } i \text{ in period } t \\ 0 & \text{otherwise} \end{cases} \tag{4.76}$$

$w_{g_i it}$: Weight of breakpoint g_i on the VPLE approximation for unit *i* in period *t*

$\varphi_{h_i it}$: Segment h_i that P_{it} lies on the VPLE approximation for unit *i* in period *t*:

$$\varphi_{h_i it} = \begin{cases} 1 \text{ if } P_{it} \text{ lies on segment } h_i \text{ for unit } i \text{ in period } t \\ 0 \text{ otherwise} \end{cases} \quad (4.77)$$

Objective Function

By adding valve point loading costs to the objective function defined in MIQP Model I in Section 4.2.4, the modified objective function becomes:

$$Min \sum_{i=1}^{|N|} (a_i u_{it} + b_i P_{it} + c_i {P_{it}}^2 + VP_{it} + q_i R_{it} + S_{it} u_{it}) + (VOLL)(EENS_t) \quad (4.78)$$

Constraints

<u>*Sine Area Identification Constraints:*</u> If unit *i* generates power in period *t*, then P_{it} should lie on sine area k_i and produce within the power generation range of that area in that period:

$$P_{it} \geq P_i^{Min} + (g_i - 1)\frac{\pi}{e_i} + m_2\left(1 - \delta_{k_i it}^{VP}\right) \quad \forall k_i, \forall i \quad (4.79)$$

where m_2 is a very small number denoting lower bounds for Sine Area Identification Constraints.

$$P_{it} \leq P_i^{Min} + g_i\frac{\pi}{e_i} + M_3\left(1 - \delta_{k_i it}^{VP}\right) \quad \forall k_i, \forall i \quad (4.80)$$

where M_3 is a very large number denoting upper bounds for Sine Area Identification Constraints.

<u>*Piecewise Linear Approximation Constraints for VPLE:*</u> For unit *i*, the absolute sinusoidal relationship between P_{it} and VP_{it} is converted into its multi-area piecewise linear approximation with the following constraints:

- The approximation of power generation level of unit *i* in period *t*:

$$P_{it} - \sum_{k_i=1}^{|K_i|} (k_i - 1) \frac{\pi}{e_i} \delta_{k_i it}^{VP} = \sum_{g_i=1}^{|G_i|} x_{g_i i}^{VP} \, w_{g_i it} \quad \forall i \tag{4.81}$$

- The approximation of valve point loading cost of unit *i* in period *t*:

$$VP_{it} = \sum_{g_i=1}^{|G_i|} y_{g_i i}^{VP} \, w_{g_i it} \quad \forall i \tag{4.82}$$

- If unit *i* is committed in period *t*, then P_{it} should lie on one of the sine areas in that period:

$$\sum_{k_i=1}^{|K_i|} \delta_{k_i it}^{VP} = u_{it} \quad \forall i \tag{4.83}$$

- If unit *i* is committed in period *t*, then P_{it} should lie on one of the sine areas; accordingly, the sum of weights should be equal to one in the approximation for unit *i* in that period:

$$\sum_{g_i=1}^{|G_i|} w_{g_i it} = \sum_{k_i=1}^{|K_i|} \delta_{k_i it}^{VP} \quad \forall i \tag{4.84}$$

- If unit *i* is committed in period *t*, then P_{it} should lie on one of the sine areas; accordingly, it should lie on one of the segments in the approximation for unit *i* in that period:

$$\sum_{h_i=1}^{|H_i|} \varphi_{h_i it} = \sum_{k_i=1}^{|K_i|} \delta_{k_i it}^{VP} \quad \forall i \tag{4.85}$$

- There is a concave relationship between P_{it} and VP_{it}. Since we are trying to minimize valve point loading cost (VP_{it}), we need to define the following set of constraints to satisfy the adjacency criterion (*at most two adjacent weights can be non-zero*) in the piecewise linear approximation for unit *i* in period *t*:

$$\begin{bmatrix} w_{1it} \\ \vdots \\ w_{|G_i|it} \end{bmatrix} \leq CM^{i}_{|G_i| \, x \, |H_i|} \begin{bmatrix} \varphi_{1it} \\ \vdots \\ \varphi_{|H_i|it} \end{bmatrix} \quad \forall i \qquad (4.86)$$

Sign Restrictions of Decision Variables for VPLE:

$$VP_{it} \geq 0 \quad \forall i \qquad (4.87)$$

$$w_{g_i it} \geq 0 \quad \forall g_i, \forall i \qquad (4.88)$$

$$\varphi_{h_i it} \in \{0,1\} \quad \forall h_i, \forall i \qquad (4.89)$$

$$\delta^{VP}_{k_i it} \in \{0,1\} \quad \forall k_i, \forall i \qquad (4.90)$$

Mathematical Model: MIQP I-VPLE

$$Min \quad \sum_{i=1}^{|N|} (a_i u_{it} + b_i P_{it} + c_i {P_{it}}^2 + VP_{it} + q_i R_{it} + S_{it} u_{it}) + (VOLL)(EENS_t)$$

$subject\ to$

$(4.40), \dots, (4.59), (4.79), \dots, (4.90)$

Mathematical Model: MIQP II-VPLE

$$Min \quad \sum_{i=1}^{|N|} (a_i u_{it} + b_i P_{it} + c_i {P_{it}}^2 + VP_{it} + q_i R_{it} + S_{it} u_{it}) + (VOLL)(EENS_t)$$

$subject\ to$

$(4.40), \dots, (4.49), (4.55), (4.57), (4.58), (4.62), \dots, (4.70), (4.79), \dots, (4.90)$

4.3 Computational Study

The proposed time-decoupled MIQP formulations are coded in MATLAB programming language and solved via CPLEX for MATLAB toolbox provided by IBM ILOG CPLEX Optimizer 12.9.0. The model is executed in Windows 10 environment in a Lenovo ultrabook with Intel(R) Core (TM) i7-6500U 2.6 GHz CPU and 8 GB RAM. Numerical experiments on the performance of the approaches are conducted by using a set of three problem instances of IEEE which are explained in detail in the subsequent sections. First of all, two EENS approximations are compared for the case without the VPLE. Then, test and sensitivity analysis results are provided for the cases with/without the VPLE. Lastly, our time-decoupled stochastic MIQP formulations are compared with the UCP formulations enforcing traditional deterministic reserve policies for both UCP variants with/without the VPLE.

4.3.1 Problem Instances

To conduct numerical experiments, the time-decoupled MIQP models are applied to IEEE 24-bus, 30-bus problem instances and its duplicated version by considering significant wind penetration with six wind farms. For each instance, the ramp rate limits are set to be 20% of the unit's maximum power output limit. The reliability of the power system is modelled via ORR of each conventional unit. The load demand forecast errors are assumed to follow Normal distribution with zero mean and a variance 0.09% of the expected load demand for each period. Similarly, wind power forecast errors in each wind farm are also assumed to follow Normal distribution with zero mean and a variance ranging from 1% and 12.25% of the expected wind power. To illustrate, the standard deviation factors are set to be 3%, 2.5%, 2%, 1%, 3.5% and 1.5% of the expected wind power in each wind farm, respectively. To model the dependencies in wind power generation within a wind farm and between wind farms, the associated correlation coefficients are taken as 0.3 and 0.2,

respectively. The reserve cost of each conventional unit is assumed to be a function of the reserve rate which is taken as 10% of its highest marginal fuel cost. To calculate the cost of $EENS_t$, VOLL is set as 1750 $/MWh for each period.

Problem Instance 1

This problem instance consists of 24-bus with 26 conventional thermal units and 6 wind farms. The hydro generating units in the original configuration are ignored. The length of the scheduling horizon is 24 hours. In each wind warm, there are 70 wind turbines, each with a capacity of 1.5 MW.

The conventional unit related data for IEEE 24-bus reliability test system are provided in Table 4.2. Load demand and wind power forecasts of the system over 24 hours are provided in Table 4.3.

Table 4.2. Conventional Unit Related Data for IEEE 24-bus Problem Instance

	Unit 1	**Unit 2**	**Unit 3**	**Unit 4**	**Unit 5**	**Unit 6**	**Unit 7**	**Unit 8**	**Unit 9**	**Unit10**
P_i^{Max} (MW)	12	12	12	12	12	20	20	20	20	76
P_i^{Min} (MW)	2.4	2.4	2.4	2.4	2.4	4	4	4	4	15.2
a_i ($)	24.3891	24.411	24.6382	24.7605	24.8882	117.7551	118.1083	118.4576	118.8206	81.1364
b_i($/$MW$)	25.5472	25.6753	25.8027	25.9318	26.0611	37.551	37.6637	37.777	37.8896	13.3272
c_i ($/$MW^2$)	0.02533	0.02649	0.02801	0.02842	0.02855	0.01199	0.01261	0.01359	0.01433	0.00876
d_i ($)	-	-	-	-	-	-	-	-	-	-
e_i (MW)	-	-	-	-	-	-	-	-	-	-
$T_{Min,i}^{on}$ (h)	0	0	0	0	0	0	0	0	0	3
$T_{Min,i}^{off}$ (h)	0	0	0	0	0	0	0	0	0	2
S_i^H($)	0	0	0	0	0	33.33562	33.33562	33.33562	33.33562	76.73219
S_i^C ($)	0	0	0	0	0	39.79139	39.79139	39.79139	39.79139	98.33637
$T_{c,i}$ (h)	1	1	1	1	1	3	3	3	3	2
Initial Status (h)	-1	-1	-1	-1	-1	-1	-1	-1	-1	3
ORR_i	0.00034	0.00034	0.00034	0.00034	0.00034	0.002222	0.002222	0.002222	0.002222	0.00051

Table 4.2 (continued)

	Unit11	Unit12	Unit13	Unit14	Unit15	Uni16	Unit17	Unit18	Unit19	Unit20	Unit21	Unit22	Unit23	Unit24	Unit25	Unit26
P_i^{Max} (MW)	76	76	76	100	100	100	155	155	155	155	197	197	197	350	400	400
P_i^{Min} (MW)	15.2	15.2	15.2	25	25	25	54.25	54.25	54.25	54.25	68.95	68.95	68.95	140	100	100
a_i $(\$/h)$	81.298	81.4641	81.6259	217.8952	218.335	218.7752	142.7348	143.0288	143.3179	143.5972	259.131	259.649	260.176	177.0575	310.0021	311.9102
$b_i(\$/MWh)$	13.3538	13.3805	13.4073	18	18.1	18.2	10.694	10.7154	10.7367	10.7583	23	23.1	23.2	10.8616	7.4921	7.5031
c_i $(\$/MW^2 - h)$	0.00895	0.0091	0.00932	0.00623	0.00612	0.00598	0.00463	0.00473	0.00481	0.00487	0.00259	0.0026	0.00263	0.00153	0.00194	0.00195
d_i ($)	-	-	-	-	-	-	-	-	-	-	-	-	-	-	-	-
e_i (MW)	-	-	-	-	-	-	-	-	-	-	-	-	-	-	-	-
$T_{Min,i}^{on}$ (h)	3	3	3	4	4	4	5	5	5	5	5	5	5	8	8	8
$T_{Min,i}^{off}$ (h)	2	2	2	2	2	2	3	3	3	3	4	4	4	5	5	5
$S_i^H(\$)$	76.73219	76.73219	76.73219	104.8308	104.8308	104.8308	212.864	212.864	212.864	212.864	274.8684	252.2441	252.2441	367.9085	658.0976	658.0976
S_i^C ($)	98.33637	98.33637	98.33637	136.3158	136.3158	136.3158	283.9379	283.9379	283.9379	283.9379	367.5661	358.1863	358.1863	464.7361	886.4964	886.4964
$T_{c,i}$ (h)	2	2	2	3	3	3	3	3	3	3	3	3	3	1	2	2
Initial Status (h)	3	3	3	-3	-3	-3	5	5	5	5	-4	-4	-4	10	10	10
ORR_i	0.00051	0.00051	0.00051	0.000833	0.000833	0.000833	0.001041	0.001041	0.001041	0.001041	0.001052	0.001052	0.001052	0.000869	0.000909	0.000909

Table 4.3. Hourly Load Demand and Wind Power Forecasts for IEEE 24-bus Problem Instance

Hour	**1**	**2**	**3**	**4**	**5**	**6**	**7**	**8**	**9**	**10**	**11**	**12**
Demand (MW)	1950	1980	1940	1950	2000	2100	2250	2680	2790	2850	2920	2840
Wind Power(MW)	454.8	422.2	407.3	403.9	379.4	362.9	377.8	433.7	420.2	369.7	358.6	420.2
Hour	**13**	**14**	**15**	**16**	**17**	**18**	**19**	**20**	**21**	**22**	**23**	**24**
Demand (MW)	2840	2800	2870	2900	2800	2780	2750	2800	2850	2730	2450	2090
Wind Power(MW)	405	428.7	362	237.3	339.7	305.3	289	208.9	225.3	183.6	140.6	165.5

Problem Instance 2

This problem instance consists of 30-bus with 6 conventional thermal units and 6 wind farms. The length of the scheduling horizon is 24 hours. In each wind warm, there are 15 wind turbines, each with a capacity of 1.5 MW.

The conventional unit related data for IEEE 30-bus test system are provided in Table 4.4. Load demand and wind power forecasts of the system over 24 hours are provided in Table 4.5.

Table 4.4. Conventional Unit Related Data for IEEE 30-bus Problem Instance

	Unit 1	**Unit 2**	**Unit 3**	**Unit 4**	**Unit 5**	**Unit 6**
P_i^{Max} (MW)	120	110	700	500	550	210
P_i^{Min} (MW)	30	20	130	100	120	45
a_i ($)	2200	2400	6500	930.5	900	130.2
b_i($/MW)	12	15	11	20	15	20,5
c_i ($/$MW^2$)	0.003	0.002	0.0022	0.0032	0.002	0.004125
d_i ($)	200	300	400	150	100	80
e_i (MW)	0.08	0.04	0.04	0.06	0.08	0.1
$T_{Min,i}^{on}$ (h)	5	4	6	4	4	3
$T_{Min,i}^{off}$ (h)	5	3	4	3	3	4
S_i^H($)	500	360	2250	3600	3300	2230
S_i^C ($)	900	780	4800	7000	6600	4200
$T_{c,i}$ (h)	1	1	2	3	3	2
Initial Status (h)	-5	-6	1	1	-1	-1
ORR_i	0.00511	0.00222	0.00034	0.000104	0.000105	0.00433

Table 4.5. Hourly Load Demand and Wind Power Forecasts for IEEE 30-bus Problem Instance

Hour	1	2	3	4	5	6	7	8	9	10	11	12
Demand (MW)	859	757	683	647	638	667	819	991	1177	1359	1609	1760
Wind Power(MW)	44	73	69	76	91	84	92	86	13	44	65	62,9
Hour	**13**	**14**	**15**	**16**	**17**	**18**	**19**	**20**	**21**	**22**	**23**	**24**
Demand (MW)	1850	1883	1809	1728	1753	1769	1782	1713	1543	1331	1138	962
Wind Power(MW)	59	58	43,2	27	3	6	7	11	7	43	54	61

Problem Instance 3

This problem instance is obtained by appropriately scaling Problem Instance 2. For this purpose, conventional generating units are replicated two times to form the 12-Unit problem instance. Also, capacities of wind turbines in each wind farm, load demand and wind power forecasts are doubled.

4.3.2 Comparison of the Proposed EENS Approximation Methods

In our time-decoupled approach, we propose two approximation methods for $EENS_t$ as explained in Section 4.2.3. The time-decoupled stochastic MIQP models using these approximations (MIQP I and MIQP II) are implemented to IEEE 24-bus and 30-bus problem instances without the VPLE. Their performances are compared for both instances in terms of model sizes such as required variables and constraints, solution qualities and computing times.

Table 4.6. Overall Performance Comparison of $EENS_t$ Approximation Methods I and II for IEEE 24-bus Problem Instance

	Approximation I	Approximation II
Total Operating Cost ($)	722,482.5	723,743.2
Total EENS (MWh)	11.24	11.18
Computing Time (min)	2.5	34.2

As it is shown in Table 4.6, both approximation methods yield similar results for total EENS and total operating costs for Problem Instance 1 consisting of 26

conventional units. It is an indication that both methods are comparable in terms of overall solution qualities. However, approximation II requires more computing time than approximation I since $EENS_t$ values are calculated for each net load demand interval, which in return increases the evaluation of unit combinations in the associated $EENS_t$ breakpoints. As a result of separate calculations of $EENS_t$ values, the model size of approximation II increases with the inclusion of additional variables and constraints, especially binary variables and equality constraints, which makes the model more complex and complicated as demonstrated in Table 4.7. Consequently, approximation II inherently needs more time for computations.

Table 4.7. Model Sizes with $EENS_t$ Approximation Methods I and II for IEEE 24-bus Problem Instance over a 24-h Scheduling Horizon

	Approximation I	Approximation II
Binary Variables	723	1308
Continuous Variables	1419	2292
Inequality Constraints	3915	4644
Equality Constraints	154	724

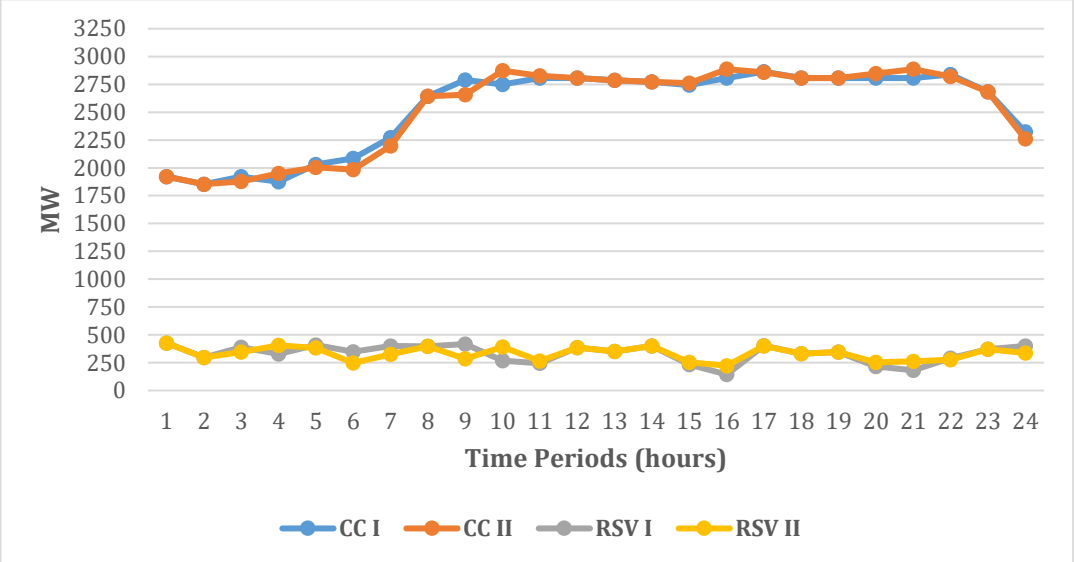

Figure 4.12. Comparison of Hourly Committed Capacities and Reserves in IEEE 24-bus Problem Instance for $EENS_t$ Approximation Methods I and II

When these approximation methods are examined further, it is observed that models using approximation I and II give similar hourly schedules although the first one is a little bit more conservative than the second one by committing more capacity and holding additional reserves. This relationship is illustrated in Figure 4.12 where CC I and CC II denote hourly committed capacities, and RSV I and RSV II indicate hourly reserves for approximation methods I and II respectively. According to Figure 4.12, for 71% of the time, committed capacities and reserves in approximation I are greater than or equal to the ones in approximation II, but they are approximately the same in general.

Similar analyses are also carried out for IEEE 30-bus problem instance which contains 6 conventional units. Different from Problem Instance 1, approximation I yields results with lower total EENS and total operating costs for Problem Instance 2 as it is shown in Table 4.8. The reason is that the model with approximation I behaves more conservatively for small-sized systems when compared to systems with moderate and large sizes. Hence, it commits more units for time periods with higher net load demands. Similar to Problem Instance 1, approximation II requires more calculation time than approximation I. Another reason is that the model size of approximation II increases by including additional variables and constraints, especially binary variables and equality constraints, which complicates the model as reported in Table 4.9. Since the problem size is relatively small for Problem Instance 2, both methods are implementable in terms of computing times though approximation I is faster than approximation II as illustrated in Table 4.8.

Table 4.8. Overall Performance Comparison of $EENS_t$ Approximation Methods I and II for IEEE 30-bus Problem Instance

	Approximation I	**Approximation II**
Total Operating Cost ($)	707,604.1	751,779.1
Total EENS (MWh)	13.94	21.18
Computing Time (sec)	1.9	11.3

Table 4.9. Model Sizes with $EENS_t$ Approximation Methods I and II for IEEE 30-bus Problem Instance over a 24-h Scheduling Horizon

	Approximation I	Approximation II
Binary Variables	214	635
Continuous Variables	430	1139
Inequality Constraints	1006	1571
Equality Constraints	159	734

When these approximation methods are examined for each time period, it is observed that models using approximation methods I and II give more conservative hourly schedules. As depicted in Figure 4.13, committed capacities and reserves in approximation I are greater than or equal to the ones in approximation II for 14 out of 24 time periods. When compared to schedules for Problem Instance 1, there are more fluctuations in both committed capacities and reserves for Problem Instance 2. However, it should be emphasized that both methods give the same schedules for time periods with larger net load demands.

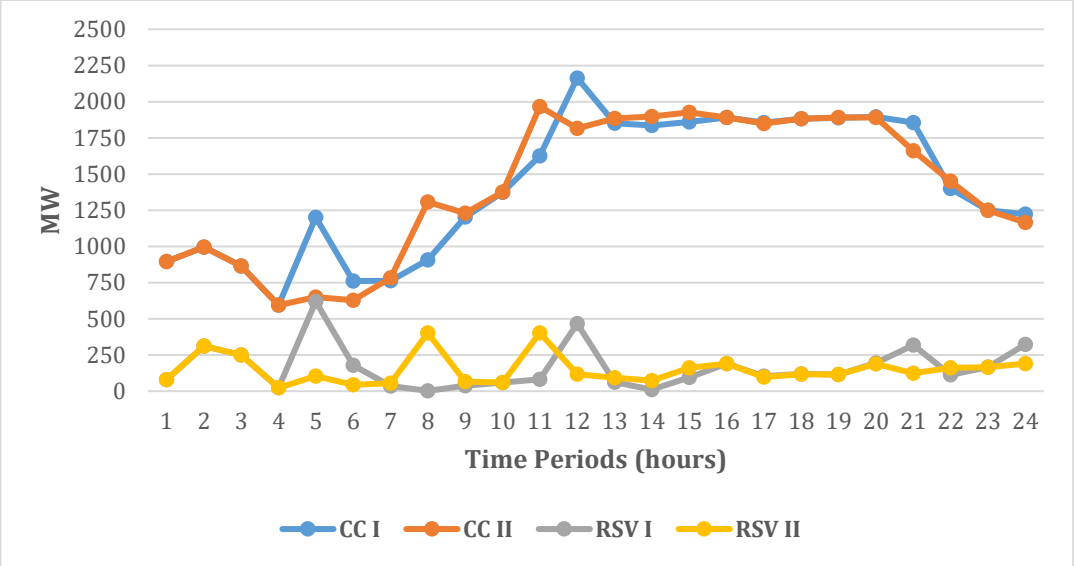

Figure 4.13. Comparison of Hourly Committed Capacities and Reserves in IEEE 30-bus Problem Instance for $EENS_t$ Approximation Methods I and II

According to these analyses, models with approximation methods I and II have similar performances in terms of solution qualities for real-sized wind integrated hybrid power systems. For small-sized systems, schedules obtained by these methods slightly differ for time periods having small net load requirements whereas they are comparable for heavily loaded periods. The reason of this difference is that $EENS_t$ values are calculated by failure combinations with less units as the problem size decreases. Nevertheless, it is not the case for the large power systems with conventional units. Therefore, these approximation methods can be used interchangeably for large systems in terms of intended solution quality. However, approximation II is more computationally intensive due to the associated $EENS_t$ calculations especially for large-scaled problems. Because of these reasons, approximation I is preferred for the $EENS_t$ approximations in our MIQP models with and without the VPLE. Hence, in the subsequent sections, approximation I is used for the sensitivity analyses of the proposed time-decoupled approaches (MIQP I and MIQP I-VPLE) and their comparisons with traditional deterministic reserve policies.

4.3.3 Sensitivity Analysis Results

Sensitivity analysis is a necessary part of the mathematical modelling because of several reasons. The first one is that model parameters might change through time. The second one is estimating some of the parameters may be very difficult; as a result, they are forecasted or estimated with common sense. Hence, it is important to assess how those changes can affect the solution. This can be done very easily for LP models by using sensitivity reports obtained by optimization packages like GAMS or LINDO. However, it is not that straightforward for mixed integer and nonlinear programming models, so the sensitivity is usually tested by solving them with different parameter values. For this reason, we examine the sensitivity of the solutions of time-decoupled models MIQP I and MIQP I-VPLE by changing parameters one at a time; accordingly, solving them with the updated parameter value. Those parameters include $VOLL$, load demand and wind speed forecast errors,

reserve costs and failure rates of conventional generating units since these are introduced to replace traditional deterministic reserve polices for the UCP. Their effects on the solution are discussed in the following sections. Firstly, the sensitivity analysis of the model MIQP I is carried out for IEEE 24-bus problem instance. Secondly, similar analysis is made for the model MIQP I-VPLE by implementing it to IEEE 30-bus problem instance.

4.3.3.1 Results for the Model MIQP I

The time-decoupled stochastic model MIQP I is implemented to IEEE 24-bus problem instance for different values of an associated parameter. First of all, the effect of $VOLL$ on spinning reserves (SR_t) and $EENS_t$ is determined by increasing $VOLL$ by 750 \$/MWh starting from 1750 \$/MWh.

In Table 4.10, the total cost of the system and its breakdown under different $VOLL$ values are summarized. It is observed that the total operating cost increases as the $VOLL$ increases.

Table 4.10. Total Operating Cost under Different $VOLL$ Values for IEEE 24-bus Problem Instance

***VOLL* (\$/MWh)**	**1750**	**2500**	**3250**	**4000**
Expected Cost of EENS (\$)	19,683.5	20,116.4	19,945.6	23,846.7
Generation & Reserve Cost (\$)	702,799.0	710,282.5	714,914.0	715,583.4
Total Operating Cost (\$)	**722,482.5**	**730,398.9**	**734,859.6**	**739,430.1**

In Figure 4.14, SR_t values differ significantly for the smallest and the largest $VOLL$ values since the trade-off between generating cost, reserve cost and expected cost of EENS averts from the side of load shedding to the side of additional reserves as $VOLL$ increases. As a result, SR_t level increases. It should also be emphasized that SR values do not change much for time periods with low net load intensity when $VOLL$ is 2500 \$/MWh, 3250 \$/MWh and 4000 \$/MWh. As a matter of fact, the overall reserve schedules are almost the same for $VOLL$ of 3250 \$/MWh and 4000

$/MWh. This is an indicator that the compromise solution is not affected much when $VOLL$ is greater than 3250 $/MWh. Similar but inverse relationship is valid for $EENS_t$ under different $VOLL$ values. $EENS_t$ values decrease as more reserves are committed (Figure 4.15).

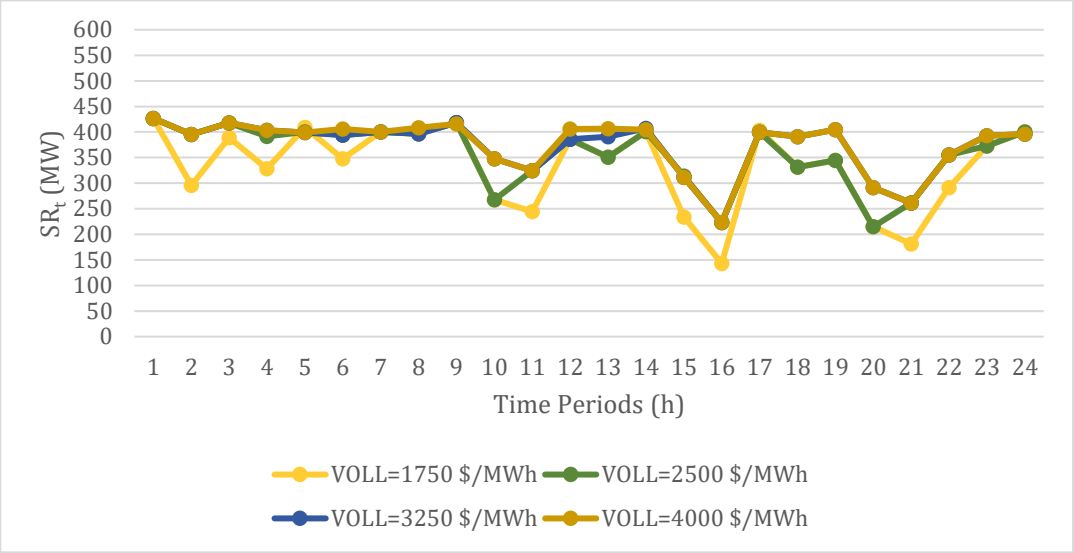

Figure 4.14. Relationship between $VOLL$ and SR_t for IEEE 24-bus Problem Instance

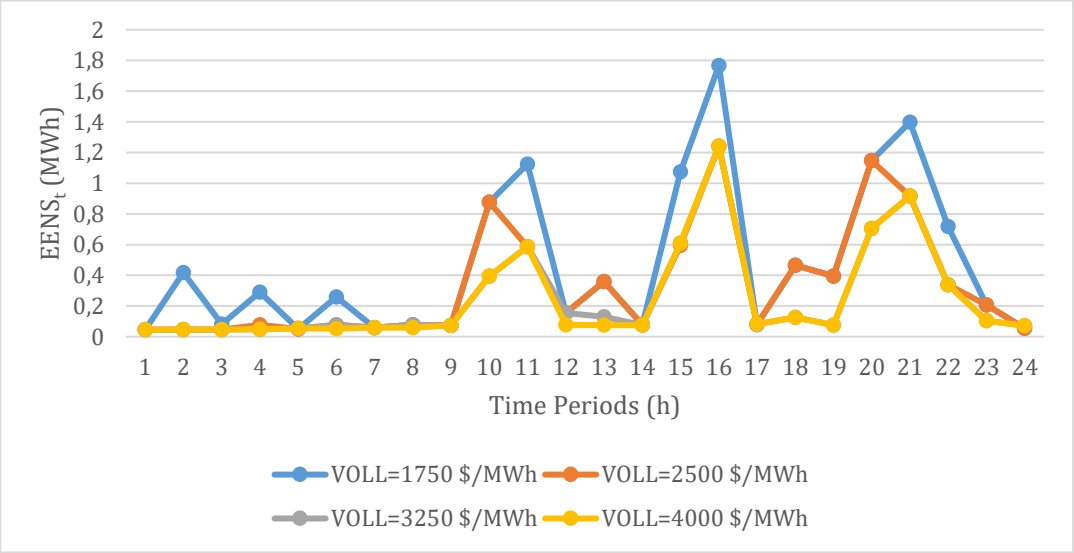

Figure 4.15. Relationship between $VOLL$ and $EENS_t$ for IEEE 24-bus Problem Instance

Secondly, we examine how changes in wind forecast errors affect the compromise solution. For this purpose, SR_t and $EENS_t$ values are plotted in Figures 4.16 and 4.17 for different scaling factors. It is observed that SR_t values do not change for time periods with high net load intensity as wind power forecast errors increase. Nevertheless, the SR_t values slightly change in time periods with low net load intensity as illustrated in Figure 4.16. That is, the effect of wind speed forecast errors on the trade-off between generating cost, reserve cost and expected cost of load shedding is not critical when net load demands are satisfied by using much of the installed conventional generation capacity.

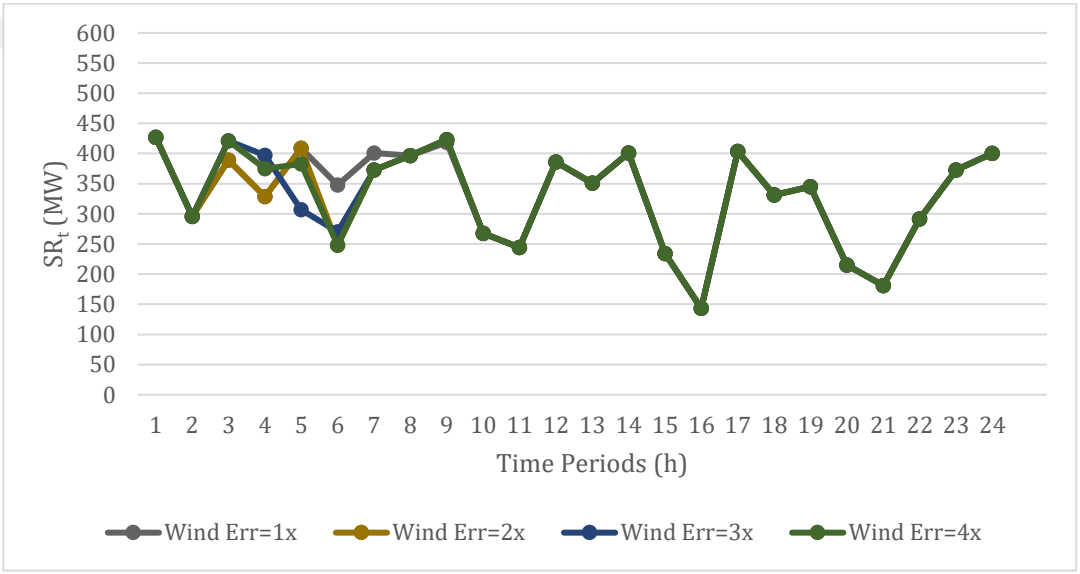

Figure 4.16. Relationship between Wind Speed Forecast Errors and SR_t for IEEE 24-bus Problem Instance

Even though decisions on SR_t do not change significantly with an increase in wind speed forecast errors, $EENS_t$ values increase as shown in Figure 4.17, which is due to increasing uncertainty of the overall power system with more error-prone wind power forecasts.

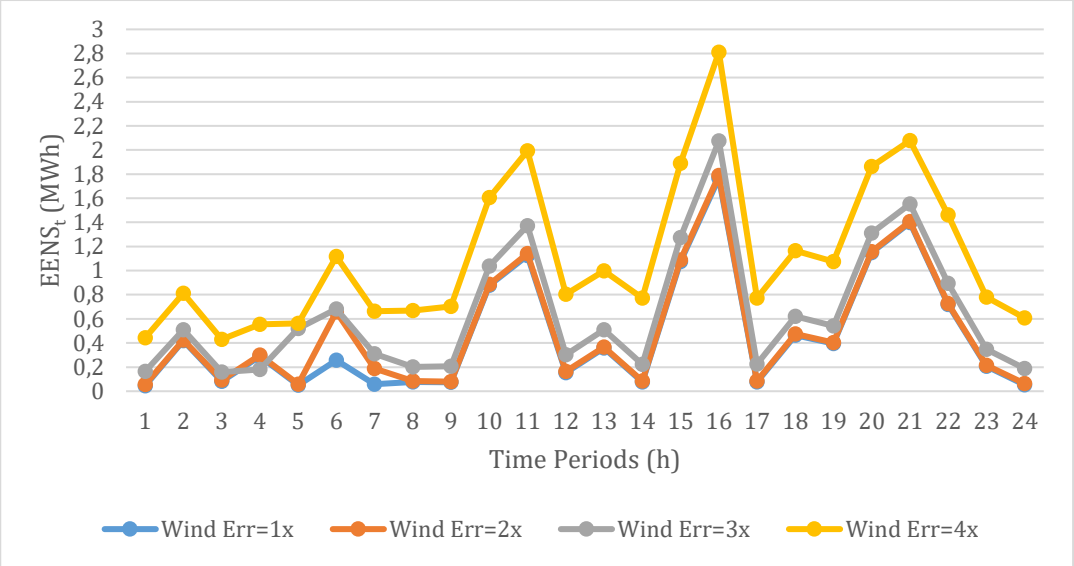

Figure 4.17. Relationship between Wind Speed Forecast Errors and $EENS_t$ for IEEE 24-bus Problem Instance

The total operating cost and its breakdowns under different wind speed errors are reported in Table 4.11. It is observed that the total operating cost increases as wind speed errors increase.

Table 4.11. Total Operating Cost under Different Wind Speed Forecast Errors for IEEE 24-bus Problem Instance

Scale of Wind Speed Error	**x1**	**x2**	**x3**	**x4**
Expected Cost of EENS ($)	19,683.5	20,979.3	26,947.2	46,599.7
Generation & Reserve Cost ($)	702,799.0	702,004.3	702,062.8	702,133.4
Total Operating Cost ($)	**722,482.5**	**722,983.6**	**729,010.0**	**748,733.1**

Thirdly, we investigate the sensitivity of the solution for different load demand forecast errors. The results are similar to the ones under different wind speed forecast errors. SR decisions are not sensitive to changes in load demand forecast errors for time periods with high net load intensity whereas $EENS_t$ values increase with high load demand forecast errors as shown in Figures 4.18 and 4.19.

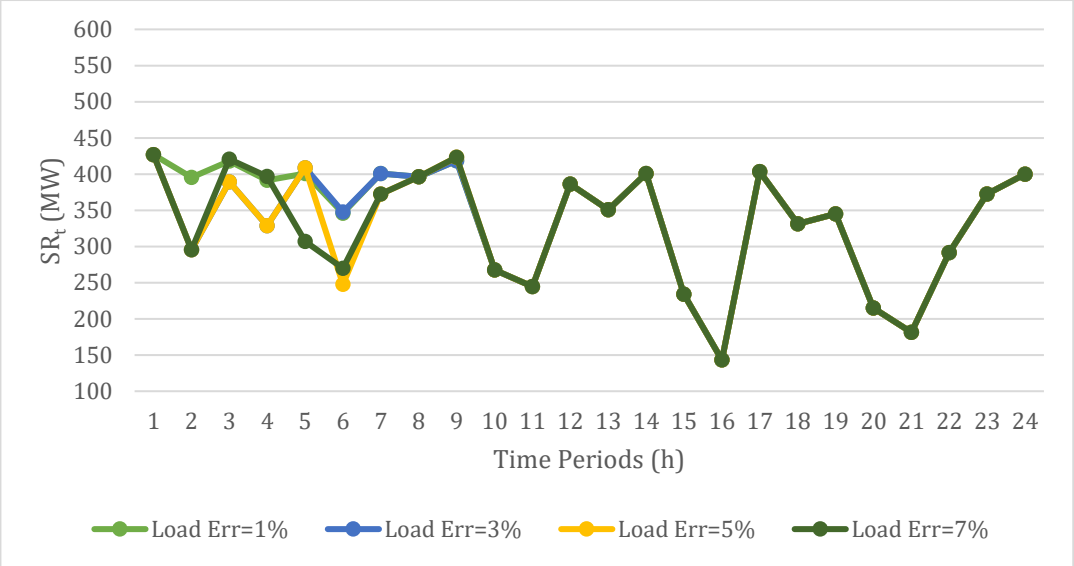

Figure 4.18. Relationship between Load Demand Forecast Errors and SR_t for IEEE 24-bus Problem Instance

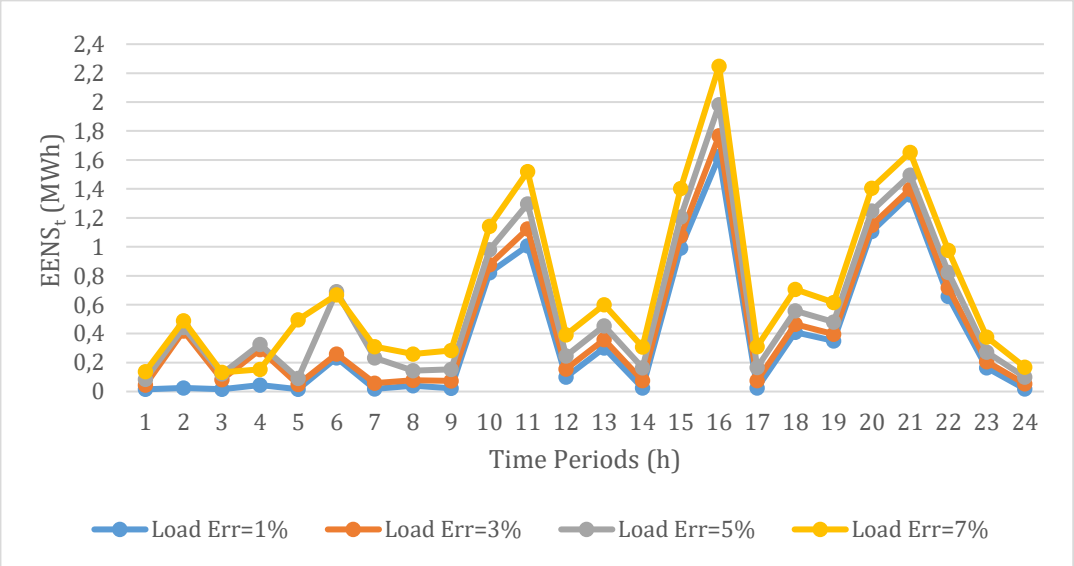

Figure 4.19. Relationship between Load Demand Forecast Errors and $EENS_t$ for IEEE 24-bus Problem Instance

Similarly, total operating cost increases with high load demand forecast errors. Its breakdown is provided in Table 4.12.

Table 4.12. Total Operating Cost under Different Load Demand Forecast Errors for IEEE 24-bus Problem Instance

Load Forecast Errors	1%	3%	5%	7%
Expected Cost of EENS ($)	16,431.7	19,683.5	24,076.1	29,321.7
Generation & Reserve Cost ($)	704,377.3	702,799.0	702,004.3	702,062.8
Total Operating Cost ($)	**720,809.0**	**722,482.5**	**726,080.4**	**731,384.5**

Another important parameter in our approach is incremental reserve cost of a conventional generating unit. To see its effects on total cost, SR_t and $EENS_t$, reserve rates are scaled in an increasing order. As the reserve rates increase, the total operating cost also increases as shown in Table 4.13. That is because charging higher incremental reserve costs makes SR_t more expensive, which in return increases total EENS since there is an inverse relationship between SR_t and $EENS_t$.

Table 4.13. Total Operating Cost under Different Incremental Reserve Rates for IEEE 24-bus Problem Instance

Scale of Reserve Rates	x1	x2	x3
Expected Cost of EENS ($)	19,683.5	24,148.5	43,110.8
Generation & Reserve Cost ($)	702,799.0	712,378.7	707,318.3
Total Operating Cost ($)	**722,482.5**	**736,527.2**	**750,429.1**

As demonstrated in Figure 4.20, SR_t values are very sensitive to changes in incremental reserve rates especially in time periods where net load intensity is low. This is not the case for time periods with high net load intensity when scales of reserves are between 1 and 2. For such periods, it may be tolerable to increase reserve rates up to the scale of 2 without changing SR_t decisions much. Nevertheless, there is a similar but inverse relationship for $EENS_t$ values under different incremental reserve rates as shown in Figure 4.21. Since the cost of holding an extra reserve increases, less reserves are committed; accordingly, $EENS_t$ values increase in general. When the scale factor is hold between 1 and 2, $EENS_t$ values do not change for time periods in which the net load intensity is high. When the scale factor is greater than 3, the compromise solution definitely changes since trade-off between

generating cost, reserve cost and expected cost of EENS averts from the side of additional reserves to the side of load shedding.

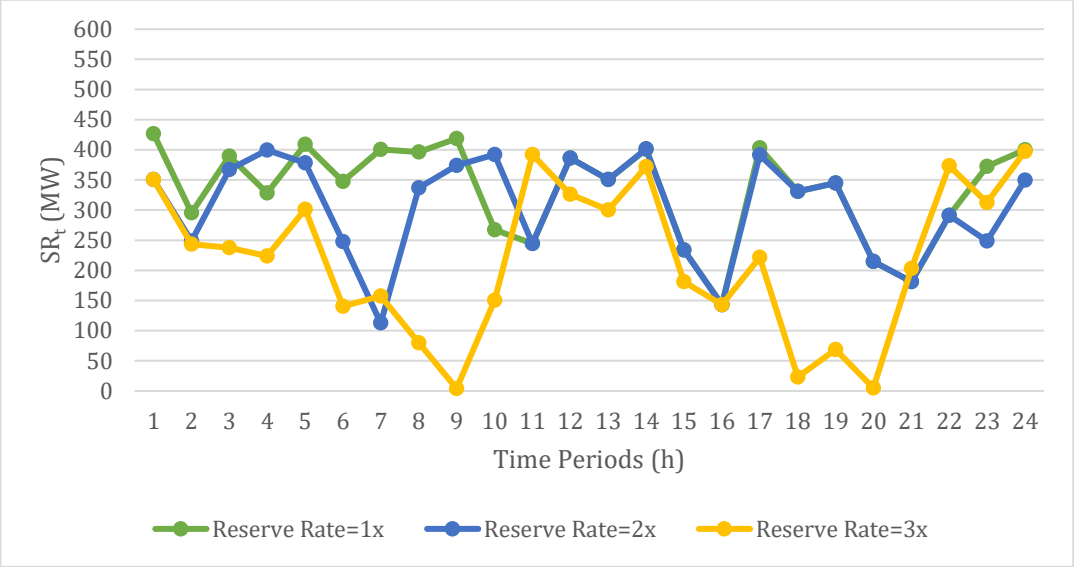

Figure 4.20. Relationship between Incremental Reserve Rates and SR_t for IEEE 24-bus Problem Instance

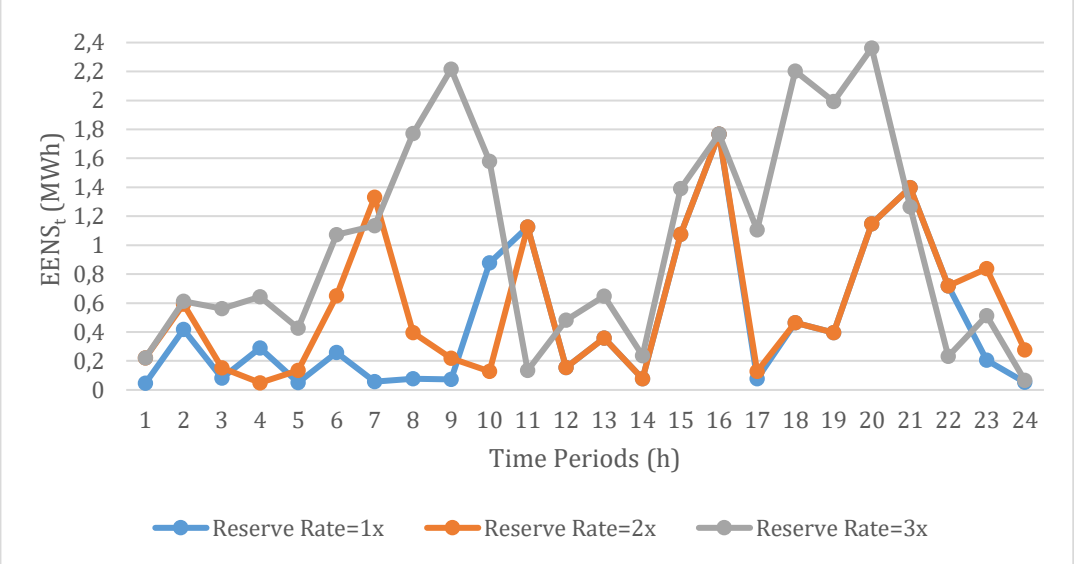

Figure 4.21. Relationship between Incremental Reserve Rates and $EENS_t$ for IEEE 24-bus Problem Instance

Lastly, we test the sensitivity of the solution by reducing the reliability of the conventional power generation system. For this purpose, we double and triple failure rates (ORR); accordingly, we solve the model with new system reliabilities. As shown in Table 4.14, total operating cost increases as the conventional system reliability reduces. That is because increasing uncertainty in conventional generation brings additional burden on the generation and reserve costs and expected cost of EENS.

Table 4.14. Total Operating Cost under Different Conventional System Reliability for IEEE 24-bus Problem Instance

Scale of *ORR*	**x1**	**x2**	**x3**
Expected Cost of EENS ($)	19,683.5	21,557.8	31,489.9
Generation & Reserve Cost ($)	702,799.0	715,135.2	716,162.6
Total Operating Cost ($)	**722,482.5**	**736,693.1**	**747,652.5**

As illustrated in Figure 4.22, the proposed model is sensitive to changes in ORR scales between 1 and 2 since SR_t values increase substantially. However, this is not the case for the changes in ORR scale between 2 and 3, so this change might be tolerable in terms of SR_t decisions although there are slight variations in several time periods.

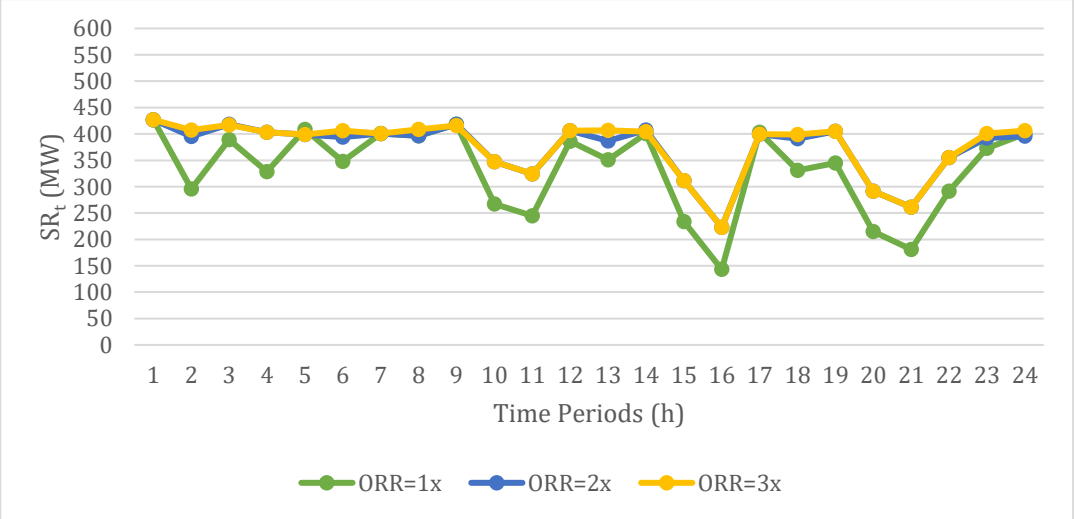

Figure 4.22. Relationship between Conventional System Reliability and SR_t for IEEE 24-bus Problem Instance

With the reduction in the reliability of the conventional system, $EENS_t$ values tend to increase as demonstrated in Figure 4.23, which is especially the case for time periods with high net load intensity. The reason is that the model fails to commit more reserves due to the ramp rate limitations and the available installed capacities for some periods in general. This results in higher $EENS_t$ values.

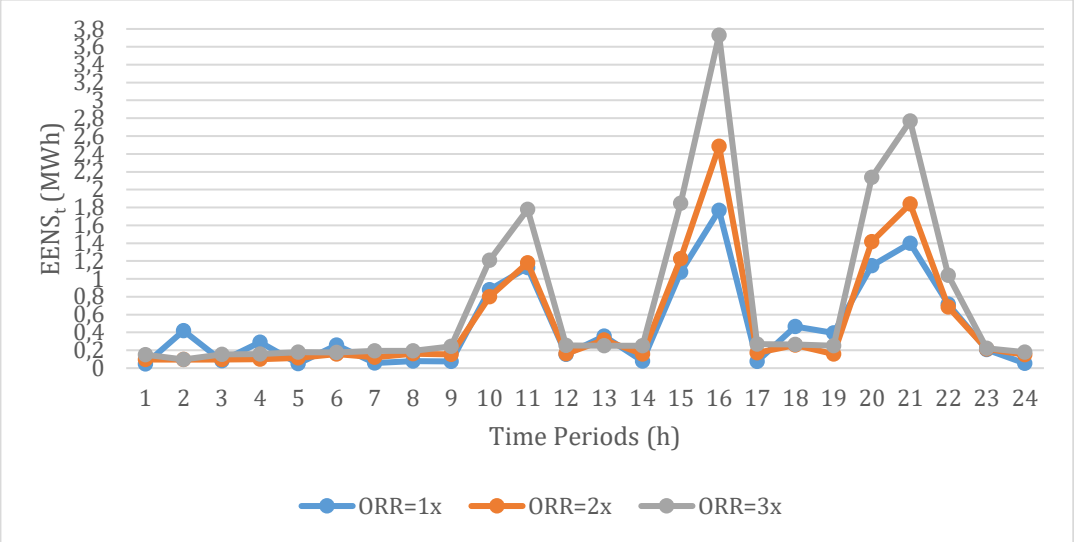

Figure 4.23. Relationship between Conventional System Reliability and $EENS_t$ for IEEE 24-bus Problem Instance

In particular, the results of sensitivity analyses verify that $VOLL$, reserve rates and conventional generation reliability have important roles in the proposed time-decoupled stochastic model MIQP I for IEEE 24-bus problem instance. Hence, their levels significantly affect the compromise solution. Similarly, load demand and wind speed forecast errors play an important role in periods with low net load intensity, but they do not change solutions for other periods.

4.3.3.2 Results for the Model MIQP I-VPLE

The time-decoupled stochastic model MIQP I-VPLE, in which rippling power plant efficiencies are also taken into account by adding the cost of VPLE in the generation

costs, is implemented to IEEE 30-bus problem instance for different values of the corresponding parameter. Firstly, the impact of $VOLL$ on SR_t and $EENS_t$ is analyzed by increasing $VOLL$ by 750 \$/MWh starting from 1750 \$/MWh.

In Table 4.15, the total cost of the system and its breakdown under different $VOLL$ values are reported. It is observed that increasing $VOLL$ directly increases the total operating cost of the system. Nonetheless, generation and reserve costs are the same for the first three levels of $VOLL$ since the corresponding commitment decisions do not change.

Table 4.15. Total Operating Cost under Different $VOLL$ Values for IEEE 30-bus Problem Instance

***VOLL* (\$/MWh)**	**1750**	**2500**	**3250**	**4000**
Expected Cost of EENS (\$)	24,304.3	34,720.4	45,136.6	49,626.8
Generation & Reserve Cost (\$)	697,383.4	697,383.4	697,383.4	701,694.4
Total Operating Cost (\$)	**721,687.7**	**732,103.8**	**742,520.0**	**751,321.1**

In Figure 4.24, SR_t values differ significantly between the first three levels and the highest level of $VOLL$. Another important observation is that SR_t values do not change over the horizon when $VOLL$ is 1750\$/MWh, 2500 \$/MWh and 3250 \$/MWh. At first glance, this relationship may seem as counterintuitive since it is shown in Section 4.3.3.1 that there is a positive correlation between SR_t and $VOLL$. However, the main reason behind these results is the dominant effect of the VPLE on the trade-off between total cost components. For the first three levels of $VOLL$, the same committed capacities are maintained due to the VPLE. With 4000 \$/MWh of $VOLL$, 62.5 percent of the time SR_t values are greater than or equal to the ones in lower $VOLL$ values although this margin is 100 percent in the case without the VPLE. Thus, we can conclude that the compromise solution is not affected for $VOLL$ between 1750 \$/MWh and 3250 \$/MWh. Similar but inverse relationship is valid for $EENS_t$ under different $VOLL$ values (Figure 4.25).

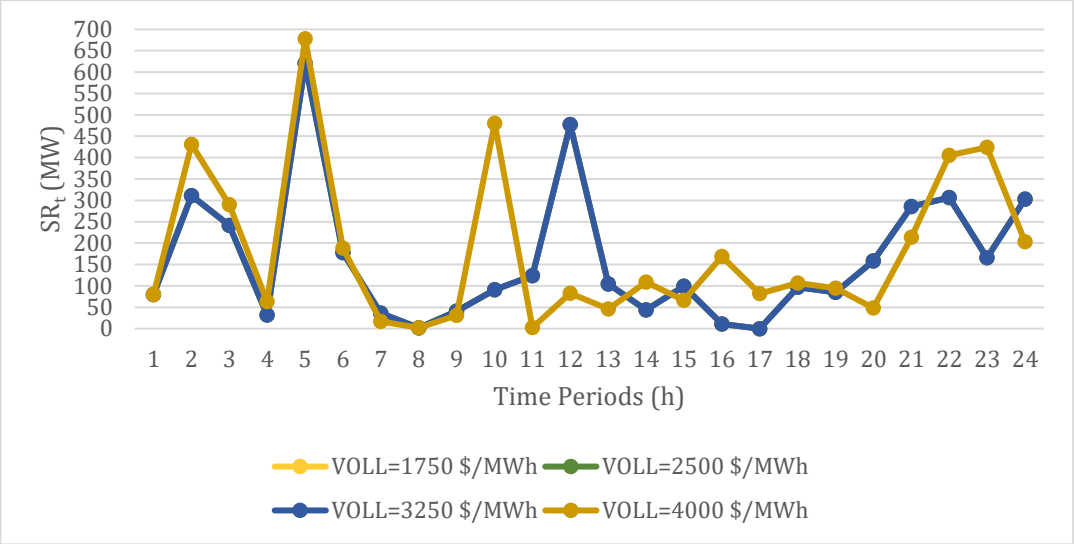

Figure 4.24. Relationship between $VOLL$ and SR_t for IEEE 30-bus Problem Instance

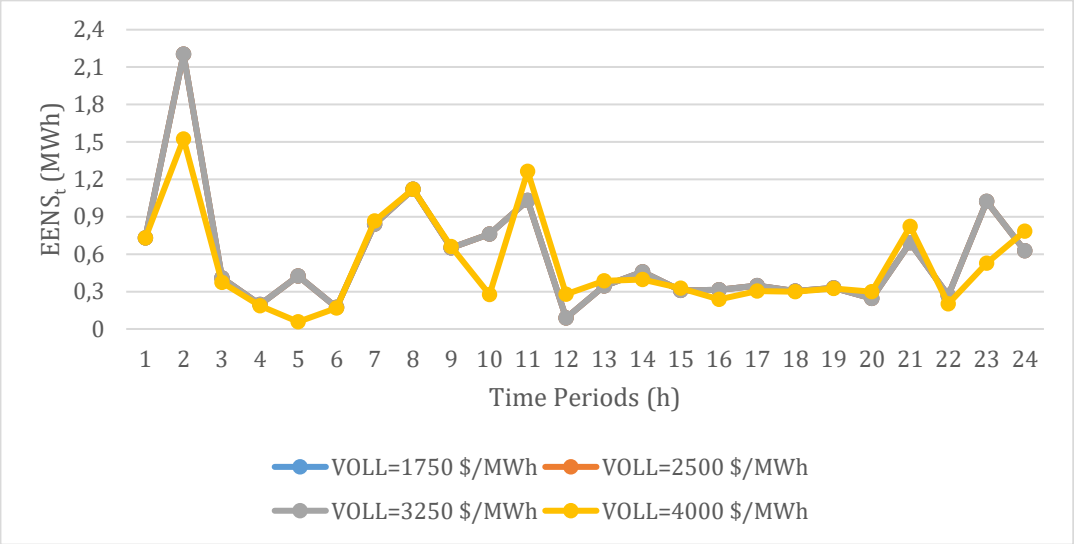

Figure 4.25. Relationship between $VOLL$ and $EENS_t$ Reserve for IEEE 30-bus Problem Instance

Secondly, we analyze how changes in wind forecast errors affect the compromise solution. For this purpose, SR_t and $EENS_t$ values are plotted in Figures 4.26 and 4.27 for different scaling factors. It is observed that SR_t values over the horizon do not change between the first two and the last two wind speed scales, since the same commitment decisions are maintained because of the VPLE. That is, for the first two

and the last two wind speed scales, the cost of the VPLE has a dominant effect on the equilibrium point in the trade-off between total cost components.

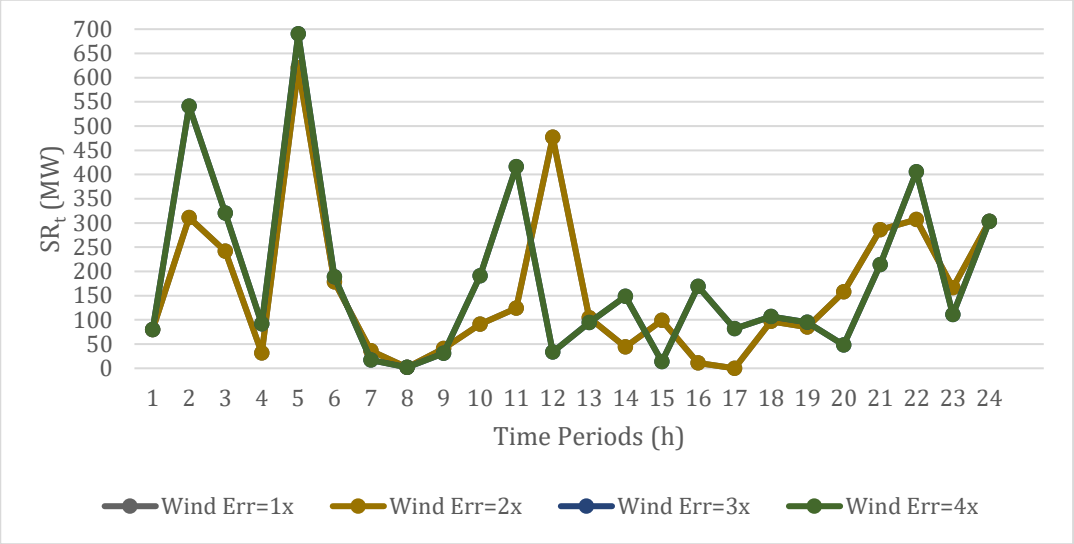

Figure 4.26. Relationship between Wind Speed Forecast Errors and SR_t for IEEE 30-bus Problem Instance

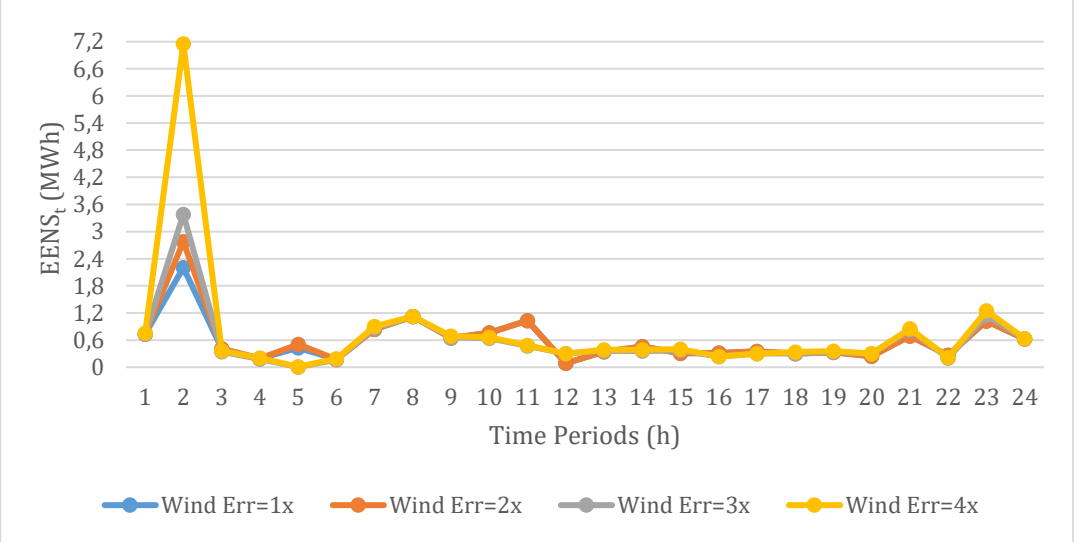

Figure 4.27. Relationship between Wind Speed Forecast Errors and $EENS_t$ for IEEE 30-bus Problem Instance

Different from SR_t values, $EENS_t$ values slightly increase with an increase in wind speed forecast errors as shown in Figure 4.27, but the change is not significant for time periods with high net load intensity. The total operating cost and its breakdown under different wind speed errors are summarized in Table 4.16. It is observed that the total operating cost increases as wind speed errors increase. Nevertheless, generation and reserve costs do not change for the first two and the last two levels of wind speed scales because of the VPLE.

Table 4.16. Total Operating Cost under Different Wind Speed Forecast Errors for IEEE 30-bus Problem Instance

Scale of Wind Speed Error	**x1**	**x2**	**x3**	**x4**
Expected Cost of EENS ($)	24,304.3	25,457.8	24,968.9	32,390.3
Generation & Reserve Cost ($)	697,383.4	697,383.4	712,876.6	712,876.6
Total Operating Cost ($)	**721,687.7**	**722,841.2**	**737,845.5**	**745,266.9**

Thirdly, we examine the sensitivity of the solution for different load demand forecast errors. The results are different from the ones under different wind speed forecast errors. SR_t decisions are very sensitive to changes in load demand forecast errors for all time periods as illustrated in Figure 4.28. Likewise, $EENS_t$ values increase with high load demand forecast errors as shown in Figure 4.29.

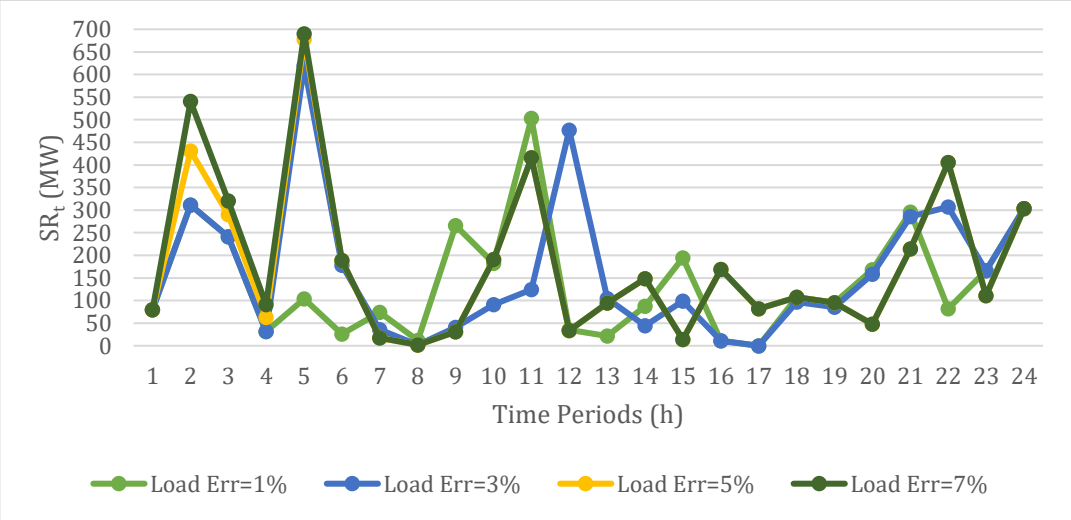

Figure 4.28. Relationship between Load Demand Forecast Errors and SR_t for IEEE 30-bus Problem Instance

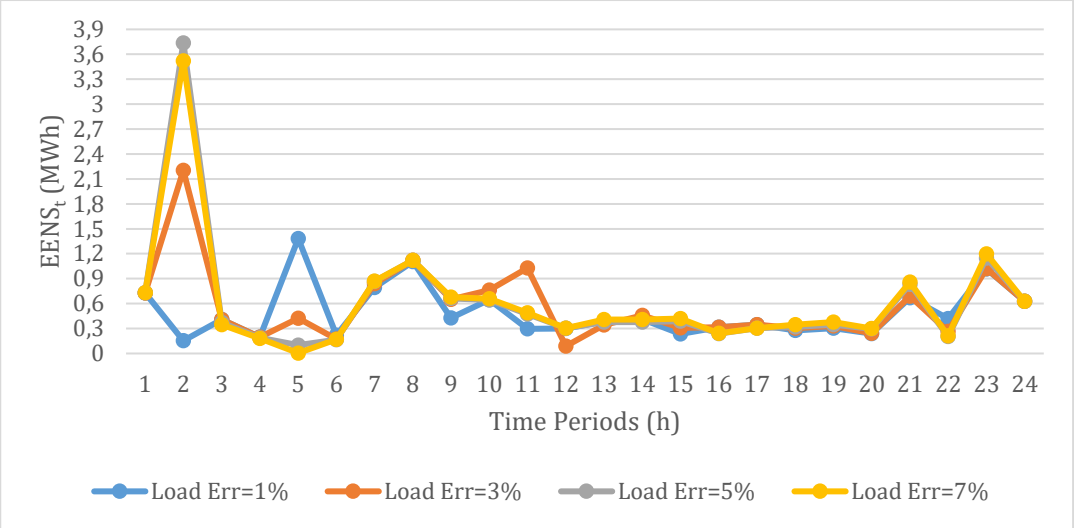

Figure 4.29. Relationship between Load Demand Forecast Errors and $EENS_t$ for IEEE 30-bus Problem Instance

However, it should also be noted that both SR_t and $EENS_t$ values are the same for time periods with high net load intensity and 5% and 7% load demand forecast errors. In particular, the cost of expected load shedding overweighs the cost of the VPLE in the trade-off between total cost components for different load demand forecast errors. Moreover, total operating cost increases with high load demand forecast errors. Its breakdown is provided in Table 4.17.

Table 4.17. Total Operating Cost under Different Load Demand Forecast Errors for IEEE 30-bus Problem Instance

Load Forecast Errors	**1%**	**3%**	**5%**	**7%**
Expected Cost of EENS ($)	20,836.6	24,304.3	25,946.2	25,857.0
Generation & Reserve Cost ($)	698,242.9	697,383.4	702,245.7	712,876.6
Total Operating Cost ($)	**719,079.5**	**721,687.7**	**728,191.9**	**738,733.6**

Another parameter is incremental reserve cost of a conventional generating unit. To see its effects on total cost, SR_t and $EENS_t$; reserve rates are scaled in an increasing order. As demonstrated in Figure 4.30, SR_t values are not sensitive to changes in incremental reserve rates since the equilibrium point in the trade-off between cost components is not affected by marginal reserve costs. This is a result of the VPLE,

which is the main determinant on this trade-off. There is a similar relationship for $EENS_t$ values under different incremental reserve rates. Hence, it is tolerable to increase reserve rates up to the scale of 3 without changing SR_t decisions much (Figure 4.31).

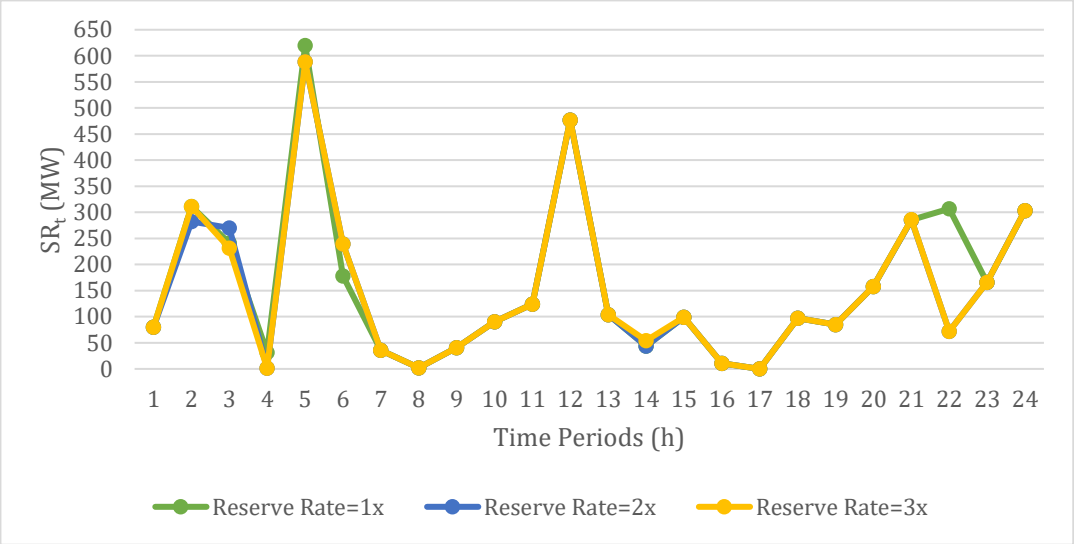

Figure 4.30. Relationship between Incremental Reserve Rates and SR_t for IEEE 30-bus Problem Instance

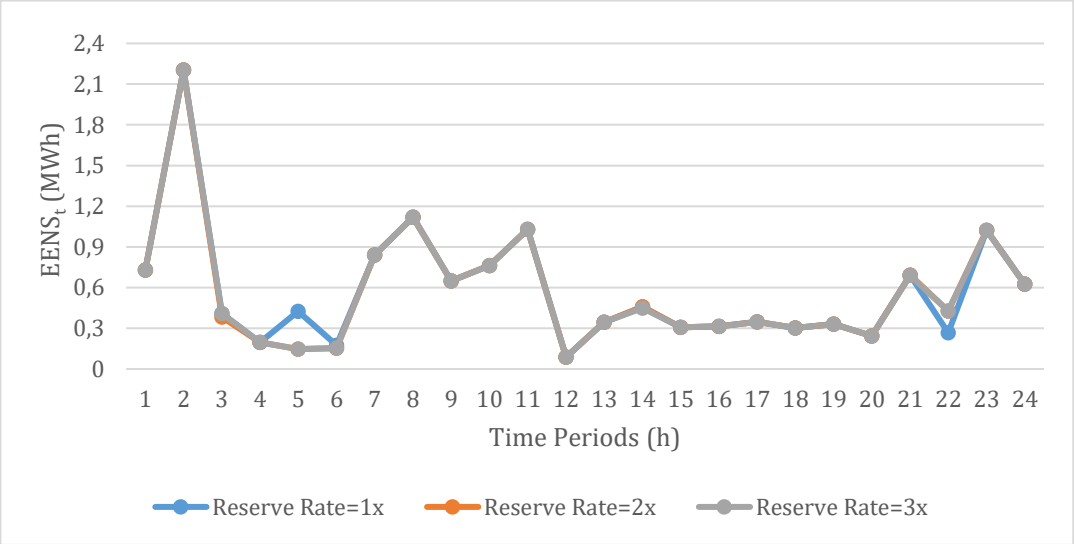

Figure 4.31. Relationship between Incremental Reserve Rates and $EENS_t$ for IEEE 30-bus Problem Instance

Although commitment and dispatching decisions are not significantly affected by the change in the cost of holding an extra reserve, total reserve costs increase with an increase in incremental reserve rates as show in Table 4.18. That is because charging higher incremental rates makes the same level of SR_t more expensive.

Table 4.18. Total Operating Cost under Different Incremental Reserve Rates for IEEE 30-bus Problem Instance

Scale of Reserve Rates	x1	x2	x3
Expected Cost of EENS ($)	24,304.3	24,015.6	24,042.3
Generation & Reserve Cost ($)	697,383.4	705,241.4	712,621.7
Total Operating Cost ($)	**721,687.7**	**729,256.9**	**736,664.1**

Lastly, we test the sensitivity of the solution by reducing the reliability of the conventional power generation system. For this purpose, we double and triple failure rates; accordingly, we solve the model with new system reliability. As shown in Table 4.19, there is an increase in total operating cost as the conventional system becomes less reliable. That is because increasing uncertainty in conventional generation brings additional burden on the expected cost of EENS.

Table 4.19. Total Operating Cost under Different Conventional System Reliability for IEEE 30-bus Problem Instance

Scale of ORR	x1	x2	x3
Expected Cost of EENS ($)	24,304.3	44,265.9	61,110.5
Generation & Reserve Cost ($)	697,383.4	697,383.4	690,395.7
Total Operating Cost ($)	**721,687.7**	**741,649.2**	**751,506.2**

As illustrated in Figure 4.32, the proposed model is not sensitive to changes in ORR scales between 1 and 2, so this change might be tolerable for SR_t decisions. However, this is not the case for the changes in ORR scales between 2 and 3. The reason is that more units become committed in time periods with high net load intensity when failure rates are tripled.

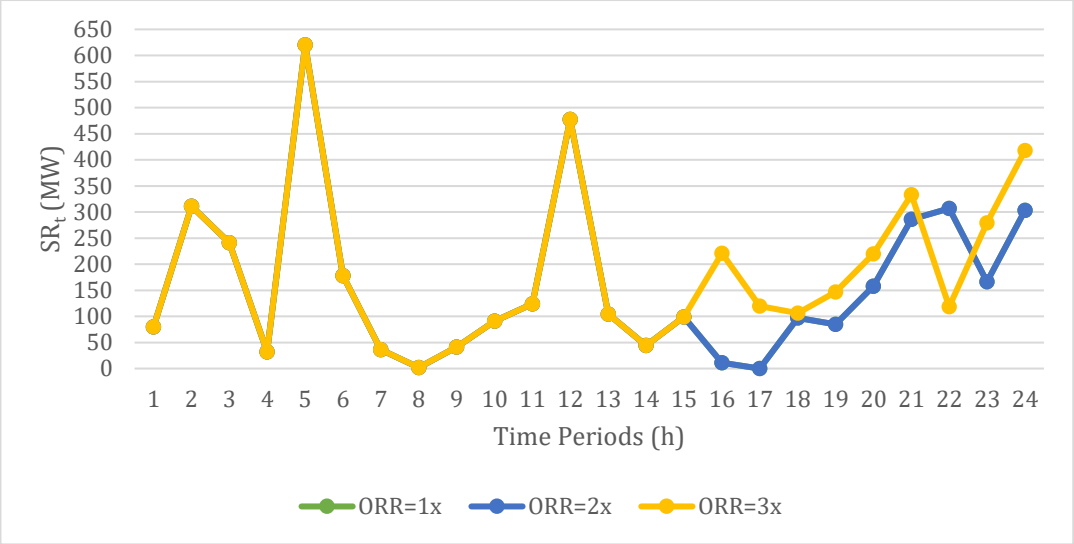

Figure 4.32. Relationship between Conventional System Reliability and SR_t for IEEE 30-bus Problem Instance

As demonstrated in Figure 4.33, $EENS_t$ values tend to increase with the reduction in the reliability of the conventional system even if the same committed capacities are maintained.

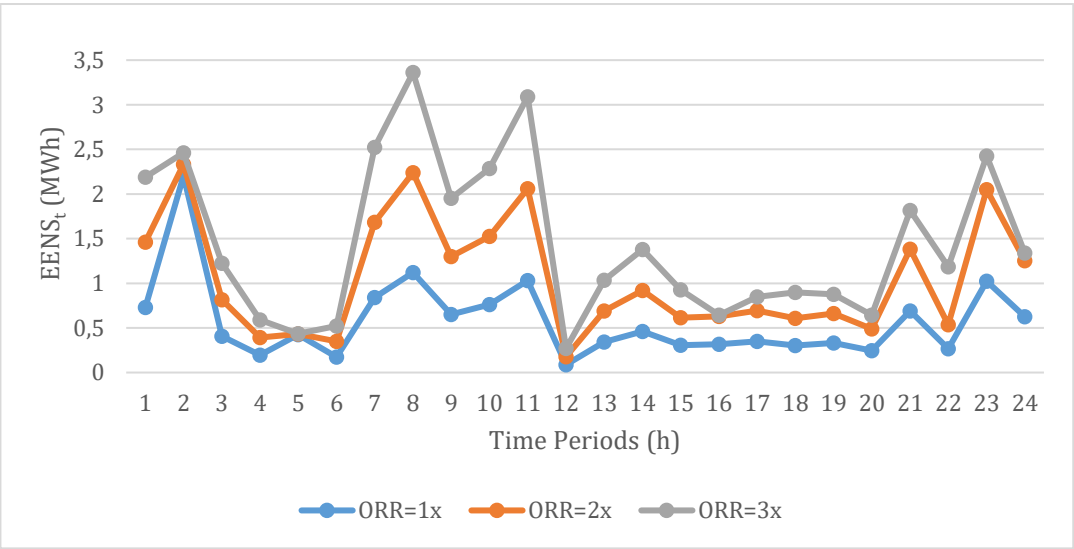

Figure 4.33. Relationship between Incremental Reserve Rates and $EENS_t$ for IEEE 30-bus Problem Instance

In particular, the results of sensitivity analyses verify that $VOLL$, load demand and wind speed forecast errors, and conventional generation reliability have important roles in the proposed time-decoupled stochastic model MIQP I-VPLE for IEEE 30-bus problem instance. Hence, the compromise solution is significantly affected for some levels of these parameters. On the other hand, reserve rates have an insignificant effect on the solution. Moreover, it is also observed that rippling efficiencies of conventional generating units due to the VPLE substantially change solution behaviors towards different parameters when compared to the ones without the VPLE.

4.3.4 Comparison with Deterministic Approaches

The proposed time-decoupled stochastic formulations MIQP I and MIQP I-VPLE are compared with traditional UCP formulations in which deterministic reserve policies are adopted in order to cope with uncertainties related to conventional generation and forecasts of load demand and wind power. The most commonly used deterministic policies are traditional, 3.5σ or hybrid approaches. They are imposed with the following constraint where SR_t^{Min} denotes the minimum spinning reserve requirement in period *t*:

$$CC_t \geq D_t^f + SR_t^{Min} \quad \forall t \tag{4.91}$$

In the traditional approach, reserves are determined according to |*N*|-1 contingency rules while ignoring variabilities in forecast errors. That is, the amount of reserve in a period is calculated by considering the failure case of a conventional generating unit and assuming that synchronized failures of two or more units are less likely to occur. For this purpose, the minimum reserve in each period is set to be at least the available capacity of the largest unit that can be committed in period *t*. However, this reserve requirement may be too conservative when the conventional system reliability is high, the forecast errors have smaller standard deviation and

socioeconomic value that customers put on the lost load is low. SR_t^{Min} is expressed with the following expression:

$$SR_t^{Min} = \max\{P_{it}^{Max}\} \quad \forall t \tag{4.92}$$

In the 3.5σ approach, reserves are determined according to the potential imbalances in net load forecasts while neglecting failure events in conventional generation. Thus, the minimum reserve in each period is set to be 3.5 times the standard deviation of net load forecast errors for period *t*. Nonetheless, this reserve requirement may not be sufficient when forecast precision is high, but the conventional system reliability is low and socioeconomic value that customers put on the lost load is high. SR_t^{Min} is expressed with the following expression:

$$SR_t^{Min} = 3.5\sigma_t^D \quad \forall t \tag{4.93}$$

In the hybrid approach, traditional and 3.5σ approaches are combined as a weighted sum in order to consider uncertainties in both conventional generation and forecast errors. In this approach, weights are determined according to the judgment and prior knowledge of the system operator. In our comparison, we assume that each approach is equally important, so SR_t^{Min} is expressed with the following expression:

$$SR_t^{Min} = [0.5 \max\{P_{it}^{Max}\} + 0.5(3.5\sigma_t^D)] \quad \forall t \tag{4.94}$$

Those deterministic approaches are also solved in a time-decoupled manner via CPLEX for MATLAB toolbox. According to schedules obtained by these approaches, their SR_t and $EENS_t$ values are computed by using $EENS_t$ Approximation I as in our MIQP models. Then, their expected costs of load shedding and reserve costs are calculated by incurring the same $VOLL$ and reserve rates.

4.3.4.1 Results for the Model MIQP I

The time-decoupled stochastic model MIQP I and conventional UCP models with deterministic reserve criteria are implemented to IEEE 24-bus problem instance. In Figure 4.34, committed capacities are compared for proposed and deterministic UCP

approaches. The traditional approach yields schedules with the largest CC_t over all periods whereas the 3.5σ approach gives schedules with the smallest CC_t. This is an indicator that the former is the most conservative one while the latter is the least conservative one. The proposed and hybrid approach are comparable in terms of committed capacities over the 24-h scheduling horizon. CC_t levels in the proposed approach ranges between 1853 MW and 2864 MW whereas they are between 1782 MW and 2905 MW for the hybrid approach. Furthermore, for 66% of the time, the proposed approach commits more capacity than that of the hybrid approach because of the real trade-off between generation, reserve and $EENS_t$ costs over all periods.

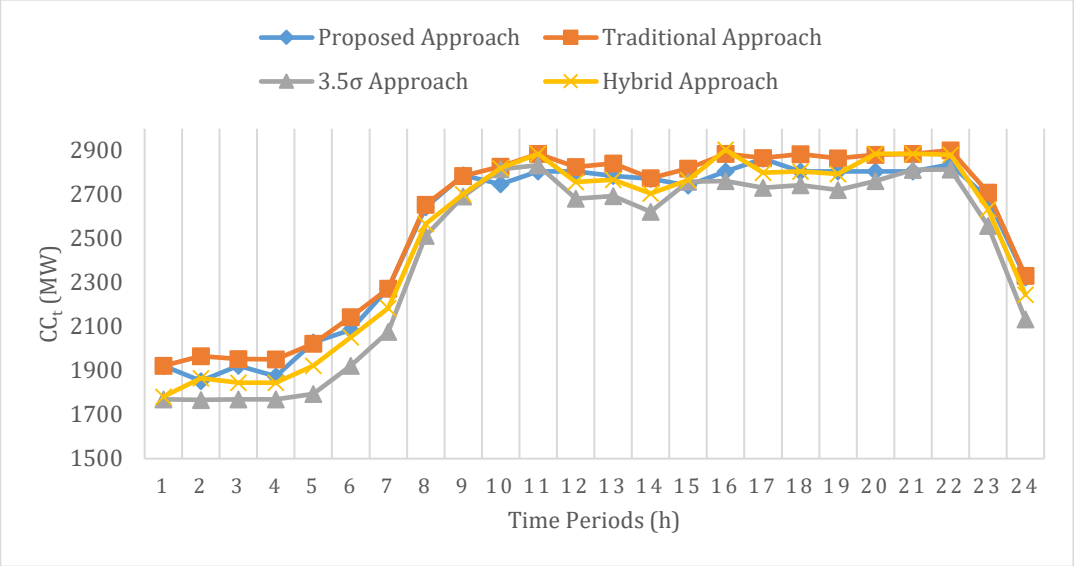

Figure 4.34. Comparison of Committed Capacities in the Proposed and Deterministic Approaches for IEEE 24-bus Problem Instance

Besides, both proposed and deterministic approaches are compared with respect to SR_t levels over the 24-h scheduling horizon as demonstrated in Figure 4.35. Similar to the relationship in CC_t levels, the traditional approach provides more SR_t than other approaches because of its conservativeness whereas the 3.5σ approach supplies less SR_t than other approaches. When compared to other approaches, the hybrid approach supplies SR_t in a steadier manner, but this stability is not economically justified. On the contrary, in the proposed approach, there is a significant fluctuation

in SR_t levels over periods, which are always less than the ones in the traditional approach and sometimes less than both 3.5σ and hybrid approaches. That is because the proposed approach tries to economically rationalize the provision of additional reserves over the abatement in $EENS_t$.

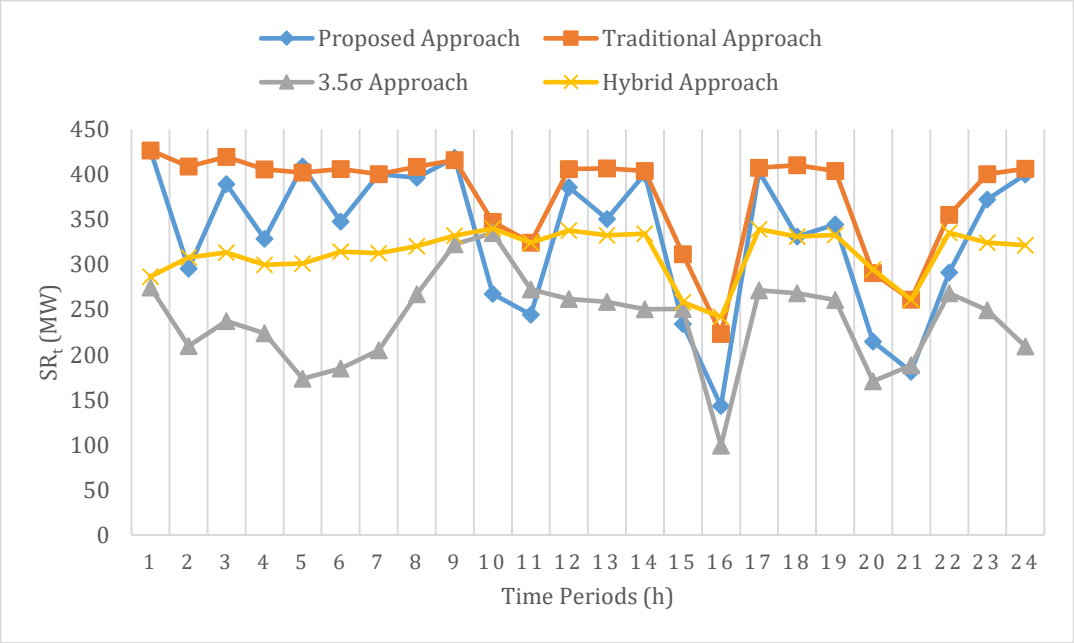

Figure 4.35. Comparison of Reserves in the Proposed and Deterministic Approaches for IEEE 24-bus Problem Instance

In addition, both proposed and deterministic approaches are compared in terms of $EENS_t$ levels over the 24-h scheduling horizon as illustrated in Figure 4.36. As expected, a similar but inverse relationship is valid for $EENS_t$ levels. As a result of the conservative nature of the traditional approach, $EENS_t$ levels are usually less than or equal to the ones in other approaches. It is followed by the proposed, hybrid and 3.5σ approaches in increasing order. Nevertheless, for the deterministic policies, $EENS_t$ levels are steadier than those for the proposed approach, which is also the result of the real trade-off between generation, reserve and $EENS_t$ costs.

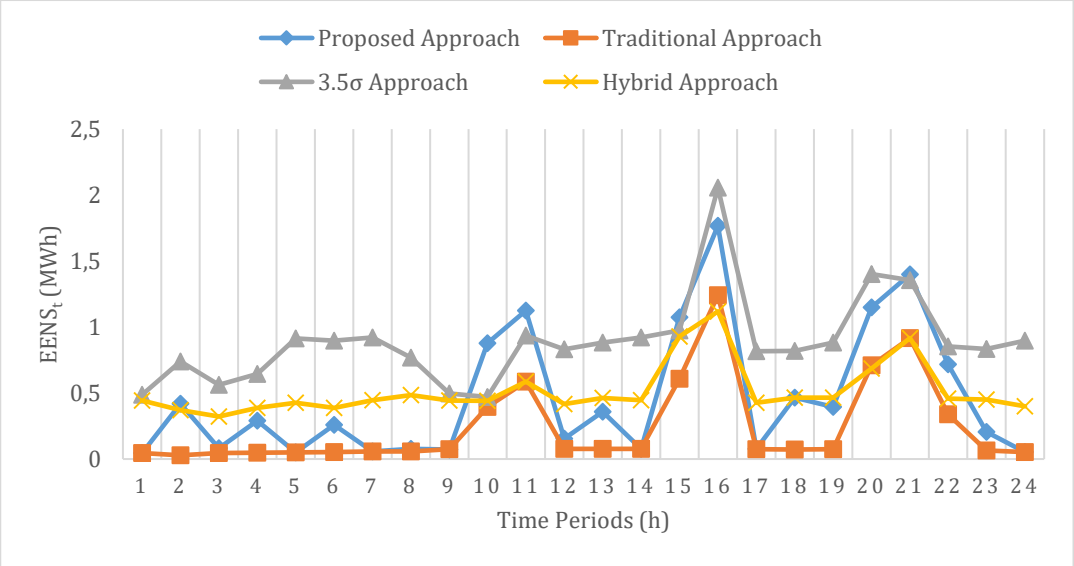

Figure 4.36. Comparison of $EENS_t$ levels in the Proposed and Deterministic Approaches for IEEE 24-bus Problem Instance

According to Table 4.20, the proposed approach outperforms deterministic approaches in terms of total operating costs including socioeconomic value of the lost load and reserve rates.

Table 4.20. Comparison of Total Operating Costs in the Proposed and Deterministic Approaches for IEEE 24-bus Problem Instance

Approaches	**Proposed**	**Traditional**	**3.5σ**	**Hybrid**
Total Operating Cost ($)	722,482.5	726,596.0	730,981.5	727,215.5

When total operating costs are divided into two components, namely the expected cost of load shedding (EENS), and generation and reserve costs as illustrated in Figure 4.37, $EENS_t$ related cost constitutes the minimal portion of the total operating cost in the traditional approach since total $EENS_t$ over the 24-h scheduling horizon has the minimum value of 6 MWh due its conservative reserve requirement. When the 3.5σ approach is compared to other approaches, total $EENS_t$ has its maximum value of 21 MWh. Thus, the cost component associated with load shedding has the largest portion. Accordingly, the 3.5σ approach yields the costliest schedule. Concerning the expected cost of EENS, the proposed and hybrid approaches are

approximately same. However, the proposed approach has the highest operational efficiency in terms of generation and reserve costs by explicitly making the cost/benefit analysis between the socioeconomic value of the lost load and the provision of extra reserves.

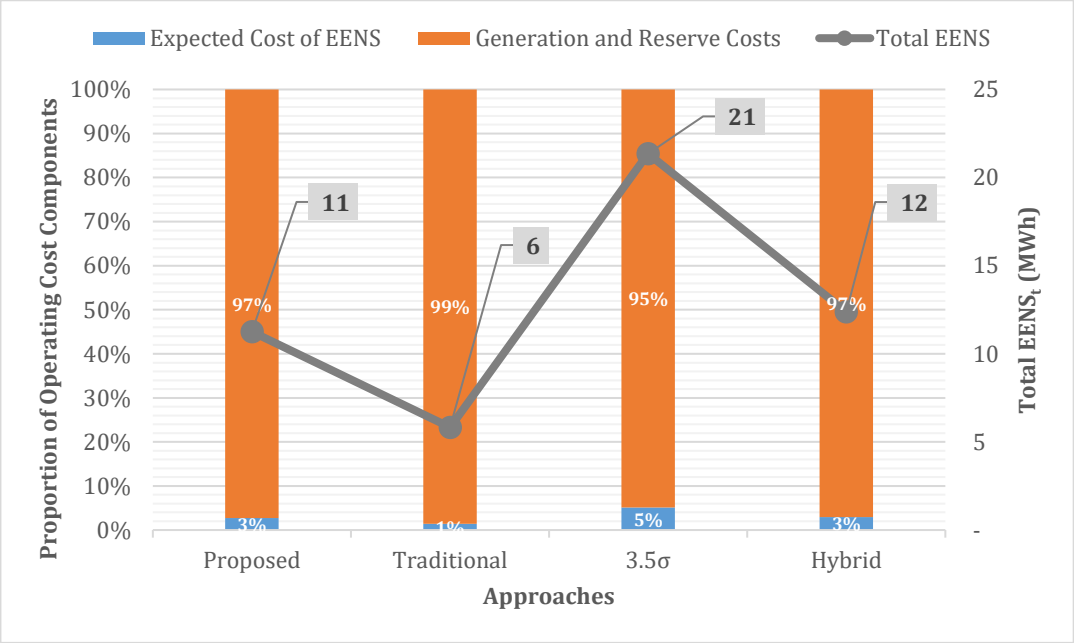

Figure 4.37. Comparison of Cost Components and Total $EENS_t$ in the Proposed and Deterministic Approaches for IEEE 24-bus Problem Instance

4.3.4.2 Results for the Model MIQP I-VPLE

The time-decoupled stochastic MIQP model and conventional UCP models with deterministic reserve criteria are applied to IEEE 30-bus problem instance and its duplicated version. In both problem instances, the VPLE is also taken into consideration. Thus, we show its impact on the schedules obtained with different approaches for smaller and medium sized conventional power systems. First, the results for the former problem instance are provided. In Figure 4.38, committed capacities are compared for the proposed and deterministic approaches for IEEE 30-bus problem instance. Schedules obtained by the traditional and hybrid approaches have the largest CC over most of the periods due to the VPLE, which is an indicator

that both approaches are too conservative. These schedules are followed by the 3.5σ approach in terms of CC although it yields similar dispatching decisions for periods with low net load intensity. That is, the 3.5σ approach behaves closer to the proposed approach when full utilization of available conventional generation capacity is not required to satisfy the net load demand. As a result of the explicit cost/benefit analysis between the provision of additional reserves and the reduction in $EENS_t$, the proposed approach suggests that there is no need for excessive number of committed units, which is the case in the deterministic policies, to meet the net load demand in almost all periods. Thus, schedules attained by the proposed approach usually have the smallest committed capacity ranging from 603 MW to 2174 MW over the 24-h scheduling horizon.

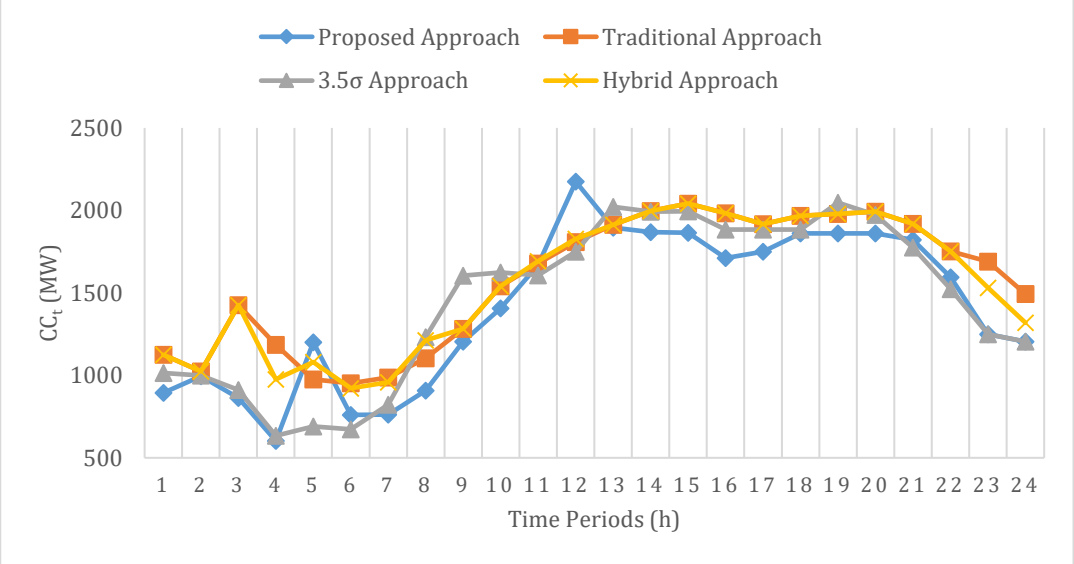

Figure 4.38. Comparison of Committed Capacities in the Proposed and Deterministic Approaches for IEEE 30-bus Problem Instance

Moreover, both proposed and deterministic approaches are compared with respect to SR_t levels over the 24-h scheduling horizon as demonstrated in Figure 4.39. Similar to the relationship in CC levels, traditional and hybrid approaches provide more SR_t than other approaches because of their conservativeness whereas the proposed approach supplies less SR_t than other approaches in most of the periods. The reason

is that the proposed approach economically justifies the supply of additional reserves over the abatement in EENS. For periods with low net load intensity, the 3.5σ approach gives schedules that are similar to the ones of the proposed approach in the sense of reserves allocated.

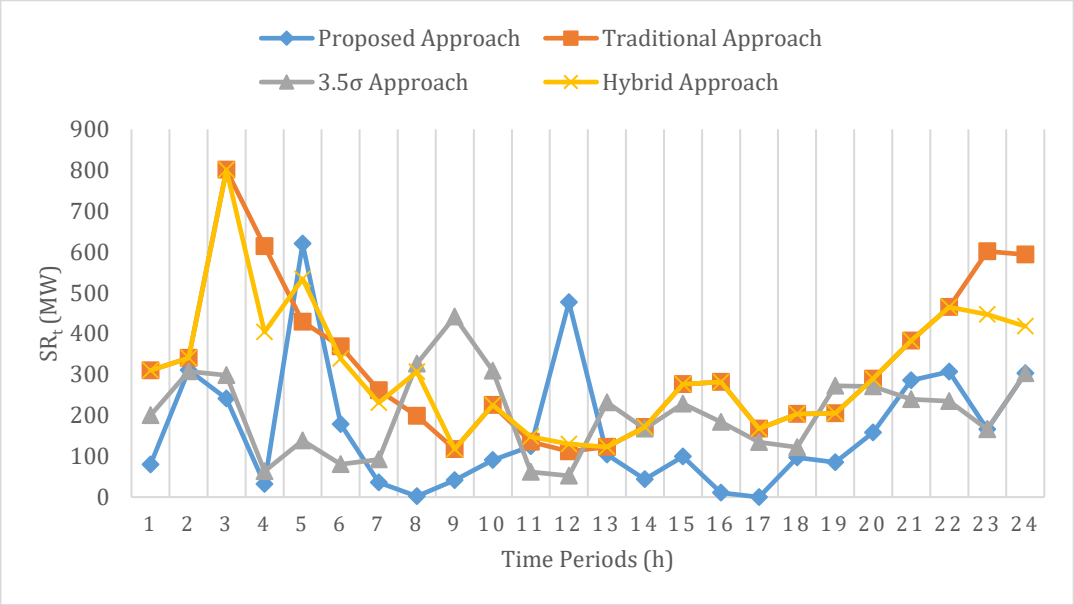

Figure 4.39. Comparison of Reserves in the Proposed and Deterministic Approaches for IEEE 30-bus Problem Instance

Both proposed and deterministic approaches are also compared in terms of $EENS_t$ levels over the 24-h scheduling horizon as illustrated in Figure 4.40. As expected, a similar but inverse relationship is valid for $EENS_t$ levels. Due to conservative natures of traditional and hybrid approaches, $EENS_t$ levels are usually less than or equal to the ones with the other approaches. They are followed by the schedules of the 3.5σ approach and the proposed approach in terms of $EENS_t$ levels. Nonetheless, for all approaches, $EENS_t$ levels are steadier for periods with high net load intensity whereas those levels significantly fluctuate over periods with low load intensity. That is because the installed conventional generation capacity is not required to be fully utilized for such periods, so the VPLE component in generation costs is the dominant factor when deciding on the allocation of SR_t and the abatement in $EENS_t$.

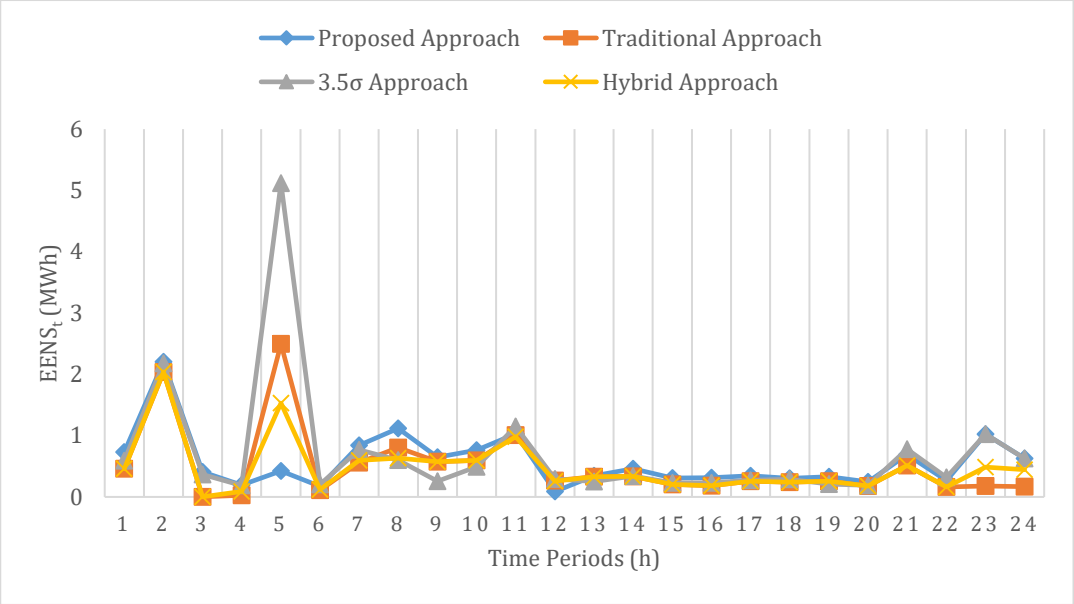

Figure 4.40. Comparison of $EENS_t$ levels in the Proposed and Deterministic Approaches for IEEE 30-bus Problem Instance

As reported in Table 4.21, the proposed approach outperforms deterministic approaches in terms of total operating costs including socioeconomic value of the lost load and reserve rates.

Table 4.21. Comparison of Total Operating Costs in the Proposed and Deterministic Approaches for IEEE 30-bus Problem Instance

Approaches	**Proposed**	**Traditional**	**3.5σ**	**Hybrid**
Total Operating Cost ($)	721,687.7	809,204.4	755,191.0	789,344.5

When total operating costs are divided into two components, namely the expected cost of load shedding (EENS), and generation and reserve costs as illustrated in Figure 4.41, $EENS_t$ related cost constitutes the minimal portion of the total operating cost in the traditional approach since total $EENS_t$ over the 24-h scheduling horizon is 12 MWh due to its conservative reserve requirement. Even if it provides smaller total $EENS_t$, the schedule obtained by the traditional approach has the highest total operating cost since more units are committed in general. The same reasoning is also valid for the hybrid approach which yields a schedule with the smallest total $EENS_t$

of 11 MWh by committing more units. When the 3.5σ approach is compared to the other approaches, total $EENS_t$ has its maximum value of 17 MWh. Hence, the load shedding component has the largest impact on its total operating cost. Although the total $EENS_t$ of the schedule attained by the proposed approach is 14 MWh, which is the second largest value when compared to the other approaches, it has the minimum total operating cost. The main reason is that the proposed approach has the highest operational efficiency in terms of generation and reserve costs by explicitly making the cost/benefit analysis between the socioeconomic value of the lost load and the provision of extra reserves. Therefore, it commits a smaller number of conventional units to satisfy the same net load level with less reserves by providing economic justification.

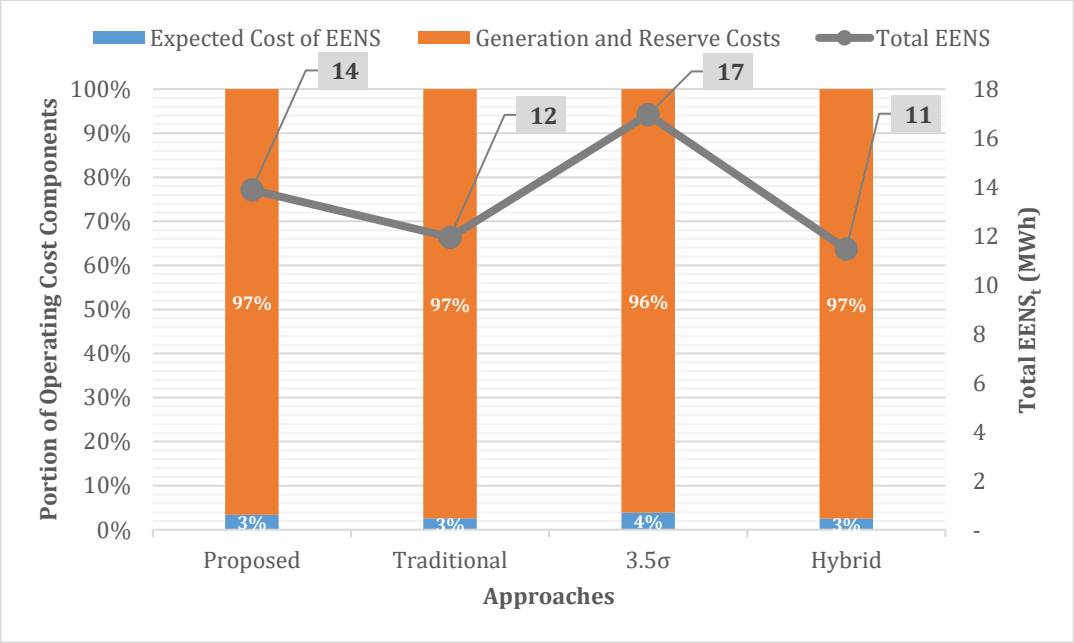

Figure 4.41. Comparison of Cost Components and Total $EENS_t$ in the Proposed and Deterministic Approaches for IEEE 30-bus Problem Instance

Similar comparisons are also made for the duplicated version of IEEE 30-bus problem instance. As illustrated in Figure 4.42, committed capacities are compared for the proposed and deterministic approaches. Traditional and hybrid approaches give the same schedules due to the VPLE even though the minimum reserve

requirements are different but close to each other. Schedules obtained by both approaches have the largest CC_t over most of the periods, which is an indicator that they are too conservative. These schedules are followed by the 3.5σ approach in terms of CC_t. Thanks to the explicit cost/benefit analysis between the supply of additional reserves and the mitigation in $EENS_t$, the proposed approach suggests that there is no need to commit an excessive number of units, which is the case in deterministic policies, to meet the net load demand in almost all periods. Thus, schedules attained by the proposed approach usually has the smallest committed capacity ranging from 1205 MW to 3670 MW over the 24-h scheduling horizon.

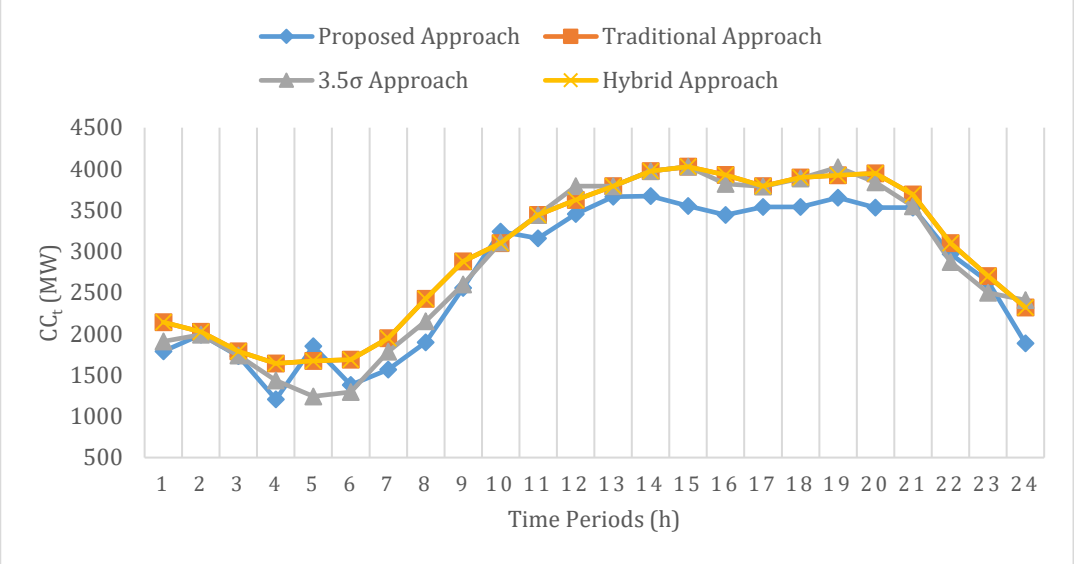

Figure 4.42. Comparison of Committed Capacities in the Proposed and Deterministic Approaches for Duplicated IEEE 30-bus Problem Instance

Both proposed and deterministic approaches are also compared with respect to SR_t levels over the 24-h scheduling horizon as demonstrated in Figure 4.43. Similar to the relationship in CC_t levels, traditional and hybrid approaches supply more SR_t than the other approaches owing to their conservativeness whereas the proposed approach provides less SR_t than other approaches in most of the periods. That is because the proposed approach economically justifies the provision of additional reserves over the reduction in $EENS_t$. It is important to emphasize that the difference

between the proposed and deterministic approaches is more significant in duplicated IEEE 30-bus problem instance than that in the original instance. The reason is that simultaneous outages are less likely to occur as the size of the conventional power generation system increases. Hence, with 1750 $/MWh of $VOLL$, the additional reduction of $EENS_t$ cannot be justified by committing additional units; accordingly, providing additional reserves. Besides, the 3.5σ approach gives schedules that are between the ones of the proposed and other deterministic approaches. Nonetheless, it provides similar schedules for periods with high net load intensity as in traditional and hybrid approaches.

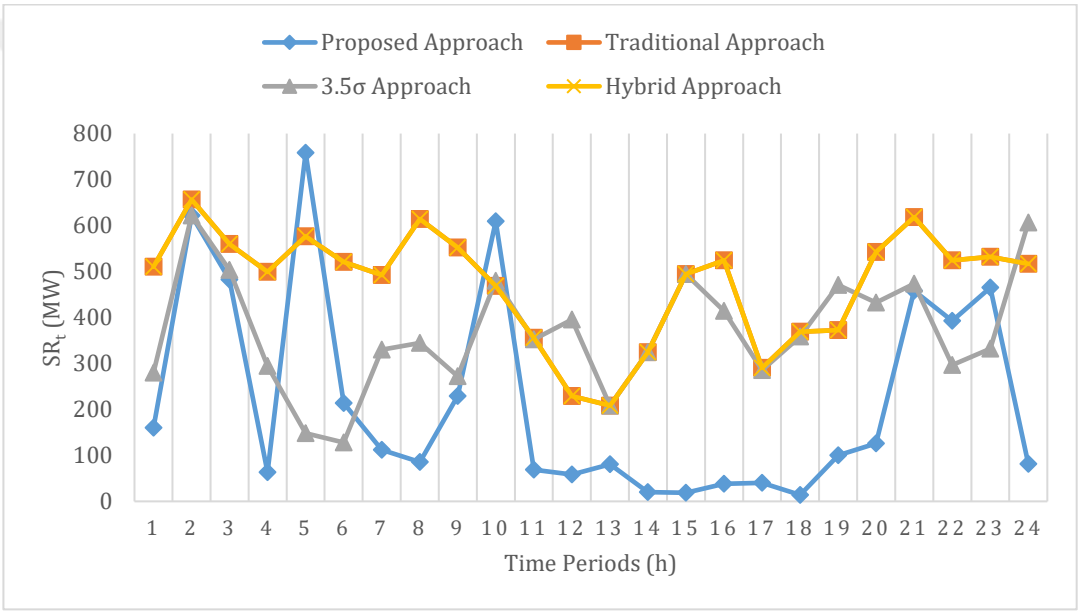

Figure 4.43. Comparison of Reserves in the Proposed and Deterministic Approaches for Duplicated IEEE 30-bus Problem Instance

In Figure 4.44, the comparison of both proposed and deterministic approaches is illustrated in terms of $EENS_t$ levels over the 24-h scheduling horizon. For $EENS_t$ levels, a similar but inverse relationship is valid. Owing to conservative natures of traditional and hybrid approaches, $EENS_t$ levels are usually less than or equal to the ones in other approaches. In general, they are followed by schedules of the 3.5σ approach and the proposed approach in terms of $EENS_t$ levels.

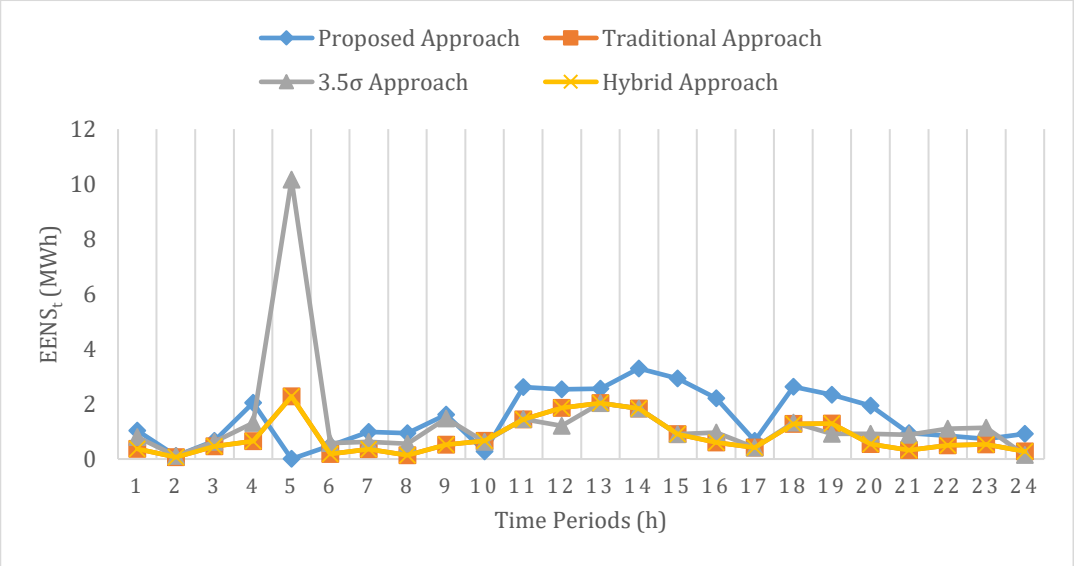

Figure 4.44. Comparison of $EENS_t$ levels in the Proposed and Deterministic Approaches for Duplicated IEEE 30-bus Problem Instance

As summarized in Table 4.22, the proposed approach outperforms deterministic approaches in terms of total operating costs including socioeconomic value of the lost load and reserve rates.

Table 4.22. Comparison of Total Operating Costs in the Proposed and Deterministic Approaches for Duplicated IEEE 30-bus Problem Instance

Approaches	**Proposed**	**Traditional**	**3.5σ**	**Hybrid**
Total Operating Cost ($)	1,418,710.3	1,488,444.1	1,467,718.5	1,488,444.1

When total operating costs are divided into two components such as the expected cost of load shedding (EENS), and generation and reserve costs as depicted in Figure 4.45, $EENS_t$ related cost constitutes the minimal portion of the total operating cost in traditional and hybrid approaches since total $EENS_t$ over the 24-h scheduling horizon is 28 MWh owing to their conservative reserve requirements. Although they provide lower total $EENS_t$, their schedules have the highest total operating cost since more units are committed in general. Total $EENS_t$ of the schedule obtained by the 3.5σ approach is 32 MWh, which is the second largest value when compared to other

approaches. Even though the total $EENS_t$ in the proposed approach is 34 MWh, which is the largest value when compared to other approaches, it has the minimum total operating cost. The same reasoning on higher operational efficiency of the proposed approach in IEEE 30-bus system is also valid for the duplicated system.

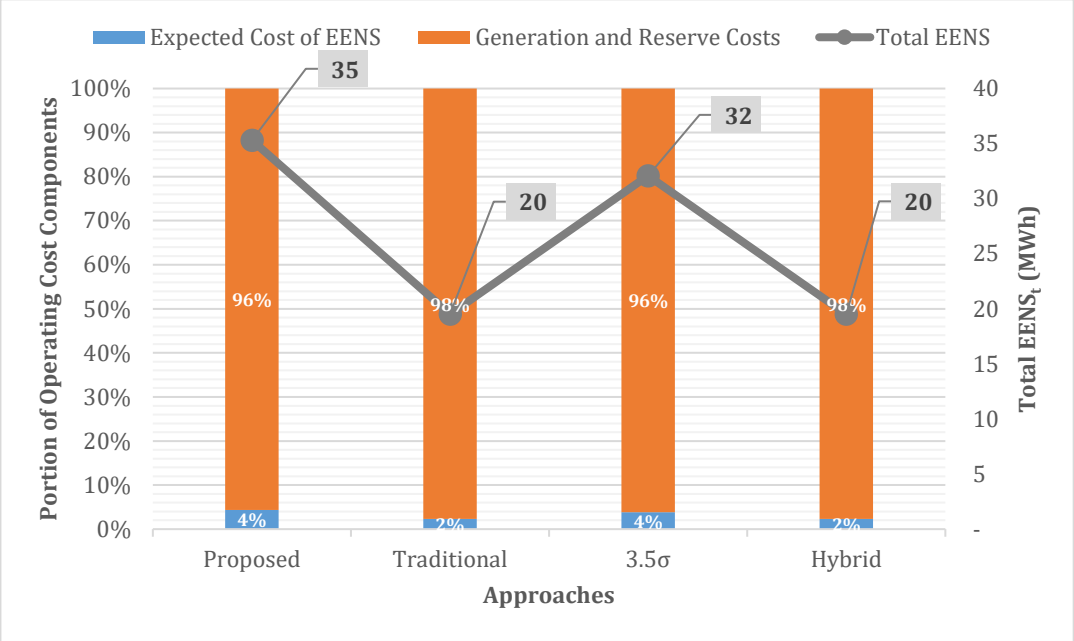

Figure 4.45. Comparison of Cost Components and EENS in Proposed and Deterministic Approaches for Duplicated IEEE 30-bus Problem Instance

CHAPTER 5

UNIT COMMITMENT PROBLEM FOR WIND INTEGRATED HYBRID POWER SYSTEMS UNDER SUPPLY/DEMAND UNCERTAINTY AND EMISSION LIMITATIONS

Due to increasing concerns on adverse effects of global warming and air pollution, a great majority of countries have been promoting policies that can mitigate emissions of greenhouse gases and air pollutants especially for the last decade. For this purpose, usage of clean energy technologies is encouraged in environmental and industrial policies, and ambitious targets have been set to increase the contribution of renewable energy sources in the power generation mix and to reduce levels of emissions that are detrimental for the environment and human health. To illustrate, wind, which is one of the promising renewable sources, is widely used for power generation in most of the countries of North America, Europe and Far East. Nevertheless, wind power generation has an intermittent nature, which makes operations in power generation more challenging by bringing additional uncertainties. As it is stated in Chapter 4, there are three major sources of uncertainty in wind-integrated hybrid power systems such as unexpected outages of conventional generating units in a power system, and forecasts of load demand and wind power generation. Consequently, uncertainties may cause an unexpected increase in emission levels even though wind generation does not directly emit greenhouse gases and air pollutants. Thus, in addition to the effect of uncertainties on conventional generation, the impact of emission control technologies and regulations must also be considered when making unit commitment and load dispatch decisions in order to guarantee more environmentally friendly and reliable power generation.

5.1 Emission Reduction Agreements and Regulations

In 1997, the Kyoto Protocol, one of the most fundamental regulations against climate change, was adopted by the United Nations. The main objective was to stabilize the concentrations of Greenhouse Gases (GHGs) in the atmosphere at a level that would prevent irrevocable changes in the climate system. The 15 countries, namely European Union (EU) members in 1997, United States (US), Canada, Hungary, Japan, Poland, Croatia, New Zealand, Russian Federation, Ukraine, Norway, Australia and Iceland were participated in this protocol. However, US had declared its intention not to ratify the protocol in the same year and Canada had withdrawn from the protocol in 2012 (UNFCCC, n.d.). According to this protocol, the maximum allowable emission amounts that each country can emit over the first commitment period (2008-2012) was determined. Since the main polluter countries such as China, US and India did not ratify this treaty, the average reduction level was targeted as 5% from the 1990 level by the participating countries.

Apart from the Kyoto Protocol, in late 2016, the Paris Agreement has been adopted by the United Nations at the Paris Climate Conference. This agreement has brought all nations including China and USA into a common cause to tackle with the global warming and climate change. According to UNFCCC (2016), the main objective is to globally respond to the threat of climate change by making commitments of:

- Keeping the increase in global temperature below 2 degrees Celsius during the 21st century,
- Contributing to the capabilities of countries to overcome the effects of climate change,
- Reducing global GHG emissions in the second half of the century by implementing the best available innovative technologies for capture and storage.

189 out of 197 Parties attending to the convention have ratified the agreement since 2016. These parties have submitted their detailed national climate action plans in

which they have declared that they are responsible of regularly reporting their emission targets and levels, countermeasures and efforts.

5.1.1 Emission Trading Systems against Greenhouse Gas Emissions

Emission Trading Systems (ETS) in different countries or regions are based on the Cap & Trade mechanism in which a cap, also known as quota, is set on the total amount of GHGs that can be emitted during a year. Companies can buy additional emission allowances if they need additional quota or they want to trade with each other to gain extra revenue. Therefore, this trading mechanism can be considered as the carbon economy where sellers and buyers of emission allowances can interact with each other. Since the authorities of ETS set some limits on the total number of allowances that can be traded, those allowances have a real value in the carbon economy, which makes them tradable commodities. As a result of the Cap & Trade mechanism, companies should have enough allowances for their emissions during a year, otherwise they will need to pay heavy penalties for emissions exceeding their allowances. When companies decrease their emissions beyond their quotas, they can transfer excess allowances to compensate for their future needs or they can trade those allowances in the carbon economy.

In Appendix A, the ETS in EU, US and China are briefly explained since they have been three major GHG emitter regions and countries for several years. The ETS in those countries differentiate from each other with respect to the regulated sectors and different regulatory rules that specify allowable emission limits, allowance allocation methods, sanctions against the noncompliance on limitations for those sectors (ICAP, 2020). Also, according to ICAP (2020), in Turkey, an ETS is planned to be built in near future. Thus, Turkey's efforts to build an ETS are also explained in Appendix A.

5.1.2 Environmental Policies against Air Pollutant Emissions

Air pollution occurs due to excessive releases of dangerous and harmful chemical, biological and physical agents to the atmosphere, which pose a significant risk on the human health and the environment. These agents consist of gases, namely Particulate Matters (PM_x), Nitrogen oxides (NO_x), Sulphur dioxide (SO_2), Carbon monoxide (CO), Methane (CH_4), Ammonia (NH_3), Chlorofluorocarbons (CFCs) and biological molecules. The release of these agents is caused by both human activities and natural phenomena. The human related sources are power generation plants burning coal, oil, natural gas or biomass, energy-intensive industrial facilities, motor vehicles and household combustion devices such as stoves and furnaces burning carbon intensive fuels. These are the major sources of air pollutant emissions although they can also occur as a result of natural disasters like forest fires. According to the World Health Organization (WHO) (2004), the exposure to ambient air pollution has adverse effects on the cardiovascular and respiratory systems by triggering stroke, ischemic heart disease, pneumonia, lung cancer, or chronic and acute respiratory diseases. The potential sources of the most common air pollutants and their adverse effects on the human health and environment are summarized in Table 5.1. (WHO, 2004).

In 1987, WHO designed Air Quality Guidelines, which were revised after 10 years, to mitigate the negative impacts on health and environment. In 2005, the last revision was made as a result of new scientific researches and advancements since 1997. As shown in Table 5.2, revisions include new guidelines for atmospheric concentrations of relatively more important air pollutants such as PM_x, NO_2 and SO_2, which pose more serious and considerable environmental and health risks (WHO, 2005).

Table 5.1. Potential Sources and Adverse Effects of Air Pollutants

Air Pollutant	Potential Sources	Adverse Effects
PM_x	- Combustion engines Motor vehicles - Solid fuel combustion Power generation plants Industrial plants	- Reduction in life expectancy - Aggravation of cardiovascular and lung diseases and cancers - Lung inflammatory reactions - Respiratory disorders - Chronic obstructive pulmonary disease
NO_x	- Fossil fuel combustion Power generation plants Industrial plants	- Acidification and eutrophication of waters and soils - Aggravation of bronchitis and asthma - Formation of particulate matters - Respiratory infections - Lung inflammatory reactions - Reduced lung function and growth
SO_2	- Sulphur-containing fossil fuel combustion Heat generation plants Power generation plants Motor vehicles - Sulphur-containing mineral ore smelting	- Acidification of waters and soils - Formation of acid rains - Adverse effects on aquatic ecosystems and forests - Respiratory disorders - Lung inflammatory reactions - Aggravation of asthma and chronic bronchitis, even pneumonia - Irritation of the eyes
CO	- Fossil fuel combustion Motor vehicle exhaust Industrial plants	- Impairment of cardiovascular system - CO poisoning

Table 5.2. Revised Guideline Thresholds for Air Pollutants by the WHO (2005)

Air Pollutant	WHO Guideline Thresholds	
	Short-Term	Long-Term
PM_2	25 μg/m3 24-h mean	10 μg/m3 annual mean
PM_{10}	50 μg/m3 24-h mean	20 μg/m3 annual mean
NO_2	200 μg/m3 1-h mean	40 μg/m3 annual mean
SO_2	500 μg/m3 10-min mean	20 μg/m3 24-h mean

Besides, the WHO strongly emphasize that achieving guideline thresholds for each air pollutant would not completely annihilate the possibility of negative effects by taking ongoing epidemiological researches and findings into consideration, so most of the countries may adopt concentration levels lower than the thresholds indicated in the guideline. In addition to guideline values, WHO has also set several interim targets for short-term and long-term exposures to progressively reduce concentrations of air pollutants in areas suffering from high air pollution. The detailed explanation of these interim targets can be found in WHO (2005).

Most of the countries in the world have been using these guidelines in order to develop their policies against air pollution. Those polices generally include command and control type regulations although there are several countries which also implement market-based approaches. Command and control type policies involve controlling air pollutant emission amounts and setting emission concentration standards. In the first one, maximum allowable emission amounts are determined according to the best available techniques (BAT) (Organization for Economic Co-operation and Development [OECD], 2017). In the BAT concept, the most effective and sophisticated technologies and their implementation methods, which are especially practical and suitable in real world applications for different sectors, are determined. By taking the emission amounts provided by the BAT as a basis, allowable emission limits for air pollutants are specified to reduce threats on the human health and environment. Different from allowable limits on emission amounts, emission concentration standards are defined by practicing guideline thresholds and interim targets specified by WHO or other air quality index specified by authorized environmental institutions. In some policies, command and control regulations are reinforced with a pollution levy. With this reinforcement, the companies are subject to pay a tax or a set of taxes for their concentrations or amounts of air pollutant emissions. For this purpose, two or three level taxes have been imposed by several countries. The first level is the emission tax for each unit of a pollutant emitted. When the emission amount exceeds the maximum allowable limit, the penalty of emission amount is added to emission tax. When the emission

concentration is greater than the emission concentration standard, the penalty of emission concentration is added to emission tax. If one of these violations exists, then companies pay the second level tax for each unit of air pollutant emission. If both violations exist, then the third level tax is imposed for each unit of air pollutant emission.

In Appendix B, air pollution prevention and reduction policies and practices in EU, US and China are briefly explained.

5.2 Emission Reduction Technologies for Conventional Power Plants

For the last two decades, climate change and air pollution has received a significant attention all over the world due to the expected global temperature rise and reduction in average life expectancy in case effective countermeasures are not taken by the end of 20^{th} century. Besides, the integration of renewable energy sources such as wind and solar into a country's energy generation portfolio will lead to an additional need to increase the installed capacities of conventional power plants requiring fossil fuel combustion. The reason is that wind and solar energy have an intermittent nature, which causes uncertainties in power generation via renewable energy sources, and uncertainties in stable and adequate energy supply of a country. As a result, governments in developed and developing countries have been studying and promoting developments of clean renewable energy sources, and implementations of innovative emission reduction technologies in conventional power plants using fossil fuel combustion processes. For those installations, various technologies have been utilized to mitigate carbon dioxide (CO_2) emissions, which is one of the major GHG emissions causing global warming. Furthermore, there are advanced and efficient air pollution control technologies available for emissions of sulphur dioxide (SO_2), nitrogen oxides (NO_x), and particulate matter (PM_x). Implementing those technologies in conventional power plants has a significant potential in the abatement of atmospheric air pollutant emissions as the air pollution control limits set by governments are becoming more stringent. If those power plants burning fossil

fuels do not benefit from these technologies, they cannot remain operational in near future with more rigorous worldwide regulations on GHG emissions and air pollution.

5.2.1 Carbon Capture and Storage Systems

Marchetti (1977) proposes the concept of sequestration and storage of CO_2 to reduce atmospheric CO_2 emissions, which is the origin of Carbon Capture and Storage (CCS) systems evolved and implemented in the industry nowadays. The main idea behind CCS systems is to sequestrate CO_2 before emitted to the atmosphere, and then transferring captured CO_2 via pipelines or shipping to geological storage areas or ocean storage areas. CCS is the most suitable and practical technology to retrofit fossil fuel burning power plants. By utilizing CCS, CO_2 emissions of these plants can be reduced up to 98% in accordance with the capture technology employed (Huaman and Lourenco, 2015).

Depending on the type of power plants, three technologies are available for CO_2 separation and capture. These are pre combustion, oxyfuel combustion and post combustion as demonstrated in Figure 5.1 (Intergovernmental Panel on Climate Change [IPCC], 2005).

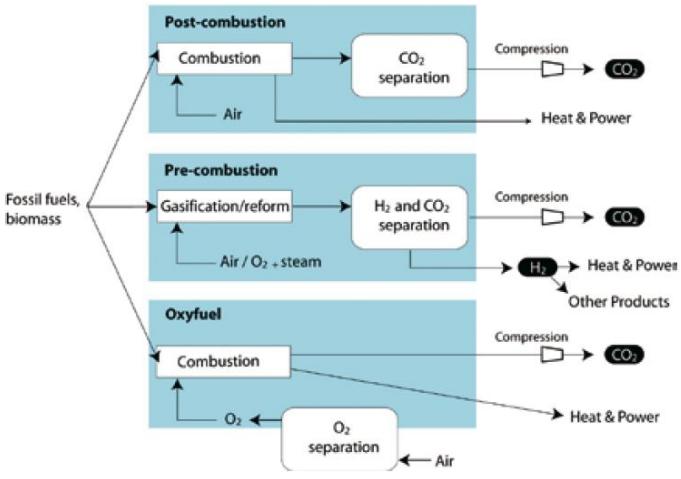

Figure 5.1. Schematic Representation of CO_2 Capture Systems, Adapted from IPCC (2005)

In pre combustion systems, the fuel is combined with steam and air before the combustion process, which results in synthesis gas comprising mostly of carbon monoxide (CO) and hydrogen (H_2). As a result of the reaction of CO with the steam, CO_2 and additional H_2 is obtained. This mixture is sequestrated into CO_2 stream and H_2 stream. Then, CO_2 is captured, and the remaining hydrogen is used for the combustion. Pre combustion systems are preferred in power plants utilizing integrated gasification combined cycle (IGCC) technology (IPCC, 2005). It is pointed out that pre combustion capture technology is not suitable for retrofitting existing power plants. Rather, it can be employed in new power plants. With this technology, up to 90% of CO_2 can be captured. However, pre combustion capture mechanism may cause a decrease of approximately 7.2% in power plant efficiency (Moazzem et al., 2012).

In oxyfuel combustion systems, the fuel is burned with pure oxygen (O_2) rather than air, so CO_2 capture takes place during the combustion. After the combustion process, a flue gas comprising of water vapor and highly concentrated CO_2 is formed. By going through a cooling and compressing process, water vapor in the flue gas is removed, and CO_2 stream is captured. Oxyfuel combustion systems can be used for new gas turbine power plants or for retrofitting existing gas turbine power plants (IPCC, 2005). Nevertheless, the separation of O_2 from air requires a considerable amount of energy, which causes an expected efficiency reduction of 23% for new installations, and 40% for retrofitting existing installations (Moazzem et al., 2012). In spite of a significant decrease in power plant efficiency, almost 100% of CO_2 can be captured with this technology.

In post combustion systems, CO_2 is captured after the combustion of the fuel with air by using several amine solvents, membrane devices or mineral carbonation process on flue gas. This technology is applicable for modern pulverized coal power plants and combined cycle gas turbine power plants, thanks to its cost-effective implementation option that requires only a capture equipment to be installed. The CO_2 capture rate of post combustion technology is between 85% and 95% (IPCC, 2005).

5.2.2 Air Pollution Control Systems

To cope with the most threatening and risky air pollutants such as sulphur dioxide (SO_2), nitrogen oxides (NO_x), and particulate matter (PM_x), there are miscellaneous state-of-the-art emission control systems applicable for conventional power plants. The most commonly used technologies for each pollutant are shown in Table 5.3.

Table 5.3. Widely Used Air Pollution Control Technologies in the Abatement of PM_x, NO_x and SO_2 Emissions

Air Pollutant	Control Technologies
PM_x	- Electrostatic Precipitator (ESP) - Cyclones - Fabric Filter (FF)
NO_x	- Low NOx Burner (LNB) - Selective Catalytic Reduction (SCR) - Selective Noncatalytic Reduction (SCNR) - Lean Premixed Combustion in Gas Turbines
SO_2	- Flue Gas Desulfurization (FGD)

NO_x control technologies are divided into two categories such as combustion and post combustion depending on the control technology used. With the combustion control technologies like Low NO_x Burner (LNB) and Lean Premixed Combustion (LPC) mode of gas turbines, NO_x capture and reduced NO_x emissions occur during the combustion of fossil fuels whereas it occurs after combustion with post combustion technologies such as Selective Catalytic Reduction (SCR) and Selective Non-catalytic Reduction (SCNR). One of the main causes of NO_x emissions from conventional power plants without any control technology is that the flame temperature increases when the fuel is burned with an excess air in the burner. LNBs utilize advanced thermodynamics and fluid mechanics to remove the excess air in the burner and accordingly to reduce the flame temperature, which leads to less NO_x emissions (Shahzad Baig and Yousaf, 2017). Nevertheless, Denny E. and O'Malley M. (2006) also note that the plant efficiency may decrease when the flame temperature is decreased. To implement this technology, LNBs are used instead of

original burners in conventional power plants. With this technology, the NO_x capture rate is estimated as almost 30% (Zhao et al., 2008). As a result of this poor capture rate, in most of the power plants, LNBs are also integrated with one of the post combustion systems to achieve the desired emission reduction level. In post combustions systems, an equipment is installed in power plants so that emitted NO_x can be separated into nitrogen (N_2) and water (H_2O) with the help of either a chemical reaction between the flue gas and a reagent like urea ($(NH_2)_2CO$) or a chemical reaction between flue gas and ammonia (NH_3) in a catalytic chamber. The former separation technology is used in SNCR systems and has a relatively low NO_x capture rate between 15% and 35%, whereas the latter one is used in SCR systems and it has relatively high NO_x capture rate between 70% and 90% (Moretti and Jones, 2012). For this reason, LNB and SCR devices are used together in case a high NO_x capture efficiency is required in conventional power plants. Apart from these technologies, combustion mode switch option is also utilized in gas fired power plants. Two modes such as diffusion (spray) combustion and lean premixed combustion are available in gas turbines. When a turbine is started up or generating at lower power output levels, the diffusion combustion mode is activated. This combustion mode emits more NO_x than lean premixed combustion mode. In gas turbines generating high power output, NO_x emissions can be reduced by switching to lean premixed combustion mode in which the fuel and air are premixed before combustion, which makes this mode more environmentally friendly in terms of reduced atmospheric NO_x emissions (Denny and O'Malley, 2006).

PM_x control technologies are based on post combustion controls requiring an installation of PM_x collectors such as Electrostatic Precipitator (ESP), Cyclones and Fabric Filter (FF). Each equipment uses a different technique to capture PM_x in the flue gas stream. To illustrate, FFs consist of finely netted filters by which PM_x in the flue gas is collected. In ESPs, there are several vertically and horizontally aligned plates. When the flue gas flows through these plates, electromagnetic forces are applied by the electrodes at the center of an ESP; accordingly, PM_x is captured. FFs and ESPs are very efficient in terms of collection performances, which are estimated

as 99.9% (Moretti and Jones, 2012). Cyclones apply centrifugal forces to the flue gas stream to collect PM_x. Their capture efficiencies are estimated as 90% for particulate matters greater than 15 microns, but they are not preferred much since their capture rates are not sufficient for particulate matters less than 15 microns (Shahzad Baig and Yousaf, 2017).

Similar to PM_x control technologies implemented in power plants, SO_2 control technologies are also based on post combustion control systems in which SO_2 is extracted from the flue gas stream. This process is known as Flue Gas Desulphurization (FGD) which has two different application techniques such as wet FGD and dry FGD. Wet FGD systems are based on wet limestone reaction. In this reaction, SO_2 in the flue gas is mixed with air, water and reagents like lime (calcium carbonate ($CaCO_3$)), magnesium-enriched lime, seawater or soda ash (sodium carbonate (Na_2CO_3)). As result of a chemical reaction in this mixture, gypsum ($CaSO_4 \cdot 2H_2O$) and carbon monoxide (CO) are formed. By this way, SO_2 is removed from the flue gas. The capture rate of wet FGD systems is estimated as almost 98% (Nolan, 2000). In dry FGD systems, semi-dry or dry solid reagent is injected into the flue gas stream, a chemical reaction occurs during the injection, SO_2 is captured and reaction byproducts like dry salts and fly ash are removed by filter units. Spray Dryer Absorber (SDA) is a SO_2 control technology based on semi-dry injection method. Atomized lime slurry is used as a semi-dry reagent which is injected into the hot exhaust gas. SDA control technology has almost 96% of SO_2 removal rate (Moretti and Jones, 2012). Different from SDA, Circulating Dry Scrubber (CDS) system is based on dry injection method. Fluid bed of hydrated lime is used as a dry reagent that reacts with the flue gas. The removal rate of wet FGD systems is found to be almost 98% (Moretti and Jones, 2012).

5.3 Proposed Time-decoupled Quadratic Programming Based Approach

Similar to the approaches proposed in Chapter 4, the UCP under both supply/demand uncertainty and emission limitations is time-decoupled by decomposing the original

UCP into T many subproblems each of which is a single-period UCP defined for each period in the planning horizon. Accordingly, each subproblem is optimally solved by balancing the potential benefits to be obtained by reducing emissions and $EENS_t$, and potential losses caused by not committing enough reserve in period *t*. For this purpose, unit commitment, economic load dispatch and reserve decisions are individually determined for each period by the time-decoupled cost-benefit optimization instead of multi-period optimization. It is important to note that time dependent UCP constraints are also taken into consideration in our approach. Nonetheless, near optimal solutions may be obtained owing to time-decoupling, but the multi-period optimization for the UCP under both supply/demand uncertainty and emission limitations is not a plausible method for real power systems which consist of many conventional and renewable generating units.

5.3.1 Emission Models with Emission Control Technologies

In the proposed approach, CO_2, NO_x, SO_2 and PM_x emissions are considered for coal-fired, gas-fired and oil-fired power plants (generating units). For each period, emission models depend on the state of the conventional generating unit whether it has been operational in previous periods or not. To illustrate, when a unit has been working in previous periods, there are only operational emissions of that unit. However, if a unit is started up in that period, then start-up emissions are also taken into account. Besides, the effects of emission reduction and control technologies on operational emissions are also integrated into emission models as follows:

- CCS systems are used against CO_2 emissions.
- LNB, SCR and LPC technologies are used against NO_x emissions.
- FGD systems are used against SO_2 emissions.
- FF systems are used against PM_x emissions.

According to European Commission's directive on monitoring and reporting regulation, two different emission estimation methodologies are available. The first one is measurement-based methodology in which real concentrations of GHGs and

air pollutants are measured from the flue gas stream via monitoring devices whereas the second one is based on arithmetic calculations, and it is further divided into two categories such as mass balance method and standard method (European Commission, 2012). In the mass balance method, fuel flow rate is calculated by considering the principle of mass balance in the boiler; accordingly, emissions are calculated by using the flow rate. The detailed explanation of this method is provided in Majanne (2014). In the standard method, emissions are estimated by the relationship between fuel consumption of the conventional power plant and fuel specific emission factors. For this purpose, fuel consumption function of the power plant is estimated first. Then, by multiplying the fuel consumption function with fuel specific emission factors, emission functions of the power plant are estimated for each GHG and air pollutant. In the proposed approach, fuel consumptions of conventional power plants are modelled by a quadratic function which is widely used in practice for power plants burning coal, oil or natural gas. The quadratic fuel consumption function of unit *i* with respect to its commitment status u_i and power output level P_i is provided by the following expression where α_i, β_i and γ_i are fuel consumption coefficients of unit *i*:

$$F_i = \alpha_i u_i + \beta_i P_i + \gamma_i P_i^2 \qquad (5.1)$$

According to the standard method, without any emission control mode or device, operational emissions of unit *i* for gas *G*, Eo_i^G, are calculated based on emission factor for gas *G* (ef^G) as follows:

$$Eo_i^G = ef^G F_i = ef^G(\alpha_i u_i + \beta_i P_i + \gamma_i P_i^2) \qquad (5.2)$$

Apart from operational emissions, there are also start-up emissions since emissions during start-up does not behave as in its operational state and they are considerably high when starting up. Emissions during start-up for unit *i* can be modelled based on how much time it has stayed inactive or nonoperational because emissions are higher in case of long period of inactivity. For this purpose, start-up emissions can be determined via an exponential function or a two-step function. In the former, an exponential increase is expected for emissions during start-ups as the number of

inactive periods increases. It is illustrated by the following function where θ_i^1 and θ_i^2 are start-up fuel consumption rates of unit *i* during start-up, and T_i^{off} and τ_i denote the number of inactive periods and start-up time constant of unit *i*, respectively:

$$SE_i^G = ef^G \left[\theta_i^1 + \theta_i^2 (1 - e^{-\frac{T_i^{off}}{\tau_i}}) \right] \tag{5.3}$$

In the two-step representation, emissions for gas *G* during start-up are categorized as hot start-up emissions ($SE_i^{G,H}$) and cold start-up emissions ($SE_i^{G,C}$). The two-step function, where $T_{Min,\,i}^{off}$ is the minimum downtime requirement for unit *i*, is illustrated below:

$$SE_i^G = \begin{cases} SE_i^{G,H} & \text{if} \quad T_{Min,\,i}^{off} \leq T_i^{off} \leq T_{Min,\,i}^{off} + \tau_i \\ SE_i^{G,C} & \text{if} \quad T_i^{off} > T_{Min,\,i}^{off} + \tau_i \end{cases} \tag{5.4}$$

In our approach, start-up emissions of a conventional generating unit are modelled via the exponential representation as in (5.3).

Geng et al. (2015) propose an environmental economic dispatch formulation in which emission reduction and control technologies for NO_x, SO_2 and PM_x emissions are also considered. By using this formulation, Geng et al. (2017) propose an environmental generation scheduling formulation to be applied in Chinese power system. We have inspired from these formulations when integrating emission control technologies into proposed emission models with several modifications which include the integration of CCS system against CO_2 emissions, the usage of FF system instead of ESP system against PM_x emissions and more precise modelling of combustion mode switch feature against NO_x emissions of gas-fired generating units.

CO_2 Emissions with Carbon Capture and Storage Systems

To reduce CO_2 emissions from a conventional generating unit, one of the most suitable systems to retrofit existing conventional generating units and to implement

on new ones is post combustion type CCS systems with chemical absorption. Operational CO_2 emissions with CCS systems can be modelled with the following expression:

$$E_i^{CO_2} = \left(1 - \eta_i^{CCS}\right) Eo_i^{CO_2} \quad (5.5)$$

where η_i^{CCS} is the CO_2 capture rate or decarbonization efficiency of unit *i* and $Eo_i^{CO_2}$ is operational CO_2 emission without carbon capture storage systems.

SO_2 Emissions with Flue Gas Desulphurization Systems

Similar to CCS systems, operational SO_2 emissions with CDS or limestone process based FGD systems can be modelled as follows:

$$E_i^{SO_2} = \left(1 - \eta_i^{FGD}\right) Eo_i^{SO_2} \quad (5.6)$$

where η_i^{FGD} is the SO_2 capture rate or desulphurization efficiency of unit *i* and $Eo_i^{SO_2}$ is operational SO_2 emission without FGD systems.

PM_x Emissions with Fabric Filters

Geng et al. (2015) use ESP as an emission control technology and model PM_x emissions of coal-fired power plants with dynamic discounted removal efficiency, which creates additional nonlinearities and complexities in their emission formulation. According to Shahzad and Yousaf (2017), FF systems are more advantageous than ESP systems in the removal of PM_x because of several reasons:

- Collection reliabilities and efficiencies of FFs are higher than ESPs,
- FFs resist more to changes in the flue gas flow,

Because of FF's high resistance to changes in the flow rate of the flue gas, using FFs instead of ESPs prevents the dynamic reduction in PM_x removal efficiency, so FFs are preferred over ESP in the proposed PM_x emission model. PM_x emissions are modelled only for coal-fired generating units because concentrations of PM_x emissions from oil-fired and gas-fired generating units are negligible (Di, 2007). Under these conditions, operational PM_x emissions with FF systems can be modelled as follows:

$$E_i^{PM_x} = (1 - \eta_i^{FF}) Eo_i^{PM_x} \quad (5.7)$$

where η_i^{FF} is the PM_x capture rate or removal efficiency of unit i and $Eo_i^{PM_x}$ is operational PM_x emission without FF systems.

NO_x Emissions with Control Technologies

For coal-fired and oil-fired conventional units, operational NO_x emissions without any emission control mode are modelled via the standard method. Different from these units, gas-fired generating units have two combustion modes, namely spray (diffusion) combustion (SC) and lean premixed combustion (LPC) as explained in Section 5.2.2. Switching from SC mode to LPC mode, NO_x emissions can be significantly reduced according to the experimental studies by Okhubo (2005) who experiments NO_x emissions of these combustion modes by using different fuel gases in gas turbines and his results are provided in Figure 5.2.

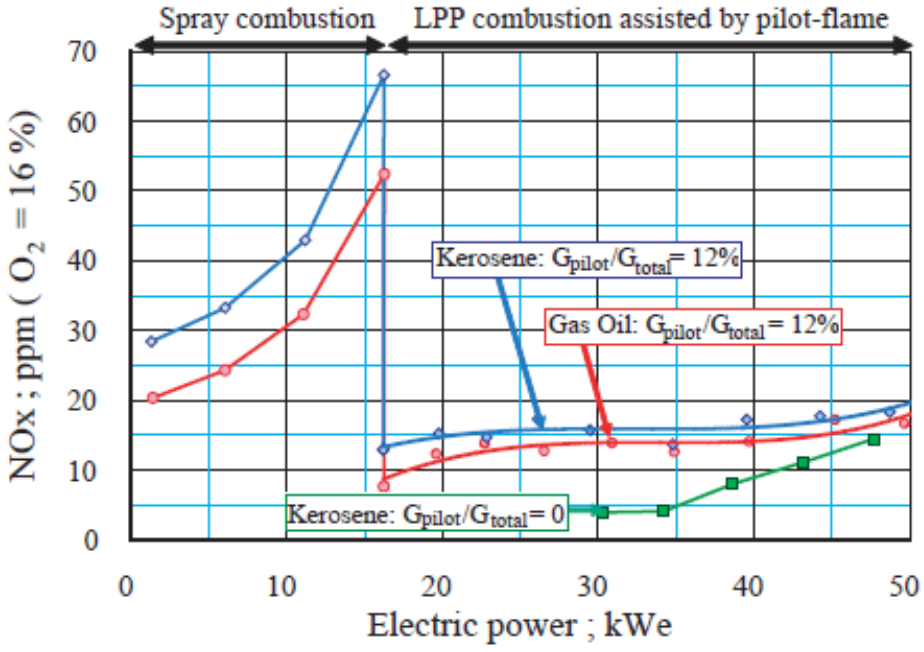

Figure 5.2. NO_x Emissions of Spray Combustion Mode and Lean Premixed Combustion Mode Using Kerosene and Gas Oil as Fuels, Adapted from Ohkubo (2005)

As it can be inferred from Figure 5.2, NO_x emissions increase quadratically in SC mode as in emissions represented by the standard method when the power output level increases whereas the relationship between NO_x emissions and the power output level is close to linear and even fixed at a lower emission level in LPC mode. Nonetheless, the LPC mode cannot be used during startup and lower power output levels due to combustion instabilities, so this mode can be activated when the power output level of the unit is greater than approximately 70% of its capacity (Denny and O'Malley, 2006). Geng et al. (2015) formulate NO_x emissions by using two linear functions representing emission levels at two combustion modes but this simplification is not precise when modelling NO_x emissions in SC mode. Thus, we formulate NO_x emissions quadratically in SC mode and linearly in LPC mode as shown in Figure 5.3.

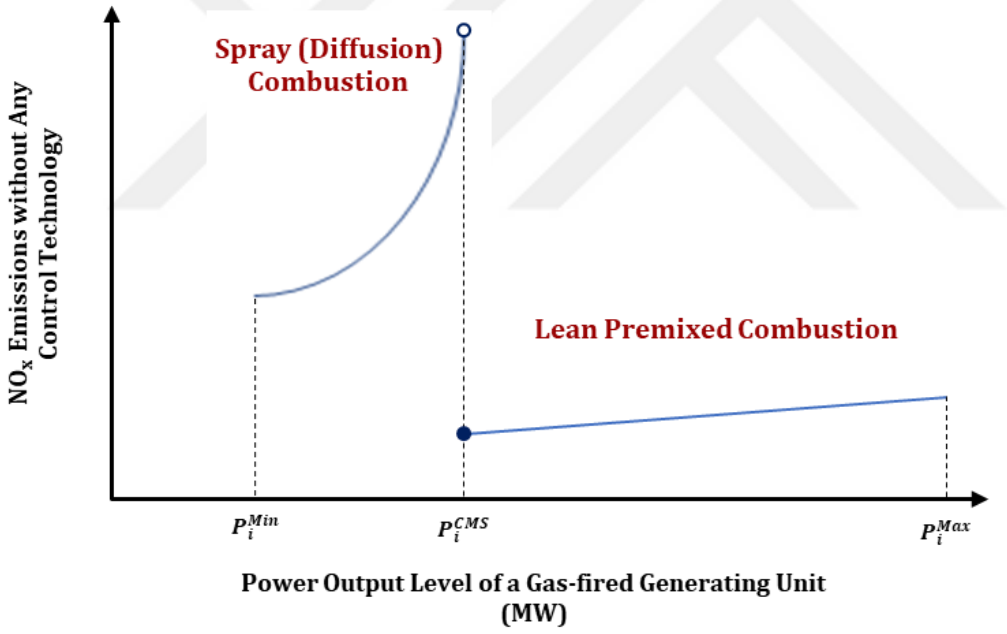

Figure 5.3. Operational NO_x Emissions of Spray Combustion and Lean Premixed Combustion in the Proposed Emission Model

For gas-fired generating units, this piecewise relationship in operational NO_x emissions without any control technology is modelled by the following piecewise function where ef^{NO_x} is NO_x emission factor of the fuel gas, α_i, β_i and γ_i are fuel

consumption coefficients of gas-fired unit *i* in SC mode, ρ_i is the emission coefficient of gas-fired unit *i* in LPC mode, and P_i^{CMS} is the power output threshold required for the combustion mode switch of gas-fired unit *i*:

$$Eo_i^{NO_x} = \begin{cases} ef^{NO_x}(\alpha_i u_i + \beta_i P_i + \gamma_i P_i^2) & \text{if} \quad P_i < P_i^{CMS} \\ \rho_i P_i & \text{if} \quad P_i \geq P_i^{CMS} \end{cases} \tag{5.8}$$

As mentioned in Section 5.2.2, there are also other control technologies against NO_x emissions. One of them is combined usage of LNB technology and a post combustion type denitration device such as SCR or SCNR since using LNBs without supported by one of these denitration equipment yields less NO_x removal efficiency than required. Therefore, in the proposed NO_x emissions model, it is assumed that LNBs in conventional generating units can be backed up with SCR devices. In spite of their high removal rate, those devices can be activated in high temperature (>300 ^oC) so they cannot operate when the power generation level of a conventional unit is less than a threshold level (Geng et al., 2015). As a result of this requirement, operational NO_x emissions with combined usage of LNB technology and SCR equipment can be modelled by the following piecewise function where $Eo_i^{NO_x}$ is operational NO_x emissions without any emission control technology, P_i^{SCR} is the power output threshold required for the activation of SCR in unit *i*, and η_i^{LNB} and η_i^{SCR} are the NO_x capture rate of LNB technology and NO_x removal efficiency of SCR equipment in unit *i*, respectively:

$$E_i^{NO_x} = \begin{cases} (1-\eta_i^{LNB})Eo_i^{NO_x} & \text{if} \quad P_i < P_i^{SCR} \\ \left(1-\eta_i^{SCR}\right)(1-\eta_i^{LNB})Eo_i^{NO_x} & \text{if} \quad P_i \geq P_i^{SCR} \end{cases} \tag{5.9}$$

5.3.2 Emission Control Regulations in Emission Models

Emission Trading System for CO_2 Emission Control

Regulations on CO_2 emissions in most of the states and countries have been based on ETS, which works with the principle of Cap & Trade mechanism. In the proposed approach, ETS is used to regulate CO_2 emissions. For this purpose, it is assumed that each company is required to have enough allowances for their CO_2 emissions otherwise they are going to pay heavy penalties for emissions exceeding their allowances. To prevent this situation, they are allowed to purchase additional emission allowances via the carbon market. When companies decrease their emissions beyond their quotas, they can transfer excess allowances to compensate for their future needs or they can trade those allowances to gain extra revenue.

Since we are solving a day ahead UCP, the length of the planning horizon is 24 hours. In our time-decoupled UCP formulation, we implement Cap & Trade mechanism according to the assumptions provided below:

- Total monthly or quarterly allowances are disaggregated into daily allowances according to several disaggregation techniques, which is out of our scope. Hence, daily allowances are considered as given and disaggregated into hourly allowances according to expected net load levels in each hour.
- In the time-decoupled UCP formulation, hourly Cap & Trade Mechanism is used for total CO_2 emissions in each hour. However, company is not allowed to trade during the 24-h planning horizon so they can trade at the end of the last hour. For this purpose, the following set of rules are applied.
    - If total CO_2 emissions during an hour do not exceed its hourly allowance in the optimal solution of the time-decoupled UCP, excess allowance is not sold, rather transferred to the total allowances of the remaining hours.

- If total CO_2 emissions during an hour exceed its hourly allowance in the optimal solution of the time-decoupled UCP, excess emissions are subtracted from the total allowances of the remaining hours.
- Then, updated allowances are disaggregated by applying the same procedure of hourly disaggregation for the remaining hours.

- No carbon tax is imposed for CO_2 emissions less than the company's total emission allowances.

Three-Level Tax System for Air Pollutant Emission Control

Owing to severe adverse effects of air pollutant emissions on the human health and environment, command and control type regulations have been adopted by a big majority of countries instead of Cap & Trade mechanism (OECD, 2017). For emissions of PM_x, NO_x and SO_2, it is assumed that amounts of air pollutant emissions are regulated with command and control type policies with three-level tax systems in the proposed approach. For this reason, each company is required to comply with tier emission limits for air pollutants while paying a pollution tax on its emission amounts. For each air pollutant, the first level tax is imposed as an emission tax for emission amounts less than the first-tier emission limits. When a company emits more than the first-tier limit but less than the second-tier limit, the second level penalty is also imposed for emission amounts exceeding the first-tier limit, which constitutes the second level tax for emissions. If a company emits more than the second-tier limit, the third level penalty is also imposed for emission amounts exceeding the second-tier limit, which constitutes the third level tax for emissions. The three-level tax system for air pollutant *G* is illustrated in Figure 5.4 where π_1^G, π_2^G and π_3^G is the emission tax, the second level penalty and the third level penalty respectively.

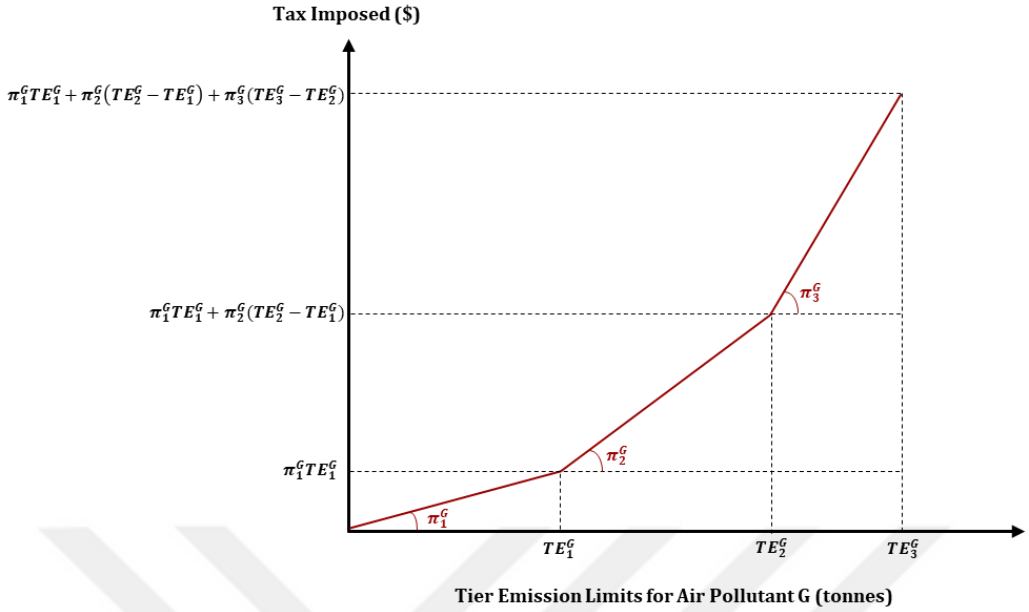

Figure 5.4. Three-Level Tax System for Air Pollutants

5.3.3 Time-decoupled Mixed Integer Quadratically Constrained Programming (MIQCP) Formulation with Quadratic Objective

The proposed method is the extension of the model MIQP I-VPLE proposed in Chapter 4. Different from these formulations, the proposed formulation with emissions is based on MIQCP formulation since emissions are represented by quadratic functions, which make the representation of emission related constraints quadratic. By taking emissions and emission taxes into consideration, the objective consists of fuel costs, start-up costs, reserve allocation costs, expected cost of load shedding, valve-point loading costs and emission taxes in this extension. Excluding fuel costs, the remaining costs have a linear relationship with corresponding decision variables such as commitment statuses, reserves, $EENS_t$, and total CO_2, NO_x, SO_2 and PM_x emissions. The fuel costs are represented by convex quadratic functions. As a result, both the objective function and constraints have quadratic terms in the extended formulation.

Standard UCP constraints such as power balance constraints and minimum/maximum generation limits, and time-dependent constraints like the minimum uptime/downtime constraints and the ramp-up/ramp-down limits are modelled similarly as in formulations in Chapter 4. Likewise, reserves are also considered as decision variables whose values are determined by the trade-off between total operational costs and the expected cost of load shedding (energy not served) instead of using standard spinning reserve requirements. For this purpose, $EENS_t$ is piecewise linearly approximated by using the Approximation Method I explained in Chapter 4. Similarly, the valve point loading effect on conventional generating units are reckoned with multi-area piecewise linear approximation of valve point loading costs. Thus, the extended formulation with emissions control is called as MIQP I-VPLE-EC. Since the model MIQP I-VPLE-EC uses the same representations for constraints excluding emission related ones, only modifications for emissions are provided in this section. For each period in the planning horizon, the extended formulation is sequentially solved to obtain near-optimal schedules for the commitment, generation and reserve by trading off generation costs, the expected cost of load shedding and costs of emissions.

Assumptions

Assumptions Defined for Emissions:

- Emissions are regulated via emission trading and taxing mechanisms only. For GHG and air pollutants, there are no zonal emission limits.
- CO_2 emissions are controlled via Cap & Trade mechanism according to assumptions provided in Section 5.3.2.
- NO_x, SO_2 and PM_x emissions are controlled via three-level tax system provided in Section 5.3.2.
- The capture rates of the emission reduction technologies applied on conventional generating units remain unchanged during their operations.

- Emissions during start-ups do not depend on the production level. Rather, they depend on how much time the units have stayed inactive or nonoperational.

Sets and Indices

For emissions of CO_2, NO_x, SO_2 and PM_x, the following sets are defined.

Additional Sets and Indices for Emissions:

AP: Set of air pollutants:

$$AP = \{\mathrm{NO}_x, \mathrm{SO}_2, \mathrm{PM}_x\} \quad (5.10)$$

$ap \in AP$: air pollutant ap

CT: Set of combustion types:

$$CT = \{coal, oil, gas\} \quad (5.11)$$

$cm_i \in CT$: Combustion type of unit i

$N^{Coal} \subset N$: Set of coal-fired conventional units:

$$N^{Coal} = \{i \in N: cm_i = coal\} \quad (5.12)$$

$N^{Oil} \subset N$: Set of oil-fired conventional units:

$$N^{Oil} = \{i \in N: cm_i = oil\} \quad (5.13)$$

$N^{Gas} \subset N$: Set of gas-fired conventional units:

$$N^{Gas} = \{i \in N: cm_i = gas\} \quad (5.14)$$

ECT: Set of emission control technologies:

$$ECT = \{LNB, SCR, FGD, FF, CCS\} \quad (5.15)$$

$ECT_i \subset ECT$: Set of emission control technologies in conventional generating unit i

$N^{SCR} \subset N$: Set of conventional units with a SCR device:

$$N^{SCR} = \{i \in N: \{SCR\} \subset ECT_i\} \quad (5.16)$$

Q: Set of three-level emission tiers for air pollutants:

$$Q = \{TE_0^{ap}, TE_1^{ap}, TE_2^{ap}, TE_3^{ap}\} \quad (5.17)$$

$q \in Q$: Sequential emission tiers for air pollutant emissions

Parameters

For emissions of CO_2, NO_x, SO_2 and PM_x, the following parameters are defined.

Additional Parameters for Emissions:

α_i, β_i, γ_i: Fuel consumption coefficients of unit $i \in N^{Coal} \cup N^{Gas}$, and fuel consumption coefficients in SC mode for $i \in N^{Gas}$ (tonnes, tonnes/MW, tonnes/MW^2, respectively)

ef^{ap}: Emission factor of air pollutant *ap* (tonnes/tonnes)

ef^{CO_2}: Emission factor of CO_2 (tonnes/tonnes)

ρ_i: Emission coefficient in LPC mode for unit $i \in N^{Gas}$ (tonnes/MW)

θ_i^1, θ_i^2: Start-up fuel consumption rates of unit *i* during start-up (tonnes)

τ_i Start-up time constant of unit *i* (hours)

η_i^{LNB}: NO_x capture rate of LNB technology in unit *i*

η_i^{SCR}: NO_x removal efficiency of SCR equipment in unit *i*

η_i^{FGD}: SO_2 capture rate or desulphurization efficiency of unit *i*

η_i^{FF}: PM_x capture rate or removal efficiency of unit *i*

η_i^{CCS}: CO_2 capture rate or decarbonization efficiency of unit *i*

P_i^{SCR}: Power output threshold required for the activation of SCR in unit $i \in N^{SCR}$ (MW)

P_i^{CMS}: Power output threshold required for the combustion mode switch of unit $i \in N^{Gas}$ (MW)

SEM_{it}^{ap}: Start-up emissions of unit *i* for air pollutant *ap* in period *t*

$SEM_{it}^{CO_2}$: Start-up CO_2 emissions of unit *i* in period *t*

π_1^{ap}: Emission tax for air pollutant *ap* ($)

π_2^{ap}: Second level penalty for air pollutant *ap* ($)

π_2^{ap}: Third level penalty for air pollutant *ap* ($)

TE_q^{ap}: q^{th}-tier maximum emission level for emissions of air pollutant *ap* (tonnes)

Tax_q^{ap}: q^{th}-tier maximum emission tax for emissions of air pollutant *ap* ($):

$$Tax_0^{ap} = 0 \tag{5.18}$$

$$Tax_1^{ap} = TE_1^{ap}\,\pi_1^{ap} \tag{5.19}$$

$$Tax_2^{ap} = Tax_1^{ap} + TE_2^{ap}\,\pi_2^{ap} \tag{5.20}$$

$$Tax_3^{ap} = Tax_2^{ap} + TE_3^{ap}\,\pi_3^{ap} \tag{5.21}$$

$CAP_t^{CO_2}$: CO_2 cap (amount of allowances) in period *t* (tonnes)

p^{CO_2}: Trading price in the carbon market ($)

Decision Variables

For emissions of CO_2, NO_x, SO_2 and PM_x, the following variables are defined.

Additional Variables for Emissions:

$\widetilde{EM}_{it}^{NO_x}$: NO_x emissions of unit *i* in period *t* without emission control technology

$EM_{it}^{NO_x}$: NO_x emissions of unit *i* in period *t* with emission control technology

TEM_t^{ap}: Total emissions of air pollutant *ap* in period *t*

$TEM_t^{CO_2}$: Total CO_2 emissions in period *t*

TEC_t^{ap}: Cost of total emissions of air pollutant *ap* in period *t*

$TEC_t^{CO_2}$: Cost/Revenue of total CO_2 emissions in period *t*

w_q^{ap}: Weight of q^{th}-tier maximum emission level for emissions of air pollutant *ap*

δ_{it}^{CMS}: Combustion mode switch of unit $i \in N^{Gas}$ in period *t* (Activation of LPC mode):

$$\delta_{it}^{CMS} = \begin{cases} 1 \text{ if LPC mode of gas fired unit } i \text{ is activated in period } t \\ 0 \text{ otherwise} \end{cases} \tag{5.22}$$

δ_{it}^{SCR}: Activation of SCR device of unit $i \in N^{SCR}$ in period *t*:

$$\delta_{it}^{SCR} = \begin{cases} 1 \text{ if SCR device of gas fired unit } i \text{ is activated } i \text{ in period } t \\ 0 \text{ otherwise} \end{cases} \quad (5.23)$$

Objective Function

Having added the emission taxes of air pollutant emissions and cost/revenue of CO_2 emissions, the objective function of the model MIQP I-VPLE is modified as:

$$Min \sum_{i=1}^{|N|} (a_i u_{it} + b_i P_{it} + c_i {P_{it}}^2 + VP_{it} + q_i R_{it} + S_{it} u_{it}) + (VOLL)(EENS_t) + TEC_t^{NO_x} + TEC_t^{SO_2} + TEC_t^{PM_x} + TEC_t^{CO_2} \quad (5.24)$$

Constraints for Emissions

<u>*Cost or Revenue of CO_2 Emissions:*</u> When total CO_2 emissions in period *t* are less than the amount of CO_2 allowances for period *t*, then remaining allowances of that period will be considered as if they can be sold with the CO_2 price in the carbon market, so the revenue from selling allowances is taken as negative cost. When total CO_2 emissions in period *t* exceed the amount of CO_2 allowances for period *t*, then the excess emissions in the same period will be considered as if they can be compensated for by buying additional allowances with the CO_2 price in the carbon market, so the cost of buying allowances is taken as positive cost.

Note: *Because of no trading assumption during 24-h planning horizon, the trading will not happen in both cases so that excess allowances in period t can be used to compensate for future needs in remaining hours, and the excess emissions in period t will be compensated for by using CO_2 allowances of remaining hours. Thus, the final decision on trading will be made at the end of the last hour in the planning horizon.*

$$TEC_t^{CO_2} = \left(TEM_t^{CO_2} - CAP_t^{CO_2}\right) p^{CO_2} \quad (5.25)$$

Constraints for Three-level Taxes for Air Pollutant Emissions:

- The constraint for locating the total emission level of air pollutant *ap* in the set of emission tiers:

$$TEM_t^{ap} = \sum_{q=0}^{3} TE_q^{ap}\, w_q^{ap} \quad \forall ap \tag{5.26}$$

- The constraint for finding the total emission cost of air pollutant *ap* depending on its total emission level:

$$TEC_t^{ap} = \sum_{q=0}^{3} Tax_q^{ap}\, w_q^{ap} \quad \forall ap \tag{5.27}$$

- If there are emissions for air pollutant *ap*, then the total emission level should lie on one of emission tiers; accordingly, the sum of weights of tiered maximum emission levels should be 1:

$$\sum_{q=0}^{3} w_q^{ap} = 1 \quad \forall ap \tag{5.28}$$

Total SO_2 Emissions: Total SO_2 emissions in period *t* is the sum of total operational emissions with FGD technology and start-up emissions in that period.

$$TEM_t^{SO_2} \geq \sum_{i=1}^{|N|} \left[\left(1-\eta_i^{FGD}\right)\left(ef^{SO_2}(\alpha_i u_{it} + \beta_i P_{it} + \gamma_i P_{it}^2)\right) + SEM_{it}^{SO_2} u_{it}\right] \tag{5.29}$$

Total PM_x Emissions: Total PM_x emissions in period *t* is the sum of total operational emissions with FF technology and start-up emissions in that period.

Note: *Since concentrations of PM_x emissions from oil-fired and gas-fired generating units are negligible, PM_x emissions are caused by only coal-fired generating units.*

$$TEM_t^{PM_x} \geq \sum_{i \in N^{Coal}} \left[(1-\eta_i^{FF})\left(ef^{PM_x}(\alpha_i u_{it} + \beta_i P_{it} + \gamma_i P_{it}^2)\right) + SEM_{it}^{PM_x} u_{it}\right] \tag{5.30}$$

Total CO_2 Emissions: Total CO_2 emissions in period *t* is the sum of total operational emissions with CCS technology and start-up emissions in that period.

$$TEM_t^{CO_2} \geq \sum_{i=1}^{|N|} \left[\left(1 - \eta_i^{CCS}\right) \left(ef^{CO_2} (\alpha_i u_{it} + \beta_i P_{it} + \gamma_i P_{it}^2) \right) + SEM_{it}^{CO_2} u_{it} \right] \quad (5.31)$$

Constraints for Total NO_x Emissions: Since NO_x emissions for coal-fired and oil-fired generating units are different from ones for oil-fired generating units, and different emission control technologies are available for conventional units, the following set of constraints are defined for modelling NO_x emissions.

- Operational NO_x Emissions without any emission control technologies for coal-fired or oil-fired generating unit *i* in period *t*:

$$\widetilde{EM}_{it}^{NO_x} \geq ef^{NO_x} (\alpha_i u_{it} + \beta_i P_{it} + \gamma_i P_{it}^2) \quad \forall i \in \left(N^{Oil} \cup N^{Coal}\right) \quad (5.32)$$

- Operational NO_x Emissions without any emission control technologies for gas-fired generating units:

  Since there are two combustion modes available for gas-fired units, the following set of constraints are defined for modelling NO_x emissions without any emission control technologies for gas-fired generating unit *i* in period *t*.

  - If power output level of gas-fired unit *i* is greater than or equal to its power output threshold required for the combustion mode switch, then the power is generated in LPC mode and emissions are modelled by LPC mode-emissions in period *t*:

$$P_{it} \geq P_i^{CMS} + m_3 \left(1 - \delta_{it}^{CMS}\right) \quad \forall i \in N^{Gas} \quad (5.33)$$

    where m_3 is a very small number denoting lower bounds for power output levels.

$$\widetilde{EM}_{it}^{NO_x} \geq \rho_i P_{it} + m_4 \left(1 - \delta_{it}^{CMS}\right) \quad \forall i \in N^{Gas} \quad (5.34)$$

    where m_4 is a very small number denoting lower bounds for NO_x emission levels.

  - If power output level of gas-fired unit *i* is less than its power output threshold required for the combustion mode switch, then the power is

generated in SC mode and emissions are modelled by SC mode-emissions in period *t*:

$$P_{it} \leq P_i^{CMS} - \varepsilon + (M_4 + \varepsilon)\delta_{it}^{CMS} \quad \forall i \in N^{Gas} \qquad (5.35)$$

where M_4 is a very large number denoting upper bounds for power output levels and $\varepsilon = 0.001$.

$$\widetilde{EM}_{it}^{NO_x} \geq ef^{NO_x}(\alpha_i u_{it} + \beta_i P_{it} + \gamma_i P_{it}^2) + M_5\, \delta_{it}^{CMS}\ \forall i \in N^{Gas} (5.36)$$

where M_5 is a very large number denoting upper bounds for NO_x emission levels.

- Combustion mode can be switched if and only if gas-fired unit *i* is committed in period *t*:

$$\delta_{it}^{CMS} \leq u_{it} \quad \forall i \in N^{Gas} \qquad (5.37)$$

- Operational NO_x Emissions with emission control technologies for conventional generating units:

  Since two emission control technologies (LNB and SCR) might be used for conventional generating units, the following set of constraints are defined for modelling NO_x emissions with emission control technologies for unit *i* in period *t*.

  - If power output level of unit *i* with a SCR device is greater than or equal to its power output threshold required for the activation of the device, then both LNB technology and SCR device are used to reduce NO_x emissions in period *t*:

$$P_{it} \geq P_i^{SCR} + m_3\left(1 - \delta_{it}^{SCR}\right) \quad \forall i \in N^{SCR} \qquad (5.38)$$

where m_3 is a very small number denoting lower bounds for power output levels.

$$EM_{it}^{NO_x} \geq (1 - \eta_i^{SCR})(1 - \eta_i^{LNB})\widetilde{EM}_{it}^{NO_x} + m_4(1 - \delta_{it}^{SCR})\ \forall i \in N^{SCR} (5.39)$$

where m_4 is a very small number denoting lower bounds for NO_x emission levels.

- If power output level of unit *i* with a SCR device is less than its power output threshold required for the activation of the device, then only LNB technology is used to reduce NO_x emissions in period *t*:

$$P_{it} \leq P_i^{SCR} - \varepsilon + (M_4 + \varepsilon)\delta_{it}^{CMS} \quad \forall i \in N^{SCR} \quad (5.40)$$

where M_4 is a very large number denoting upper bounds for power output levels and $\varepsilon = 0.001$.

$$EM_{it}^{NO_x} \geq (1 - \eta_i^{LNB})\widetilde{EM}_{it}^{NO_x} + M_5\, \delta_{it}^{SCR} \quad \forall i \in N^{SCR} \quad (5.41)$$

where M_5 is a very large number denoting upper bounds for NO_x emission levels.

- SCR device can be activated if and only if unit *i* is committed in period *t*:

$$\delta_{it}^{SCR} \leq u_{it} \quad \forall i \in N^{SCR} \quad (5.42)$$

- For unit *i* without a SCR device, only LNB technology is used to reduce NO_x emissions in period *t*:

$$EM_{it}^{NO_x} \geq (1 - \eta_i^{LNB})\widetilde{EM}_{it}^{NO_x} \quad \forall i \notin N^{SCR} \quad (5.43)$$

- Total NO_x emissions in period *t* is the sum of total operational emissions with emission control technologies and start-up emissions in that period:

$$TEM_t^{NO_x} \geq \sum_{i=1}^{|N|} \left[EM_{it}^{NO_x} + SEM_{it}^{NO_x} u_{it}\right] \quad (5.44)$$

Sign Restrictions of Decision Variables for Emissions:

$$\widetilde{EM}_{it}^{NO_x}, EM_{it}^{NO_x} \geq 0 \quad \forall i \quad (5.45)$$

$$TEC_t^{ap}, TEM_t^{ap}, w_q^{ap} \geq 0 \quad \forall ap \quad (5.46)$$

$$TEM_t^{CO_2} \geq 0 \quad (5.47)$$

$$TEC_t^{CO_2} \quad urs \quad (5.48)$$

$$\delta_{it}^{CMS} \in \{0,1\} \quad \forall i \in N^{Gas} \quad (5.49)$$

$$\delta_{it}^{SCR} \in \{0,1\} \quad \forall i \in N^{SCR} \tag{5.50}$$

Mathematical Model: MIQP I-VPLE-EC

$$Min \sum_{i=1}^{|N|} (a_i u_{it} + b_i P_{it} + c_i {P_{it}}^2 + VP_{it} + q_i R_{it} + S_{it} u_{it}) + (VOLL)(EENS_t) + TEC_t^{NO_x} + TEC_t^{SO_2} + TEC_t^{PM_x} + TEC_t^{CO_2}$$

$subject\ to$

$(4.40), \dots, (4.59), (4.79), \dots, (4.90), (5.25), \dots, (5.50)$

5.4 Computational Study

The proposed time-decoupled environmental MIQCP formulation (MIQP I-VPLE-EC) is coded in MATLAB programming language and solved via CPLEX for MATLAB toolbox provided by IBM ILOG CPLEX Optimizer 12.9.0. The model is executed in Windows 10 environment in a Lenovo ultrabook with Intel(R) Core (TM) i7-6500U 2.6 GHz CPU and 8 GB RAM. Numerical experiments on the performance of the approach is conducted by using modified versions of Problem Instance 2 described in Section 4.3.1. Those modifications are explained in detail in the subsequent sections. Then, test and sensitivity analysis results are provided for the proposed model. Lastly, our time-decoupled environmental formulation MIQP I-VPLE-EC is compared with the UCP formulations enforcing traditional deterministic reserve policies.

5.4.1 Problem Instances

To conduct numerical experiments, the time-decoupled model MIQP I-VPLE-EC is implemented to modified versions of IEEE 30-bus problem instance by considering significant wind penetration and emission considerations as well. For wind farms, conventional generation reliability, load demand and wind power forecast errors,

ramp rate limits, reserve rates and socioeconomic value that customers put on the value of the lost load, we use the same settings provided in Section 4.3 in our stochastic and environmental model MIQP I-VPLE-EC. Hence, only modifications are provided in the following sections.

Problem Instance 1

This problem instance consists of 30-bus with 6 conventional thermal units and 6 wind farms which have a total installed capacity of 135 MW. The length of the scheduling horizon is 24 hours. The power output thresholds for SCR activation and CMS are assumed to be 30% and 70% of the unit's maximum rated capacity. Concerning emissions, additional unit related data for modified IEEE 30-bus test system are provided in Table 5.4.

Table 5.4. Conventional Units' Emissions Related Data for Modified IEEE 30-bus Problem Instance

	Unit 1	**Unit 2**	**Unit 3**	**Unit 4**	**Unit 5**	**Unit 6**
Fuel Type	Coal	Coal	Coal	Gas	Gas	Oil
$\boldsymbol{\alpha_i}$	45	50	90	2430.5	2000	1.248
$\boldsymbol{\beta_i}$	0.3	0.25	0.14	55	0.212	0.334
$\boldsymbol{\gamma_i}$	0.00005	0.00004	0.00003	0,009	0.007	0.0000342
$\boldsymbol{\theta_i^1}$	90	100	180	4861	4000	2.496
$\boldsymbol{\theta_i^2}$	90	100	180	4861	4000	2.496
$\boldsymbol{\rho_i}$	0.075	0.0625	0.035	13.75	0.053	0.0835
$\boldsymbol{\tau_i}$ $(\boldsymbol{h})$	8	5	6	5	5	6
LNB System	Yes	Yes	Yes	Yes	Yes	Yes
SCR System	Yes	No	Yes	No	Yes	No
FF System	No	No	Yes	No	No	No
FGD System	Yes	Yes	Yes	No	Yes	No
CCS System	No	No	Yes	Yes	No	No

NOTE: 1. The coefficients of $\boldsymbol{\alpha_i, \beta_i, \gamma_i, \theta_i^1, \theta_i^2}$ are in $\mathbf{t}$, $\mathbf{t/MW}$, $\mathbf{t/MW^2}$, $\mathbf{t}$ and $\mathbf{t}$ for coal & oil type units

2. The coefficients of $\boldsymbol{\alpha_i, \beta_i, \gamma_i, \rho_i, \theta_i^1, \theta_i^2}$ are in $\mathbf{m^3}$, $\mathbf{m^3/MW}$, $\mathbf{m^3/MW^2}$, $\mathbf{m^3/MW}$, $\mathbf{m^3}$ and $\mathbf{m^3}$ for gas type units

Table 5.5 shows removal efficiencies of each emission control technology.

Table 5.5. Emission Control Systems' Removal Efficiencies for Modified IEEE 30-bus Problem Instance

	LNB	**SCR**	**FF**	**FGD**	**CCS**
Removal Efficiencies (η)	30%	70%	95%	90%	80%

Fuel based emissions factors for CO_2 and air pollutants are determined according to Di et al. (2007). These factors are reported in Table 5.6.

Table 5.6. Fuel-based Emission Factors for Modified IEEE 30-bus Problem Instance

	Coal (kg/kg)	**Oil (kg/kg)**	**Gas (kg/m³)**
ef^{CO_2}	3.1604	2.8523	1.84
ef^{NO_x}	0.0122	0.0172	0.002543
ef^{PM_x}	0.0026	-	-
ef^{SO_2}	0.01701	0.02232	0.00026

Carbon trading price and CO_2 cap over the scheduling horizon are shown in Table 5.7.

Table 5.7. Carbon Trading Environment for Modified IEEE 30-bus Problem Instance

	p^{CO_2}	CAP^{CO_2}
Carbon Economy	86.22	8,846.99

NOTE: Carbon price and cap are in $\$/\mathbf{t}$ and **t**

The CO_2 cap is dynamically disaggregated for individual hours by applying rules provided in Section 5.3.2. Three-level emission tax systems for each pollutant are illustrated in Table 5.8.

Table 5.8. Three-Level Emission Tax Systems of Air Pollutants for Modified IEEE 30-bus Problem Instance

	NOx		**PMx**		**SO_2**	
	$\pi_q^{NO_x}$	$TE_q^{NO_x}$	$\pi_q^{PPM_x}$	$TE_q^{PPM_x}$	$\pi_q^{SO_2}$	$TE_q^{SO_2}$
Tier 1	13.78	1.07	10.88	0.19	3.21	1.37
Tier 2	30.00	3.83	14.50	0.57	5.98	4.63
Tier 3	46.25	6.60	18.12	0.94	8.76	7.89

NOTE: The units of emission taxes and emission tiers are in $\$/\mathbf{kg}$ and **t**

Problem Instance 2

This problem instance is obtained by appropriately scaling Problem Instance 1. For this purpose, generating units are replicated two times to form 12-Unit problem instance. Also, capacities of wind turbines in each wind farm, load demand and wind power forecasts, CO_2 cap and emission levels on tiers are doubled. Nevertheless, removal efficiencies of emission control technologies, fuel-based emission factors, carbon trading price and emission taxes remain unchanged.

5.4.2 Sensitivity Analysis Results

Similar to sensitivity analyses made in Chapter 4, we test the sensitivity of the solutions of our time-decoupled model MIQP I-VPLE-EC by changing parameters one at a time and solving them with the updated parameter value. Those parameters involve $VOLL$, carbon trading price, air pollutant emission taxes, load demand and wind speed forecast errors, failure rates of conventional generating units. The sensitivity of the model is examined by applying it to the modified IEEE 30-bus problem instance.

First of all, the impact of $VOLL$ on CC_t is determined by increasing VOLL by 750 \$/MWh starting from 1750 \$/MWh. In Table 5.9, the total operating cost of the system and its breakdowns under different $VOLL$ values are summarized. Emission related costs or revenues are not included in total operating costs. It is observed that the total operating cost increases. For the first two levels, this increase is attributed

to the increase in the expected cost of load shedding because increasing $VOLL$ has a minor effect on generation and reserve cost. However, this increase is attributed to the increase in both cost components. That is, commitment and dispatching decisions are affected significantly when the $VOLL$ is increased to 3250 $/MWh.

Table 5.9. Total Operating Cost under Different $VOLL$ Values for Modified IEEE 30-bus Problem Instance

***VOLL* ($/MWh)**	**1750**	**2500**	**3250**
Expected Cost of EENS ($)	31,664.5	45,025.4	57,801.4
Generation & Reserve Cost ($)	698,277.4	698,287.5	706,449.5
Total Operating Cost ($)	**729,941.9**	**743,312.9**	**764,250.9**

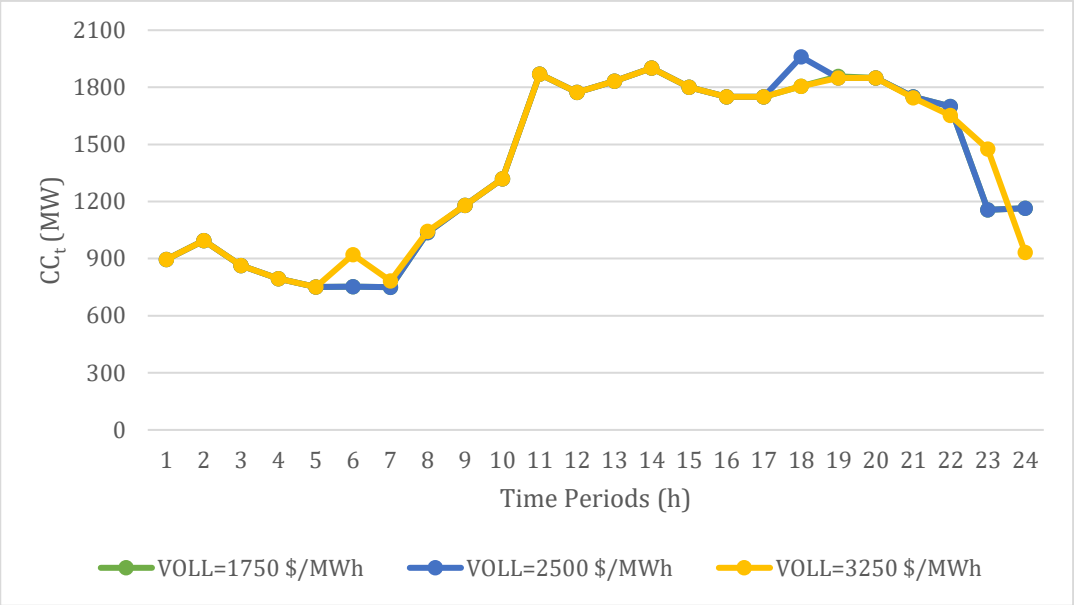

Figure 5.5. Relationship between $VOLL$ and CC_t for Modified IEEE 30-bus Problem Instance

This situation is also illustrated in Figure 5.5 which shows the relationship between $VOLL$ and CC_t over the 24-h scheduling horizon. Increasing $VOLL$ does not change CC_t levels except for five periods since emission related costs/revenues remain the dominant factor in the cost/benefit analysis. By increasing $VOLL$ to 3250 MWh/$,

CC_t levels generally increase in those periods. Also, we examine how total emission amounts change by increasing $VOLL$, which is demonstrated in Figure 5.6 where the primary and secondary vertical axes represent GHG emissions such as CO_2, and air pollutant emissions consisting of NO_x, SO_2 and PM_x.

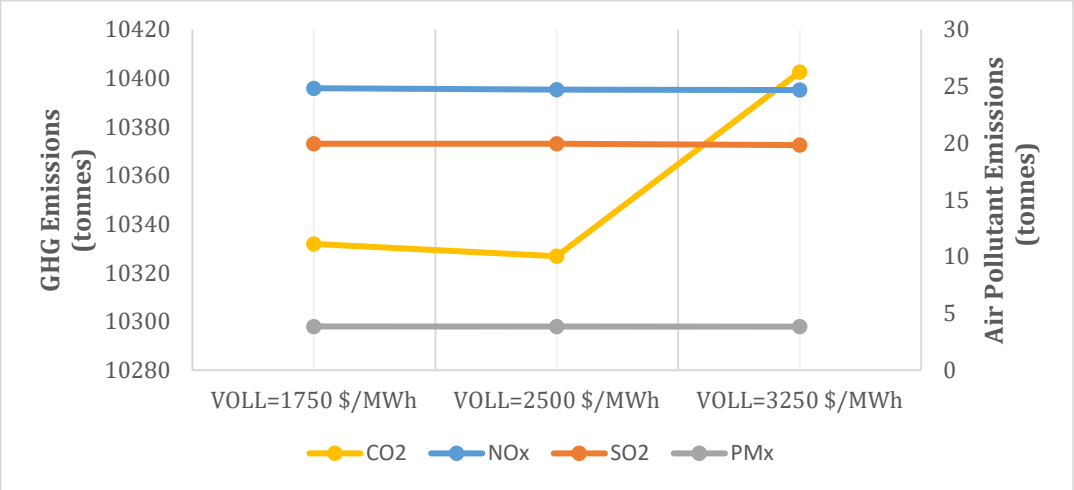

Figure 5.6. Relationship between $VOLL$ and Total Emission Amounts for Modified IEEE 30-bus Problem Instance

Air pollutant emissions do not change significantly as $VOLL$ increases. NO_x emissions are 24.68, 24.73 and 24.85 tonnes, SO_2 emissions are 19.95, 19.94 and 19.83 tonnes, and PM_x emissions are 3.86, 3.86 and 3.84 for increasing levels of $VOLL$, respectively. Nevertheless, by increasing $VOLL$ from 1750 $/MWh to 2500 $/MWh, CO_2 emissions are slightly reduced from the level of 10,331.96 tonnes to 10,326.87 tonnes. However, they increase substantially by reaching to the top level of 10,402.62 tonnes with a further 750 $/MWh increase. The reason is that more carbon intensive units such as coal-fired and oil-fired units become committed to decrease $EENS_t$ levels.

Secondly, we test the sensitivity of the solution by increasing the system uncertainty. Since solution behaviors are similar for both increasing forecast errors and decreasing conventional power generation reliability, we provide the solutions where the reliability of the conventional generation is reduced. For this purpose, we double

and triple failure rates (ORR); accordingly, we solve the model with new conventional system reliability. In Figure 5.7, the relationship between ORR and CC_t over the 24-h scheduling horizon is illustrated. Changing ORR does not affect CC_t levels much except for five periods since emission related costs/revenues dominate the overall cost/benefit analysis. It is important to note that schedules under doubled ORR are similar to the ones in original ORR for the first 20 periods, but schedules under doubled ORR behaves like the ones in tripled ORR due to the VPLE.

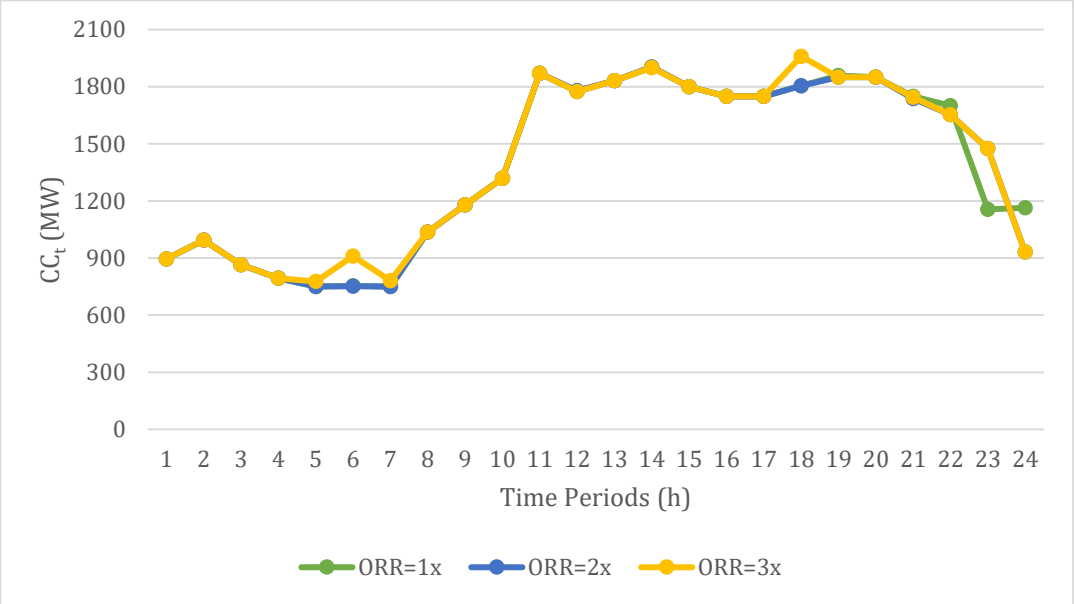

Figure 5.7. Relationship between Conventional System Reliability and CC_t for Modified IEEE 30-bus Problem Instance

Also, we examine how total emission amounts change by decreasing the conventional system reliability, which is shown in Figure 5.8 where the primary and secondary vertical axes represent GHG emissions such as CO_2, and air pollutant emissions consisting of NO_x, SO_2 and PM_x.

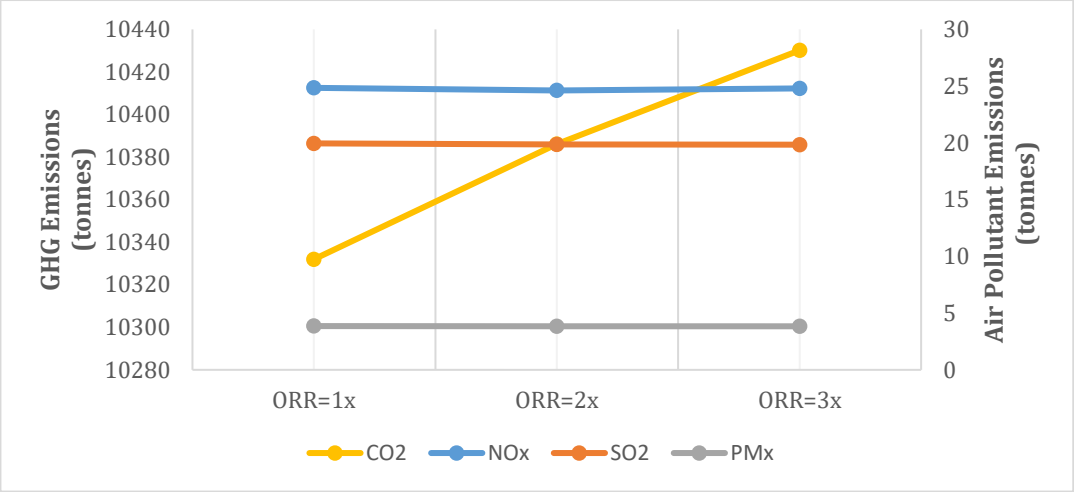

Figure 5.8. Relationship between Conventional System Reliability and Total Emission Amounts for Modified IEEE 30-bus Problem Instance

There is no significant change in air pollutant emissions by increasing ORR as depicted in Figure 5.8. NO_x emissions are 24.85, 24.62 and 24.79 tonnes, SO_2 emissions are 19.95, 19.87 and 19.84 tonnes, and PM_x emissions are 3.86, 3.84 and 3.84 for increasing levels of ORR, respectively. Nonetheless, CO_2 emissions increase substantially as the conventional system reliability is reduced. The emission levels start with 10,331.96 tonnes, then they increase by 54.13 tonnes when ORR is doubled. They further increase by 44.08 tonnes when ORR is tripled. The reason is that more carbon intensive units such as coal-fired and oil-fired units become committed to increase CC_t levels. Moreover, there is an increase in total operating cost when the conventional system becomes less reliable as reported in Table 5.10. That is because both generation and reserve costs and total $EENS_t$ increases with the reduction in the conventional system reliability.

Table 5.10. Total Operating Cost under Different Conventional System Reliability for Modified IEEE 30-bus Problem Instance

Scale of *ORR*	**x1**	**x2**	**x3**
Expected Cost of EENS ($)	31,664.5	51,124.8	69,539.9
Generation & Reserve Cost ($)	698,277.4	703,513.3	707,433.5
Total Operating Cost ($)	**729,941.9**	**754,638.1**	**776,973.4**

Another parameter is the trading price in the carbon economy. To see its effects on total cost, CC_t and emissions, the carbon price is scaled in an increasing order. As shown in Figure 5.9, CC_t values are sensitive to changes in the carbon price. In periods with low net load intensity, there is a downward effect on CC_t levels when the trading price is doubled and tripled. However, this effect is generally reversed for periods with high net load intensity. That is because more units become committed for these periods, but they are dispatched more environmentally friendly to abate GHG and air pollutant emissions.

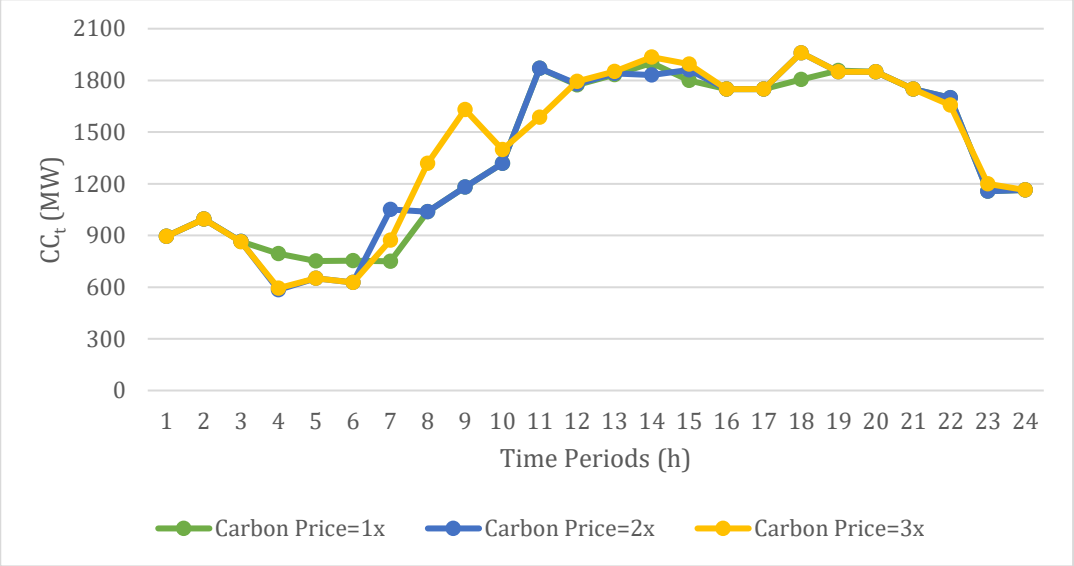

Figure 5.9. Relationship between Carbon Trading Price and CC_t for Modified IEEE 30-bus Problem Instance

Except for NO_x and SO_2 emissions, PM_x and CO_2 emissions reduce as the carbon price increases. In Figure 5.10, PM_x emissions are 3.86, 3.71 and 2.97, and CO_2 emissions are 10,331.96, 10,192.96 and 8,976.43 tonnes for increasing levels of the trading price, respectively. Nevertheless, NO_x emissions slightly increase by 1.75 tonnes and reaches to 26.60 tonnes for doubled trading price. Then, they reduce to 23.58 tonnes for tripled trading price. Similarly, SO_2 emissions slightly increases for doubled carbon price from 19.95 tonnes to 19.98 tonnes. When the carbon price is tripled, they reduce by 3.53 tonnes.

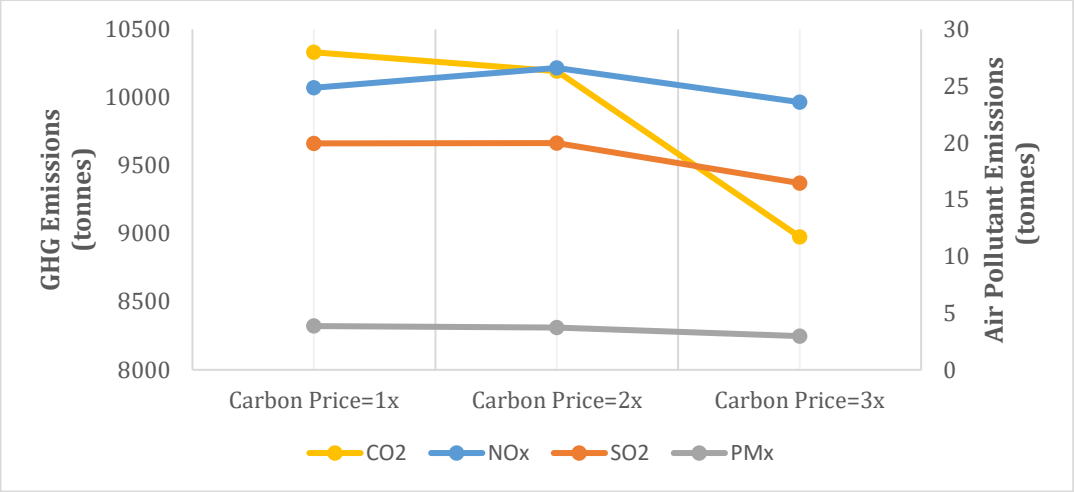

Figure 5.10. Relationship between Carbon Trading Price and Total Emission Amounts for Modified IEEE 30-bus Problem Instance

As reported in Table 5.11, total operating costs increase with an increase in the carbon price due to the increase in generation and reserve costs. While this cost component increases, the expected cost of load shedding slightly fluctuates around the level of $ 31,600.

Table 5.11. Total Operating Cost under Different Carbon Trading Price for Modified IEEE 30-bus Problem Instance

Scale of Carbon Price	**x1**	**x2**	**x3**
Expected Cost of EENS ($)	31,664.5	32,683.8	31,960.6
Generation & Reserve Cost ($)	698,277.4	700,994.6	702,400.4
Total Operating Cost ($)	**729,941.9**	**733,678.5**	**734,360.9**

Like carbon trading price, we also examine how NO_x taxes change the commitment and dispatching decisions. For this purpose, NO_x taxes in three levels are doubled and tripled at the same time. As illustrated in Figure 5.11, CC_t values are very sensitive to changes in NO_x taxes. In general, increasing NO_x taxes have a downward effect on CC_t levels, but those levels with tripled taxes are greater than or equal to the ones with lower taxes for periods with high net load intensity.

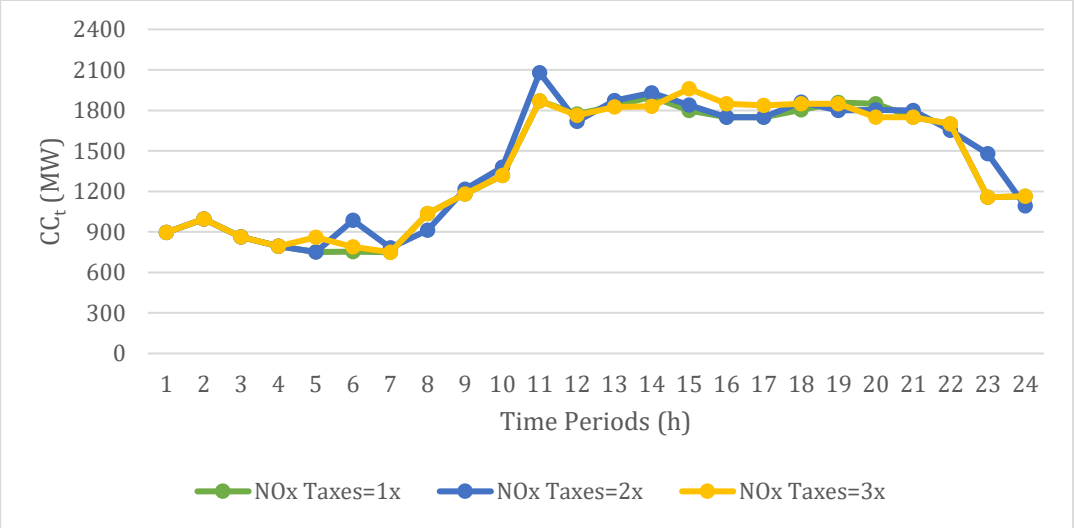

Figure 5.11. Relationship between Three-level NO_x Taxes and CC_t for Modified IEEE 30-bus Problem Instance

Except for CO_2 emissions, NOx, SO_2, PM_x emissions reduce as NO_x taxes increase as demonstrated in Figure 5.12. NO_x emissions are 24.85, 25.44 and 21.37 tonnes, SO_2 emissions are 19.95, 19.76 and 16.30 tonnes, and PM_x emissions are 3.86, 3.59 and 2.66 for increasing NO_x taxes, respectively. However, CO_2 emissions substantially increase by 185.52 tonnes and reaches to 10,517.48 tonnes for doubled NO_x taxes. Then, they significantly abate to 8,978.84 tonnes for tripled NO_x taxes.

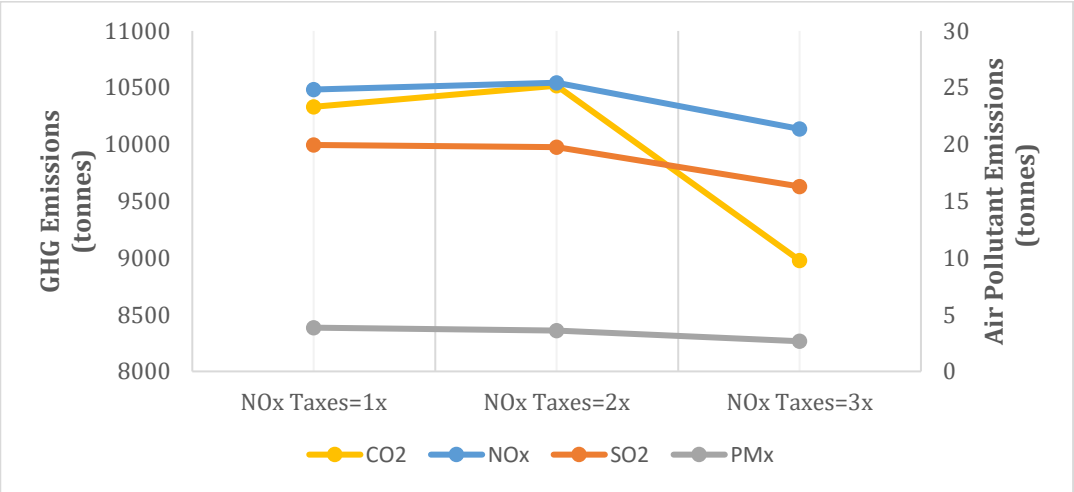

Figure 5.12. Relationship between Three-level NO_x Taxes and Total Emission Amounts for Modified IEEE 30-bus Problem Instance

When the expected costs of EENS are compared for different levels of NO_x taxes, they decrease because of the reduction in total $EENS_t$. In contrast, generation and reserve costs fluctuates, so the total operating costs. It should be pointed out that both components are decreased for the initial and tripled NO_x taxes (Table 5.12).

Table 5.12. Total Operating Cost under Different Three-level NO_x Taxes for Modified IEEE 30-bus Problem Instance

Scale of NO_x Taxes	x1	x2	x3
Expected Cost of EENS ($)	31,664.5	29,873.6	29,713.7
Generation & Reserve Cost ($)	698,277.4	710,832.6	689,425.8
Total Operating Cost ($)	**729,941.9**	**740,706.2**	**719,139.5**

Similar analyses are also made for scaled SO_2 taxes. Different from other parameters, CC_t levels generally increase with higher SO_2 taxes (Figure 5.13). The reason is that gas-fired units do not have an FGD technology whereas coal-fired and oil-fired units have this control technology. However, gas-fired units have more capacity than other units except 700 MW coal-fired unit. Therefore, more units become committed for the same net load level as SO_2 taxes increase, which in return increases CC_t. This effect becomes more significant when SO_2 taxes are tripled.

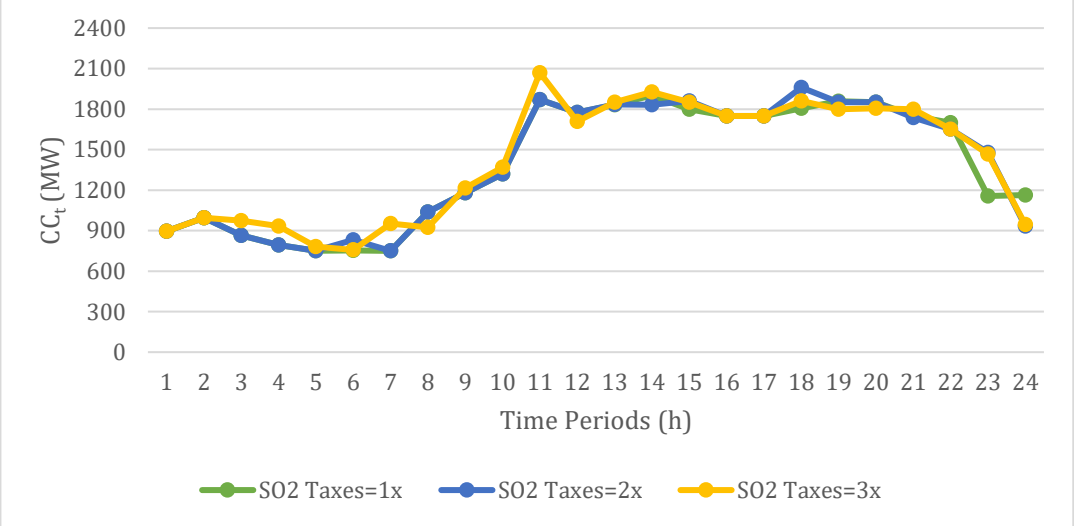

Figure 5.13. Relationship between Three-level SO_2 Taxes and CC_t for Modified IEEE 30-bus Problem Instance

Excluding CO_2 emissions, NOx, SO_2, PM_x emissions are not affected when SO_2 taxes are kept in the original levels and doubled as depicted in Figure 5.14. NO_x emissions are 24.85 and 24.87 tonnes, SO_2 emissions are 19.95 and 19.76 tonnes, and PM_x emissions are 3.86 and 3.71 for the first two scales, respectively. However, CO_2 emissions substantially decrease by 79.61 tonnes and become 10,252.35 tonnes for doubled SO_2 taxes. Nonetheless, both GHG and air pollutant emissions increase significantly when compared to the ones in previous scales. To illustrate, NO_x, SO_2, PM_x and CO_2 emissions reach their top levels of 31.87, 21.80, 4.48 and 11,708.87 tonnes, respectively. The same reasoning in the increase in CC_t levels is also valid for the increase in emission levels. Although coal-fired and oil-fired units do not utilize FGD technology, they are more carbon intensive. Hence, emission levels skyrocket for tripled SO_2 taxes.

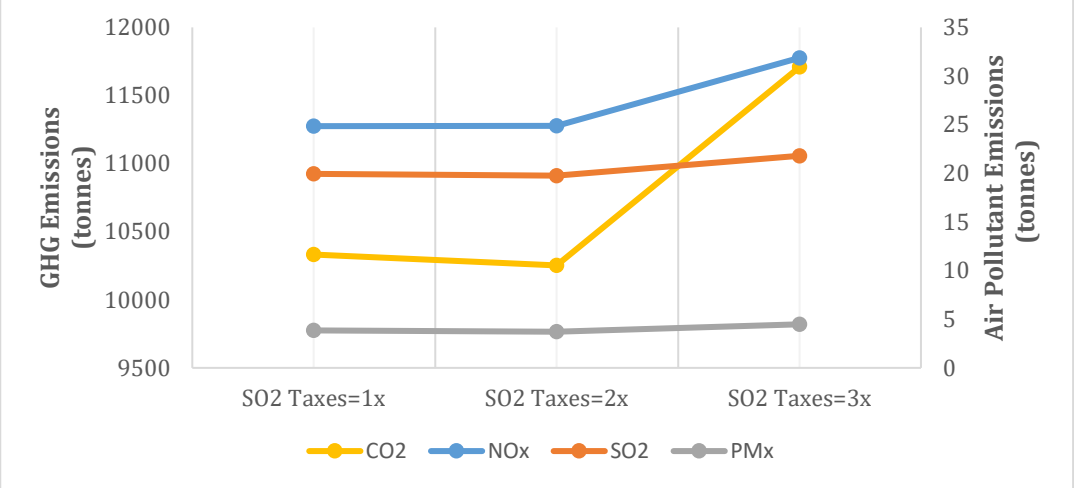

Figure 5.14. Relationship between Three-level SO_2 Taxes and Total Emission Amounts for Modified IEEE 30-bus Problem Instance

When total operating costs are compared for different SO_2 taxes, there is an increasing trend, which is caused by generation and reserve costs as reported in Table 5.13. Since CC_t levels increase, generation and reserve costs also increase whereas the expected cost of load shedding decreases.

Table 5.13. Total Operating Cost under Different Three-level SO_2 Taxes for Modified IEEE 30-bus Problem Instance

Scale of SO_2 Taxes	x1	x2	x3
Expected Cost of EENS ($)	31,664.5	31,177.1	29,393.9
Generation & Reserve Cost ($)	698,277.4	703,700.6	730,019.9
Total Operating Cost ($)	**729,941.9**	**734,877.8**	**759,413.9**

Lastly, we examine the sensitivity of the solution under different PM_x taxes. It is observed that, different PM_x tax regimes do not have a significant impact on CC_t levels as demonstrated in Figure 5.15. The reason is that PM_x emissions are caused by only coal-fired units, and only 700 MW coal-fired unit is committed in the original tax regime since it has the FF technology. Hence, increasing PM_x taxes does not change the commitment and dispatching decisions.

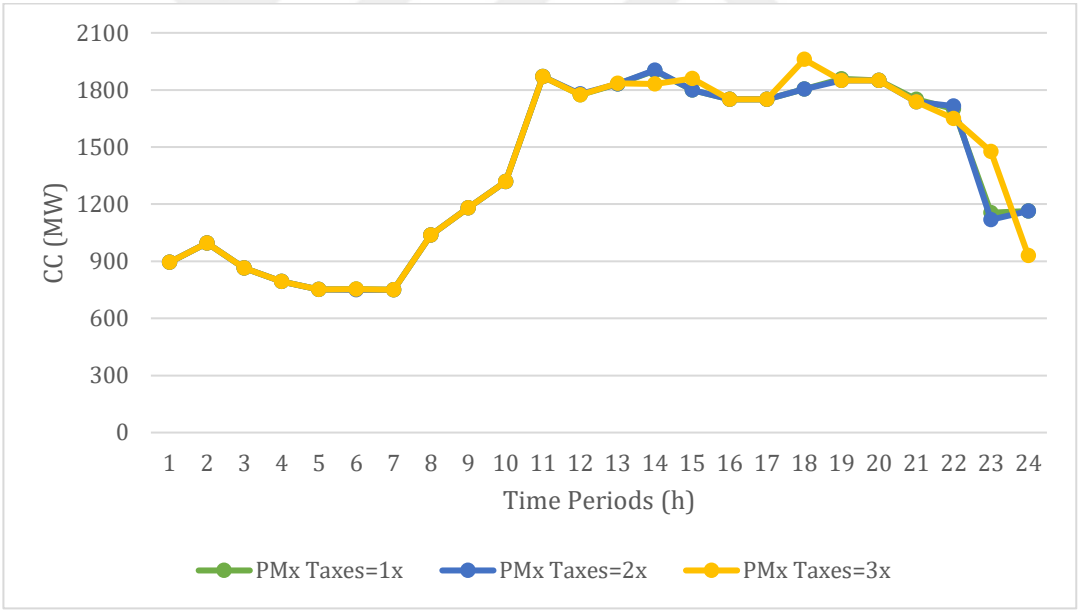

Figure 5.15. Relationship between Three-level PM_x Taxes and CC_t for Modified IEEE 30-bus Problem Instance

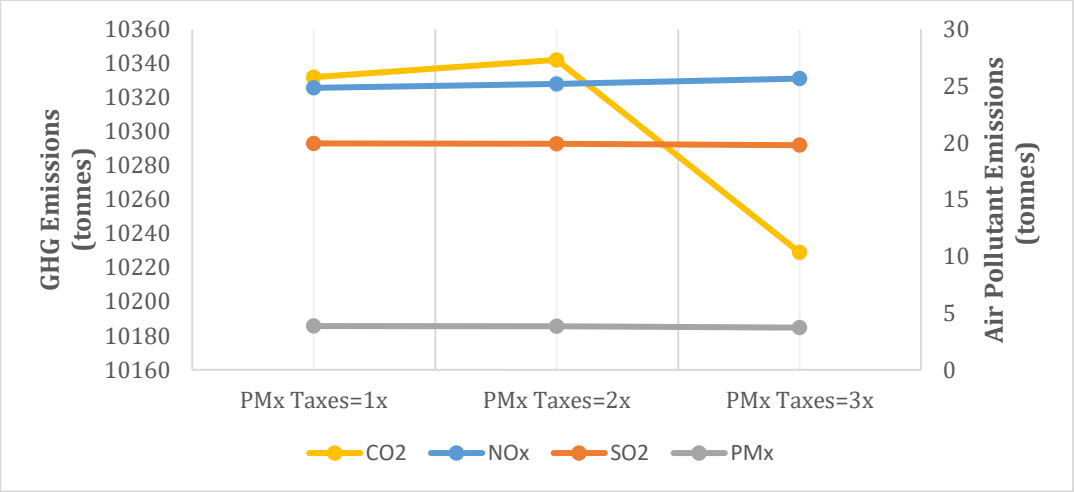

Figure 5.16. Relationship between Three-level PM_x Taxes and Total Emission Amounts for Modified IEEE 30-bus Problem Instance

In Figure 5.16, emission levels under different PM_x tax regimes are shown. PM_x emissions are slightly reduced with the increasing PM_x tax regime. The emission levels are 3.86, 3.85 and 3.72 tonnes. Likewise, SO_2 emissions are also abated by increasing PM_x taxes. The associated emission levels are 19.95, 19.92 and 19.79 tonnes. That is because committed coal fired unit generates less power. Nevertheless, NO_x emissions increase as PM_x taxes increase. The corresponding emission levels are 24.85, 25.20 and 25.66 tonnes. Different from air pollutant emissions, when PM_x taxes are doubled, CO_2 emissions are increased by 10.16 tonnes first and become 10,342.12 tonnes. Then, they decrease by 113.16 tonnes when taxes are tripled. When total operating costs are compared for different PM_x tax regimes, total operating cost increases as a result of the increase in generation and reserve costs as shown in Table 5.14.

Table 5.14. Total Operating Cost under Different Three-level PM_x Taxes for Modified IEEE 30-bus Problem Instance

Scale of PM_x Taxes	**x1**	**x2**	**x3**
Expected Cost of EENS ($)	31,664.5	31,814.6	31,246.4
Generation & Reserve Cost ($)	698,277.4	699,076.3	701,936.6
Total Operating Cost ($)	**729,941.9**	**730,890.9**	**733,182.9**

In particular, the results of sensitivity analyses verify that the carbon trading price, tax regimes for air pollutant emissions have a substantial impact on both commitment and dispatching decisions, and GHG and air pollutant emissions in our time-decoupled, stochastic and environmental model MIQP I-VPLE-EC for modified IEEE 30-bus problem instance. Different from models introduced in Chapter 4, $VOLL$ and the system uncertainty due to forecast errors and potential failures in conventional generation have an insignificant effect on commitment and dispatching decisions, and air pollutant emissions in the proposed approach. Even so, it should be emphasized that total CO_2 emissions are always affected by the changes in almost all parameters.

5.4.3 Comparison of Results

For modified IEEE 30-bus problem instance and its duplicated version, the proposed time-decoupled, stochastic and environmental formulation MIQP I-VPLE-EC is compared with traditional UCP formulations with deterministic reserve policies and the time-decoupled model MIQP I-VPLE proposed in Chapter 4. According to schedules obtained by these approaches, their SR_t and $EENS_t$ values are computed by using $EENS_t$ Approximation I. Similarly, their GHG and air pollutant emissions are calculated via emission models explained in Section 5.3.

5.4.3.1 Comparison with Deterministic Approaches

For both problem instance, the proposed approach and deterministic approaches are compared in terms of total emissions and total operating costs that consist of generation costs, reserve rates and socioeconomic value of the lost load. First, the results for Problem Instance 1 are provided. In Table 5.15, total operating costs of each approach and their components are reported for modified IEEE 30-bus problem instance. Total operating cost of the proposed approach is lower than the deterministic approaches thanks to the complete trade-off between generation and

reserve costs, the expected cost of load shedding and emission related costs/revenues. Nonetheless, the proposed approach yields schedules with larger total $EENS_t$, so its expected cost of lost load is greater than other deterministic approaches.

Table 5.15. Comparison of Total Operating Costs in the Proposed and Deterministic Approaches for Modified IEEE 30-bus Problem Instance

Approaches	Proposed	Traditional	3.5σ	Hybrid
Expected Cost of EENS ($)	31,664.5	20,904.3	29,673.3	20,061.2
Generation & Reserve Cost ($)	698,277.4	788,300.1	725,517.7	769,283.4
Total Operating Cost ($)	**729,941.9**	**809,204.4**	**755,191.0**	**789,344.5**

As shown in Figure 5.17, total NO_x and PM_x emissions are significantly reduced by the proposed approach. For NO_x emissions, the overall reduction ranges between 39% and 45%. This range is between 46% and 60% for PM_x emissions. In terms of SO_2 emissions, the proposed approach gives schedules with lower emissions when compared to the ones in the 3.5σ and hybrid approaches. The corresponding reduction amounts are 8% and 15%, respectively. However, schedules obtained by the proposed and traditional approaches emit the same amount of SO_2 which is approximately 20 tonnes. Furthermore, by using the proposed approach, CO_2 emissions are also cut by 30% to 42% as illustrated in Figure 5.18.

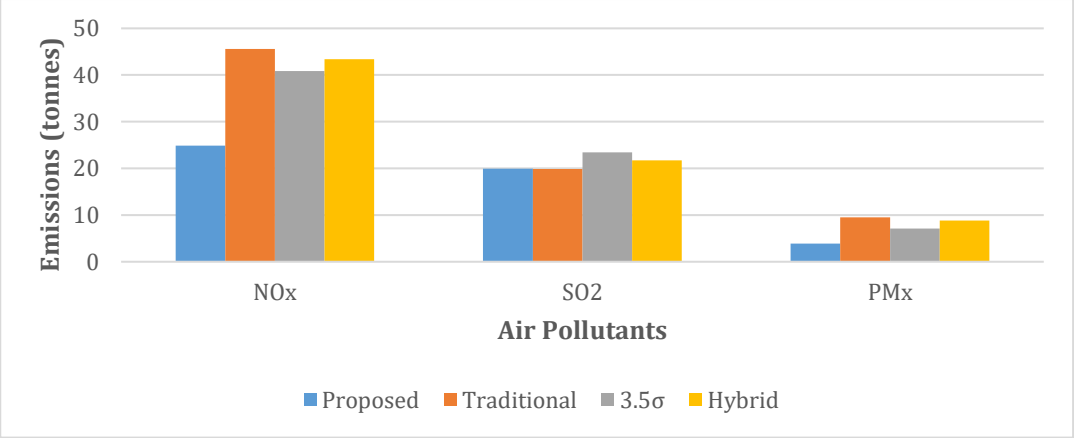

Figure 5.17. Comparison of Air Pollutant Emissions in the Proposed and Deterministic Approaches for Modified IEEE 30-bus Problem Instance

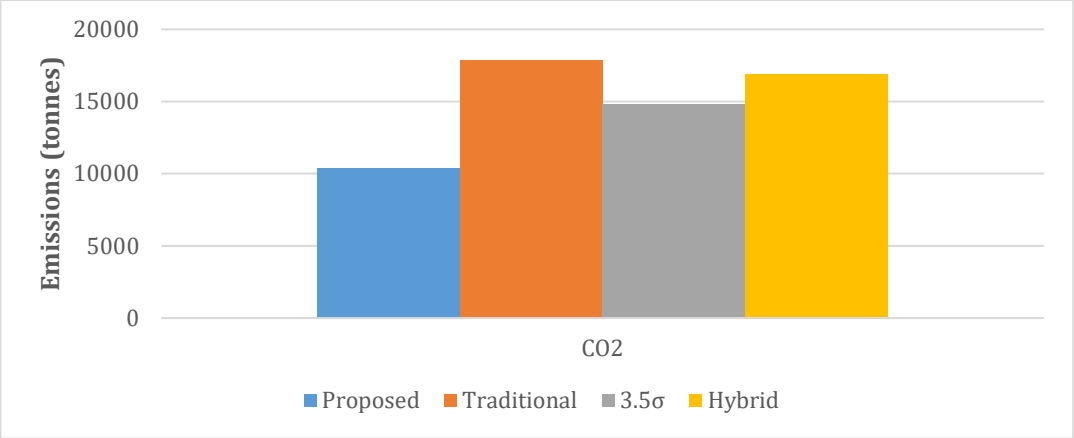

Figure 5.18. Comparison of CO_2 Emissions in the Proposed and Deterministic Approaches for Modified IEEE 30-bus Problem Instance

Similar comparisons are also made for the duplicated version of modified IEEE 30-bus problem instance. Considering total operating costs, the proposed approach outperforms the deterministic approaches since it explicitly makes the trade-off between generation and reserve costs, the expected cost of EENS and emission related costs/revenues (Table 5.16). Nevertheless, the proposed approach yields schedules with larger total $EENS_y$ as in modified IEEE 30-bus problem instance.

Table 5.16. Comparison of Total Operating Costs in the Proposed and Deterministic Approaches for Modified and Duplicated IEEE 30-bus Problem Instance

Approaches	**Proposed**	**Traditional**	**3.5σ**	**Hybrid**
Expected Cost of EENS ($)	74,845.9	34,162.7	56,140.9	34,162.7
Generation & Reserve Cost ($)	1,355,239.6	1,454,281.4	1,411,577.6	1,454,281.4
Total Operating Cost ($)	**1,430,085.4**	**1,488,444.1**	**1,467,718.5**	**1,488,444.1**

Different from modified IEEE 30-bus problem instance, all air pollutant emissions are substantially reduced by the proposed approach as depicted in Figure 5.19. For NO_x emissions, the total abatement is 43% when compared to the 3.5σ approach whereas it is 50% when compared to the traditional and hybrid approaches. For PM_x emissions, these are 56% and 67%, respectively. For SO_2 emissions, the corresponding reduction amounts are 20% and 26%, respectively. Likewise, by using

the proposed approach, CO_2 emissions are also cut by 30 percent to 41 percent as shown in Figure 5.20.

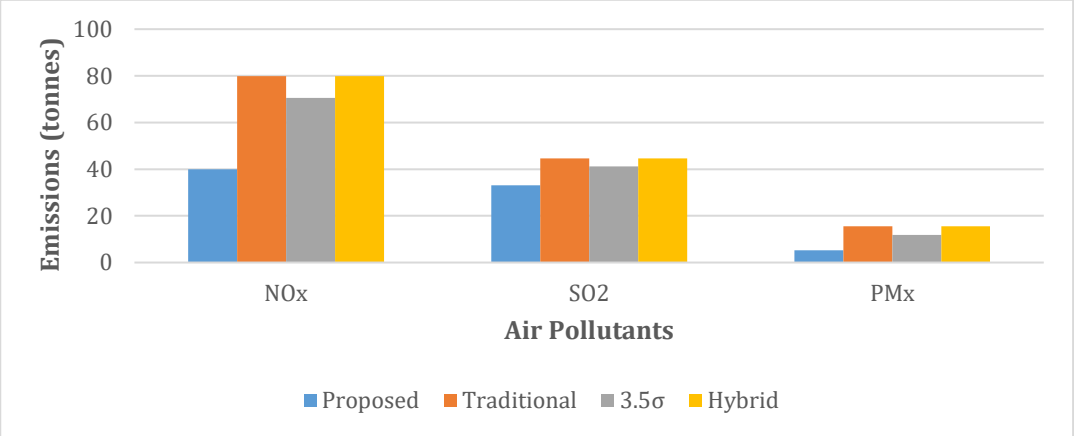

Figure 5.19. Comparison of Air Pollutant Emissions in the Proposed and Deterministic Approaches for Modified and Duplicated IEEE 30-bus Problem Instance

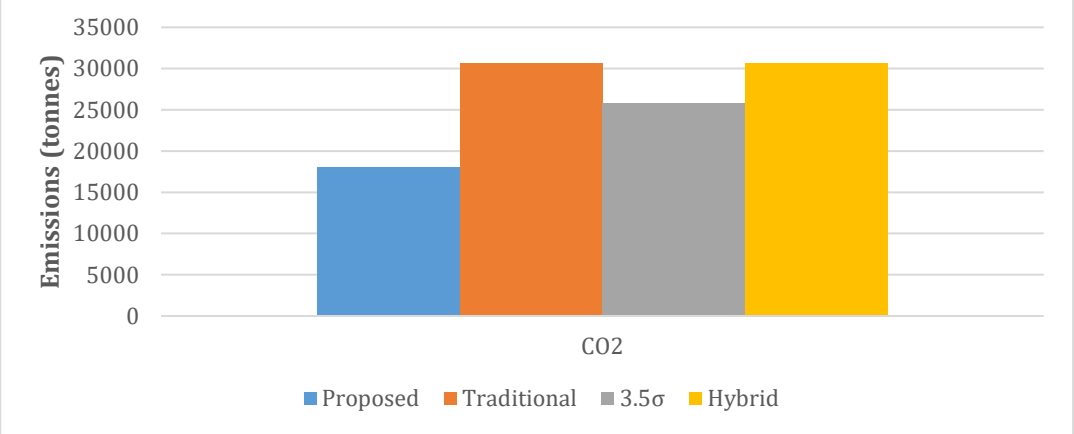

Figure 5.20. Comparison of CO_2 Emissions in the Proposed and Deterministic Approaches for Modified and Duplicated IEEE 30-bus Problem Instance

5.4.3.2 Comparison with the Pure Stochastic Approach

For both problem instance, the proposed formulation MIQP I-VPLE-EC and the formulation MIQP I-VPLE are compared in terms of committed capacities, reserves, total $EENS_t$, total emissions, total operating costs that consist of generation costs,

reserve rates and socioeconomic value of the lost load. For the sake of clarity, in this section, the proposed model MIQP I-VPLE-EC is called as the environmental stochastic approach while the model MIQP I-VPLE is called as the pure stochastic approach. First, the results for Problem Instance 1 are provided.

In Figure 5.21, CC_t levels are compared for the environmental stochastic and pure stochastic approaches for modified IEEE 30-bus problem instance. In 10 out of 24 periods, the environmental stochastic approach yields schedules having CC_t greater than or equal to that in the pure stochastic approach. Hence, the former behaves less conservative when emission limitations are considered. To illustrate, total $EENS_t$ over the 24-h scheduling horizon is 18 MWh in the environmental stochastic whereas it is 14 MWh in the pure stochastic approach. Nevertheless, commitment decisions are approximately the same for both approaches when periods are net load intensive.

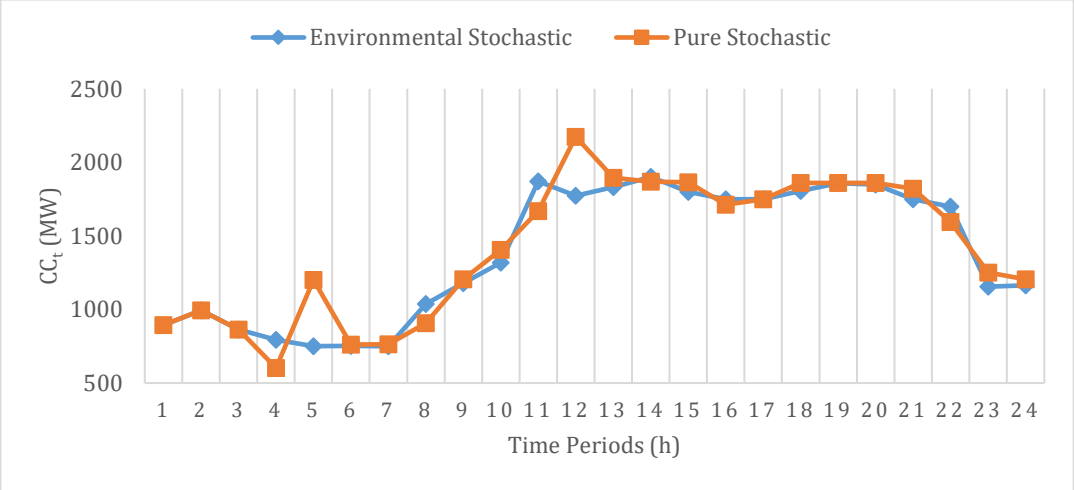

Figure 5.21. Comparison of Committed Capacities in the Environmental Stochastic and Pure Stochastic Approaches for Modified IEEE 30-bus Problem Instance

Also, we compare how the overall power generation mix changes when emission limitations are also considered. As shown in Figure 5.22, the power generation is coal intensive with 55% share in the pure stochastic approach, whereas it is gas intensive with 61% share in the environmental stochastic approach. That is because coal-fired units are cheaper in the sense of power generation. When emission

limitations are considered, it is more plausible to generate more power from gas-fired units because these units are more environmentally friendly. In any case, the share of oil-fired units in the power generation mix remains unchanged.

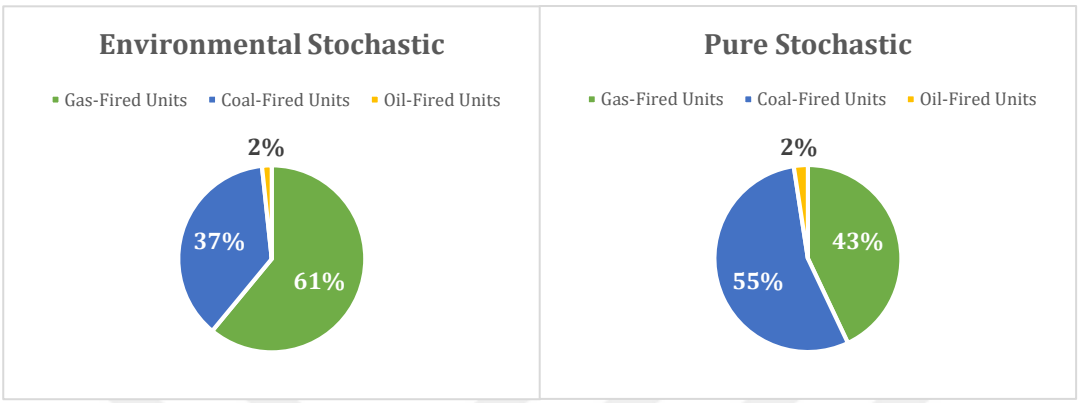

Figure 5.22. Comparison of Power Generation Mixes in the Environmental Stochastic and Pure Stochastic Approaches for Modified IEEE 30-bus Problem Instance

It is important to note that the shift in overall power generation mix is due to the change in unit-based hourly loading profiles as shown in Figures 5.23 and 5.24 where combustion types of units are specified in parenthesis. The share of gas-fired generation increases in every period when the environmental stochastic approach is used. This increase is more prevalent in periods with low and medium load intensity.

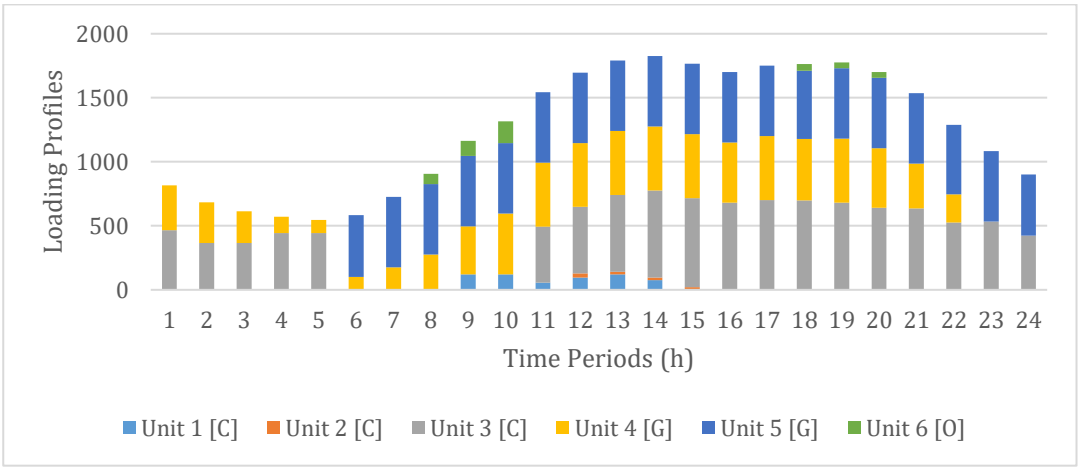

Figure 5.23. Hourly Loading Profiles of Conventional Units in the Environmental Stochastic Approach for Modified IEEE 30-bus Problem Instance

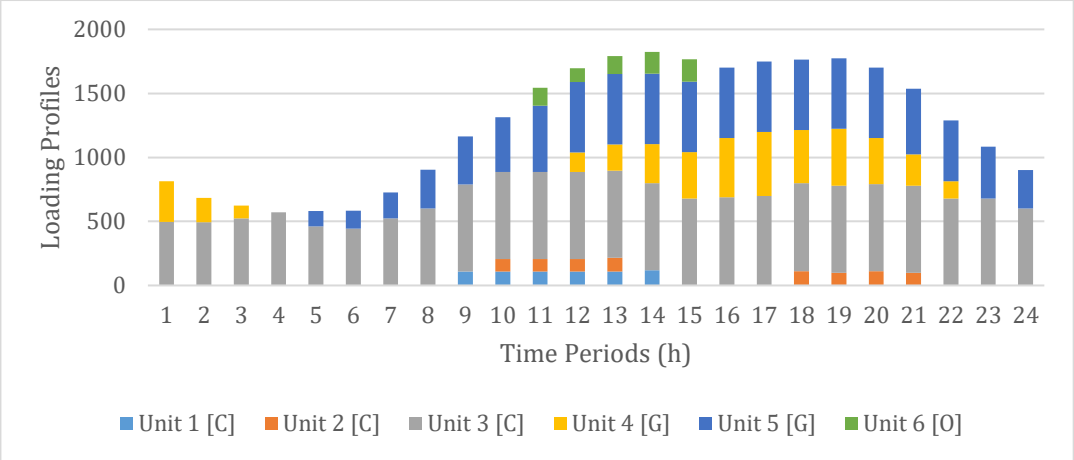

Figure 5.24. Hourly Loading Profiles of Conventional Units in the Pure Stochastic Approach for Modified IEEE 30-bus Problem Instance

As illustrated in Figure 5.25, the reductions in total NO_x and PM_x emissions are significant in the environmental stochastic approach. Both emissions are cut by 19%. However, total SO_2 emissions is approximately the same for both approaches, which is around 20 tonnes. Besides, in terms of GHG emissions, by using the environmental stochastic approach, CO_2 emissions are reduced by 8% as depicted in Figure 5.25.

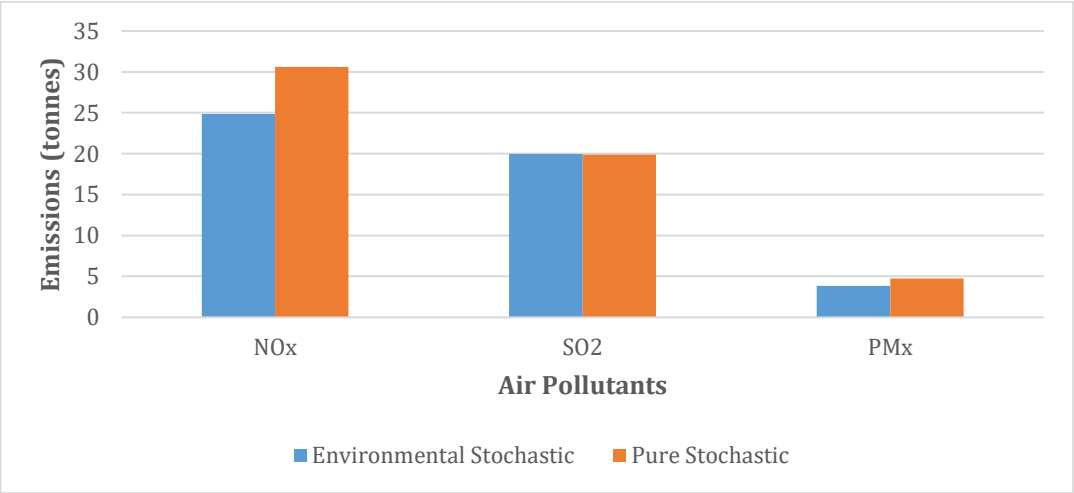

Figure 5.25. Comparison of Air Pollutant Emissions in the Environmental Stochastic and Pure Stochastic Approaches for Modified IEEE 30-bus Problem Instance

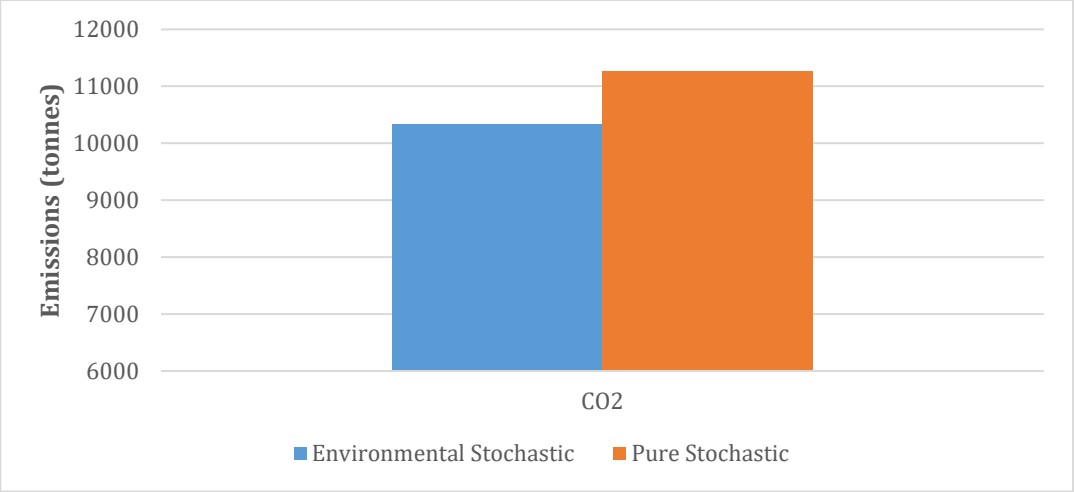

Figure 5.26. Comparison of CO_2 Emissions in the Environmental Stochastic and Pure Stochastic Approaches for Modified IEEE 30-bus Problem Instance

When both approaches are compared in terms of total operating costs, the environmental approach yields a generation schedule that is more expensive than that in the pure stochastic approach, which is mainly due to the difference between total $EENS_t$ in each approach as shown in Table 5.17. In the environmental stochastic approach, 18 MWh of energy is expected to be not served whereas it is 14 MWh in the pure stochastic approach. The reason is that the former provides less reserves in order to reduce GHG and air pollutant emissions.

Table 5.17. Comparison of Total Operating Costs in the Environmental Stochastic and Pure Stochastic Approaches for Modified IEEE 30-bus Problem Instance

Approaches	**Environmental Stochastic**	**Pure Stochastic**
Expected Cost of EENS ($)	31,664.5	24,304.3
Generation & Reserve Cost ($)	698,277.4	697,383.4
Total Operating Cost ($)	**729,941.9**	**721,687.7**

Similar comparisons are also made for the duplicated version of modified IEEE 30-bus problem instance. In Figure 5.27, for Problem Instance 2, CC_t levels are provided for the environmental stochastic and pure stochastic approaches. In 15 out of 24 periods, CC_t in the environmental stochastic approach is greater than or equal

to the ones in the pure stochastic approach. Thence, the former behaves more conservative in those periods, but it gives a schedule with larger total $EENS_t$ over the 24-h scheduling horizon. To illustrate, total $EENS_t$ is 43 MWh in the environmental stochastic approach, whereas it is 35 MWh in the pure stochastic approach. This is an indicator that the latter preserves its conservativeness as in Problem Instance 1. Nonetheless, commitment decisions in periods with high net load intensity are similar for both approaches.

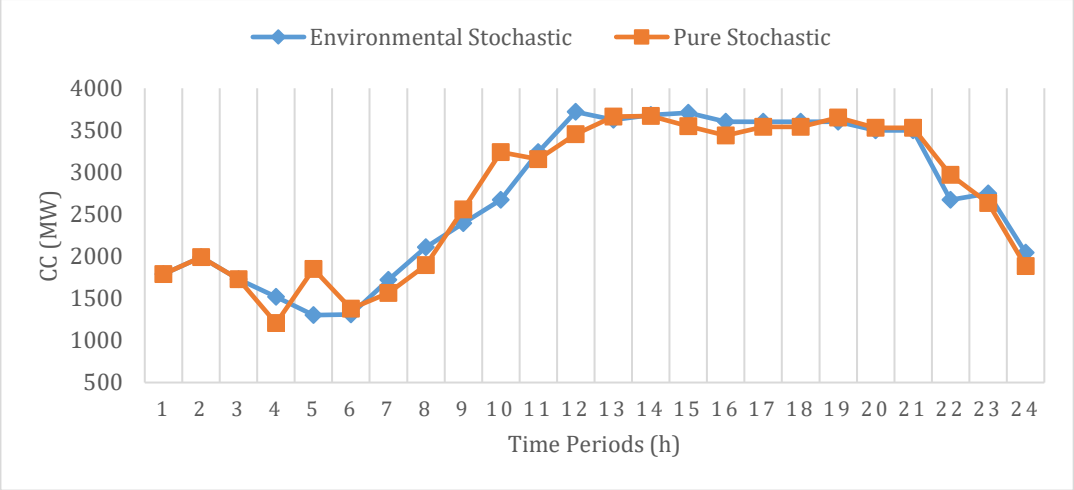

Figure 5.27. Comparison of Committed Capacities in the Environmental Stochastic and Pure Stochastic Approaches for Modified and Duplicated IEEE 30-bus Problem Instance

Secondly, the change in the overall power generation mix is compared for both environmental stochastic and pure stochastic approaches. As shown in Figure 5.28, the power generation is coal intensive with 52% share in the pure stochastic approach while it is gas intensive with 64% share in the environmental stochastic approach. The same reasoning in the first problem instance is also valid in its duplicated version. Different from Problem Instance 1, the share of oil-fired units in the power generation mix is also decreased by 4% in this case.

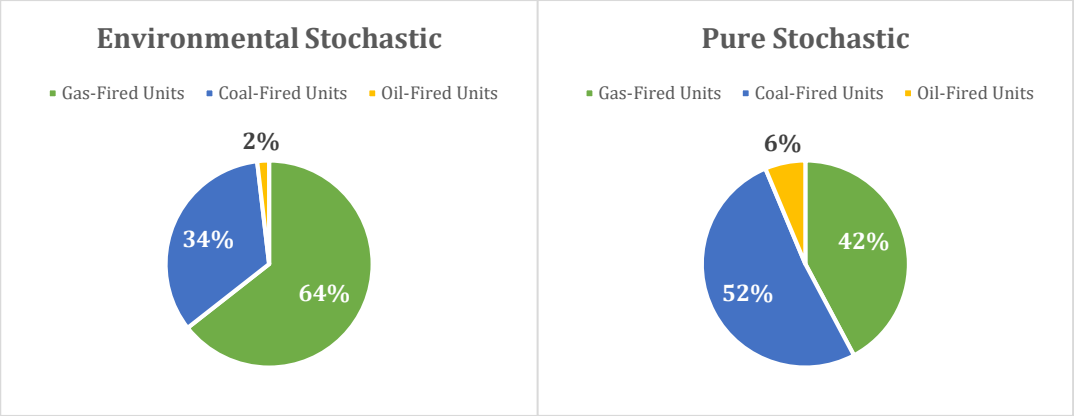

Figure 5.28. Comparison of Power Generation Mixes in the Environmental Stochastic and Pure Stochastic Approaches for Modified and Duplicated IEEE 30-bus Problem Instance

The shift in overall power generation mix is due to the change in unit-based hourly loading profiles as shown in Figures 5.29 and 5.30. When environmental stochastic approach is implemented, it is observed that the share of gas fired generation increases significantly in every period. In fact, only gas-fired units become committed or most of the load demand is met by those units after the 4th period.

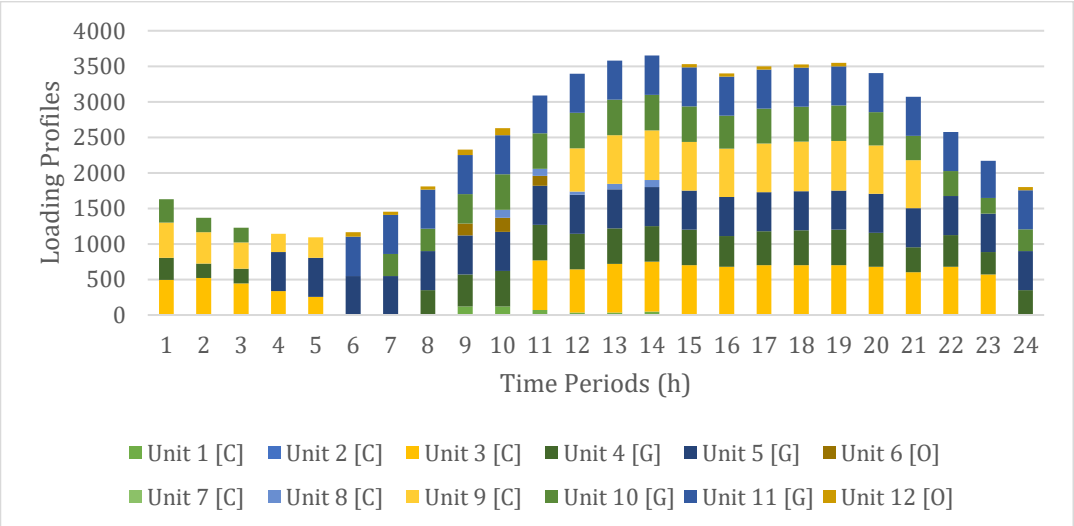

Figure 5.29. Hourly Loading Profiles of Conventional Units in the Environmental Stochastic Approach for Modified and Duplicated IEEE 30-bus Problem Instance

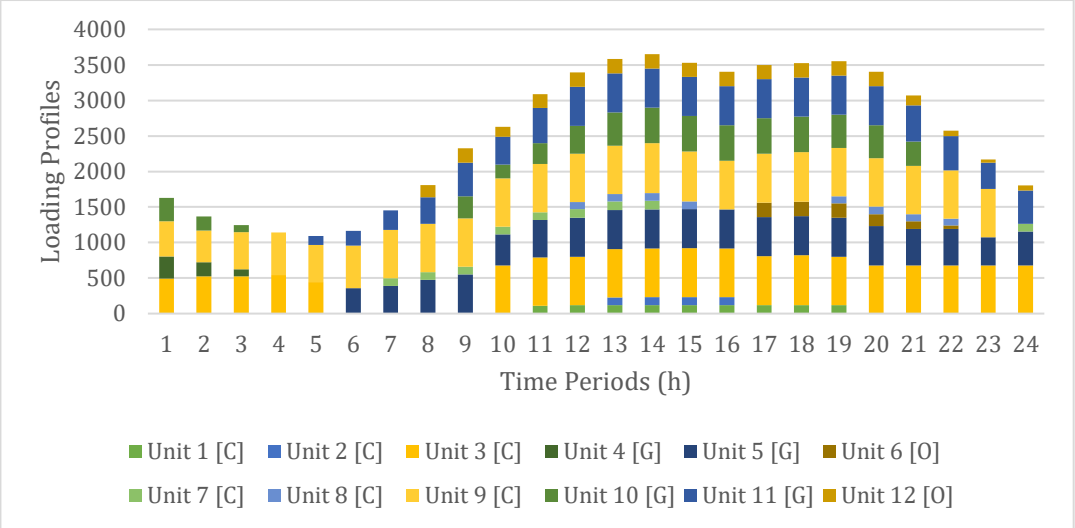

Figure 5.30. Hourly Loading Profiles of Conventional Units in Pure Stochastic Approach for Modified and Duplicated IEEE 30-bus Problem Instance

Unlike Problem Instance 1, all air pollutant emissions are significantly reduced by the environmental stochastic approach as illustrated in Figure 5.31. The associated reductions in total NO_x, SO_2 and PM_x emissions are 42%, 26% and 51%, respectively. Moreover, in terms of GHG emissions, by using the proposed approach, CO_2 emissions are cut by 29% as shown in Figure 5.32.

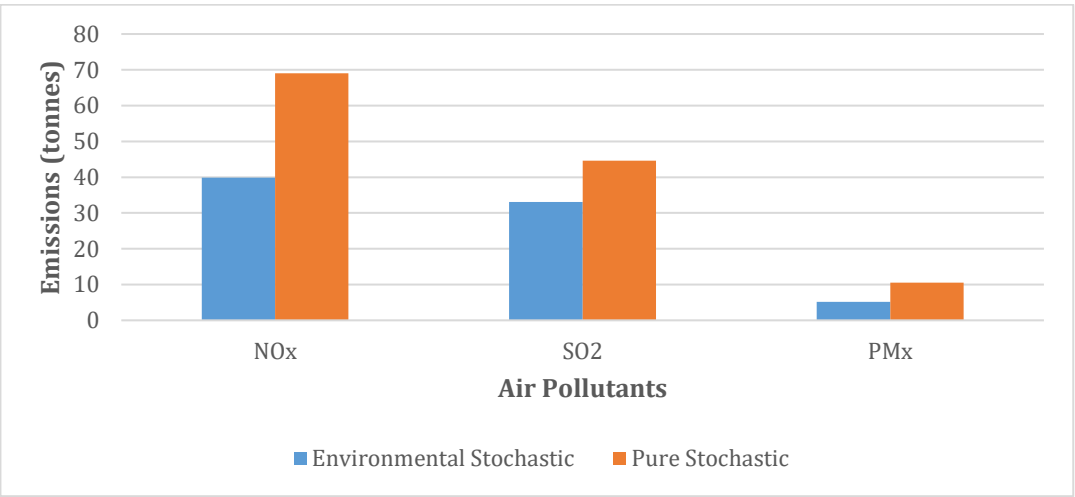

Figure 5.31. Comparison of Air Pollutant Emissions in the Environmental Stochastic and Pure Stochastic Approaches for Modified and Duplicated IEEE 30-bus Problem Instance

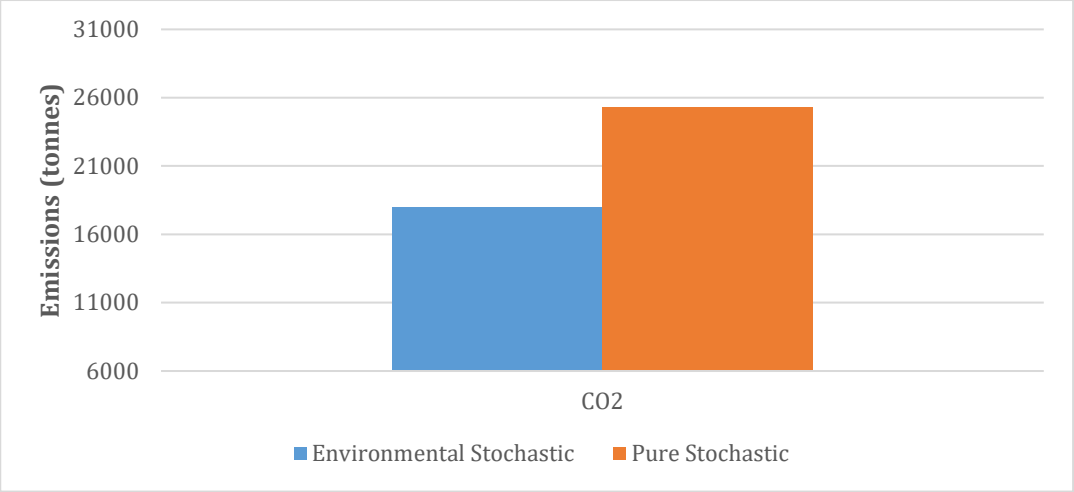

Figure 5.32. Comparison of CO_2 Emissions in the Environmental Stochastic and Pure Stochastic Approaches for Modified and Duplicated IEEE 30-bus Problem Instance

As in Problem Instance 1, the environmental stochastic approach yields a generation schedule that is more expensive than that in the pure stochastic approach in terms of total operating costs. Even if generation and reserve costs are reduced by $ 1,693.2 in environmental stochastic approach, its expected cost of load shedding is larger than that of the pure stochastic approach as shown in Table 5.18. The reason is that 43 MWh of energy is expected to be not served in the former which keeps less reserve to mitigate emissions, whereas it is 35 MWh in the latter.

Table 5.18. Comparison of Total Operating Costs in the Environmental Stochastic and Pure Stochastic Approaches for Modified and Duplicated IEEE 30-bus Problem Instance

Approaches	**Environmental Stochastic**	**Pure Stochastic**
Expected Cost of EENS ($)	74,845.9	61,777.4
Generation & Reserve Cost ($)	1,355,239.6	1,356,932.8
Total Operating Cost ($)	**1,430,085.4**	**1,418,710.3**

CHAPTER 6

CONCLUSION AND FUTURE RESEARCH

This thesis addresses solution approaches for unit commitment problems in traditional and wind integrated hybrid power systems. These problems have a critical role in effective planning and efficient operation of modern power systems. For this purpose, operating cost reduction has been a top priority objective for power generation companies in the vertically integrated electricity markets. Nevertheless, with the increasing concerns on global warming and air pollution, a great majority of countries have been promoting policies to abate GHG and air pollutant emissions. Hence, power generation companies are forced to also consider the minimization of atmospheric emissions in their operations planning.

At the first stage of this study, we propose a Mixed Integer Coded Genetic Algorithm (MICGA) combined with Improved Lambda Iteration Method (I-LIM) to solve the UCP in traditional power systems where the sole priority is to minimize total operating costs of conventional power plants ignoring the inherent uncertainties. In the proposed algorithm, commitment decisions are given according to genetic operations while load dispatching decisions are made with the combined usage of the I-LIM and genetic operators. The MICGA incorporates a special chromosome representation strategy and initial population algorithm, problem specific genetic operators, penalty mechanisms and a modified version of the LIM. Those features assure the convergence of the algorithm, the feasibility and optimality of the solutions. The algorithm is applied to a set of widely used benchmark problem instances. According to statistical analyses conducted, the algorithm yields robust and precise solutions, which is very important in operations planning of power systems. Also, the solutions are compared with other GA-based approaches in terms

of both solution qualities and computing times. The results indicate that the MICGA can determine satisfactorily good unit schedules and power generation mix in a reasonable computation time. The main contributions of the proposed approach are listed as follows:

- Different from most of the genetic algorithm-based approaches reviewed in Chapter 2, mixed integer coding scheme is first utilized when representing commitment schedules as chromosomes. By doing so, the required memory usage is reduced, and the computation is expedited significantly.
- For initial population generation, an intelligent algorithm is first devised to ensure that chromosomes in the initial population always satisfy the minimum uptime/downtime constraints. Similarly, various problem specific mutation operators are developed to enhance the solution quality and the convergence rate of the MICGA. With the special initial population algorithm and smart mutation operators, minimum uptime/downtime constraints are always met during the evolution.
- Different from the original LIM, the proposed I-LIM can also use the notion of Average Fuel Cost Optimization in addition to its main logic of the Total Fuel Cost Optimization. Accordingly, the I-LIM yields dispatching schedules with less total fuel costs. Moreover, the original LIM cannot cope with the ramp rate limits of conventional generating units. To overcome this problem, the I-LIM is also strengthened with a set of rules that can guarantee the non-violation of the ramp rate limits. As a result, both generation limits and ramp-rate limits are satisfied with this improved version.

For the first stage of this study (Chapter 3), there are several future research directions, including, but not limited to, the following ideas:

- The proposed MICGA can be improved by integrating other local search techniques so that the regions around the local optimum can be explored even further.

- Making use of some diversity measures that will enable the algorithm to adjust its genetic operation probabilities on its own during the evolution may improve the exploitation capability of the MICGA.
- In the proposed MICGA, dispatching subproblem is solved via an improved version of the LIM (I-LIM). Without requiring such an exogenous algorithm, the solution of this subproblem can also be integrated to the GA itself. By doing so, the convergence rate of the MICGA can be improved.
- In real power systems, conventional power plant efficiencies oscillate when their power output levels increase gradually. This is called as valve point loading effect (VPLE) which results in nonconvex operating cost functions. To integrate this phenomenon into the MICGA, a new set of rules can be defined to reinforce the I-LIM, or the MICGA can be combined with another heuristic.

At the second stage of this study, we propose different time-decoupled and stochastic Mixed Integer Quadratic Programming (MIQP) models to solve the UCP in wind integrated hybrid power systems, where the main objective is to minimize the sum of total power generation costs of conventional power plants and the socioeconomic value of the expected energy not served (EENS) due to wind and load demand forecast errors, and unexpected unit outages in conventional generation. In those models, load demand forecasts and wind power generation forecasts are linked with each other by considering wind power supply as a negative load under certain assumptions, while the unexpected outages of conventional generating units are modeled as a two-state Discrete Time Markov Process. To integrate EENS due to forecast errors and sudden outages in conventional generation, two modelling techniques are developed. In these techniques, EENS is piecewise linearly approximated by using additional auxiliary variables and linear constraints. It is shown that one of these estimation techniques has a superior performance in terms of model complexity and required computing time. Then, that model is extended to also take into account the VPLE in conventional generation. In this extension, the absolute sinusoidal oscillation in conventional power plant efficiencies is piecewise

linearly approximated by introducing additional auxiliary variables and linear constraints. The proposed models are implemented on a set of widely used benchmark problem instances. To examine the effects of changes in problem parameters on the solutions, sensitivity analyses are carried out for critical problem parameters. Then, the proposed time-decoupled and stochastic approaches are compared with the standard UCP models enforcing deterministic reserve criteria. The results indicate that the MIQP stochastic models outperform the standard UCP formulations in terms of total operating costs. The main contributions of the proposed MIQP approaches are listed as follows:

- An efficient algorithm is devised to construct the Capacity Outage Probability Table (COPT) for medium and large scale wind integrated hybrid power systems.
- Some novel EENS estimation techniques, which make use of the concept of piecewise linear approximation, are developed and integrated to the MIQP models. By this way, the proposed models accurately calculate EENS approximations without requiring any deterministic reserve criteria or risk targets. Accordingly, total power generation cost and the expected cost of EENS are explicitly traded off when making commitment and dispatching decisions.
- An efficient piecewise linear approximation method is developed for the VPLE in conventional power plant efficiencies. This approximation includes fewer auxiliary variables and constraints than that of its current counterparts. As a result, the proposed MIQP model, which is reinforced with the VPLE approximation, remains computationally tractable. Accordingly, the required memory usage is reduced, and the computation is expedited significantly.
- As a result of the above techniques, a practical and yet effective methodology, which combines both supply and demand uncertainties in wind integrated hybrid power systems, has been developed. This methodology is implemented in a single mathematical model (MIQP I-VPLE).

At the last stage of this study, the model MIQP I-VPLE is further extended to also consider the effects of emission limitations and emission reduction technologies on the conventional generation in wind integrated hybrid power systems. Owing to nonlinear representations of GHG and air pollutant emissions, the extended version of the model MIQP I-VPLE now becomes a time-decoupled, stochastic and environmental Mixed Integer Quadratically Constrained Programming (MIQCP≡MIQP I-VPLE-EC) model. In this extension, the main objective is to minimize the sum of total power generation costs of conventional generating units, the socioeconomic value of the expected energy not served as well as the cost of emissions. The proposed MIQCP model is applied to a set of widely used benchmark problem instances. To examine the effects of changes in problem parameters on the solutions, sensitivity analyses are conducted for several problem parameters. Then, the proposed time-decoupled, stochastic and environmental approach (MIQCP model) is compared with the standard UCP models enforcing deterministic reserve criteria and the model MIQP I-VPLE. The results indicate that the MIQCP model outperforms others in terms of both operating costs and emission amounts. The main contributions of the proposed MIQCP approach are listed as follows:

- To the best of our knowledge, the proposed methodology is the first that considers both supply/demand uncertainty, the VPLE, emission limitations and clean energy technologies in wind integrated hybrid power systems. By this way, total power generation costs, the expected cost of EENS and emission costs/revenues are explicitly traded off when making commitment and dispatching decisions.
- As far as we know, the proposed methodology is the only study that deals with CO_2, NO_x, SO_2 and PM_x emissions at the same time by taking emission trading and taxing mechanisms into consideration.
- In the UCP in wind integrated hybrid power systems, the proposed MIQCP approach provides effective and integrated modelling of Carbon Capture Storage Systems against CO_2 emissions; Low NO_x Burner and Selective Catalytic Reduction Technologies against NO_x emissions; Fabric Filters

against PM_x emissions; and Flue Gas Desulfurization Technique against SO_2 emissions. Likewise, the Combustion Mode Switch Feature against NO_x emissions of gas-fired generating units is modelled more precisely than that of its current applications. Hence, the proposed MIQCP formulation is the first environmentally friendly model that integrates those emission control technologies in a single mathematical model (MIQP I-VPLE-EC).

For the last two stages of this study (Chapters 4 and 5), we can point out several future research directions, including, but not limited to, the following ideas:

- In the proposed models, it is assumed that there are no constraints on the transmission of the produced power to the demand points. In reality, each transmission line has a power transmission limit. Also, some portion of the produced power might be lost during transmission especially over long distances. Hence, the impacts of transmission infrastructure on the UCP should also be taken into account. Thanks to time-decoupled features of the proposed models, power transmission limits and transmission losses can also be integrated without losing the tractability of the models.
- Due to the thermal stress limitations and mechanical characteristics of the conventional generating units, they might not be able to produce power output in several operating zones. These zones are called as prohibited operating zones, which results in discontinuities on their fuel cost curves. In the proposed models, this requirement is relaxed by assuming that conventional power generating units can produce within their power output and ramp-rate limits. Nevertheless, by defining additional auxiliary variables and constraints to the proposed models, these discontinuities can also be handled.
- In addition to wind turbines, solar panels have also grabbed a significant attention in several countries. Nonetheless, solar power generation has an intermittent nature like wind power generation. Thus, the variation in solar power forecasts is another source of uncertainty in wind and solar

integrated hybrid power systems. However, modelling solar uncertainty is not as straightforward as in wind power and load demand forecasts. The reason is that solar power forecast errors follow a bimodal distribution. On the contrary, wind power and load demand forecast errors follow a unimodal distribution. Hence, integrating solar power generation to the proposed models is a challenging but a promising research area.

- To reduce electricity prices by increasing the competition and the service quality among power generation companies; electricity markets have started to be deregulated in several developed countries. In the deregulated electricity market, power generation companies have a freedom in such a way that they are not required to satisfy the whole energy demand of their customers. That is, they can meet some portion of the demand which maximizes their profit. This relaxation introduces a new problem called as Profit Based UCP (PBUCP) in which the objective changes from cost minimization to profit maximization. The PBUC will bring another source of uncertainty arising from the variabilities in forecasted energy price (spot price) profiles. Our approach can be extended to solve this new variant of the UCP by relaxing load demand constraints and developing effective spot price forecasting methods or employing stochastic programming techniques for different energy price scenarios.
- The proposed EENS approximations can be improved even further by representing the relationship between EENS and the committed capacity as a combination of a negative definite quadratic equation and an absolute sine function, or stepwise functions ignoring the curvatures in the original relationship by introducing breaks to the approximations. These will require an additional set of experiments. By doing so, the quality of the approximations will increase but the models will become more complex to solve since these modifications will cause nonconvex feasible regions.

- In some countries, emissions are also controlled via zonal emission limits in addition to emission trading and taxing mechanisms. In the proposed approach in Chapter 5, only the latter is modelled. Those zonal emission limits can easily be added to the proposed approach as additional constraints limiting total emissions of conventional generating units in those specific zones

In real life, the proposed approaches can be used for the following purposes:

- Power generation companies can obtain efficient commitment and dispatching schedules, and adjust them in a rolling horizon basis in case of unexpected deviations from the schedules that are originally set.
- Power generation companies can also make effective What-if analyses for the parameters that are critical to their operations planning.
- Policymakers can develop effective policies to reduce both greenhouse gas and air pollutant emissions of conventional power plants.
- Both policymakers and power generation companies can quantify supply/demand uncertainty in wind integrated hybrid power systems, socioeconomic value of EENS, rippling effects in conventional power plant efficiencies, importance of Emission Control Technologies and impacts of Emission Trading and Taxing Mechanisms.

REFERENCES

Ahmadian, A., Sedghi, M. and Golkar, M. A. (2014). Solving Multiobjective Unit Commitment Problem to Minimize Operation Cost and Emissions Using HBMO Algorithm. International Conference on Machine Learning, Electrical and Mechanical Engineering, Dubai, UAE.

Alabedin, A. M. Z., El-Saadany, E. F. and Salama, M. M. A. (2012). Generation Scheduling in Microgrids under Uncertainties in Power Generation. IEEE Electrical Power and Energy Conference, London, ON, Canada.

Alham, M. H., Elshahed, M., Ibrahim, D. K. and El Zahab, E. E. D. A. (2016). A Dynamic Economic Emission Dispatch Considering Wind Power Uncertainty Incorporating Energy Storage System and Demand Side Management. Renewable Energy, 96, 800-811.

Álvarez-Miranda, E., Campos-Valdés, C. and Rahmann, C. (2015). Two-Stage Robust UC Including a Novel Scenario-Based Uncertainty Model for Wind Power Applications. Energy Conversion and Management, 101, 94-105.

Amjady, N. and Shirzadi, A. (2009). Unit Commitment Using a New Integer Coded Genetic Algorithm. European Transactions on Electrical Power, 19, 1161-1176.

Anita, J. M. and Raglend, I. J. (2013). Solution of Emission Constrained Unit Commitment Problem Using Shuffled Frog Leaping Algorithm. International Conference on Circuits, Power and Computing Technologies, Nagercoil, India.

Azizipanah-Abarghooee, R., Niknam, T., Roosta, A., Malekpour, A. R. and Zare, M. (2011). Probabilistic Multiobjective Wind-Thermal Economic Emission Dispatch Based on Point Estimated Method. Energy, 37, 322-335.

Bendotti, P., Fouilhoux, P. and Rottner, C. (2017). On the Complexity of the Unit Commitment Problem, Annals of Operations Research, 274, 119-130.

Billinton, R. and Allan, R. N (1996). Reliability evaluation of power systems. Plenum Press, 2nd Ed. New York, London.

Bofinger, S., Luig, A., and Beyer, H. G. (2002). Qualification of Wind Power Forecasts. Proceedings of Global Wind Power Conference. Poster P_GWP093 on the Global Windpower Conference and Exhibition, Paris, France.

Bouffard, F. and Galiana, F. D. (2008). Stochastic Security for Operations Planning with Significant Wind Power Generation. IEEE Transactions on Power Systems, 23 (2), 306-316.

Bradley, S. P., Hax, A. C. and Magnanti, T. L. (1977). Applied Mathematical Programming. Addison Wesley.

Bukhari, S. B. A., Ahmad, A., Raza, S. A., and Sıddıque, M. N. (2016). A Ring Crossover Genetic Algorithm for the Unit Commitment Problem. Turkish Journal of Electrical Engineering & Computer Sciences, 24, 3862-3876.

California Air Resources Board. (2012). How Does the Cap-And-Trade Program Work? Cap-and-Trade Regulation Instructional Guidance. Retrieved from https://ww3.arb.ca.gov/cc/capandtrade/guidance/chapter1.pdf

California Air Resources Board. (2016). AB 32 Scoping Plan. Retrieved from https://ww3.arb.ca.gov/cc/scopingplan/scopingplan.htm

Catalão, J. P. S., Mariano, S. J. P. S., Mendes, V. M. F. and Ferreira, L. A. F. M. (2010). A Practical Approach for Profit-Based Unit Commitment with Emission Limitations. Electrical Power and Energy Systems, 32, 218-224.

Chaiyabut, N. and Damrongkulkumjorn, P. (2014). Optimal Spinning Reserve for Wind Power Uncertainty by Unit Commitment with EENS Constraint. Innovative Smart Grid Technologies, Washington, DC, USA.

Che, P. and Shi, G. (2014). An MILP Approach for a Profit-Based Unit Commitment Problem with Emissions Penalty. The 26th Chinese Control and Decision Conference, Changsha, China.

Chen, H., Kong, Y., Li, G. and Bai, L. (2016). Conditional Value-at-Risk-Based Optimal Spinning Reserve for Wind Integrated Power System. International Transactions on Electrical Energy Systems, 26 (8).

Chen, J., Wu, W., Zhang, B., Wang, B. and Guo, Q. (2013). A Spinning Reserve Allocation Method for Power Generation Dispatch Accommodating Large-Scale Wind Power Integration. Energies, 6, 5357-5381.

Chinnadurrai, C. L. and Victoire, T. A. A. (2019). Enhanced Multi-Objective Crisscross Optimization for Dynamic Economic Emission Dispatch Considering Demand Response and Wind Power Uncertainty. Soft Computing, 24, 9021-9038.

Cobos, N. G., Arroyo, J. M., Alguacil, N. and Street, A. (2018). Robust Energy and Reserve Scheduling under Wind Uncertainty Considering Fast-Acting Generators. IEEE Transactions on Sustainable Energy, 10 (4), 2142-2151.

Cui, N., Zhang, Z., Liu, W., Zhang, Y. and Li, Q. (2015). Probabilistic Spinning Reserve Model of Power System Containing Wind. Applied Mechanics and Materials, 1238-1243.

Damousis, I. G., Bakirtzis, A. G. and Dokopoulos, P. S. (2004). A Solution to the Unit Commitment Problem Using Integer-Coded Genetic Algorithm. IEEE Transactions on Power Systems, 19 (2), 1165–1172.

Datta, D. (2013). Unit Commitment Problem with Ramp Rate Constraint Using a Binary-Real-Coded Genetic Algorithm. Applied Soft Computing, 13 (9), 3873-3883.

Decker, G. L. and Brooks, A. D. (1958). Valve Point Loading of Turbines. IEEE Transactions of the American Institute of Electrical Engineers. Part III: Power Apparatus and Systems, 77 (3), 481-484.

Denny, E. and O'Malley, M. (2006). Wind Generation, Power System Operation, and Emissions Reduction. IEEE Transactions on Power Systems, 21 (1), 341-347.

Di, X., Nie, Z., Yuan, B. and Zu, T. (2007). Life Cycle Inventory for Electricity Generation in China. The International Journal of Life Cycle Assessment, 12 (4), 217-224.

Dudek, G. (2013). Genetic Algorithm with Binary Representation of Generating Unit Start-Up and Shut-Down Times for the Unit Commitment Problem. Expert Systems with Applications, 40 (15), 6080-6086.

Effatnejad, R. and Rouhi, F. (2015). Unit Commitment in Power System t by Combination of Dynamic Programming (DP), Genetic Algorithm (GA) and Particle Swarm Optimization (PSO). Indian Journal of Science and Technology, 8 (2), 134-141.

European Commission. (2012). Accreditation and Validation Regulation: Commission Regulation No. 600/2012. Directive 2003/87/EC of the European Parliament and of the Council.

European Commission. (2012). Monitoring and Reporting Regulation No 601/2012. Directive 2003/87/EC of the European Parliament and of the Council.

European Commission. (2014). Commission Regulation No 176/2014. Directive 96/61/EC of the European Parliament and of the Council.

European Commission. (2014). 2030 Climate & Energy Framework. Retrieved from https://ec.europa.eu/clima/policies/strategies/2030_en

European Commission. (2018). Revision for Phase 4 (2021-2030). Retrieved from https://ec.europa.eu/clima/policies/ets/revision_en#tab-0-0

European Commission. (n.d.). Emissions Cap and Allowances. Retrieved from https://ec.europa.eu/clima/policies/ets/cap_en

European Commission. (n.d.). EU Emissions Trading System (EU ETS). Retrieved from https://ec.europa.eu/clima/policies/ets_en

European Commission. (n.d.). Free Allocation. Retrieved from https://ec.europa.eu/clima/policies/ets/allowances_en

European Commission. (n.d.). Market Stability Reserve. Retrieved from https://ec.europa.eu/clima/policies/ets/reform_en

European Commission. (n.d.). Phases 1 and 2 (2005-2012). Retrieved from https://ec.europa.eu/clima/policies/ets_en

Fabbri, A., GomezSanRoman, T., RivierAbbad, J., and MendezQuezada, V. H. (2005). Assessment of The Cost Associated with Wind Generation Prediction Errors in A Liberalized Electricity Market, IEEE Transactions on Power Systems, 20 (3), 1440-1446.

Farag, M. A., El-Shorbagy, M. A., El-Desoky, I. M., El-Sawy, A. A. and Mousa, A. A. (2015). Binary-Real Coded Genetic Algorithm Based k-Means Clustering for Unit Commitment Problem. Applied Mathematics, 6, 1873-1890.

Franz, A., Rieck, J. and Zimmermann, J. (2018). Fix-and-Optimize Procedures for Solving the Long-Term Unit Commitment Problem with Pumped Storages. Annals of Operations Research, 274, 241-265.

Franz, A., Rieck, J. and Zimmermann, J. (2020). A Long-Term Unit Commitment Problem with Hydrothermal Coordination for Economic and Emission Control in Large-Scale Electricity Systems. OR Spectrum, 42, 235-259.

Geng, Z, Chen, Q., Chen, X., Xia, Q., Li, J., Wang, Y. and Chen, Y. (2015). Environmental Economic Dispatch towards Multiple Emissions Control Coordination Considering a Variety of Clean Generation Technologies. IEEE Power & Energy Society General Meeting, Denver, CO, USA.

Geng, Z., Chen, Q., Xia, Q., Kirschen, D. S., and Kang, C. (2017). Environmental Generation Scheduling Considering Air Pollution Control Technologies and Weather Effects. IEEE Transactions on Power Systems, 32 (1), 127-136.

Geng, Z., Conejo, A. J., Chen, Q. and Kang, C. (2018). Power Generation Scheduling Considering Stochastic Emission Limits. Electrical Power and Energy Systems, 95, 374-383.

Ghadi, M. J., Karin, A. I., Baghramian, A. and Imani, M. H. (2016). Optimal Power Scheduling of Thermal Units Considering Emission Constraint for Gencos' Profit Maximization. Electrical Power and Energy Systems, 82, 124-135.

Gjengedal, T. (1996). Emission Constrained Unit-Commitment (ECUC). IEEE Transactions on Energy Conversion, 11 (1), 132-138.

Govardhan, M. (2016). Joint Energy and Spinning Reserve Scheduling Integrating Uncertain Wind Power. IEEE Students' Conference on Electrical, Electronics and Computer Science, Bhopal, India.

Gross, G. and Galiana, F. D. (1987). Short-Term Load Forecasting. Proceedings of the IEEE, 75 (12),1558-1573.

Guo, D., Yu, J. and Ban, M. (2018). Day-Ahead Scheduling of Thermal Generation under Air Quality Ecological Compensation System Considering Wind Power Uncertainty. 2nd IEEE Conference on Energy Internet and Energy System Integration, Beijing, China.

Haddadiana, G., Khalilia, N., Khodayarb, M. and Shahidehpour, M. (2015). Optimal Scheduling of Distributed Battery Storage for Enhancing the Security and the Economics of Electric Power Systems with Emission Constraints. Electric Power Systems Research, 124, 152-159.

Haddi, S. and Bouktir, T. (2015). Economic/Emission Dispatch Including Wind Power Using ABC-Weighted-Sum. International Journal of Engineering and Technical Research, 3 (10), 61-66.

Hedayati-Mehdiabadi, M., Hedman, K. W. and Zhang, J. (2017). Reserve Policy Optimization for Scheduling Wind Energy and Reserve. IEEE Transactions on Power Systems, 33 (1), 19-31.

Hetzer, J., Yu, D. C. and Bhattarai, K. (2008). An Economic Dispatch Model Incorporating Wind Power. IEEE Transactions on Energy Conversion, 23 (2), 603-611.

Hu, F., Hughes, K. J., Ma, L. and Pourkashanian, M. (2017). Combined Economic and Emission Dispatch Considering Conventional and Wind Power Generating Units. International Transactions on Electrical Energy Systems, 27 (4), DOI: 10.1002/etep.2424.

Huaman, R. N. E. and Lourenco, S. (2015). A Review on: CO_2 Capture Technology on Fossil Fuel Power Plant. Journal of Fundamentals of Renewable Energy and Applications, 5 (3), 1-11.

Intergovernmental Panel on Climate Change. (2005). Carbon Dioxide Capture and Storage: Summary for Policymakers. IPCC Special Report.

Intergovernmental Panel on Climate Change. (2005). Carbon Dioxide Capture and Storage: Technical Summary. IPCC Special Report.

International Carbon Action Partnership. (2020). ETS Detailed Information: Turkey. Retrieved from https://icapcarbonaction.com/en/?option=com_etsmap&task=export&format=pdf&layout=list&systems[]=66

International Carbon Action Partnership. (2020). China - Beijing pilot ETS. Retrieved from https://icapcarbonaction.com/en/?option=com_etsmap&task=export&format=pdf&layout=list&systems[]=53

International Carbon Action Partnership. (2020). China - Chongqing pilot ETS. Retrieved from

https://icapcarbonaction.com/en/?option=com_etsmap&task=export&format=pdf&layout=list&systems[]=56

International Carbon Action Partnership. (2020). China - Fujian pilot ETS. Retrieved from https://icapcarbonaction.com/en/?option=com_etsmap&task=export&format=pdf&layout=list&systems[]=87

International Carbon Action Partnership. (2020). China - Guangdong pilot ETS. Retrieved from https://icapcarbonaction.com/en/?option=com_etsmap&task=export&format=pdf&layout=list&systems[]=57

International Carbon Action Partnership. (2020). China - Hubei pilot ETS. Retrieved from https://icapcarbonaction.com/en/?option=com_etsmap&task=export&format=pdf&layout=list&systems[]=58

International Carbon Action Partnership. (2020). China National ETS. Retrieved from https://icapcarbonaction.com/en/?option=com_etsmap&task=export&format=pdf&layout=list&systems[]=55

International Carbon Action Partnership. (2020). China - Shanghai pilot ETS. Retrieved from https://icapcarbonaction.com/en/?option=com_etsmap&task=export&format=pdf&layout=list&systems[]=53

International Carbon Action Partnership. (2020). China - Shenzhen pilot ETS. Retrieved from https://icapcarbonaction.com/en/?option=com_etsmap&task=export&format=pdf&layout=list&systems[]=63

International Carbon Action Partnership. (2020). China - Tianjin pilot ETS. Retrieved from https://icapcarbonaction.com/en/?option=com_etsmap&task=export&format=pdf&layout=list&systems[]=65

International Carbon Action Partnership. (2020). USA - California Cap-and-Trade Program. Retrieved from https://icapcarbonaction.com/en/?option=com_etsmap&task=export&format=pdf&layout=list&systems[]=45

Jacobson, M. Z. and Delucchi, M. A. (2011). Providing All Global Energy with Wind, Water, and Solar Power, Part I: Technologies, Energy Resources, Quantities and Areas of Infrastructure, and Materials. Energy Policy, 39, 1154-1169.

Jacobson, M. Z., Delucchi, M. A., Cameron, M. A. and Mathiesen, B. V. (2018). Matching Demand with Supply at Low Cost in 139 Countries among 20 World Regions with 100% Intermittent Wind, Water, and Sunlight (WWS) for All Purposes. Renewable Energy, 123, 236-248.

Jacobson, M. Z., Delucchi, M. A., Cameron, M. A., Coughlin, S. J., Hay, C. A., Manogaran, I. P., Shu Y. and Von Krauland, A. K. (2019). Impacts of Green New Deal Energy Plans on Grid Stability, Costs, Jobs, Health, and Climate in 143 Countries. One Earth, 1 (4), 449-463.

Jadhav, H. T. and Roy, R. (2013). Gbest Guided Artificial Bee Colony Algorithm for Environmental/Economic Dispatch Considering Wind Power. Expert Systems with Applications, 40, 6385-6399.

Kåberger, T. (2018). Progress of Renewable Electricity Replacing Fossil Fuels. Global Energy Interconnection, 1 (1), 48-52.

Kariuki, K. K. and Allan, R. N. (1996). Evaluation of Reliability Worth and Value of Lost Load. IEE Proceedings-Generation, Transmission and Distribution, 143 (2), 171-180.

Kazarlis, S. A., Bakirtzis, A. G., Petridis, V. (1996). A Genetic Algorithm Solution to the Unit Commitment Problem. IEEE Transactions on Power Systems, 11(1), 83-92.

Khazali, A. and Kalantar, M. (2015). Spinning Reserve Quantification by A Stochastic–Probabilistic Scheme for Smart Power Systems with High Wind Penetration. Energy Conversion and Management, 96, 242-257.

Kuo, C. (2009). Generation Dispatch Under Large Penetration of Wind Energy Considering Emission and Economy. Energy Conversion and Management, 51, 89-97.

Kyu-Hyung, J. and Mun-Kyeom, K. (2018). Improved Genetic Algorithm-Based Unit Commitment Considering Uncertainty Integration Method. Energies, 11 (6), 1387-1405.

Laia, R., Pousinho, H. M. I., Melicio, R., Collares-Pereira, M. and Mendes, V. M. F. (2014). Spinning Reserve and Emission Unit Commitment through Stochastic Optimization. International Symposium on Power Electronics, Electrical Drives, Automation and Motion, Ischia, Italy.

Lazo, B. P. and Cartes, J. S. (2011). A Deterministic Annular Crossover Genetic Algorithm Optimisation for the Unit Commitment Problem. Expert Systems with Applications, 38, 6523-6529.

Lee, T. Y. (2007). Optimal Spinning Reserve for a Wind-Thermal Power System Using EIPSO. IEEE Transactions on Power Systems, 22 (4), 1612-1621.

Li, Y., Pedroni, N., and Zio, E. (2013). A Memetic Evolutionary Multi-Objective Optimization Method for Environmental Power Unit Commitment. IEEE Transactions on Power Systems, 28 (3), 2660-2669.

Liao, G. (2011). A Novel Evolutionary Algorithm for Dynamic Economic Dispatch with Energy Saving and Emission Reduction in Power System Integrated Wind Power. Energy, 36, 1018-1029.

Lin, J., Cheng, L., Chang, Y., Zhang, K., Shu, B. and Liu, G. (2014). Reliability Based Power Systems Planning and Operation with Wind Power Integration: A Review to Models, Algorithms and Applications. Renewable and Sustainable Energy Reviews, 31, 921-934.

Liu, G. and Tomsovic, K., (2012). Quantifying Spinning Reserve in Systems with Significant Wind Power Penetration. IEEE Transactions on Power Systems, 27 (4), 2385-2393.

Liu, S., Chevallier, J. and Zhu, B. (2016). Self-Scheduling of a Power Generating Company: Carbon Tax Considerations. Computers & Operations Research, 66, 384-392.

Liu, X. (2012). Optimization of A Combined Heat and Power System with Wind Turbines. Electrical Power and Energy Systems, 43, 1421-1426.

Liu, X. and Xu, W. (2010). Minimum Emission Dispatch Constrained by Stochastic Wind Power Availability and Cost. IEEE Transactions on Power Systems, 25 (3), 1705-1713.

Madraswala, H. S. and Deshpande, A. S. (2016). Genetic Algorithm Solution to Unit Commitment Problem. IEEE 1st International Conference on Power Electronics, Intelligent Control and Energy Systems, Delhi, India.

Majanne, Y., Korpela, T. and Uotila, T. (2014). EU Emission Trading Related CO2 Monitoring in Power Plants. Proceedings of the 19th World Congress the International Federation of Automatic Control, 1361-1366.

Mallipeddi, R. and Suganthan, P. N. (2014). Unit Commitment – A Survey and Comparison of Conventional and Nature Inspired Algorithms. International Journal of Bio-Inspired Computation, 6 (2), 71-90.

Mantawy, A. H., Abdel-Magid, Y. L. and Selim, S. Z. (1997). A New Genetic Algorithm Approach for Unit Commitment Problem. Genetic Algorithms in Engineering Systems: Innovations and Applications, 446, 215-220.

Marchetti, C. (1977). On geo engineering and the CO_2 problem. Climatic Change, 1, 59-68.

Marrouchi, S., Hessine, M. B. and Chebbi, S. (2018). Combined Use of an Improved PSO and GA to Solve the Unit Commitment Problem. 15th IEEE International Multi-Conference on Systems, Signals & Devices, Hammamet, Tunisia.

Marwali, M. K. C. and Shahidehpour, S. M. (1999). Long-Term Transmission and Generation Maintenance Scheduling with Network, Fuel and Emission Constraints. IEEE Transactions on Power Systems, 14 (3), 1160-1165.

Moazzem, S., Rasul, M. G. and Khan, M. M. K. (2012). A Review on Technologies for Reducing CO_2 Emission from Coal Fired Power Plants. InTech Thermal Power Plants, 228-254.

Moretti, A. L. and Jones, C. S. (2012). Advanced Emissions Control Technologies for Coal-Fired Power Plants. Babcock & Wilcox Power Generation Group Inc Technical Paper BR-1886.

Nanda, J., Hari, L. and Kothari, M. L. (1994). Economic Emission Load Dispatch with Line Flow Constraints Using A Classical Technique. IEE Proceedings-Generation, Transmission and Distribution, 141 (1), 1-10.

Navin, N. K. and Sharma, R. (2016). A Modified Differential Evolution Approach to Emission Constrained Thermal Unit Commitment Problem. 2016 IEEE 1st International Conference on Power Electronics, Intelligent Control and Energy Systems, Delhi, India.

Nazari, M. E., Ardehali, M. M. and Jafari, S. (2010). Pumped-Storage Unit Commitment with Considerations for Energy Demand, Economics, and Environmental Constraints. Energy, 35, 4092-4101.

Negi, D., Naresh, R. and Singhal, P. K. (2016). Improved Binary PSO for Wind-Thermal Unit Commitment Considering Wind Power Uncertainity and Emission. IEEE 1st International Conference on Power Electronics, Intelligent Control and Energy Systems, Delhi, India.

Nolan, P. S. (2000). Flue Gas Desulfurization Technologies for Coal-Fired Power Plants. Babcock & Wilcox Power Generation Group Inc Coal-Tech 2000 International Conference BR-1709.

Ohkubo, Y. (2005). Low-NO_x Combustion Technology. R&D Review of Toyota CRDL, 41 (1), 12-23.

Olamaei, J., Nazari, M. E. and Bahravar, S. (2018). Economic Environmental Unit Commitment for Integrated CCHP-Thermal-Heat Only System with Considerations for Valve-Point Effect Based on a Heuristic Optimization Algorithm, Energy, 159, 737-750.

Organization for Economic Co-operation and Development. (2017). Report on OECD Project on Best Available Techniques for Preventing and Controlling Industrial Chemical Pollution. OECD Environment, Health and Safety Publications Series on Risk Management, 40, 15-75.

Ortega-Vazquez, M. A., Kirschen, D. S. and Pudjianto D. (2006). Optimising the Scheduling of Spinning Reserve Considering the Cost of Interruptions. IEEE Proceedings-Generation, Transmission and Distribution, 153 (5), 570-575.

Ortega-Vazquez, M. A. and Kirschen, D. S. (2007). Optimizing the Spinning Reserve Requirements Using a Cost/Benefit Analysis. IEEE Transactions on Power Systems, 22 (1), 24-33.

Ortega-Vazquez, M. A. and Kirschen, D. S. (2009). Estimating the Spinning Reserve Requirements in Systems with Significant Wind Power Generation Penetration. IEEE Transactions on Power Systems, 24 (1), 114-124.

Pappala, V. S., Erlich, I. and Singh, S. N. (2008). Unit Commitment under Wind Power and Demand Uncertainties. Joint International Conference on Power System Technology and IEEE Power India Conference, New Delhi, India.

Piperagkas, G. S., Anastasiadis, A. G. and Hatziargyriou, N. D. (2010). Stochastic PSO-Based Heat and Power Dispatch Under Environmental Constraints Incorporating CHP and Wind Power Units. Electric Power Systems Research, 81, 209-218.

Potomac Economics. (2020). Annual Report on the Market for RGGI CO_2 Allowances: 2019.

Prada, J. F. (1999). The Value of Reliability in Power Systems-Pricing Operating Reserves. Massachusetts Institute of Technology Energy Laboratory.

Qian, T., Wang, X., Zhang, W., Wang, J., Zhou, B. and Lu, S. (2016). Spinning Reserve Optimization with Wind Power Output and Electric Vehicles Considering the Operator's Risk Preference. IEEE Conference on Energy Internet and Energy System Integration, Beijing, China.

Qu, B. Y., Liang, J. J., Zhu, Y. S. and Suganthan, P. N. (2017). Solving Dynamic Economic Emission Dispatch Problem Considering Wind Power by Multi-Objective Differential Evolution with Ensemble of Selection Method. Natural Computing, 18, 695-703.

Qu, B. Y., Liang, J. J., Zhu, Y. S., Wang, Z. Y. and Suganthan, P. N. (2016). Economic Emission Dispatch Problems with Stochastic Wind Power Using Summation Based Multi-Objective Evolutionary Algorithm. Information Sciences, 351, 48-66.

Raglend, I. J. and Padhy, N. P. (2006). Solutions to Practical Unit Commitment Problems with Operational, Power Flow and Environmental Constraints, Montreal, Que., Canada.

Ramanathan, R. (1994). Emission Constrained Economic Dispatch. IEEE Transactions on Power Systems, 9 (4), 1994-2000.

Reddy, G. V. S., Ganesh, V. and Rao, C. S. (2019). Cost Reduction in Clustering Based Unit Commitment Employing Hybrid Genetic-Simulated Annealing Technique. Journal of Electrical Engineering & Technology, 14, 27–35.

Reddy, S. S., Panigrahi, B. K., Kundu, R., Mukherjee, R., Debchoudhury, S. (2013). Energy and spinning reserve scheduling for a wind-thermal power system using CMA-ES with mean learning technique. Electrical Power and Energy Systems, 53, 113-122.

Regional Greenhouse Gas Initiative. (2009). The Regional Greenhouse Gas Initiative: An Initiative of the New England and Mid-Atlantic States of the US.

Ross, S. M. (2007). Introduction to Probability Models. Elsevier, 9th Ed. New York.

Roque, L. A. C. (2014). Optimization Methods for the Unit Commitment Problem in Electric Power Systems. Doctoral thesis, University of Porto.

Roque, L. A. C., Fontes, D. B. M. M. and Fontes, F. A. C. C. (2014). A Hybrid Biased Random Key Genetic Algorithm Approach for the Unit Commitment Problem. Journal of Combinatorial Optimization, 28 (1), 140-166.

Roy, P. K. and Hazra, S. (2014). Economic Emission Dispatch for Wind–Fossil-Fuel-Based Power System Using Chemical Reaction Optimisation. International Transactions on Electrical Energy Systems, 25 (12), 3248-3274.

Rudolf, A. and Bayrleithner, R. (1999). A Genetic Algorithm for Solving the Unit Commitment Problem of a Hydro-Thermal Power System. IEEE Transactions on Power Systems, 14 (4), 1460-1468.

Saber, N. A., Salimi, M. and Mirabbasi, D. (2016). A Priority List Based Approach for Solving Thermal Unit Commitment Problem with Novel Hybrid Genetic-Imperialist Competitive Algorithm. Energy, 117, 272-280.

Salimian, M. R. and Ameli, M. T. (2015). HGAPSO based Method for Solving Unit Commitment Problem. International Electrical Engineering Journal, 6 (3), 1834-1840.

Saravanan, B. and Vasudevan, E. R. (2014). Emission Constrained Unit Commitment Problem Solution Using Invasive Weed Optimization Algorithm. 2014 International Conference on Advances in Electrical Engineering, Vellore, India.

Sen, T. and Mathur, H. D. (2016). A New Approach to Solve Economic Dispatch Problem Using A Hybrid ACO–ABC–HS Optimization Algorithm. Electrical Power and Energy Systems, 78, 735-744.

Senjyu, T., Yamashiro, H., Uezato, K. and Funabashi, T. (2002). A Unit Commitment Problem by Using Genetic Algorithm Based on Unit Characteristic Classification. IEEE Power Engineering Society Winter Meeting, Conference Proceedings, New York, USA.

Shahzad Baig, K. and Yousaf, M. (2017). Coal Fired Power Plants: Emission Problems and Controlling Techniques. Journal of Earth Science & Climatic Change, 8 (7).

Shao, J., Sun, R., Wei, Z., Mei, J., Zhao, X., Dai, W. and Lu, Q. (2018). Risk Decision-making Model for Scheduling for Wind Integrated Power System Considering Optimal Configuration of Reserve Capacity. International Conference on Power System Technology, Guangzhou, China.

Singhal, P. K., Naresh, R., Sharma, V. and Kumar, G. (2014). Solution of Unit Commitment Problem Using Enhanced Genetic Algorithm. Eighteenth National Power Systems Conference, Guwahati, India.

Söder, L. (1993). Reserve Margin Planning in a Wind-Hydro-Thermal Power System. IEEE Transactions on Power Systems, 8 (2), 564-571.

Sundaram, C. S., Sudhakaran, M. and Raj, P. A. (2017). Tabu Search-Enhanced Artificial Bee Colony Algorithm to Solve Profit-Based Unit Commitment Problem with Emission Limitations in Deregulated Electricity Market, International Journal of Metaheuristic, 6 (1/2), 107-132.

Sundararajan, D., Subramanian, B., Subramanian, K. and Krishnan, M. (2013). Generation Scheduling problem by Intelligent Genetic Algorithm. Computers and Electrical Engineering 39, 79-88.

Swarup, K. S. and Yamashiro, S. (2003). A Genetic Algorithm Approach to Generator Unit Commitment. Electrical Power and Energy Systems, 25, 679-687.

Tang, L. and Che, P. (2013). Generation Scheduling Under a CO_2 Emission Reduction Policy in the Deregulated Market, IEEE Transactions on Engineering Management, 60 (2), 386-397.

Trivedi, A., Srinivasan, D., Biswas, S. and Reindl, T. (2016). A Genetic Algorithm – Differential Evolution Based Hybrid Framework: Case Study on Unit Commitment Scheduling Problem. Information Sciences, 354, 275-300.

Trivedi, A., Srinivasan, D., Pal, K. and Reindl, T. (2016). A Multiobjective Evolutionary Algorithm Based on Decomposition for Unit Commitment Problem with Significant Wind Penetration. IEEE Congress on Evolutionary Computation, Vancouver, BC, Canada.

Tsalavoutis, V., Vrionis, C. and Tolis, A. (2019). A Hybrid Multi-Objective Evolutionary Algorithm for Economic-Environmental Generation Scheduling. Genetic and Evolutionary Computation Conference, Prague, Czech Republic.

Ummels, C. B., Gibescu, M., Pelgrum, E., Kling, W. L. and Brand, A.J. (2007). Impacts of Wind Power on Thermal Generation Unit Commitment and Dispatch. IEEE Transactions on Energy Conversion, 22 (1), 44-51.

United Nations Framework Convention on Climate Change. (1997). Kyoto Protocol - Targets for the first commitment period. Retrieved from https://unfccc.int/process-and-meetings/the-kyoto-protocol/what-is-the-kyoto-protocol/kyoto-protocol-targets-for-the-first-commitment-period

United Nations Framework Convention on Climate Change. (2015). The Paris Agreement. Retrieved from https://unfccc.int/process-and-meetings/the-paris-agreement/the-paris-agreement

Valenzuela, J. and Smith, A. E. (2002). A Seeded Memetic Algorithm for Large Unit Commitment Problems. Journal of Heuristics, 8 (2), 173-195.

Van Dinter, J., Rebennack, S., Kallrath, J., Denholm, P. and Newman, A. (2012). The Unit Commitment Model with Concave Emissions Costs: A Hybrid Benders' Decomposition with Nonconvex Master Problems. Annals of Operations Research, 210, 361-386.

Verma, Y. P. and Kumar, A. (2011). Economic-Emission Unit Commitment Solution for Wind Integrated Hybrid System. International Journal of Energy Sector Management, 5 (2), 287-305.

Wang, B., Wang, S., Zhou, X. and Watada, J. (2016). Multi-Objective Unit Commitment with Wind Penetration and Emission Concerns under Stochastic and Fuzzy Uncertainties. Energy, 111, 18-31.

Wang, M., Bai, H., Zhou, M. and Wang, J. (2015). A Generation-Reserve Co-Optimization Dispatching Model for Wind Power Integrated Power System Based on Risk Reserve Constraints. International Conference on Renewable Power Generation, Beijing, China.

Wang, S. J., Shahidehpour, S. M., Kirschen, D. S., Mokhtari, S. and Irisarri, G. D. (1995). Short-term Generation Scheduling with Transmission and Environmental Constraints Using an Augmented Lagrangian Relaxation. IEEE Transactions on Power Systems, 10 (3), 1294-1301.

Wang, Z., Shen, C., Liu, F., Wu, X., Liu, C. and Gao, F. (2017). Chance-Constrained Economic Dispatch with Non-Gaussian Correlated Wind Power Uncertainty. IEEE Transactions on Power Systems, 32 (6), 4880-4893.

Wood, A. J. and Wollenberg, B. F. (1996). Power Generation, Operation, and Control. Wiley, 2nd Ed. New York.

World Health Organization. (2004) Health Aspects of Air Pollution Results from the Who Project: Systematic Review of Health Aspects of Air Pollution in Europe. WHO Press.

World Health Organization. (2005). WHO Air Quality Guidelines for Particulate Matter, Ozone, Nitrogen Dioxide and Sulfur Dioxide. WHO Press.

Wu, J., Zhang, B., Deng, W. and Zhang, K. (2015). Application of Cost-CVaR Model in Determining Optimal Spinning Reserve for Wind Power Penetrated System. Electrical Power and Energy Systems, 66, 110-115.

Wu, X., Zhang, B., Li, J., Luo, G. and Duan, Y. (2013). Solving Power System Unit Commitment with Wind Farms Using Multiobjective Quantum-Inspired Binary Particle Swarm Optimization. Journal of Renewable and Sustainable Energy, 5 (2), DOI: 10.1063/1.4798487.

Xia, S., Zhou, M., Li, G., Liu, Y., and Xiang, M. (2012). On Spinning Reserve Determination and Power Generation Dispatch Optimization for Wind Power Integration Systems. IEEE Power and Energy Society General Meeting, San Diego, CA, USA.

Xia, Y., Ghiocel, S. G., Dotta, D., Shawhan, D., Kindle, A., and Chow, J. H. (2013). A Simultaneous Perturbation Approach for Solving Economic Dispatch Problems with Emission, Storage, and Network Constraints. IEEE Transactions on Smart Grid, 4 (4), 2356-2363.

Xing, W. and Wu, F. F. (2002). Genetic Algorithm Based Unit Commitment with Energy Contracts. Electrical Power and Energy Systems, 24 (5), 329-336.

Yamashita, D., Niimura, T., Yokoyama, R. and Marmiroli, M. (2010). Trade-Off Analysis of CO_2 versus Cost by Multi-Objective Unit Commitment. IEEE PES General Meeting, Providence, RI, USA.

Yazandoost, A., Khazaei, P., Kamali, R. and Saadatian, S. (2018). An Efficient Scheduling for Security Constraint Unit Commitment Problem via Modified Genetic Algorithm Based on Multicellular Organisms Mechanisms. World Automation Congress, Stevenson, WA, USA.

Zhang, L., Yuan, Y. and Chen, B. (2017). Cost-Benefit Analysis Method for Optimizing Spinning Reserve Requirements with Consideration of Wind Power Generation under Carbon Trading Environment. IEEE International Conference on Energy Internet, Beijing, China.

Zhang, L., Yuan, Y., Yuan, X., Chen, B, Su, D. and Li, Q. (2017). Spinning Reserve Requirements Optimization Based on an Improved Multiscenario Risk Analysis Method. Hindawi Mathematical Problems in Engineering, 1-12.

Zhang, Y., Liu, K., Liao, X., Qin, L. and An, X. (2017). Stochastic Dynamic Economic Emission Dispatch with Unit Commitment Problem Considering Wind Power Integration. International Transactions on Electrical Energy Systems, 28 (1), DOI: 10.1002/etep.2472.

Zhang, Y., Yao, F., Iu, H. H. C., Fernando T. and Trinh H. (2014). Wind–Thermal Systems Operation Optimization Considering Emission Problem. Electrical Power and Energy Systems, 65, 238-245.

Zhang, N., Hu, Z., Dai, D., Dang, S., Yao, M. and Zhou, Y. (2016). Unit Commitment Model in Smart Grid Environment Considering Carbon Emissions Trading. IEEE Transactions on Smart Grid, 7 (1), 420-427.

Zhao, Y., Wang, S., Duan, L., Lei, Y., Cao, P. and Hao, J. (2008). Primary Air Pollutant Emissions of Coal-Fired Power Plants in China: Current Status and Future Prediction. Atmospheric Environment, 42, 8442-8452.

Zhou, W., Peng, Y. and Sun, H. (2010). Optimal Wind-Thermal Coordination Dispatch Based on Risk Reserve Constraints. European Transactions on Electrical Power, 21, 740-756.

Zobaa, A. F., Abdel Aleem, S. H. E., Abdelaziz, A. Y. (2018). Classical and Recent Aspects of Power System Optimization. Elsevier.

APPENDICES

A. Emission Trading Systems in EU, US, China and Turkey

European Union

For the first commitment period of the Kyoto Protocol, EU set a more ambitious target of 8% reduction from its 1990 level. To achieve this target, in 2005, European Commission set up EU Emission Trading System (EU ETS), which is the world's first international emissions trading system (European Commission, n.d.), to mitigate GHG emissions caused by different industrial sectors in EU. The EU ETS is based on the Cap & Trade mechanism.

The first ETS period was set for three years between 2005 and 2007. According to EC, in this period, only CO_2 emissions were monitored for power plants and energy-intensive industries. By considering EC guidelines, emission trading authorities in each EU country were responsible of setting the quotas for their country and issuing the emission allowances to power plants and energy-intensive industries. Since the first period was a trial phase and there was no reliable emission data related to those industries, total emission allowances were estimated and provided for free. Hence, the total amount of allowances issued was greater than the emission realizations at the end of 2007. In 2008, Iceland, Liechtenstein and Norway were joined to the initial 15 countries. The second ETS period was stricter in terms of emission reduction targets when compared to the ones in the previous period because it would cover the first commitment period of the Kyoto Protocol (2008-2012). First of all, EC reduced the caps by 6.5% from the ones in 2005 with respect to the emission data collected during the first ETS period. Most of the allocations of emission allowances to companies in the carbon market remained free in the second phase although the proportion of the free allocations was decreased by 10%. Furthermore, the fines imposed for non-compliance to total allowances were increased by €60 per tonnes of emission and became €100 per tonnes being subject to an increase in accordance

with the EU consumer price index (CPI). Due to the economic crisis in 2008, most of the energy-intensive plants were not fully used during that year, which leads to more excessive reduction in GHG emissions than anticipated and a large allowance surplus in the carbon economy. With the help of the economic downturn in 2008 and more binding rules on the EU ETS, EU achieved 11.7% of GHG emissions reduction at the end of the second ETS period. Besides, in 2014, EC implemented a back-loading system by making a new legislation on the surplus of allowances in the carbon market caused by 2008 economic downturn resulting in decrease in the carbon price (European Commission, 2014). As a result of lower carbon prices, the effectiveness of the EU ETS would have been weakened. To prevent this situation, according to this legislation, auctions of the significant amount of the allowance surplus had been postponed until 2019-2020, which was considered to be a short-term solution to prevent lower carbon prices in the third period. As a long-term solution, EC has also established a new mechanism called as Market Stability Reserve (MSR) in 2019. With this mechanism, the surplus of allowances will be transferred to the reserve operated by pre-defined rules. According to the allowances in circulation published by EC, this reserve will be used in the carbon economy.

In 2013, Croatia joined to the EU ETS. In the third period of ETS (2013-2020), EC has made more stringent modifications on monitoring and reporting of GHG emissions. To illustrate, EC has brought in *Accreditation and Verification Regulation* and *Monitoring and Reporting Regulation* in late 2012. These regulations specify requirements for risk and uncertainty assessment and expected data quality in continuous CO_2 monitoring system (European Commission, 2012). Moreover, EC has decided to centrally set EU-wide quota on emissions instead of quotas set by emission trading authorities of each member country. For the third ETS period, EC has also determined an annual linear reduction factor of 1.74% for the emission quota by considering EU-wide climate action targets for 2020, which are summarized below.

- 20% reduction in greenhouse gas emissions from the 1990 level
- 20% renewables integration to the EU's energy supply

- 20% improvement in energy efficiency

In addition to those regulations and modifications, auctioning has started to be the default allowance allocation method for the companies, especially in power generation sector since 2013, though some allowances have been freely provided for some member countries that joined in EU in 2004 so that they could deploy renewable energy technologies and emission reduction technologies like carbon capture and storage systems (CCSS) to modernize their power systems (European Commission, n.d.). With the auctioning method, the companies must buy their emission allowances at auctions, which have been held on a daily basis since 2012, where allowances other than freely allocated ones are auctioned. Besides, in late 2012, EC has declared that the ownership of allowances will be kept and monitored by the union registry. For this reason, the emission registries of each country were centralized into the union registry to ensure that all allowances issued under the EU ETS can be accounted accurately.

To comply with the national climate action plan under the Paris Agreement, EC has revised 2030 climate and energy framework consisting of EU-wide objectives and policies for the fourth ETS period (2021-2030). The key objectives are listed below.

- 40% reduction in greenhouse gas emissions from the 1990 level
- 32% renewables integration to the EU's energy supply
- 32.5% improvement in energy efficiency

To achieve those targets, EC is going to increase annual linear reduction factor of emission caps to 2.2%, which is going to be effective starting from 2021. EC will also provide several incentives to encourage the implementation of low-carbon technologies especially in power plants and energy-intensive industries. For this purpose, *Modernization Fund* will be provided to support modernization investments in power sectors of member countries in addition to the option of free allocation of allowances. *Innovation Fund* will be provided to support the use of innovative technologies in power plants and energy-intensive industries to lower GHG emissions.

United States

In the United States (US), GHG emissions have not been regulated on the federal level due to the legal oppositions against the GHG emission regulation plans of United States Environmental Protection Agency. Hence, State-Based Emissions Trading Programs have been undertaken by individual states and a group of states.

In 2009, the Regional Greenhouse Gas Initiative (RGGI), the first legally binding Cap & Trade mechanism in US, was adopted by the states of Connecticut, Delaware, Maine, Maryland, Massachusetts, New Hampshire, New York, Rhode Island and Vermont to reduce GHG emissions in power sector by encouraging power plants in the participating states to make investments on the development and the implementation of clean and renewable energy technologies (Regional Greenhouse Gas Initiative [RGGI], 2009). In 2020, New Jersey has also joined in RGGI.

The RGGI is based on the Cap & Trade mechanism. In 2009, RGGI has determined a region-wide cap for total CO_2 emissions for power plants in the participating states by taking regulations in the RGGI Model Rule into account. Each state has individual trading program that limits CO_2 emissions to comply with the region-wide cap. Electricity generating plants with the capacity of 25 MW and above must possess CO_2 allowances enough to cover their CO_2 emissions during each control period of RGGI. Those plants can sell their excess allowances or buy additional allowances through quarterly RGGI auctions. They can also trade allowances in the secondary CO_2 market during times between RGGI auctions so that they can protect themselves against the potential price volatility in the next auction. Similar to EU ETS, RGGI has revised its program by setting an annual linear reduction factor of 2.5% for emission caps, which will be effective between 2015 and 2020. According to 2019 RGGI Annual Report, RGGI is going to implement Emissions Containment Reserve (ECR) intending to decrease the surplus of allowances in the carbon economy in case of unexpected reductions in emission costs by enabling the participating states to withhold their allowances. The maximum amount of allowances to be withheld has been determined as 10% of the state's allowances in circulation. The ECR

mechanism resembles to MSR in the EU ETS. RGGI established CO_2 Allowance Tracking System (COATS) to monitor the ownerships of allowances, and to ensure that all allowances issued under the RGGI can accurately be accounted. As a result of the Cap & Trade system, at the end of 2020, RGGI expects to reduce CO_2 emissions of power plants in the region by 45% from the corresponding emission levels in 2005.

In 2013, the state of California has established its own GHG ETS which is the world's second largest international emissions trading system after the EU ETS (International Carbon Action Partnership [ICAP], 2020). The main objective is to combat with climate change by returning the level of GHG emissions to the 1990 level. Different from the RGGI, both power plants and industrial facilities, which account for 80% of GHG emissions in California, have to comply with the California Cap & Trade rules relying on the Mandatory Reporting of Greenhouse Gas Emissions Regulation (MRR). These rules are also valid for GHG emissions other than CO_2 emissions.

Emission allowances are allocated by means of free allocations and auctions. The former has been applied to electricity and natural gas utilities while the latter has been applied to large industrial facilities. The firms can also sell their excess allowances or buy additional allowances through auctions as in the RGGI and the EU ETS. Besides, California Air Resources Board (ARB) has also introduced another method for facilities to cover their emissions, which is known as ARB offset credit. An ARB offset credit is accounted for investments in GHG emission reduction techniques in order to support the developments and implementations of clean energy technologies. However, it can be used to satisfy up to 8% of a facility’s compliance obligation (California ARB, 2012). At the end of each compliance period, those firms have to hand over their allowances and offset credits sufficient to cover their GHG emissions during the compliance period. Facilities that do not comply with the requirements of the California Cap & Trade Program will be subject to stringent penalties. All trades are monitored and controlled by ARB centralized allowance tracking system.

By the end of 2020, California ARB has set a target of 15% reduction in GHG emissions from the level of the business-as-usual scenario. For this purpose, from 2015 to 2020, California ARB has determined an annual linear reduction factor of 3% for emission caps. For 2030, California ARB has set a more ambitious target of 40% reduction in GHG emissions from the 1990 level, which was legislated in 2016 by the California Legislature (California ARB, 2016).

China

Since mid-2013, China has initiated its operations to launch a national emission trading system by launching pilot ETSs in 8 regions. In 2013, Shenzhen pilot ETS, Shanghai pilot ETS, Beijing pilot ETS, Guangdong pilot ETS and Tianjin pilot ETS have started their operations. In 2014, two new pilot ETSs in Hubei and Chongqing have been launched. In 2016, Fujian pilot ETS has launched by the National Development and Reform Commission (NDRC). These pilots are differentiated by various aspects such as GHG emission coverage, sectors obliged to comply with ETS regulations, allowance allocation methods and penalties for the noncompliance.

Except Chongqing pilot ETS, only CO_2 emissions have been regulated by 7 ETS pilots. Chongqing pilot ETS has covered other GHGs as well. According to ICAP (2020), the sectors that comply with ETS regulations and their overall shares in GHG emissions are provided in Table A.1.

Table A.1. Sectors Regulated by China ETS Pilots

Sector	Shenzhen	Shanghai	Beijing	Guangdong	Tianjin	Hubei	Chongqing	Fujian
Power	x	x	x	x	x	x	x	x
Heat		x	x		x	x		
Water	x	x				x		
Gas	x				x			
Industry	x	x	x	x	x	x	x	x
Aviation		x		x	x			x
Transportation	x		x					
Total Share	**40%**	**57%**	**40%**	**60%**	**55%**	**45%**	**50%**	**60%**

The allowance allocation methods and their sector-by-sector implementations are varying in the ETS pilots as shown in Table A.2. In general, both free allocations and auctioning have been applied for allocating allowances to sectors.

Table A.2. Means of Allowance Allocations in China ETS Pilots

Method	Shenzhen	Shanghai	Beijing	Guangdong	Tianjin	Hubei	Chongqing	Fujian
Free Allocation	x	x	x	x	x	x	x	x
Auctioning		x	x	x	x	x	x	x

Moreover, as in California Cap & Trade Program, project-based carbon offset credits have also been used in the ETS pilots to account for investments in GHG emission reduction techniques in order to support the developments and implementations of clean energy technologies. Those credits are subject to maximum allowable limits on annual compliance obligation, which are demonstrated in Table A.3 (ICAP, 2020).

Table A.3. Maximum Allowable Limits on Annual Compliance Obligation in China ETS Pilots

	Shenzhen	Shanghai	Beijing	Guangdong	Tianjin	Hubei	Chongqing	Fujian
Quantitative Limit	10%	1%	5%	-	10%	10%	8%	5-10%

Furthermore, companies that do not comply with the annual requirements of the ETS pilots will be subject to financial and nonfinancial sanctions. In several pilot ETSs of China, financial penalties have been implemented for not complying with the regulations or not having enough allowances to cover their emissions during a year. The nonfinancial sanctions include investigation on the credit records, disqualification from special energy and emission related funds, bank loans and subsidy programs for several years, a reduction in the emission allowances for next years and publication on the internet. Sanction types used in the ETS pilots of China is demonstrated in Table A.4.

Table A.4. Types of Sanctions for the Noncompliance in China ETS Pilots

Type	Shenzhen	Shanghai	Beijing	Guangdong	Tianjin	Hubei	Chongqing	Fujian
Financial	x	x	x	x		x		x
Nonfinancial	x	x	x	x	x	x	x	x

By 2020, the China National ETS is expected to be partially operational for power sector and it will be regulated by Ministry for Ecology and Environment. In the short run, the existing pilot ETSs are going to work with the national ETS by being responsible of non-power sectors. In the long run, these pilots are going to be integrated into the national ETS. According to ICAP (2020), the environmental targets of the national ETS is listed below.

- 45% reduction in carbon intensity from the 2005 level by 2020
- 65% reduction in CO_2 emissions per unit of gross domestic product from the 2005 level by 2030

Turkey

Currently, Turkey does not have an emission trading system, but it is under consideration because of the environmental obligations of the Paris Agreement and the EU accession according to ICAP (2020). In 2012, Ministry of Environment and Urbanization has initiated a new regulatory framework to design a comprehensive and legally binding Monitoring, Reporting and Verification system for GHG emissions. For this reason, the ministry has been collaborating with the Partnership of Market Readiness (PMR) to improve the regulation on GHG emissions by making pilot studies in different sectors. In 2018, Turkish government has delivered its detailed national climate action plan to the Climate Change and Air Management Coordination Board under the Paris Agreement. According to this action plan, Turkey has set a target of 21% reduction in GHG emissions from the level of the business-as-usual scenario by the end of 2030. With additional financial support provided by the PMR in 2018, Ministry of Environment and Urbanization has also drafted legislation and developed its technical and institutional groundwork for a suitable pilot carbon economy (ICAP, 2020). The sectors that are considered for the

pilot consist of power plants with the capacity of 20 MW and above and several industrial facilities, which accounts for 69% of total GHG emissions of Turkey as shown in Figure A.1.

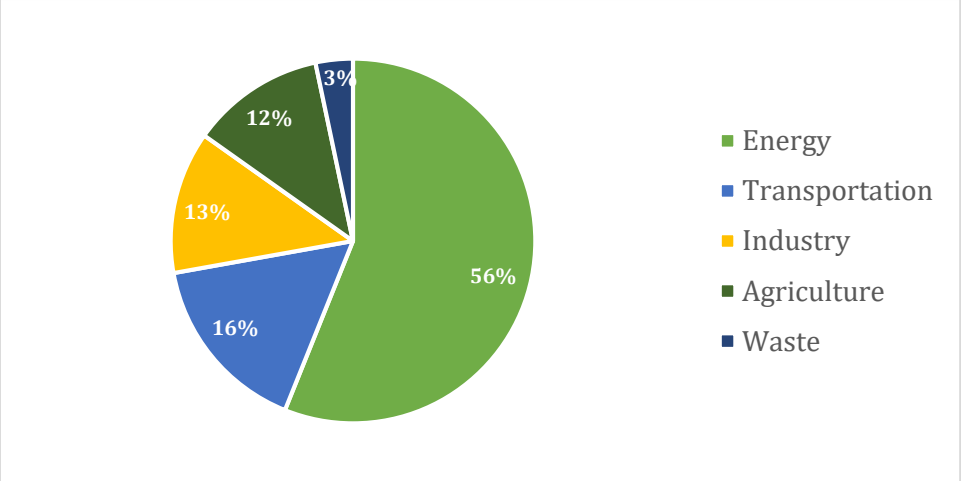

Figure A.1. Overall Share of Greenhouse Gas Emissions by Sectors in Turkey

B. Air Pollution Reduction Policies in EU, US and China

Air pollution prevention and reduction policies and practices in US, EU and China are summarized in Table B.1 (OECD, 2017). The summary consists of regulation enaction year, regulation type, types of emission standards and air pollutants, and sectors covered.

Table B.1. Legislations and Regulations against Air Pollution in United States, European Union and China

Country	Legislation and Regulation	Scope
United States	**Clean Air Act (CAA)** - Federal law enacted in 1963 - Major amendments in 1970, 1977 and 1990	- **Regulation type:** Command and Control - **Sectors covered:** Energy (power plants), energy-intensive industries, mineral and chemical industry, manufacturing, agriculture and livestock industry - **National ambient air quality standards (NAAQS)** **Air pollutants:** PM_x, NO_x, SO_2, CO, O_3 and heavy metals Sector and zone specific For new sources: based on Best Available Control Technology Lowest Achievable Emission Rate For existing sources: based on Reasonably available control technology Periodically reviewed in every 5 years
European Union	**Industrial Emissions Directive (IED)** - Revision of legislation on industrial emissions - Enacted in 2011	- **Regulation type:** Command and Control - **Sectors covered:** Energy (power plants), energy-intensive industries, mineral and chemical industry, manufacturing, agriculture and livestock industry - **Emission controls:** based on Environmental Quality Standards Best Available Technology Energy efficiency Total rated thermal input, capacity and zone specific

Table B.1 (continued)

	Eco-Management and Audit Scheme (EMAS) Regulation - Revision of previous EMAS regulations - Enacted in 2010	- **Regulation type:** Voluntary Evaluation of environmental performance of an organization - **Sectors covered:** Energy (power plants), energy-intensive industries, mineral and chemical industry, manufacturing, agriculture and livestock industry - **Air pollutants:** GHGs, PM_x, NO_x, SO_2, CO, O_3 and heavy metals - Based on Best Environmental Management Practice
	The Medium Combustion Plant (MCP) Directive - Enacted in 2015	- **Regulation type:** Command and Control - **Sector covered:** Energy (heat and power plants), energy-intensive industries (industrial plants) - **Emission controls:** **Air pollutants:** PM_x, NO_x, SO_2 and CO Total rated thermal input and zone specific Based on Best Available and Emerging Technology
China	**Atmospheric Pollution Prevention and Control Law** - Law enacted in 2000 - Revised in 2015	- **Regulation type:** Command and Control - **Sectors covered:** Energy (power plants), energy-intensive industries, mineral and chemical industry, manufacturing, agriculture, livestock industry and motor vehicles - **Air pollutants:** GHGs, PM_x, NO_x, SO_2, CO, O_3, heavy metals and PAHs - **Emission controls:** Environmental quality standards and emission standards Based on air quality standards, economic and technological status.